DEPARTMENT OF TRANSPORTATION

Cone Penetration Test Design Guide for State Geotechnical Engineers

Author: David Saftner

Report Number: 2018-32

Date Published: November 2018

Minnesota Department of Transportation
Research Services & Library
395 John Ireland Boulevard, MS 330
St. Paul, Minnesota 55155-1899
mndot.gov/research

To request this document in an alternative format, such as braille or large print, call 651-366-4718 or 1-800-657-3774 (Greater Minnesota) or email your request to ADArequest.dot@state.mn.us. Please request at least one week in advance.

Technical Report Documentation Page

1. Report No.	2.	3. Recipients Accession No.	
MN/RC 2018-32			
4. Title and Subtitle Cone Penetration Test Design Guide for State Geotechnical Engineers		5. Report Date November 2018 6.	
7. Author(s) Ryan Dagger, David Saftner, and Paul Mayne		8. Performing Organization Report No.	
9. Performing Organization Name and Address Department of Civil Engineering University of Minnesota Duluth 1405 University Drive Duluth, MN 55812		10. Project/Task/Work Unit No. CTS#2017022 11. Contract (C) or Grant (G) No. (C) 99008 (WO) 249	
12. Sponsoring Organization Name and Address Minnesota Department of Transportation Research Services & Library 395 John Ireland Boulevard, MS 330 St. Paul, Minnesota 55155-1899		13. Type of Report and Period Covered Final Report 14. Sponsoring Agency Code	
15. Supplementary Notes http://mndot.gov/research/reports/2018/201832.pdf			
16. Abstract (Limit: 250 words) The objectives of this project are focused on a new cone penetration testing (CPT) geotechnical design manual for highway and transportation applications based on recent research and innovation covering the period from 2000 to 2018. A step-by-step procedure is outlined on how to use CPT data in the analysis and design of common geotechnical tasks. Previous manuals are either very outdated with information from 1970-1996, or not appropriately targeted to transportation works. This design document introduces modern and recent advancements in CPT research not otherwise captured in legacy manuals from the 1990's and earlier. Examples and case studies are provided for each topic interpreted using CPT measures. In the manual, a step-by-step procedure is outlined on how to use CPT data in analysis and design for typical geotechnical practices. These topics, which are applicable both to state highways and local roads, include bridge foundations (including shallow footings and deep foundations) and soil characterization (including determination of standard soil engineering properties).			
17. Document Analysis/Descriptors Cone penetrometers, Geographic information systems, Soils by properties, Bridge foundations, Soil mechanics		18. Availability Statement No restrictions. Document available from: National Technical Information Services, Alexandria, Virginia 22312	
19. Security Class (this report) Unclassified	20. Security Class (this page) Unclassified	21. No. of Pages 225	22. Price

CONE PENETRATION TEST DESIGN GUIDE FOR STATE GEOTECHNICAL ENGINEERS

Prepared by:

Ryan Dagger
David Saftner
Department of Civil Engineering
University of Minnesota Duluth

Paul W. Mayne
School of Civil & Environmental Engineering
Georgia Institute of Technology, Atlanta

November 2018

Published by:

Minnesota Department of Transportation
Research Services & Library
395 John Ireland Boulevard, MS 330
St. Paul, Minnesota 55155-1899

TABLE OF CONTENTS

LIST OF FIGURES

LIST OF TABLES

CHAPTER 1: INTRODUCTION

The purpose of this manual is to provide an analysis of soil characterization, shallow footings, and deep foundations using direct cone penetration testing (CPT) methods. Geotechnical site characterization is important for evaluating soil parameters that will be used in the analysis and design of foundations, retaining walls, embankments and situations involving slope stability. Common practice is to determine these soil parameters through conventional lab and in-situ testing. An alternative method uses CPT readings of cone tip resistance (q_t) sleeve friction (f_s), and pore pressure (u_2) directly to determine these parameters, such as unit weight, effective friction angle, undrained shear strength and many others (Figure 1). Direct CPT methods are provided for these parameters, which will be used in the designs for shallow and deep foundations.

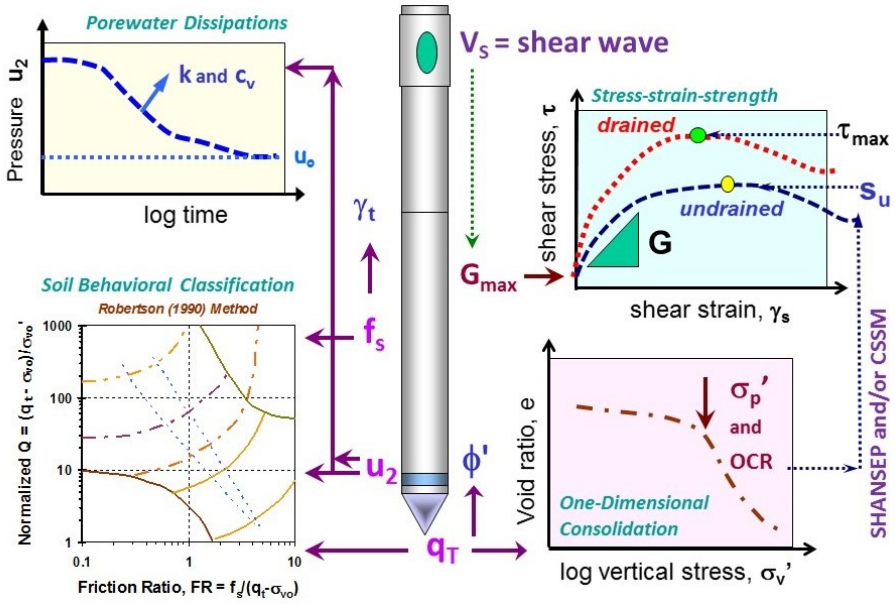

Figure 1. Geoparameters determined from CPT.

Designing shallow foundations is typically done in a two-part process, determining the bearing capacity and expected settlement (commonly referred to as displacement) of the soil, to approximate the required size and shape of a foundation. The older traditional methods are no longer required with many approaches existing for using CPT directly in the design of shallow foundations. Results from these methods can provide a direct assessment of bearing capacity and/or settlement. A specific approach to the direct method has been recommended and tested using a database of 166 full-scale field load tests (Figure 2). A one-part process is used to scale the measured cone penetrometer readings (i.e., measured cone tip resistance, sleeve friction, and pore water pressure) to obtain the bearing capacity and settlement of the soil. A step-by-step procedure has been created to transition from the CPT data to bearing capacity with settlement accounted for. The steps consist of estimating a design footing width

and length while using the process in the Soil Characterization section to determine soil parameters directly from the CPT data.

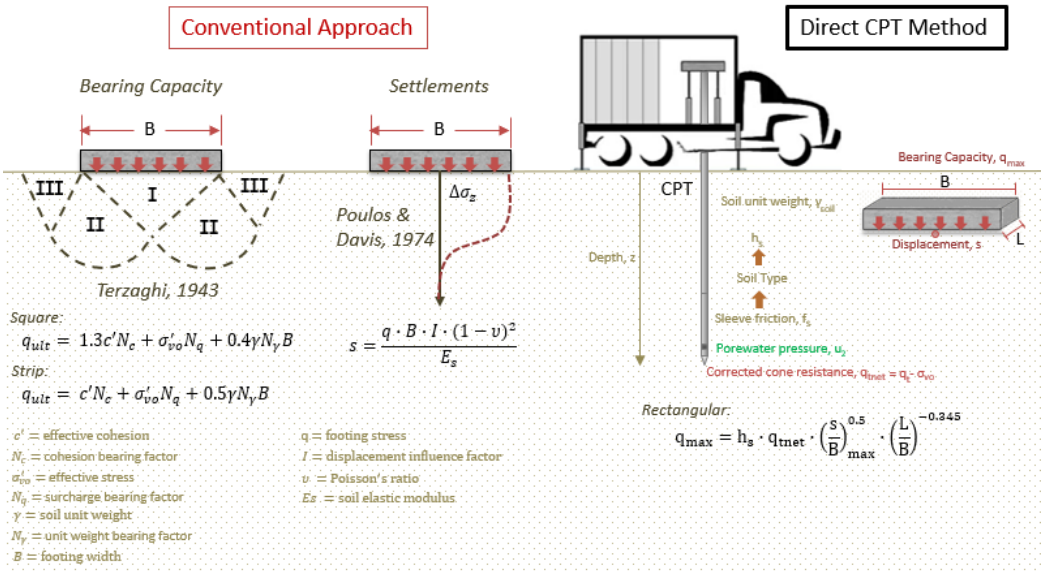

Figure 2. Conventional method for shallow foundation design compared to direct CPT method.

There are upwards of 40 different direct CPT methods that have been developed over the past five decades to determine the axial compression capacity of a piling foundation. Earlier direct CPT methods relied on hand-recorded information where mechanical-type CPT cone tip resistance data would be collected at 20 cm intervals.

Herein, the method recommended for deep foundation design is the Modified UniCone method, which uses all three readings of the modern electronic piezocone penetrometer (CPTu) while addressing a variety of pile foundation types (Figure 3). The modified UniCone Method is based on a total of 330 pile load tests (three times the original UniCone database) that were associated with SCPTu data. Two computer software programs have been recommended for analyzing pile movements and/or settlements.

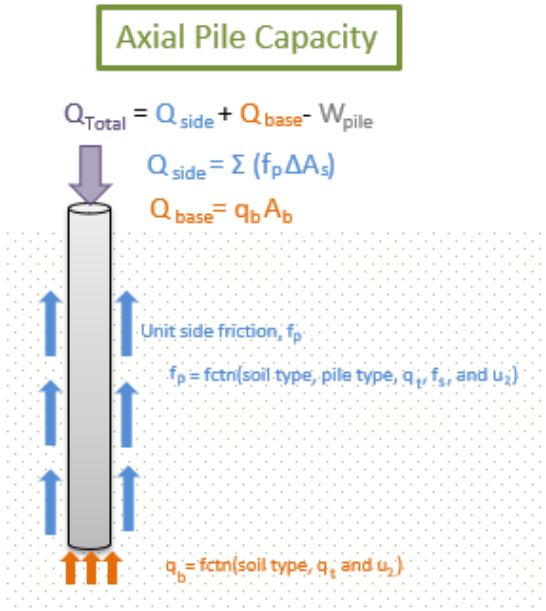

Figure 3. Direct CPT evaluation of axial pile capacity.

CHAPTER 2: DIRECT CPT METHOD FOR SOIL CHARACTERIZATION

2.1 INTRODUCTION

A direct CPT method for determining the value of each of various geoparameters, shown in Table 1, is provided. The parameter I_c is used in the derivation of several sequential parameters. This section of the guide may be referred to as these parameters are used in calculations throughout the shallow foundations and deep foundations sections.

Table 1. Geoparameters calculated directly from CPT

Symbol	Parameter
γ_t	Soil total unit weight
I_c	CPT material index
SBT	Soil behavior type (SBT)
σ_p'	Preconsolidation stress
YSR	Yield stress ratio
ϕ'	Effective friction angle
K_o	Lateral stress coefficient
s_u	Undrained shear strength
D'	Constrained modulus
E'	Drained Young's modulus

K'	Bulk modulus
k_s	Subgrade reaction modulus
M_R	Resilient modulus
G_{max}	Small-strain shear modulus
k	Coefficient of permeability
c_v	Coefficient of consolidation

Other minor parameters can be used in calculations of the geoparameters in Table 1. These minor parameters are provided in Table 2.

Table 2. Minor Geoparameters

Symbol	Parameter	Equation
ρ_t	Mass Density	$\rho_t = \gamma_t / g_a$ where $g_a = 9.8\ m/s^2$
σ_{vo}	Total Stress	$\sigma_{vo} \approx \Sigma\ (\gamma_{ti} \cdot \Delta z_i)$
c'	Effective cohesion	Empirical: $c' \approx 0.03\sigma_p'$ In clays: $c' \approx 0.1 c_u$

2.2 SOIL UNIT WEIGHT

The total soil unit weight can be estimated from CPT sleeve friction resistance as shown in Figure 4 (Mayne 2014). This method is not applicable to organic clays, diatomaceous soils, peats, or sensitive soils.

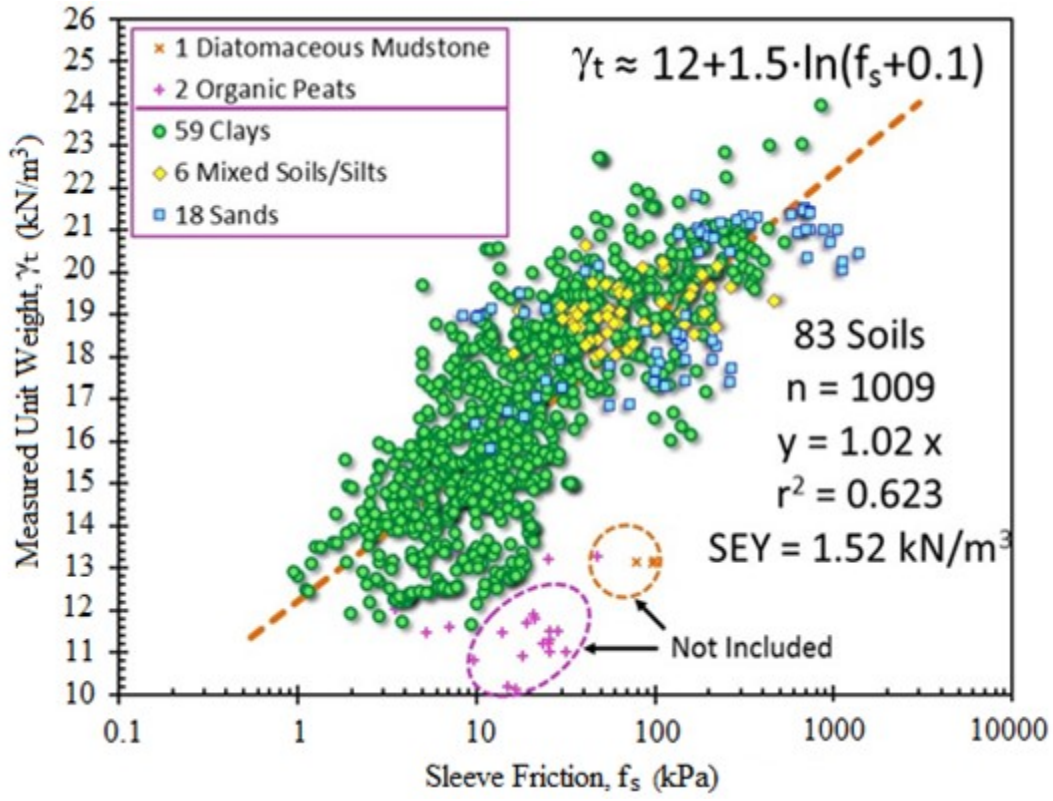

Figure 4. Soil unit weight from CPT sleeve friction.

Use Equation 1 to calculate the soils total unit weight.

$$\gamma_t = \gamma_w \cdot \left[1.22 + 0.15 \cdot \ln\left(100 \cdot \frac{f_s}{\sigma_{atm}} + 0.01\right)\right] \qquad 1$$

Since soil unit weight is required for determining most geoparameters (including Soil Behavior Type), estimating the soil type of the layers using the "rules of thumb" method is a good first step before determining more precise layering (Figure 5). Once a unit weight is determined for each noticeable layer change, these results can be used in later calculations such as "CPT Material Index." To use the "rules of thumb" method, some helpful guidelines are to assume sands are identified when $q_t > 725$ psi and $u_2 \approx u_o$, while the presence of intact clays are prevalent when $q_t < 725$ psi and $u_2 > u_o$. The magnitude of porewater pressures help to indicate intact clays such as, soft ($u_2 \approx 2 \cdot u_o$), firm ($u_2 \approx 4 \cdot u_o$), stiff ($u_2 \approx 8 \cdot u_o$), and hard ($u_2 \approx 20 \cdot u_o$). Fissured overconsolidated clays tend to have negative u_2 values such that $u_2 < 0$.

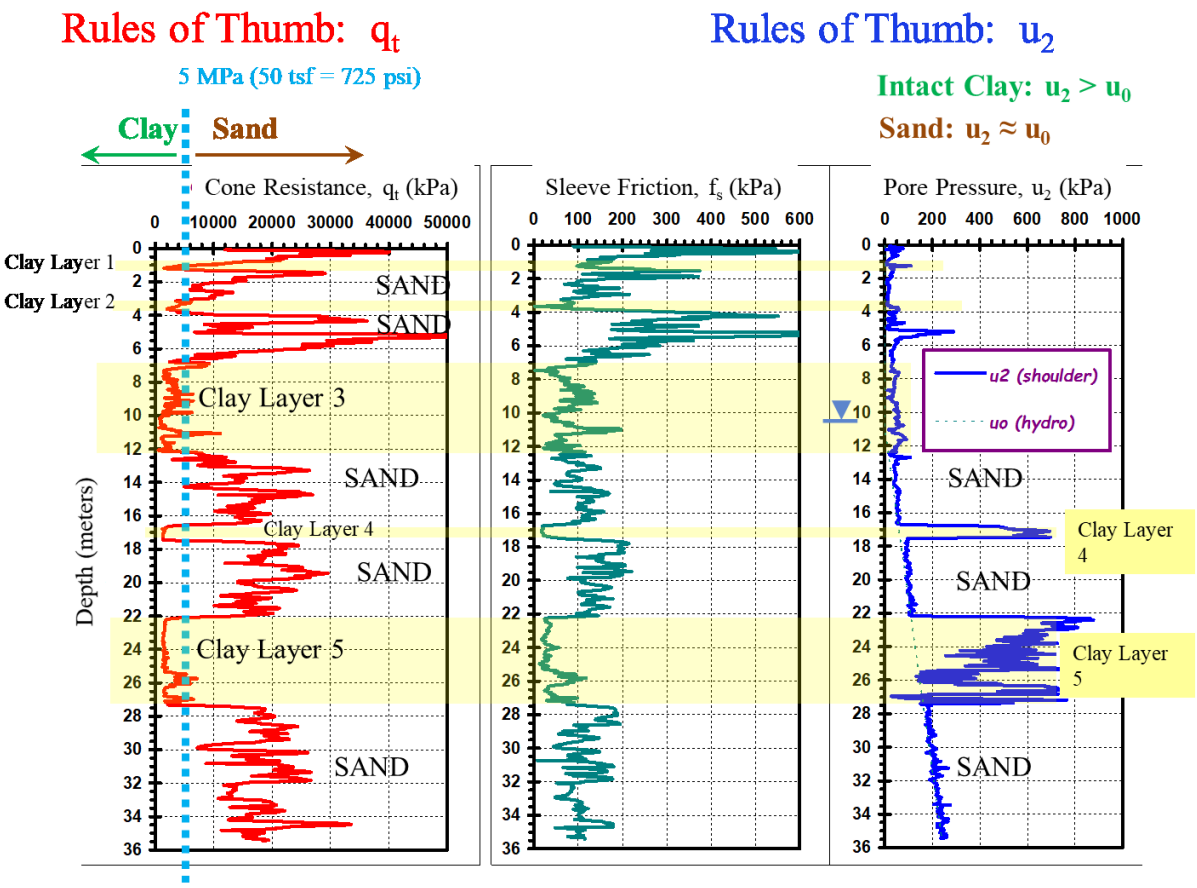

Figure 5. Approximate "rules of thumb" method using CPT sounding from Wakota Bridge, MN.

2.3 CPT MATERIAL INDEX

The development of the CPT material index I_c has improved the initial classification of soil types and calculation of soil parameters as shown in Table 1. To calculate I_c follow steps 1 and 2.

2.3.1 Step 1. Normalized Sleeve Friction

Calculate F_r using Equation 2 if not provided with the CPT data gathered.

$$F_r(\%) = 100 \cdot \frac{f_s}{(q_t - \sigma_{vo})} \qquad 2$$

2.3.2 Step 2. Iteration

Iterate using Equations 3-5 to determine I_c by initially using n = 1 to calculate a starting value of I_c. The exponent n is soil-type dependent: n = 1 (clays); $n \approx 0.75$ (silts); and $n \approx 0.5$ (sands). Iteration converges quickly which is generally after the 3rd cycle.

$$\boldsymbol{Q_{tn}} = \frac{(\boldsymbol{q_t} - \boldsymbol{\sigma_{vo}})/\boldsymbol{\sigma_{atm}}}{(\boldsymbol{\sigma'_{vo}}/\boldsymbol{\sigma_{atm}})^{\boldsymbol{n}}} \quad \textbf{3}$$

$$n = 0.381 \cdot I_c + 0.05\left(\frac{\sigma'_{vo}}{\sigma_{atm}}\right) - 0.15 \quad 4$$

$$n \leq 1.0$$

$$\boldsymbol{I_c} = \sqrt{[\boldsymbol{3.47} - \boldsymbol{logQ_{tn}}]^2 + [\boldsymbol{1.22} + \boldsymbol{logF_r}]^2} \quad \textbf{5}$$

2.4 SOIL BEHAVIOR TYPE (SBT)

Typically soil samples are not taken when using CPT. The soil types are then inferred from the q_t, f_s, and u_2 readings. To determine the types of soil from CPT data follow steps 1 and 2.

2.4.1 Step 1.

To determine the soil layers from CPT results, calculate I_c by following the steps under section "CPT Material Index." After I_c has been determined through all specified depths, use Figure 6 to classify the type of soil by comparing each I_c value to normalized CPT readings (F_r and Q_{tn}) from Equations 2 and 3.

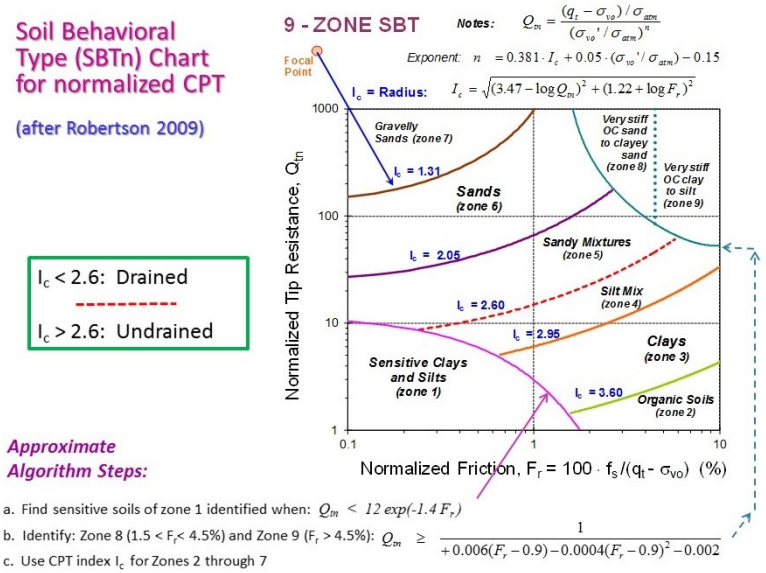

Figure 6. SBT zones using CPT Ic.

2.4.2 Step 2.

To determine if any of the soil layers contain "sensitive clays and silts" from zone 1 or "very stiff overconsolidated (OC) soil" from zones 8 and 9, use Equations 6 and 7. If any soil layers are found within zone 1 by Equation 6, then caution should be taken as these clays are prone to instability, collapses, and difficulties in construction performance. Very stiff OC sands to clayey sands of zone 8 (1.5% < F_r < 4.5%) and very stiff OC clays to silts of zone 9 (F_r > 4.5%) can be identified by Equation 7.

$$Q_{tn} < 12exp(-1.4 \cdot F_r) \quad (6)$$

Equation 6 errata. This is an exponential expression (see Figure 5)

$$Q_{tn} > \frac{1}{0.005(F_r-1)-0.0003(F_r-1)^2-0.002} \quad (7)$$

Errata: See terms and coefficients in Figure 5 above (numbers cannot be rounded off)

After each CPT reading has been assigned a zone from Figure 14, a visual representation can be made to show the predominant layers by soil types (Figure A5).

2.5 EFFECTIVE STRESS FRICTION ANGLE

The effective friction angle (ϕ') is used to govern the strength for sands and clays where Equation 8 is used for sands and Equation 9 is used for clays. The value of ϕ' for sands is derived from I_c so before ϕ' can be calculated refer to the iteration of Q_{tn} under the "CPT Material Index" section. Once the values

of I_c and Q_{tn} are calculated, the type of soil can be determined from the section "Soil Behavior Type SBT". The type of soil will dictate which equation to use for ϕ'.

Sands

$$\phi'(\text{deg}) = 17.6° + 11.0° \log(Q_{tn}) \quad (8)$$

Clays

$$\phi'(\text{deg}) = 29.5° \cdot B_q^{0.121} \cdot \left[0.256 + 0.336 \cdot B_q + \log\left(\frac{q_t - \sigma_{vo}}{\sigma'_{vo}}\right)\right] \quad (9)$$

Where:

$$B_q = (u_2 - u_o)/(q_t - \sigma_{vo})$$

2.6 STRESS HISTORY

Determining the stress history can be characterized by an apparent yield stress ratio of the form:

$$YSR = \frac{\sigma'_p}{\sigma'_{vo}} \quad (10)$$

Where σ_p' is defined as the preconsolidation stress or effective yield stress (Equation 10). The *YSR* is the same equation as the more common overconsolidation ratio (OCR), but is now generalized to accommodate mechanisms of preconsolidation such as ageing, desiccation, repeated cycles of wetting-drying, repeated freeze thaw cycles and other factors.

$$\sigma'_p = \sigma'_y = 0.33(q_t - \sigma_{vo})^{m'} \quad (11)$$

Where σ_p', σ_y', σ_{vo}, and q_t have units of kPa and the value of m' depends on soil type with typical values shown in Table 3.

Table 3. Soil type compared to exponent m'.

Soil Type	m'
Fissured clays	1.1
Intact clays	1.0
Sensitive clays	0.9
Silt mixtures	0.85
Silty sands	0.80
Clean sands	0.72
Note: m' may be higher than 1.1 in fissured clays.	

The value of m' for non-fissured soils and inorganic clays and silts is derived from I_c (Figure 7) so before m' can be calculated (Equation 12) refer to the iteration of I_c under the "CPT Material Index" section. Determine I_c for all soil layers before calculating m'.

$$m' = 1 - \frac{0.28}{1+\left(I_c/2.65\right)^{25}} \quad (12)$$

Once m' is known for all soil layers, the *YSR* can be determined.

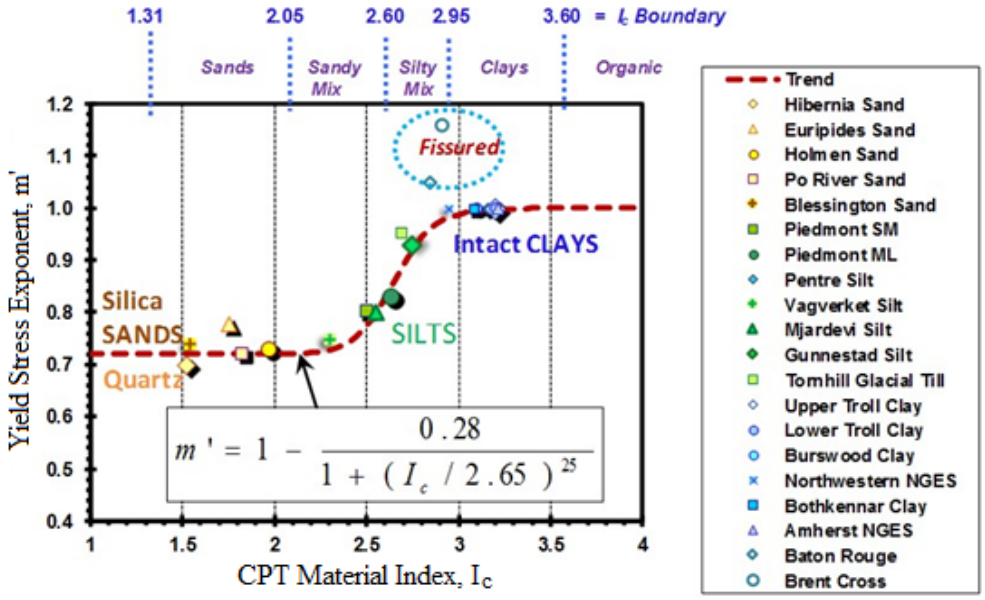

Figure 7. Yield stress exponent compared to CPT material index.

A limiting value of *YSR* can be reached for clays and sands. It can be calculated using Equation 13.

$$YSR_{limit} = \left[\frac{(1+\sin(\emptyset'))}{(1-\sin(\emptyset'))^2}\right]^{(1/\sin(\emptyset'))} \quad (13)$$

2.7 LATERAL STRESS COEFFICIENT

The lateral stress coefficient, $K_o = \sigma_{ho}'/\sigma_{vo}'$, commonly referred to as the at-rest condition is used to represent the horizontal geostatic state of soil stress. K_o can be calculated using Equation 14, but

sections such as "Stress History" and "Effective Stress Friction Angle" will need to be referred to for determining parameters ϕ' and *YSR*.

$$K_o = (1 - \sin(\emptyset')) \cdot YSR^{\sin(\emptyset')} \quad 14$$

A maximum value for K_o can be determined by Equation 15.

$$K_{o,max} = \frac{(1+\sin(\emptyset'))}{(1-\sin(\emptyset'))} = tan^2(45° + \emptyset'/2) \quad 15$$

2.8 UNDRAINED SHEAR STRENGTH

Loading on soils can result in fully drained, partially drained, or fully undrained conditions. Sands typically produce drained cases due to their high permeability, but exceptions may occur in loose sands during fast loading where the water does not have sufficient time to dissipate. Clays exhibit low permeability and thus often result in undrained loading cases when a load is applied quickly. For soft-firm clays, the undrained shear strength (s_u) can be determined from CPT via Equation 16, where the value of the bearing factor N_{kt} can be taken as 12.

$$s_u = \frac{q_t - \sigma_{vo}}{N_{kt}} \quad 16$$

In the case of remolded undrained shear strength from CPT, $s_u \approx f_s$.

2.9 GROUND STIFFNESS AND SOIL MODULI

Determining the grounds stiffness can be measured from geoparameters such as the constrained modulus (D'), drained Young's modulus (E'), bulk modulus (K'), subgrade reaction modulus (k_s), resilient modulus (M_R), and small-strain shear modulus (G_{max}).

$$D' \approx 5 \cdot (q_t - \sigma_{vo}) \quad 17$$

$$E' = \frac{D'}{1.1} \quad 18$$

$$K' = \frac{E'}{[3\cdot(1-2v')]} \quad 19$$

The subgrade modulus (k_s) is a combination of soil-structural properties, which creates a parameter that depends on the ground stiffness and the size of the loaded element.

$$k_s = \frac{E'}{[d\cdot(1-v^2)]} \quad 20$$

The resilient modulus M_R applies to pavement analysis and design and can be calculated using Equation 21 where q_t and f_s are in MPa.

$$M_R = (1.46q_t^{0.53} + 13.55f_s^{1.4} + 2.36)^{2.44} \quad 21$$

The small strain shear modulus G_{max} is a representation of the initial stiffness of all soils and rocks. Graphically it is the beginning portion of all stress-strain-strength curves for geomaterials. Use Equation 22 to determine G_{max}.

$$G_{max} = \rho_t \cdot V_s^2 \quad 22$$

Where: V_s = shear wave velocity (Equation 23), as measured by seismic cone penetration tests (SCPT). If only cone penetration tests (CPT) or piezocone (CPTu) data are available, the shear wave velocity may be estimated from:

$$V_s\ (m/s) = [10.1 \cdot \log(q_t) - 11.4]^{1.67} \cdot \left(100 \cdot \frac{f_s}{q_t}\right)^{0.3} \quad 23$$

Where: q_t and f_s have units of (kPa)

2.10 COEFFICIENT OF CONSOLIDATION

The coefficient of consolidation (c_v) controls the rate that foundation and embankment settlements occur. By using results of CPT dissipation tests, that measure the change in u_2 readings over time, the value of c_v can be determined. Using Equation 24, c_v can be determined based on piezocone dissipation

curves. The equation below requires an estimate of the in-situ rigidity index (I_R) of the soil. If results of SCPTU are available, then I_R may be determined from G_{max} and q_t per equation A38.

$$c_v = \frac{0.030 \cdot (a_c)^2 \cdot (I_R)^{0.75}}{t_{50}} \quad 24$$

Where:

a_c = penetrometer radius (1.78 cm for 10-cm^2 cone; 2.20 cm for 15-cm^2 cone)
t_{50} = time to reach 50% dissipation
$I_R = G/s_u$ = undrained rigidity index
G can be determined from the "Ground Stiffness and Soil Moduli" section.

2.11 HYDRAULIC CONDUCTIVITY

The hydraulic conductivity, also known as the coefficient of permeability (k), expresses the flow characteristics of soils and has units of cm/s or feet/day. One method of calculation would be to use Equation 25 where c_v would need to be determined from "Coefficient of Consolidation" and D' would need to be determined from "Ground Stiffness and Soil Moduli."

$$k = \frac{c_v \cdot \gamma_w}{D'} \quad 25$$

An alternative approach, developed for soft normally-consolidated soils (Figure 8), is shown in Equation 26 where t_{50} (sec) values are used directly in assessing k in (cm/s).

$$k \approx \left(\frac{1}{251 \cdot t_{50}}\right)^{1.25} \quad 26$$

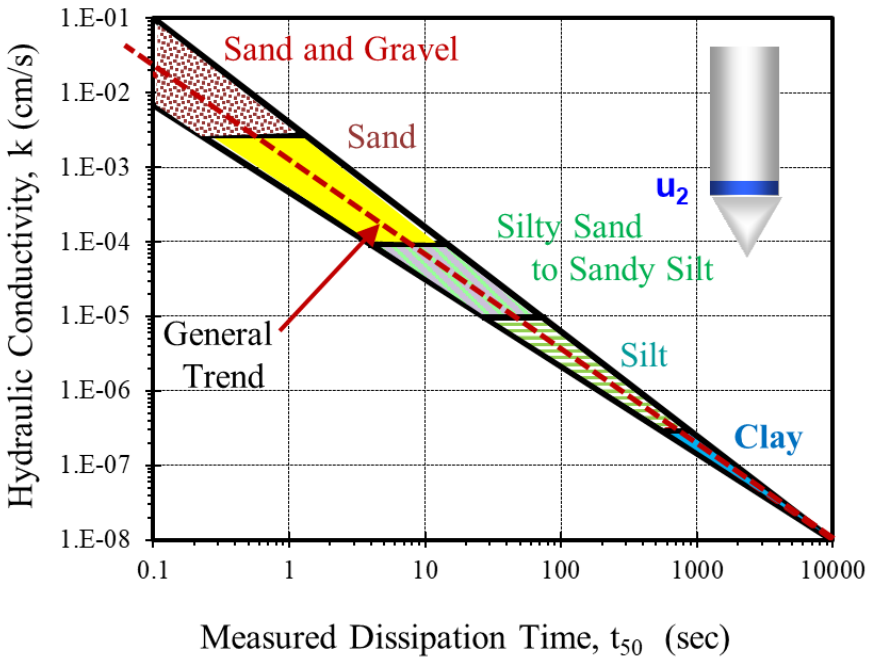

Figure 8. k vs. dissipation time for 50% consolidation (Mayne 2017).

2.12 EXAMPLE PROBLEMS

2.12.1 Example 1: Direct CPT Methods for Geoparameters on Sands

Several geoparameters need to be determined based on the given CPT data collected for the South Abutment of a bridge in Benton County, MN (Figure 9). The groundwater table (GWT) was measured at 17 feet. Determine all the geoparameters found in Table 4 at depths of 0 feet to 30 feet. All sand layers can be assumed “drained” with v = 0.2.

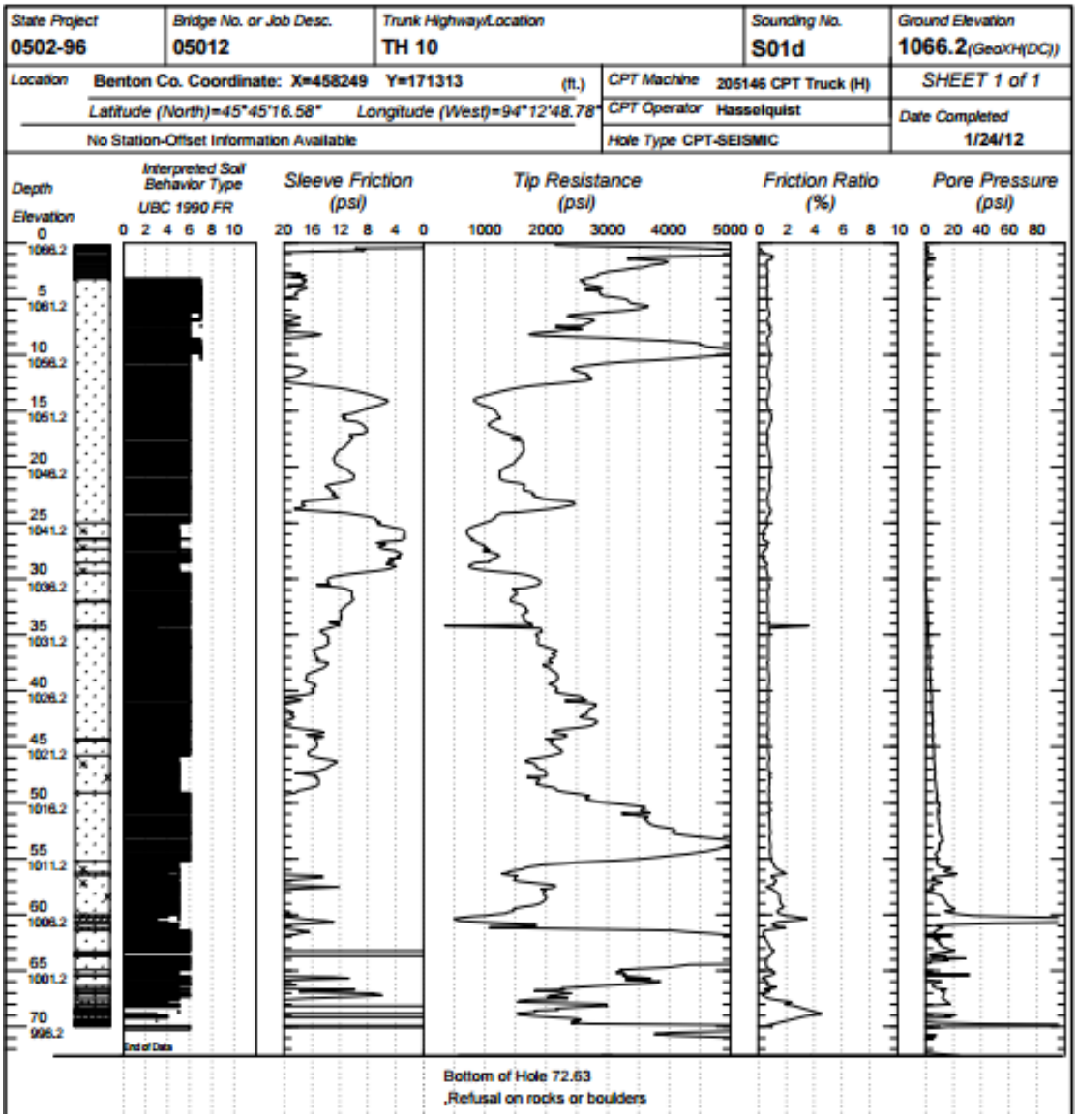

Figure 9. CPT data from Benton County, Minnesota for example problem 1.

Table 4. Geoparameters evaluated for Case Example 1

Symbol	Parameter	Symbol	Parameter
γ_t	Soil total unit weight	K_o	Lateral stress coefficient
I_c	CPT material index	D'	Constrained modulus
SBT	Soil behavior type (SBT)	E'	Drained Young's modulus
σ_p'	Preconsolidation stress	K'	Bulk modulus
YSR	Yield stress ratio	M_R	Resilient modulus
ϕ'	Effective friction angle	G_{max}	Small-strain shear modulus

Solution

Soil total unit weight

Estimate soil layering using "rules of thumb."

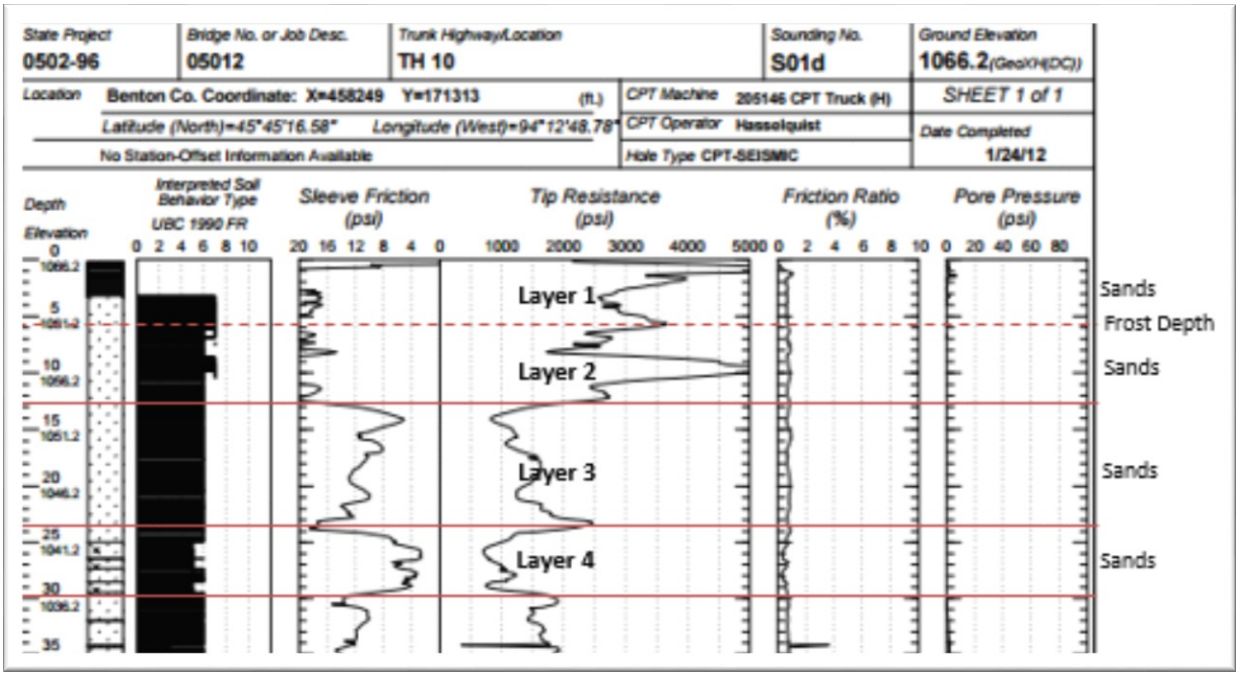

Figure 10. Soil layers using "rules of thumb."

γ_w = 62.24 pcf

Layer 1

From Figure 10: f_s = 17 psi taken as a representative value of the layer

$$\gamma_t = 62.4\ \text{pcf} \cdot \left[1.22 + 0.15 \cdot \ln\left(100 \cdot \frac{17\ \text{psi}}{14.5\ \text{psi}} + 0.01\right)\right] = 120.4\ \text{pcf}$$

Layer 2

From Figure 10: f_s = 17 psi taken as a representative value of the layer

$$\gamma_t = 62.4\ \text{pcf} \cdot \left[1.22 + 0.15 \cdot \ln\left(100 \cdot \frac{17\text{psi}}{14.5\ \text{psi}} + 0.01\right)\right] = 120.4\ \text{pcf}$$

Layer 3

From Figure 10: f_s = 12 psi taken as a representative value of the layer

$$\gamma_t = 62.4\ \text{pcf} \cdot \left[1.22 + 0.15 \cdot \ln\left(100 \cdot \frac{12\ \text{psi}}{14.5\ \text{psi}} + 0.01\right)\right] = 117.2\ \text{pcf}$$

Layer 4

From Figure 10: f_s = 7 psi taken as a representative value of the layer

$$\gamma_t = 62.4\ \text{pcf} \cdot \left[1.22 + 0.15 \cdot \ln\left(100 \cdot \frac{7\ \text{psi}}{14.5\ \text{psi}} + 0.01\right)\right] = 112.1\ \text{pcf}$$

CPT Material Index

Layer 1

From Figure 10: f_s = 17 psi and q_c = 3500 psi

$$q_t = q_c + u_2 \cdot (1 - a) = 3500 \text{ psi} + 3 \text{ psi} \cdot (1 - 0.8) = 3501 \text{ psi}$$

$$\sigma_{vo} = \gamma_t \cdot 6 \text{ feet} = 120.4 \text{ pcf} \cdot 6 \text{ feet} = 722.5 \text{ psf} = 5.0 \text{ psi}$$

$$F_r(\%) = 100 \cdot \frac{f_s}{(q_t - \sigma_{vo})} = 100 \cdot \frac{17 \text{ psi}}{(3501 \text{ psi} - 5.0 \text{ psi})} = 0.49$$

Step 2. Iterate to solve for I_c. Steps are not shown for brevity.

$$u_o = 0 \text{ psi}$$

$$\sigma'_{vo} = \sigma_{vo} - u_o = 5 \text{ psi} - 0 \text{ psi} = 5.0 \text{ psi}$$

$$Q_{tn} = \frac{(q_t - \sigma_{vo})/\sigma_{atm}}{(\sigma'_{vo}/\sigma_{atm})^n} = \frac{(3501 \text{ psi} - 5.0 \text{ psi})/14.5 \text{ psi}}{(5.0 \text{ psi}/14.5 \text{ psi})^n}$$

$$n = 0.381 \cdot I_c + 0.05\left(\frac{\sigma'_{vo}}{\sigma_{atm}}\right) - 0.15 = 0.381 \cdot I_c + 0.05\left(\frac{5.0 \text{ psi}}{14.5 \text{ psi}}\right) - 0.15$$

$$I_c = \sqrt{[3.47 - \log(Q_{tn})]^2 + [1.22 + \log(0.49)]^2}$$

$$Q_{tn} = 353.29 \qquad n = 0.36 < 1.0 \qquad I_c = 1.3$$

Layer 2

From Figure 10: f_s = 17 psi and q_c = 3500 psi

$$q_t = q_c + u_2 \cdot (1 - a) = 3500 \text{ psi} + 0 \text{ psi} \cdot (1 - 0.8) = 3500 \text{ psi}$$

$$\sigma_{vo} = 722.5 \text{ psf} + \gamma_t \cdot 6 \text{ feet} = 722.5 \text{ psf} + 120.4 \text{ pcf} \cdot 6 \text{ feet} = 1445 \text{ psf} = 10.0 \text{ psi}$$

$$F_r(\%) = 100 \cdot \frac{f_s}{(q_t - \sigma_{vo})} = 100 \cdot \frac{17 \text{ psi}}{(3500 \text{ psi} - 10.0 \text{ psi})} = 0.49$$

Step 2. Iterate to solve for I_c. Steps are not shown for brevity.

$$u_o = 0 \text{ psi}$$

$$\sigma'_{vo} = \sigma_{vo} - u_o = 10.0 \text{ psi} - 0 \text{ psi} = 10.0 \text{ psi}$$

$$Q_{tn} = \frac{(q_t - \sigma_{vo})/\sigma_{atm}}{(\sigma'_{vo}/\sigma_{atm})^n} = \frac{(3500 \text{ psi} - 10.0 \text{ psi})/14.5 \text{ psi}}{(10.0 \text{ psi}/14.5 \text{ psi})^n}$$

$$n = 0.381 \cdot I_c + 0.05\left(\frac{\sigma'_{vo}}{\sigma_{atm}}\right) - 0.15 = 0.381 \cdot I_c + 0.05\left(\frac{10.0 \text{ psi}}{14.5 \text{ psi}}\right) - 0.15$$

$$I_c = \sqrt{[3.47 - \log(Q_{tn})]^2 + [1.22 + \log(0.49)]^2}$$

$$Q_{tn} = 279.47 \qquad n = 0.41 < 1.0 \qquad I_c = 1.4$$

Layer 3

From Figure 10: f_s = 12 psi and q_c = 1500 psi

$$q_t = q_c + u_2 \cdot (1 - a) = 1500 \text{ psi} + 0 \text{ psi} \cdot (1 - 0.8) = 1500 \text{ psi}$$

$$\sigma_{vo} = 1445 \text{ psf} + \gamma_t \cdot 11 \text{ feet} = 1445 \text{ psf} + 117.2 \text{ pcf} \cdot 11 \text{ feet} = 2734 \text{ psf} = 19.0 \text{ psi}$$

$$F_r(\%) = 100 \cdot \frac{f_s}{(q_t - \sigma_{vo})} = 100 \cdot \frac{12 \text{ psi}}{(1500 \text{ psi} - 19.0 \text{ psi})} = 0.81$$

Step 2. Iterate to solve for I_c. Steps are not shown for brevity.

$$u_o = \gamma_{water} \cdot (z - z_w) = 62.24 \text{ pcf} \cdot (23 \text{ feet} - 17 \text{ feet}) = 373.4 \text{ psf} = 9.9 \text{ psi}$$

$$\sigma'_{vo} = \sigma_{vo} - u_o = 19.0 \text{ psi} - 9.9 \text{ psi} = 16.4 \text{ psi}$$

$$Q_{tn} = \frac{(q_t - \sigma_{vo})/\sigma_{atm}}{(\sigma'_{vo}/\sigma_{atm})^n} = \frac{(1500 \text{ psi} - 19.0 \text{ psi})/14.5 \text{ psi}}{(16.4 \text{ psi}/14.5 \text{ psi})^n}$$

$$n = 0.381 \cdot I_c + 0.05\left(\frac{\sigma'_{vo}}{\sigma_{atm}}\right) - 0.15 = 0.381 \cdot I_c + 0.05\left(\frac{16.4 \text{ psi}}{14.5 \text{ psi}}\right) - 0.15$$

$$I_c = \sqrt{[3.47 - \log(Q_{tn})]^2 + [1.22 + \log(0.81)]^2}$$

$$Q_{tn} = 94.7 \qquad n = 0.6 < 1.0 \qquad I_c = 1.9$$

Layer 4

From Figure 10: f_s = 7 psi and q_c = 1200 psi

$$q_t = q_c + u_2 \cdot (1 - a) = 1200 \text{ psi} + 0 \text{ psi} \cdot (1 - 0.8) = 1200 \text{ psi}$$

$$\sigma_{vo} = 2734 \text{ psf} + \gamma_t \cdot 11 \text{ feet} = 2734 \text{ psf} + 112.1 \text{ pcf} \cdot 7 \text{ feet} = 3519 \text{ psf} = 24.4 \text{ psi}$$

$$F_r(\%) = 100 \cdot \frac{f_s}{(q_t - \sigma_{vo})} = 100 \cdot \frac{7 \text{ psi}}{(1200 \text{ psi} - 24.4 \text{ psi})} = 0.60$$

Step 2. Iterate to solve for I_c. Steps are not shown for brevity.

$$u_o = \gamma_{water} \cdot (z - z_w) = 62.24 \text{ pcf} \cdot (30 \text{ feet} - 17 \text{ feet}) = 809.1 \text{ psf} = 13.0 \text{ psi}$$

$$\sigma'_{vo} = \sigma_{vo} - u_o = 24.4 \text{ psi} - 13.0 \text{ psi} = 18.8 \text{ psi}$$

$$Q_{tn} = \frac{(q_t - \sigma_{vo})/\sigma_{atm}}{(\sigma'_{vo}/\sigma_{atm})^n} = \frac{(1200 \text{ psi} - 24.4 \text{ psi})/14.5 \text{ psi}}{(18.8 \text{ psi}/14.5 \text{ psi})^n}$$

$$n = 0.381 \cdot I_c + 0.05\left(\frac{\sigma'_{vo}}{\sigma_{atm}}\right) - 0.15 = 0.381 \cdot I_c + 0.05\left(\frac{18.8 \text{ psi}}{14.5 \text{ psi}}\right) - 0.15$$

$$I_c = \sqrt{[3.47 - \log(Q_{tn})]^2 + [1.22 + \log(0.60)]^2}$$

$$Q_{tn} = 68.6 \qquad n = 0.64 < 1.0 \qquad I_c = 1.9$$

Soil Behavior Type (SBT)

Layer 1

Based on values of I_c, Q_{tn}, and F_r, the first layer is defined as a "Drained Gravelly Sand" from Figure 11.

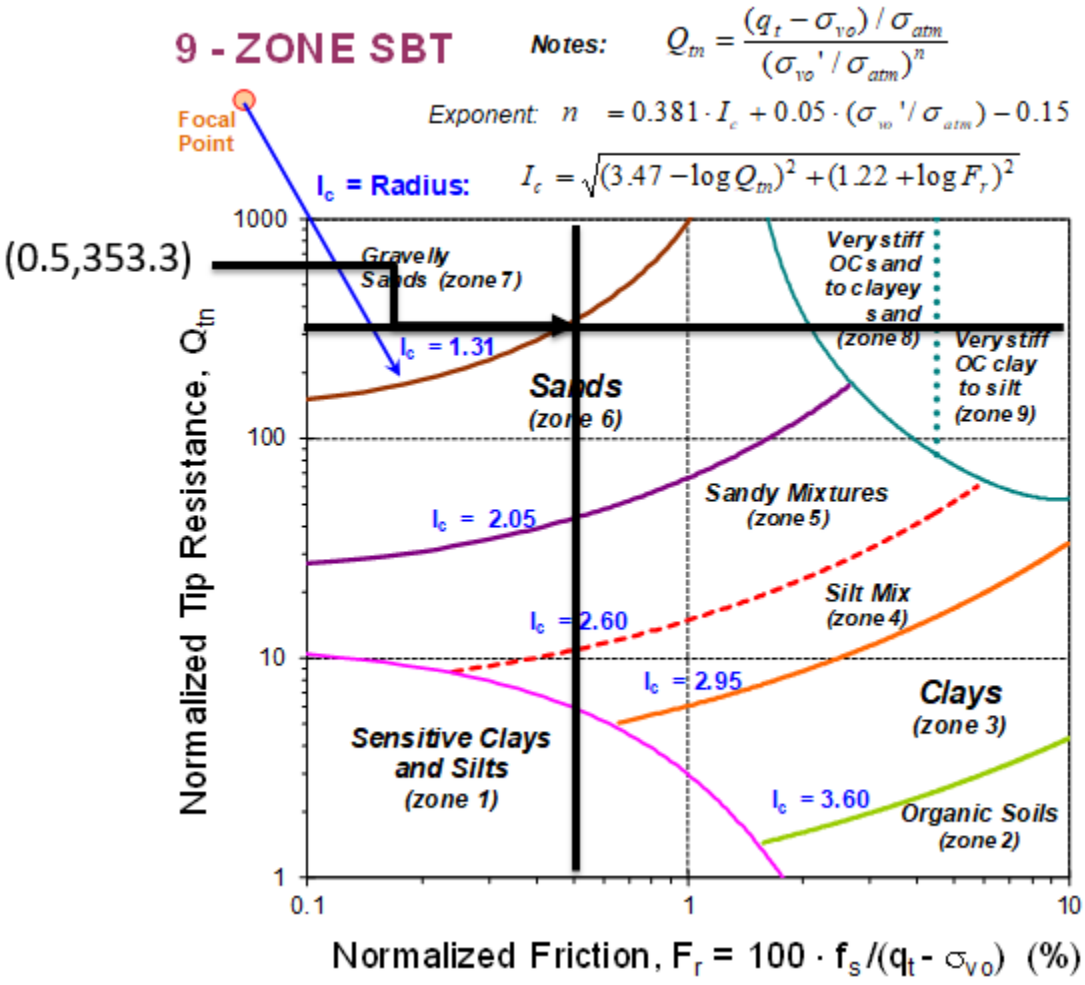

Figure 11. Soil layer 1 using SBT method.

Layer 2

Based on values of I_c, Q_{tn}, and F_r, the second layer is defined as a "Drained Sand" from Figure 12.

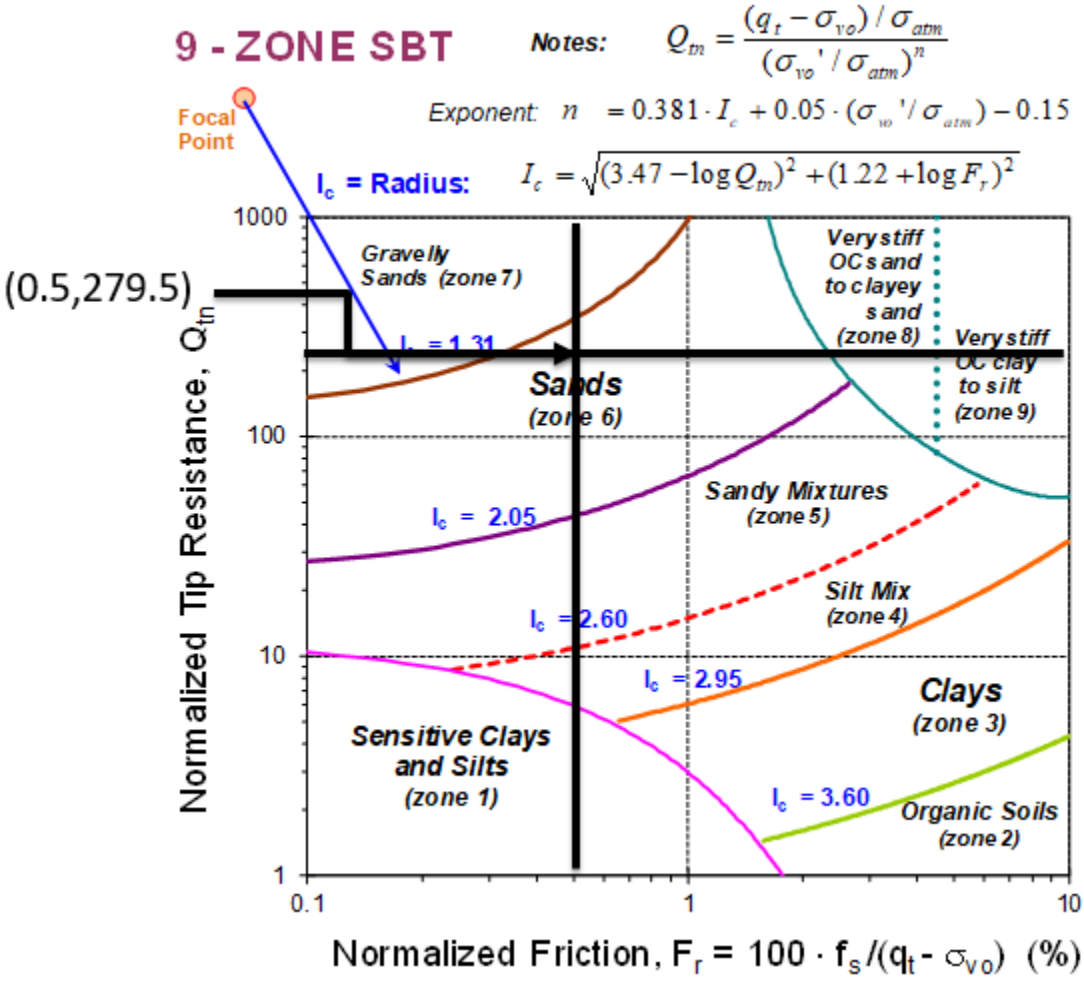

Figure 12. Soil layer 2 using SBT method.

Layer 3

Based on values of I_c, Q_{tn}, and F_r, the third layer is defined as a "Drained Sand" from Figure 13.

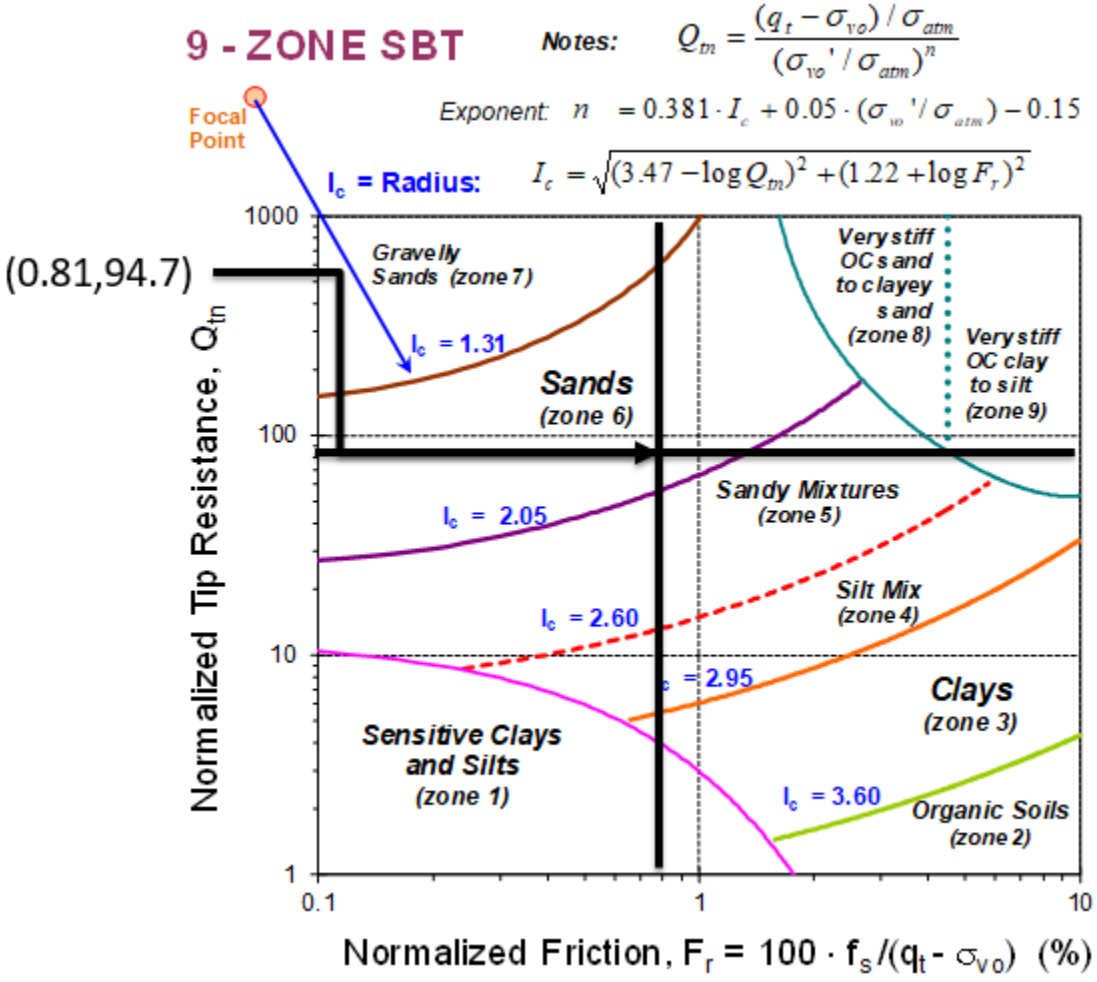

Figure 13. Soil layer 3 using SBT method.

Layer 4

Based on values of I_c, Q_{tn}, and F_r, the fourth layer is defined as a "Drained Sand" from Figure 14.

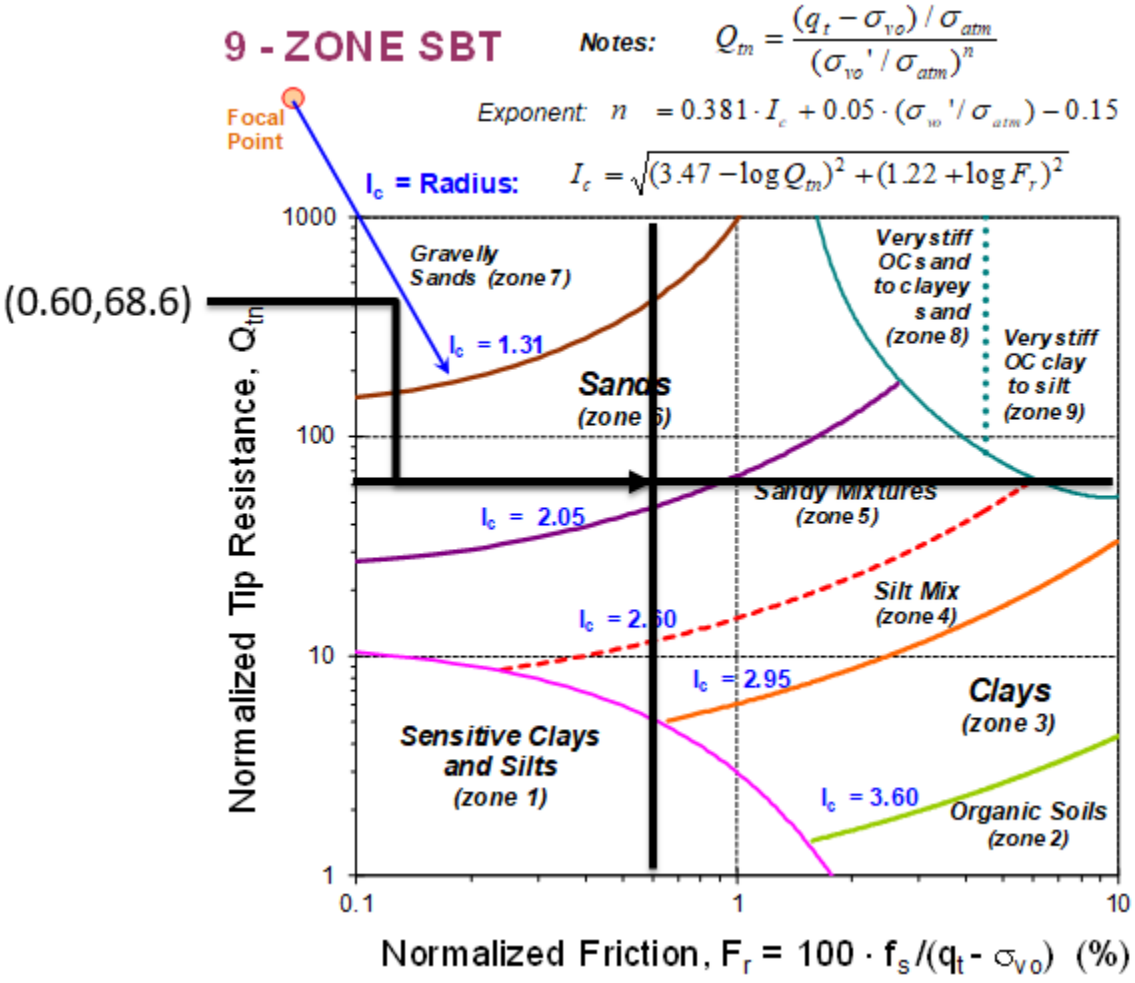

Figure 14. Soil layer 4 using SBT method.

Effective Stress Friction Angle

Layer 1

$$\phi'(\text{deg}) = 17.6° + 11.0° \log(Q_{tn}) = 17.6° + 11.0° \log(353.3) = 45.6°$$

Layer 2

$$\phi'(\text{deg}) = 17.6° + 11.0° \log(Q_{tn}) = 17.6° + 11.0° \log(279.5) = 44.5°$$

Layer 3

$$\phi'(\text{deg}) = 17.6° + 11.0° \log(Q_{tn}) = 17.6° + 11.0° \log(94.7) = 39.3°$$

Layer 4

$$\phi'(\text{deg}) = 17.6° + 11.0° \log(Q_{tn}) = 17.6° + 11.0° \log(68.6) = 37.8°$$

Stress History

Layer 1

$$m' = 1 - \frac{0.28}{1 + \left(I_c/2.65\right)^{25}} = 1 - \frac{0.28}{1 + \left(1.3/2.65\right)^{25}} = 0.72$$

$$\sigma'_p = \sigma'_y = 0.33(q_t - \sigma_{vo})^{m'} = 0.33(24139 \text{ kPa} - 34.5 \text{ kPa})^{0.72} = 471.7 \text{ kPa} = 68.4 \text{ psi}$$

$$\text{YSR} = \frac{\sigma'_p}{\sigma'_{vo}} = \frac{68.4 \text{ psi}}{5.0 \text{ psi}} = 13.6$$

Layer 2

$$m' = 1 - \frac{0.28}{1 + \left(I_c/2.65\right)^{25}} = 1 - \frac{0.28}{1 + \left(1.4/2.65\right)^{25}} = 0.72$$

$$\sigma'_p = \sigma'_y = 0.33(q_t - \sigma_{vo})^{m'} = 0.33(34132 \text{ kPa} - 68.9 \text{ kPa})^{0.72} = 605 \text{ kPa} = 87.7 \text{ psi}$$

$$\text{YSR} = \frac{\sigma'_p}{\sigma'_{vo}} = \frac{87.7 \text{ psi}}{10.0 \text{ psi}} = 8.7$$

Layer 3

$$m' = 1 - \frac{0.28}{1 + \left(I_c/2.65\right)^{25}} = 1 - \frac{0.28}{1 + \left(1.9/2.65\right)^{25}} = 0.72$$

$$\sigma'_p = \sigma'_y = 0.33(q_t - \sigma_{vo})^{m'} = 0.33(10342\ \text{kPa} - 131\ \text{kPa})^{0.72} = 254\ \text{kPa} = 36.8\ \text{psi}$$

$$YSR = \frac{\sigma'_p}{\sigma'_{vo}} = \frac{36.8\ \text{psi}}{16.4\ \text{psi}} = 2.2$$

Layer 4

$$m' = 1 - \frac{0.28}{1 + \left(I_c/2.65\right)^{25}} = 1 - \frac{0.28}{1 + \left(1.9/2.65\right)^{25}} = 0.72$$

$$\sigma'_p = \sigma'_y = 0.33(q_t - \sigma_{vo})^{m'} = 0.33(8274\ \text{kPa} - 168\ \text{kPa})^{0.72} = 215\ \text{kPa} = 31.2\ \text{psi}$$

$$YSR = \frac{\sigma'_p}{\sigma'_{vo}} = \frac{31.2\ \text{psi}}{18.8\ \text{psi}} = 1.7$$

Lateral Stress Coefficient

Layer 1

$$K_o = (1 - \sin(\emptyset')) \cdot YSR^{\sin(\emptyset')} = (1 - \sin(45.6°)) \cdot 13.6^{\sin(45.6°)} = 1.8$$

Layer 2

$$K_o = (1 - \sin(\emptyset')) \cdot YSR^{\sin(\emptyset')} = (1 - \sin(44.5°)) \cdot 8.7^{\sin(44.5°)} = 1.4$$

Layer 3

$$K_o = (1 - \sin(\emptyset')) \cdot YSR^{\sin(\emptyset')} = (1 - \sin(39.3°)) \cdot 2.2^{\sin(39.3°)} = 0.6$$

Layer 4

$$K_o = (1 - \sin(\emptyset')) \cdot YSR^{\sin(\emptyset')} = (1 - \sin(37.8°)) \cdot 1.7^{\sin(37.8°)} = 0.5$$

Ground Stiffness and Soil Moduli

Layer 1

$$D' \approx 5 \cdot (q_t - \sigma_{vo}) = 5 \cdot (3501 \text{ psi} - 5.0 \text{ psi}) = 17480 \text{ psi}$$

$$E' = \frac{D'}{1.1} = \frac{17480 \text{ psi}}{1.1} = 15890 \text{ psi}$$

$$K' = \frac{E'}{[3 \cdot (1 - 2v')]} = \frac{15890 \text{ psi}}{[3 \cdot (1 - 2(0.2))]} = 8828 \text{ psi}$$

$$M_R = (1.46 q_t^{0.53} + 13.55 f_s^{1.4} + 2.36)^{2.44}$$

Values of q_t and f_s need to be in MPa.

$$M_R = (1.46(24.1 \text{ MPa})^{0.53} + 13.55(0.12 \text{ MPa})^{1.4} + 2.36)^{2.44} = 341.6 \text{ MPa} = 49575 \text{ psi}$$

$$V_s \text{ (m/s)} = [10.1 \cdot \log(q_t) - 11.4]^{1.67} \cdot \left(100 \cdot \frac{f_s}{q_t}\right)^{0.3}$$

Values of q_t and f_s need to be in kPa.

$$V_s \text{ (m/s)} = [10.1 \cdot \log(24139 \text{ kPa}) - 11.4]^{1.67} \cdot \left(100 \cdot \frac{117.2 \text{ kPa}}{24139 \text{ kPa}}\right)^{0.3} = 274.5 \frac{\text{m}}{\text{s}}$$

$$V_s = 901.2 \text{ ft/s}$$

$$\rho_t = \frac{\gamma_t}{g_a} = \frac{120.4\ \text{pcf}}{32.2\ \text{ft/s}^2} = 3.7\ \frac{\text{slug}}{\text{ft}^3}$$

$$G_{max} = \rho_t \cdot V_s^2 = 3.7 \cdot \left(901.2\ \frac{\text{ft}}{\text{s}}\right)^2 = 3.04 \cdot 10^6 \text{psf} = 21000\ \text{psi}$$

Layer 2

$$D' \approx 5 \cdot (q_t - \sigma_{vo}) = 5 \cdot (3500\ \text{psi} - 10.0\ \text{psi}) = 17480\ \text{psi}$$

$$E' = \frac{D'}{1.1} = \frac{17480\ \text{psi}}{1.1} = 15890\ \text{psi}$$

$$K' = \frac{E'}{[3 \cdot (1 - 2v')]} = \frac{15890\ \text{psi}}{[3 \cdot (1 - 2(0.2))]} = 8828\ \text{psi}$$

$$M_R = (1.46 q_t^{0.53} + 13.55 f_s^{1.4} + 2.36)^{2.44}$$

Values of q_t and f_s need to be in MPa.

$$M_R = (1.46(24.1\ \text{MPa})^{0.53} + 13.55(0.12\ \text{MPa})^{1.4} + 2.36)^{2.44} = 341.5\ \text{MPa} = 49562\ \text{psi}$$

$$V_s\ (\text{m/s}) = [10.1 \cdot \log(q_t) - 11.4]^{1.67} \cdot \left(100 \cdot \frac{f_s}{q_t}\right)^{0.3}$$

Values of q_t and f_s need to be in kPa.

$$V_s\ (\text{m/s}) = [10.1 \cdot \log(24133\ \text{kPa}) - 11.4]^{1.67} \cdot \left(100 \cdot \frac{117.2\ \text{kPa}}{24133\ \text{kPa}}\right)^{0.3} = 274.5\ \frac{\text{m}}{\text{s}}$$

$$V_s = 901.2\ \text{ft/s}$$

$$\rho_t = \frac{\gamma_t}{g_a} = \frac{120.4\ \text{pcf}}{32.2\ \text{ft/s}^2} = 3.7\ \frac{\text{slug}}{\text{ft}^3}$$

$$G_{max} = \rho_t \cdot V_s^2 = 3.7 \cdot \left(901.2 \frac{ft}{s}\right)^2 = 3.04 \cdot 10^6 psf = \ 21000 psi$$

Layer 3

$$D' \approx 5 \cdot (q_t - \sigma_{vo}) = 5 \cdot (1500 \text{ psi} - 19.0 \text{ psi}) = 7405 \text{ psi}$$

$$E' = \frac{D'}{1.1} = \frac{7405 \text{ psi}}{1.1} = 6732 \text{ psi}$$

$$K' = \frac{E'}{[3 \cdot (1 - 2v')]} = \frac{6732 \text{ psi}}{[3 \cdot (1 - 2(0.2))]} = 3740 \text{ psi}$$

$$M_R = \ (1.46 q_t^{0.53} + 13.55 f_s^{1.4} + 2.36)^{2.44}$$

Values of q_t and f_s need to be in MPa.

$$M_R = \ (1.46(10.3 \text{ MPa})^{0.53} + 13.55(0.08 \text{ MPa})^{1.4} + 2.36)^{2.44} = 150.6 \text{ MPa} = 21854 \text{ psi}$$

$$V_s \text{ (m/s)} = \ [10.1 \cdot \log(q_t) - 11.4]^{1.67} \cdot \left(100 \cdot \frac{f_s}{q_t}\right)^{0.3}$$

Values of q_t and f_s need to be in kPa.

$$V_s \text{ (m/s)} = \ [10.1 \cdot \log(10343 \text{ kPa}) - 11.4]^{1.67} \cdot \left(100 \cdot \frac{82.7 \text{ kPa}}{10343 \text{ kPa}}\right)^{0.3} = 261.1 \frac{m}{s}$$

$$V_s = 856.6 \text{ ft/s}$$

$$\rho_t = \frac{\gamma_t}{g_a} = \frac{117.2 \text{ pcf}}{32.2 \text{ ft/s}^2} = 3.6 \frac{slug}{ft^3}$$

$$G_{max} = \rho_t \cdot V_s^2 = 3.6 \cdot \left(856.6 \frac{ft}{s}\right)^2 = 2.7 \cdot 10^6 psf = \ 19000 \text{ psi}$$

Layer 4

$$D' \approx 5 \cdot (q_t - \sigma_{vo}) = 5 \cdot (1200 \text{ psi} - 24.4 \text{ psi}) = 5878 \text{ psi}$$

$$E' = \frac{D'}{1.1} = \frac{5878\ \text{psi}}{1.1} = 5343\ \text{psi}$$

$$K' = \frac{E'}{[3 \cdot (1 - 2v')]} = \frac{5343\ \text{psi}}{[3 \cdot (1 - 2(0.2))]} = 2969\ \text{psi}$$

$$M_R = (1.46 q_t^{0.53} + 13.55 f_s^{1.4} + 2.36)^{2.44}$$

Values of q_t and f_s need to be in MPa.

$$M_R = (1.46(8.3\ \text{MPa})^{0.53} + 13.55(0.05\ \text{MPa})^{1.4} + 2.36)^{2.44} = 16.5\ \text{MPa} = 16901\ \text{psi}$$

$$V_s\ (\text{m/s}) = [10.1 \cdot \log(q_t) - 11.4]^{1.67} \cdot \left(100 \cdot \frac{f_s}{q_t}\right)^{0.3}$$

Values of q_t and f_s need to be in kPa.

$$V_s\ (\text{m/s}) = [10.1 \cdot \log(8274\ \text{kPa}) - 11.4]^{1.67} \cdot \left(100 \cdot \frac{48.3\ \text{kPa}}{8274\ \text{kPa}}\right)^{0.3} = 224.3\ \frac{\text{m}}{\text{s}}$$

$$V_s = 736.0\ \text{ft/s}$$

$$\rho_t = \frac{\gamma_t}{g_a} = \frac{112.1\ \text{pcf}}{32.2\ \text{ft/s}^2} = 3.5\ \frac{\text{slug}}{\text{ft}^3}$$

$$G_{max} = \rho_t \cdot V_s^2 = 3.5 \cdot \left(736.0\ \frac{\text{ft}}{\text{s}}\right)^2 = 3.89 \cdot 10^6 \text{psf} = 13000\ \text{psi}$$

2.12.2 Example 2: Direct CPT Methods for Geoparameters on Clay

Several geoparameters need to be determined based on the given CPT data collected for the South Abutment (Figure 15). The groundwater table (GWT) was measured at 60 feet. Determine all the geoparameters found in Table 5 at depths of 0 feet to 42 feet. All sand layers can be assumed “drained” $\nu = 0.2$. All clay layers can assume $\nu = 0.49$.

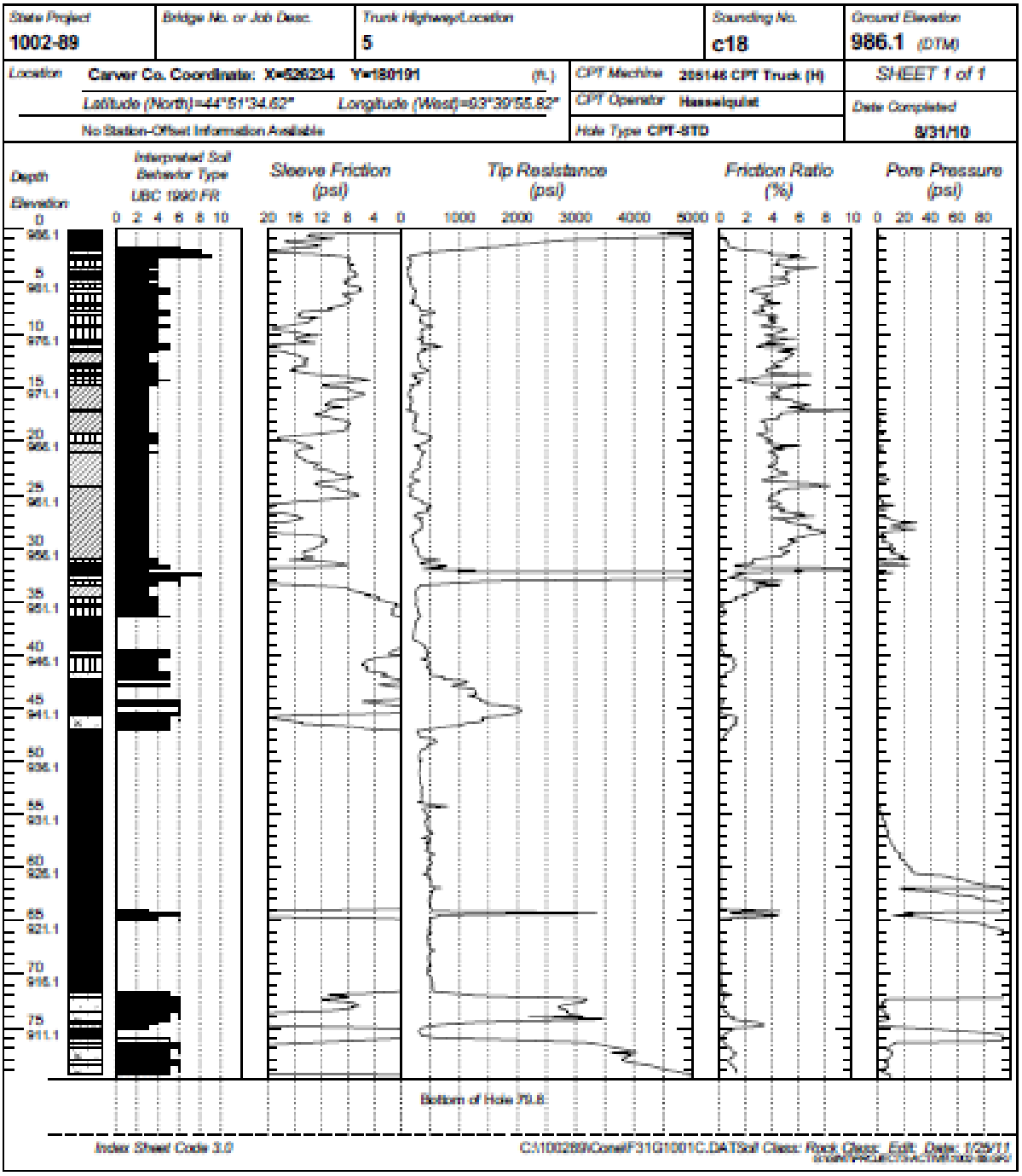

Figure 15. CPT data from Minnesota for example problem 2.

Table 5. Geoparameters

Symbol	Parameter	Symbol	Parameter
γ_t	Soil total unit weight	E'	Drained Young's modulus
I_c	CPT material index	K'	Bulk modulus
SBT	Soil behavior type (SBT)	M_R	Resilient modulus
σ_p'	Preconsolidation stress	G_{max}	Small-strain shear modulus
YSR	Yield stress ratio	s_u	Undrained shear strength
ϕ'	Effective friction angle	c_v	Coefficient of consolidation
K_o	Lateral stress coefficient	k	Hydraulic conductivity
D'	Constrained modulus		

Solution

Soil total unit weight

Estimate soil layering using "rules of thumb."

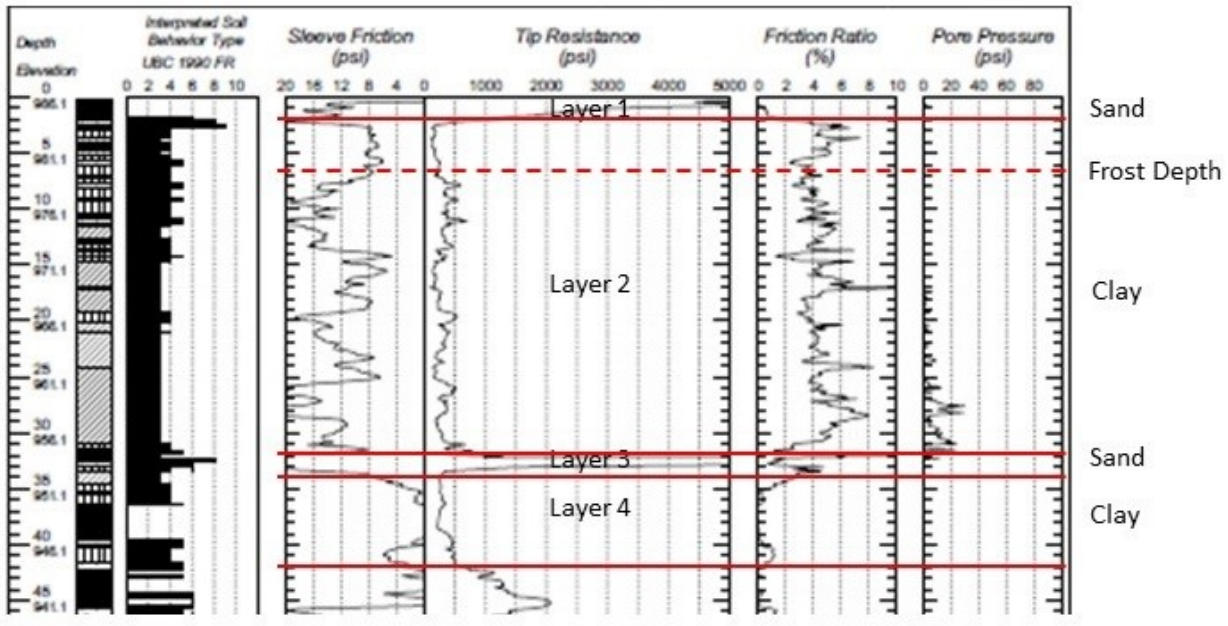

Figure 16. Soil layers using "rules of thumb."

Unit weight of water: $\gamma_w = 62.24$ pcf

Layer 1

From Figure 16: $f_s = 13$ psi taken as a representative value of the layer

$$\gamma_t = 62.4 \text{ pcf} \cdot \left[1.22 + 0.15 \cdot \ln\left(100 \cdot \frac{13 \text{ psi}}{14.5 \text{ psi}} + 0.01\right)\right] = 117.9 \text{ pcf}$$

Layer 2

From Figure 16: $f_s = 12$ psi taken as a representative value of the layer

$$\gamma_t = 62.4 \text{ pcf} \cdot \left[1.22 + 0.15 \cdot \ln\left(100 \cdot \frac{12 \text{ psi}}{14.5 \text{ psi}} + 0.01\right)\right] = 117.2 \text{ pcf}$$

Layer 3

From Figure 16: $f_s = 20$ psi taken as a representative value of the layer

$$\gamma_t = 62.4\ \text{pcf} \cdot \left[1.22 + 0.15 \cdot \ln\left(100 \cdot \frac{20\ \text{psi}}{14.5\ \text{psi}} + 0.01\right)\right] = 121.9\ \text{pcf}$$

Layer 4

From Figure 16: f_s = 2 psi taken as a representative value of the layer

$$\gamma_t = 62.4\ \text{pcf} \cdot \left[1.22 + 0.15 \cdot \ln\left(100 \cdot \frac{2\ \text{psi}}{14.5\ \text{psi}} + 0.01\right)\right] = 100.4\ \text{pcf}$$

CPT Material Index

Layer 1

From Figure 10: f_s = 13 psi and q_c = 3000 psi

$$q_t = q_c + u_2 \cdot (1 - a) = 3000\ \text{psi} + 0\ \text{psi} \cdot (1 - 0.8) = 3000\ \text{psi}$$

$$\sigma_{vo} = \gamma_t \cdot 2\ \text{feet} = 117.9\ \text{pcf} \cdot 2\ \text{feet} = 235\ \text{psf} = 1.6\ \text{psi}$$

$$F_r(\%) = 100 \cdot \frac{f_s}{(q_t - \sigma_{vo})} = 100 \cdot \frac{13\ \text{psi}}{(3000\ \text{psi} - 1.6\ \text{psi})} = 0.43$$

Step 2. Iterate to solve for I_c. Steps are not shown for brevity.

$$u_o = 0\ \text{psi}$$

$$\sigma'_{vo} = \sigma_{vo} - u_o = 1.6\ \text{psi} - 0\ \text{psi} = 1.6\ \text{psi}$$

$$Q_{tn} = \frac{(q_t - \sigma_{vo})/\sigma_{atm}}{(\sigma'_{vo}/\sigma_{atm})^n} = \frac{(3000\ \text{psi} - 1.6\ \text{psi})/14.5\ \text{psi}}{(1.6\ \text{psi}/14.5\ \text{psi})^n}$$

$$n = 0.381 \cdot I_c + 0.05\left(\frac{\sigma'_{vo}}{\sigma_{atm}}\right) - 0.15 = 0.381 \cdot I_c + 0.05\left(\frac{1.6\ \text{psi}}{14.5\ \text{psi}}\right) - 0.15$$

$$I_c = \sqrt{[3.47 - \log(Q_{tn})]^2 + [1.22 + \log(0.43)]^2}$$

$$Q_{tn} = 412.6 \qquad n = 0.32 < 1.0 \qquad I_c = 1.21 \qquad \text{therefore sand}$$

Layer 2

From Figure 10: f_s = 12 psi and q_c = 250 psi

$$q_t = q_c + u_2 \cdot (1 - a) = 250 \text{ psi} + 10 \text{ psi} \cdot (1 - 0.8) = 252 \text{ psi}$$

$$\sigma_{vo} = 235 \text{ psf} + \gamma_t \cdot 30 \text{ feet} = 235 \text{ psf} + 117.2 \text{ pcf} \cdot 30 \text{ feet} = 3751 \text{ psf} = 26.0 \text{ psi}$$

$$F_r(\%) = 100 \cdot \frac{f_s}{(q_t - \sigma_{vo})} = 100 \cdot \frac{12 \text{ psi}}{(252 \text{ psi} - 26.0 \text{ psi})} = 5.3$$

Step 2. Iterate to solve for I_c. Steps are not shown for brevity.

$$u_o = 0 \text{ psi}$$

$$\sigma'_{vo} = \sigma_{vo} - u_o = 26.0 \text{ psi} - 0 \text{ psi} = 26.0 \text{ psi}$$

$$Q_{tn} = \frac{(q_t - \sigma_{vo})/\sigma_{atm}}{(\sigma'_{vo}/\sigma_{atm})^n} = \frac{(250 \text{ psi} - 26.0 \text{ psi})/14.5 \text{ psi}}{(26.0 \text{ psi}/14.5 \text{ psi})^n}$$

$$n = 0.381 \cdot I_c + 0.05\left(\frac{\sigma'_{vo}}{\sigma_{atm}}\right) - 0.15 = 0.381 \cdot I_c + 0.05\left(\frac{26.0 \text{ psi}}{14.5 \text{ psi}}\right) - 0.15$$

$$I_c = \sqrt{[3.47 - \log(Q_{tn})]^2 + [1.22 + \log(5.3)]^2}$$

$$Q_{tn} = 8.7 \qquad n = 1.0 \leq 1.0 \qquad I_c = 3.2 \quad \text{therefore clay}$$

Layer 3

From Figure 10: f_s = 20 psi and q_c = 4000 psi

$$q_t = q_c + u_2 \cdot (1 - a) = 4000 \text{ psi} + 8 \text{ psi} \cdot (1 - 0.8) = 4001.6 \text{ psi}$$

$$\sigma_{vo} = 3751 \text{ psf} + \gamma_t \cdot 2 \text{ feet} = 3751 \text{ psf} + 121.9 \text{ pcf} \cdot 2 \text{ feet} = 3995 \text{ psf} = 27.7 \text{ psi}$$

$$F_r(\%) = 100 \cdot \frac{f_s}{(q_t - \sigma_{vo})} = 100 \cdot \frac{16 \text{ psi}}{(3001.6 \text{ psi} - 27.7 \text{ psi})} = 0.54$$

Step 2. Iterate to solve for I_c. Steps are not shown for brevity.

$$u_o = 0 \text{ psi}$$

$$\sigma'_{vo} = \sigma_{vo} - u_o = 27.7 \text{ psi} - 0 \text{ psi} = 27.7 \text{ psi}$$

$$Q_{tn} = \frac{(q_t - \sigma_{vo})/\sigma_{atm}}{(\sigma'_{vo}/\sigma_{atm})^n} = \frac{(3001.6 - 27.7)/14.5 \text{ psi}}{(27.7 \text{ psi}/14.5 \text{ psi})^n}$$

$$n = 0.381 \cdot I_c + 0.05\left(\frac{\sigma'_{vo}}{\sigma_{atm}}\right) - 0.15 = 0.381 \cdot I_c + 0.05\left(\frac{27.7 \text{ psi}}{14.5 \text{ psi}}\right) - 0.15$$

$$I_c = \sqrt{[3.47 - \log(Q_{tn})]^2 + [1.22 + \log(0.54)]^2}$$

$$Q_{tn} = 196.2 \qquad n = 0.52 \leq 1.0 \qquad I_c = 1.5 \text{ therefore sand}$$

Layer 4

From Figure 10: f_s = 2 psi and q_c = 250 psi

$$q_t = q_c + u_2 \cdot (1 - a) = 250 \text{ psi} + 0 \text{ psi} \cdot (1 - 0.8) = 250 \text{ psi}$$

$$\sigma_{vo} = 3994 \text{ psf} + \gamma_t \cdot 8 \text{ feet} = 3994 \text{ psf} + 100.4 \text{ pcf} \cdot 8 \text{ feet} = 4798 \text{ psf} = 33.3 \text{ psi}$$

$$F_r(\%) = 100 \cdot \frac{f_s}{(q_t - \sigma_{vo})} = 100 \cdot \frac{2 \text{ psi}}{(250 \text{ psi} - 33.3 \text{ psi})} = 0.92$$

Step 2. Iterate to solve for I_c. Steps are not shown for brevity.

$$u_o = 0 \text{ psi}$$

$$\sigma'_{vo} = \sigma_{vo} - u_o = 33.3 \text{ psi} - 0 \text{ psi} = 33.3 \text{ psi}$$

$$Q_{tn} = \frac{(q_t - \sigma_{vo})/\sigma_{atm}}{(\sigma'_{vo}/\sigma_{atm})^n} = \frac{(250 \text{ psi} - 33.3 \text{ psi})/14.5 \text{ psi}}{(33.3 \text{ psi}/14.5 \text{ psi})^n}$$

$$n = 0.381 \cdot I_c + 0.05\left(\frac{\sigma'_{vo}}{\sigma_{atm}}\right) - 0.15 = 0.381 \cdot I_c + 0.05\left(\frac{33.3\ \text{psi}}{14.5\ \text{psi}}\right) - 0.15$$

$$I_c = \sqrt{[3.47 - \log(Q_{tn})]^2 + [1.22 + \log(0.92)]^2}$$

$$Q_{tn} = 6.5 \qquad n = 1.0 < 1.0 \qquad I_c = 2.9$$ therefore clayey silt

Soil Behavior Type (SBT)

Layer 1

Based on values of I_c, Q_{tn}, and F_r, the first layer is defined as a "Drained Sand" from Figure 17.

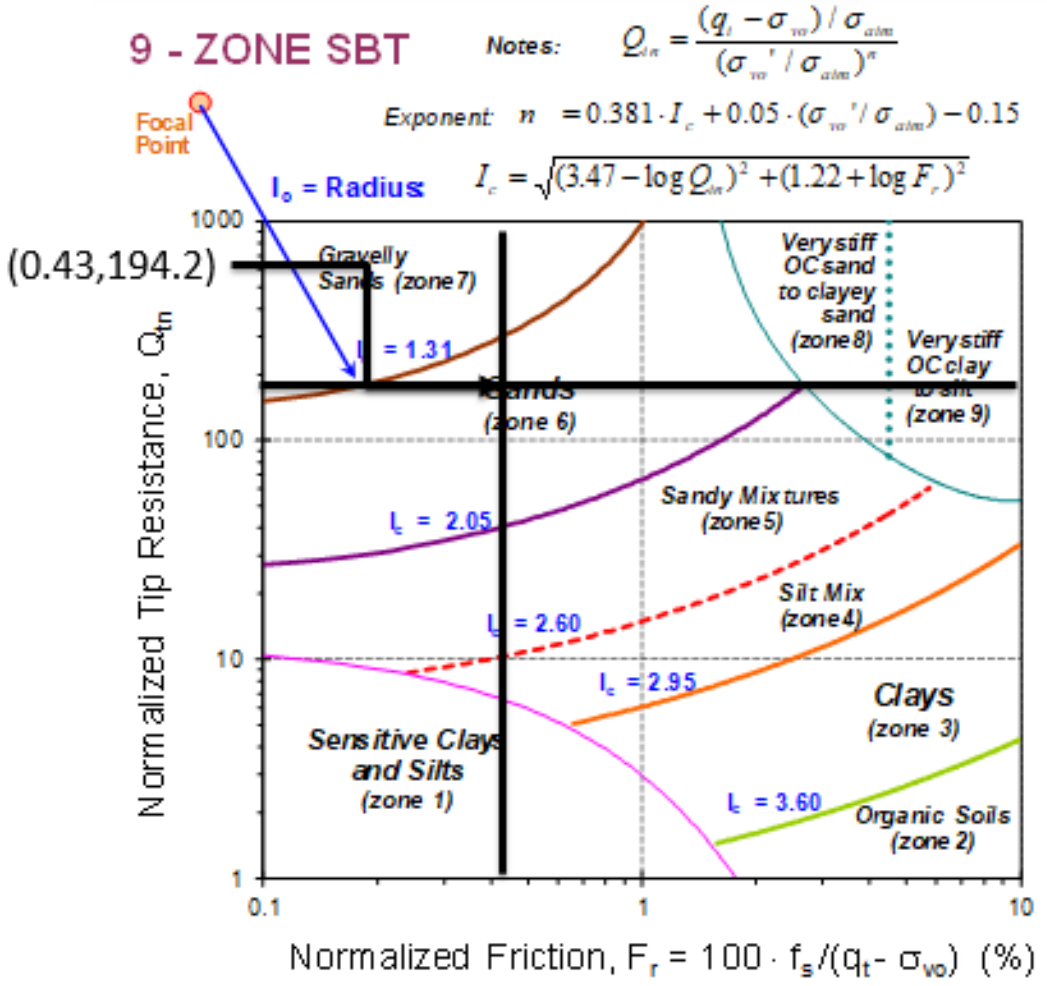

Figure 17. Soil layer 1 using SBT method.

Layer 2

Based on values of I_c, Q_{tn}, and F_r, the second layer is defined as a "Undrained Clay" from Figure 18.

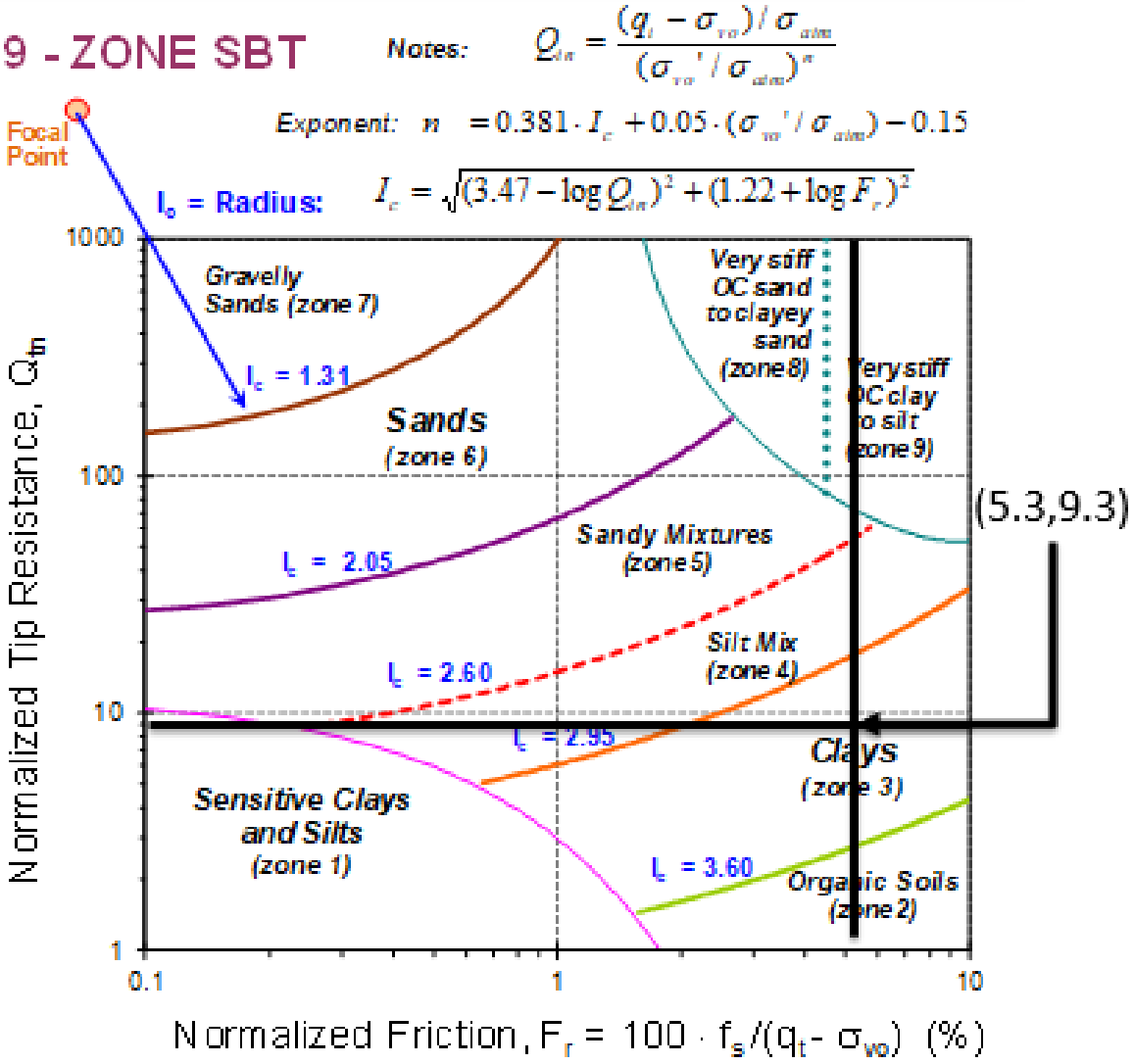

Figure 18. Soil layer 2 using SBT method.

Layer 3

Based on values of I_c, Q_{tn}, and F_r, the third layer is defined as a "Drained Sand" from Figure 19.

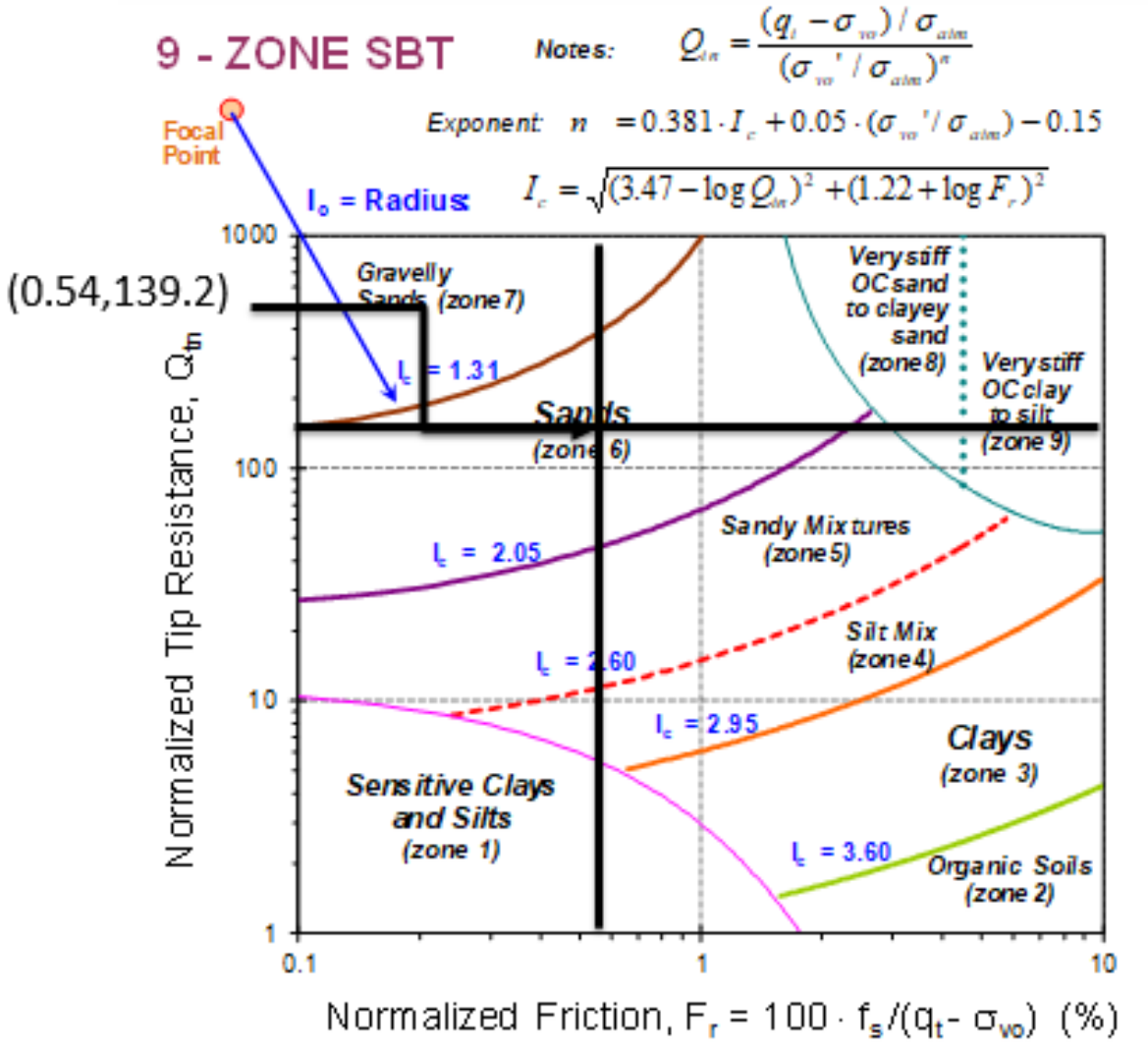

Figure 19. Soil layer 3 using SBT method.

Layer 4

Based on values of I_c, Q_{tn}, and F_r, the fourth layer is defined as a "Undrained Silty Mix" from Figure 20.

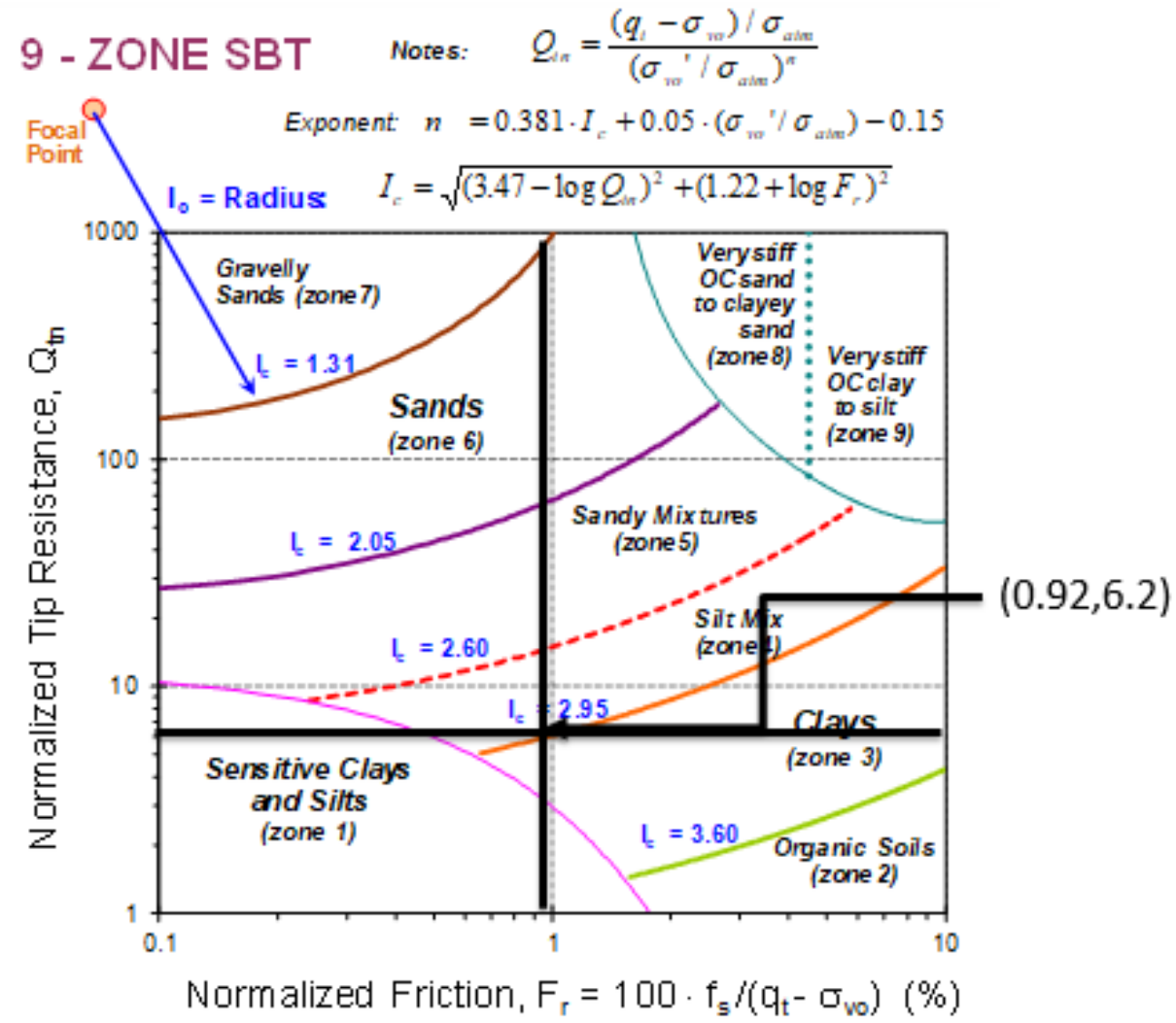

Figure 20. Soil layer 4 using SBT method.

Effective Stress Friction Angle

Layer 1 (sand)

$$\phi'(\text{deg}) = 17.6° + 11.0° \log(Q_{tn}) = 17.6° + 11.0° \log(412.6) = 46.4°$$

Layer 2 (clay)

$$\phi'(\text{deg}) = 29.5° \cdot \ B_q^{0.121} \cdot \left[0.256 + 0.336 \cdot B_q + \log\left(\frac{q_t - \sigma_{vo}}{\sigma'_{vo}}\right)\right]$$

Where:

$$B_q = \frac{(u_2 - u_o)}{(q_t - \sigma_{vo})} = \frac{(10 \text{ psi} - 0 \text{ psi})}{(252 \text{ psi} - 26.0 \text{ psi})} = 0.04$$

$$\phi'(\text{deg}) = 29.5° \cdot \ 0.044^{0.121} \cdot \left[0.256 + 0.336 \cdot 0.044 + \log\left(\frac{252 \text{ psi} - 26.0 \text{ psi}}{26.0 \text{ psi}}\right)\right]$$

$$\phi'(\text{deg}) = 24.5°$$

Layer 3 (sand)

$$\phi'(\text{deg}) = 17.6° + 11.0° \log(Q_{tn}) = 17.6° + 11.0° \log(196.2) = 42.8°$$

Layer 4 (clay)

$$\phi'(\text{deg}) = 29.5° \cdot \ B_q^{0.121} \cdot \left[0.256 + 0.336 \cdot B_q + \log\left(\frac{q_t - \sigma_{vo}}{\sigma'_{vo}}\right)\right]$$

Where:

$$B_q = \frac{(u_2 - u_o)}{(q_t - \sigma_{vo})} = \frac{(5 \text{ psi} - 0 \text{ psi})}{(251 \text{ psi} - 33.3 \text{ psi})} = 0.02$$

$$\phi'(\text{deg}) = 29.5° \cdot \ 0.02^{0.121} \cdot \left[0.256 + 0.336 \cdot 0.02 + \log\left(\frac{252 \text{ psi} - 33.3 \text{ psi}}{33.3 \text{ psi}}\right)\right]$$

$$\phi'(\text{deg}) = 26.5°$$

Stress History

Layer 1

$$m' = 1 - \frac{0.28}{1 + \left(I_c/2.65\right)^{25}} = 1 - \frac{0.28}{1 + \left(1.2/2.65\right)^{25}} = 0.72$$

$$\sigma'_p = \sigma'_y = 0.33(q_t - \sigma_{vo})^{m'} = 0.33(3000\ \text{psi} - 3.3)^{0.72} = 105.1\ \text{psi}$$

$$\text{YSR} = \frac{\sigma'_p}{\sigma'_{vo}} = \frac{105.1\ \text{psi}}{1.6\ \text{psi}} = 64.2$$

Layer 2

$$m' = 1 - \frac{0.28}{1 + \left(I_c/2.65\right)^{25}} = 1 - \frac{0.28}{1 + \left(3.2/2.65\right)^{25}} = 0.99$$

$$\sigma'_p = \sigma'_y = 0.33(q_t - \sigma_{vo})^{m'} = 0.33(252\ \text{psi} - 26.0)^{0.99} = 73.4\ \text{psi}$$

$$\text{YSR} = \frac{\sigma'_p}{\sigma'_{vo}} = \frac{73.4\ \text{psi}}{26.0\ \text{psi}} = 2.8$$

Layer 3

$$m' = 1 - \frac{0.28}{1 + \left(I_c/2.65\right)^{25}} = 1 - \frac{0.28}{1 + \left(1.5/2.65\right)^{25}} = 0.72$$

$$\sigma'_p = \sigma'_y = 0.33(q_t - \sigma_{vo})^{m'} = 0.33(4002\ \text{psi} - 27.7)^{0.72} = 128.8\ \text{psi}$$

$$YSR = \frac{\sigma'_p}{\sigma'_{vo}} = \frac{128.8\ psi}{27.7\ psi} = 4.6$$

Layer 4

$$m' = 1 - \frac{0.28}{1 + \left(I_c/2.65\right)^{25}} = 1 - \frac{0.28}{1 + \left(2.9/2.65\right)^{25}} = 0.97$$

$$\sigma'_p = \sigma'_y = 0.33(q_t - \sigma_{vo})^{m'} = 0.33(250\ psi - 33.3)^{0.97} = 62.6\ psi$$

$$YSR = \frac{\sigma'_p}{\sigma'_{vo}} = \frac{62.6\ psi}{33.3\ psi} = 1.9$$

Lateral Stress Coefficient

Layer 1

$$K_o = (1 - \sin(\emptyset')) \cdot YSR^{\sin(\emptyset')} = (1 - \sin(46.4°)) \cdot 64.2^{\sin(46.4°)} = 5.6$$

Layer 2

$$K_o = (1 - \sin(\emptyset')) \cdot YSR^{\sin(\emptyset')} = (1 - \sin(24.5°)) \cdot 2.8^{\sin(24.5°)} = 0.90$$

Layer 3

$$K_o = (1 - \sin(\emptyset')) \cdot YSR^{\sin(\emptyset')} = (1 - \sin(42.8°)) \cdot 4.6^{\sin(42.8°)} = 0.91$$

Layer 4

$$K_o = (1 - \sin(\emptyset')) \cdot YSR^{\sin(\emptyset')} = (1 - \sin(26.6°)) \cdot 1.9^{\sin(26.6°)} = 0.73$$

Ground Stiffness and Soil Moduli

Layer 1

$$D' \approx 5 \cdot (q_t - \sigma_{vo}) = 5 \cdot (3000 \text{ psi} - 1.6 \text{ psi}) = 14991 \text{ psi}$$

$$E' = \frac{D'}{1.1} = \frac{14991 \text{ psi}}{1.1} = 13629 \text{ psi}$$

$$K' = \frac{E'}{[3 \cdot (1 - 2v')]} = \frac{13629 \text{ psi}}{[3 \cdot (1 - 2(0.2))]} = 7571 \text{ psi}$$

$$M_R = (1.46 q_t^{0.53} + 13.55 f_s^{1.4} + 2.36)^{2.44}$$

Values of q_t and f_s need to be in MPa.

$$M_R = (1.46(20.7 \text{ MPa})^{0.53} + 13.55(0.09 \text{ MPa})^{1.4} + 2.36)^{2.44} = 281.6 \text{ MPa} = 40873 \text{ psi}$$

$$V_s \text{ (m/s)} = [10.1 \cdot \log(q_t) - 11.4]^{1.67} \cdot \left(100 \cdot \frac{f_s}{q_t}\right)^{0.3}$$

Values of q_t and f_s need to be in kPa.

$$V_s \text{ (m/s)} = [10.1 \cdot \log(20685 \text{ kPa}) - 11.4]^{1.67} \cdot \left(100 \cdot \frac{89.6 \text{ kPa}}{20685 \text{ kPa}}\right)^{0.3} = 256.4 \frac{\text{m}}{\text{s}}$$

$$V_s = 841.2 \text{ ft/s}$$

$$\rho_t = \frac{\gamma_t}{g_a} = \frac{117.9 \text{ pcf}}{32.2 \text{ ft/s}^2} = 3.7 \frac{\text{slug}}{\text{ft}^3}$$

$$G_{max} = \rho_t \cdot V_s^2 = 3.7 \cdot \left(841.2 \frac{\text{ft}}{\text{s}}\right)^2 = 2.60 \cdot 10^6 \text{psf} = 17992 \text{ psi}$$

Layer 2

$$D' \approx 5 \cdot (q_t - \sigma_{vo}) = 5 \cdot (252 \text{ psi} - 26.0 \text{ psi}) = 1129.8 \text{ psi}$$

$$E' = \frac{D'}{1.1} = \frac{1129.8 \text{ psi}}{1.1} = 1027.1 \text{ psi}$$

$$K' = \frac{E'}{[3 \cdot (1 - 2\nu')]} = \frac{1027.1 \text{ psi}}{[3 \cdot (1 - 2(0.49))]} = 17118 \text{ psi}$$

$$M_R = (1.46 q_t^{0.53} + 13.55 f_s^{1.4} + 2.36)^{2.44}$$

Values of q_t and f_s need to be in MPa.

$$M_R = (1.46(1.7 \text{ MPa})^{0.53} + 13.55(0.08 \text{ MPa})^{1.4} + 2.36)^{2.44} = 44.3 \text{ MPa} = 6430.9 \text{ psi}$$

$$V_s \text{ (m/s)} = [10.1 \cdot \log(q_t) - 11.4]^{1.67} \cdot \left(100 \cdot \frac{f_s}{q_t}\right)^{0.3}$$

Values of q_t and f_s need to be in kPa.

$$V_s \text{ (m/s)} = [10.1 \cdot \log(1737.5 \text{ kPa}) - 11.4]^{1.67} \cdot \left(100 \cdot \frac{82.7 \text{ kPa}}{1737.5 \text{ kPa}}\right)^{0.3} = 264.6 \frac{\text{m}}{\text{s}}$$

$$V_s = 868.0 \text{ ft/s}$$

$$\rho_t = \frac{\gamma_t}{g_a} = \frac{117.2 \text{ pcf}}{32.2 \text{ ft/s}^2} = 3.6 \frac{\text{slug}}{\text{ft}^3}$$

$$G_{max} = \rho_t \cdot V_s^2 = 3.6 \cdot \left(868.0 \frac{\text{ft}}{\text{s}}\right)^2 = 2.74 \cdot 10^6 \text{psf} = 19036 \text{ psi}$$

Layer 3

$$D' \approx 5 \cdot (q_t - \sigma_{vo}) = 5 \cdot (4002 \text{ psi} - 27.7 \text{ psi}) = 19869 \text{ psi}$$

$$E' = \frac{D'}{1.1} = \frac{19869 \text{ psi}}{1.1} = 18063 \text{ psi}$$

$$K' = \frac{E'}{[3 \cdot (1 - 2v')]} = \frac{18063 \text{ psi}}{[3 \cdot (1 - 2(0.2))]} = 10035 \text{ psi}$$

$$M_R = (1.46q_t^{0.53} + 13.55f_s^{1.4} + 2.36)^{2.44}$$

Values of q_t and f_s need to be in MPa.

$$M_R = (1.46(27.6 \text{ MPa})^{0.53} + 13.55(0.14 \text{ MPa})^{1.4} + 2.36)^{2.44} = 401.7 \text{ MPa} = 58309 \text{ psi}$$

$$V_s \text{ (m/s)} = [10.1 \cdot \log(q_t) - 11.4]^{1.67} \cdot \left(100 \cdot \frac{f_s}{q_t}\right)^{0.3}$$

Values of q_t and f_s need to be in kPa.

$$V_s \text{ (m/s)} = [10.1 \cdot \log(27591 \text{ kPa}) - 137.9]^{1.67} \cdot \left(100 \cdot \frac{137.9 \text{ kPa}}{27591 \text{ kPa}}\right)^{0.3} = 285.4 \frac{\text{m}}{\text{s}}$$

$$V_s = 936.3 \text{ ft/s}$$

$$\rho_t = \frac{\gamma_t}{g_a} = \frac{121 \text{ pcf}}{32.2 \text{ ft/s}^2} = 3.8 \frac{\text{slug}}{\text{ft}^3}$$

$$G_{max} = \rho_t \cdot V_s^2 = 3.8 \cdot \left(936.3 \frac{\text{ft}}{\text{s}}\right)^2 = 3.3 \cdot 10^6 \text{psf} = 23050 \text{ psi}$$

Layer 4

$$D' \approx 5 \cdot (q_t - \sigma_{vo}) = 5 \cdot (250 \text{ psi} - 33.3 \text{ psi}) = 1088 \text{ psi}$$

$$E' = \frac{D'}{1.1} = \frac{1088 \text{ psi}}{1.1} = 989 \text{ psi}$$

$$K' = \frac{E'}{[3 \cdot (1 - 2v')]} = \frac{989 \text{ psi}}{[3 \cdot (1 - 2(0.49))]} = 16490 \text{ psi}$$

$$M_R = (1.46q_t^{0.53} + 13.55f_s^{1.4} + 2.36)^{2.44}$$

Values of q_t and f_s need to be in MPa.

$$M_R = (1.46(1.7\ \text{MPa})^{0.53} + 13.55(0.01\ \text{MPa})^{1.4} + 2.36)^{2.44} = 36.0\ \text{MPa} = 5218.9\ \text{psi}$$

$$V_s\ (\text{m/s}) = [10.1 \cdot \log(q_t) - 11.4]^{1.67} \cdot \left(100 \cdot \frac{f_s}{q_t}\right)^{0.3}$$

Values of q_t and f_s need to be in kPa.

$$V_s\ (\text{m/s}) = [10.1 \cdot \log(1723.8\ \text{kPa}) - 11.4]^{1.67} \cdot \left(100 \cdot \frac{13.8\ \text{kPa}}{1723.8\ \text{kPa}}\right)^{0.3} = 154.5\ \frac{\text{m}}{\text{s}}$$

$$V_s = 506.9\ \text{ft/s}$$

$$\rho_t = \frac{\gamma_t}{g_a} = \frac{100.4\ \text{pcf}}{32.2\ \text{ft/s}^2} = 3.1\ \frac{\text{slug}}{\text{ft}^3}$$

$$G_{max} = \rho_t \cdot V_s^2 = 3.1 \cdot \left(506.9\ \frac{\text{ft}}{\text{s}}\right)^2 = 8.0 \cdot 10^5 \text{psf} = 5565\ \text{psi}$$

Undrained Shear Strength

Layer 2

$$s_u = \frac{q_t - \sigma_{v0}}{12} = \frac{250\ \text{psi} - 26\ \text{psi}}{12} = 18.7\ \text{psi}$$

Layer 4

$$s_u = \frac{q_t - \sigma_{v0}}{12} = \frac{250\ \text{psi} - 33.3\ \text{psi}}{12} = 18.1\ \text{psi}$$

Coefficient of Consolidation

Example dissipation data are shown in Figure 21. Example calculations are provided.

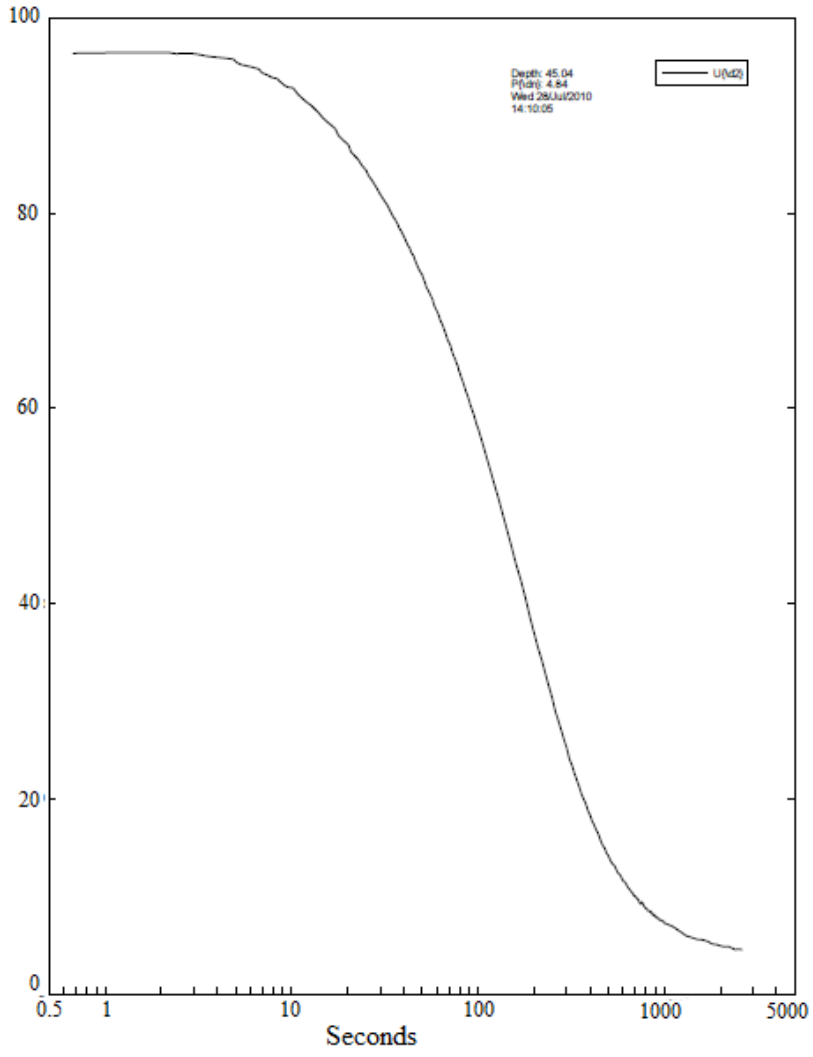

Figure 21. Dissipation, t50 data.

Layer 1

$$c_v = \frac{0.030 \cdot (a_c)^2 \cdot (I_R)^{0.75}}{t_{50}} = \frac{0.030 \cdot (2.20\ \text{cm})^2 \cdot (71.97)^{0.75}}{1\ \text{sec}} = 3.59\ \text{cm/sec}$$

Layer 2

$$c_v = \frac{0.030 \cdot (a_c)^2 \cdot (I_R)^{0.75}}{t_{50}} = \frac{0.030 \cdot (2.20\ \text{cm})^2 \cdot (943.92)^{0.75}}{3000\ \text{sec}} = 0.008\ \text{cm/sec}$$

Layer 3

$$c_v = \frac{0.030 \cdot (a_c)^2 \cdot (I_R)^{0.75}}{t_{50}} = \frac{0.030 \cdot (2.20\ \text{cm})^2 \cdot (83.03)^{0.75}}{0.6\ \text{sec}} = 6.65\ \text{cm/sec}$$

Layer 4

$$c_v = \frac{0.030 \cdot (a_c)^2 \cdot (I_R)^{0.75}}{t_{50}} = \frac{0.030 \cdot (2.20\ \text{cm})^2 \cdot (267.14)^{0.75}}{11\ \text{sec}} = 0.87\ \text{cm/sec}$$

Hydraulic Conductivity

Layer 1

$$k = \frac{c_v \cdot \gamma_w}{D'} = \frac{3.59\frac{\text{cm}}{\text{sec}} \cdot 62.24\ \text{pcf} \cdot \frac{1\ \text{psi}}{144\ \text{pcf}}}{14984\ \text{psi}} = 1.0 \cdot 10^{-4}\ \text{cm/sec}$$

Layer 2

$$k = \frac{c_v \cdot \gamma_w}{D'} = \frac{0.008\frac{\text{cm}}{\text{sec}} \cdot 62.24\ \text{pcf} \cdot \frac{1\ \text{psi}}{144\ \text{pcf}}}{1137.9\ \text{psi}} = 7.3 \cdot 10^{-7}\ \text{cm/sec}$$

Layer 3

$$k = \frac{c_v \cdot \gamma_w}{D'} = \frac{6.65\frac{\text{cm}}{\text{sec}} \cdot 62.24\ \text{pcf} \cdot \frac{1\ \text{psi}}{144\ \text{pcf}}}{14865.0\ \text{psi}} = 2.0 \cdot 10^{-5}\ \text{cm/sec}$$

Layer 4

$$k = \frac{c_v \cdot \gamma_w}{D'} = \frac{0.87\,\frac{cm}{sec} \cdot 62.24\ pcf \cdot \frac{1\ psi}{144\ pcf}}{1086.1\ psi} = 1.8 \cdot 10^{-4}\ cm/sec$$

CHAPTER 3: DIRECT CPT METHOD FOR SHALLOW FOUNDATIONS

3.1 PROCEDURE

Shallow foundation analysis is typically done in a two-part traditional procedure. The traditional techniques are no longer required as a direct CPT method for square, rectangular and circular shallow footings is available (Figure 22). This process has the soil types grouped into four main categories: sands, silts, fissured clays, and intact clays. When determining soil types for each design it is believed footings on sands and silts act in a fully drained manner, while intact clays act in an undrained manner under conditions of constant volume. In order to determine the vertical stress-displacement-capacity of square, rectangular and circular shallow footings, follow the steps provided towards the solution given by Equation 27.

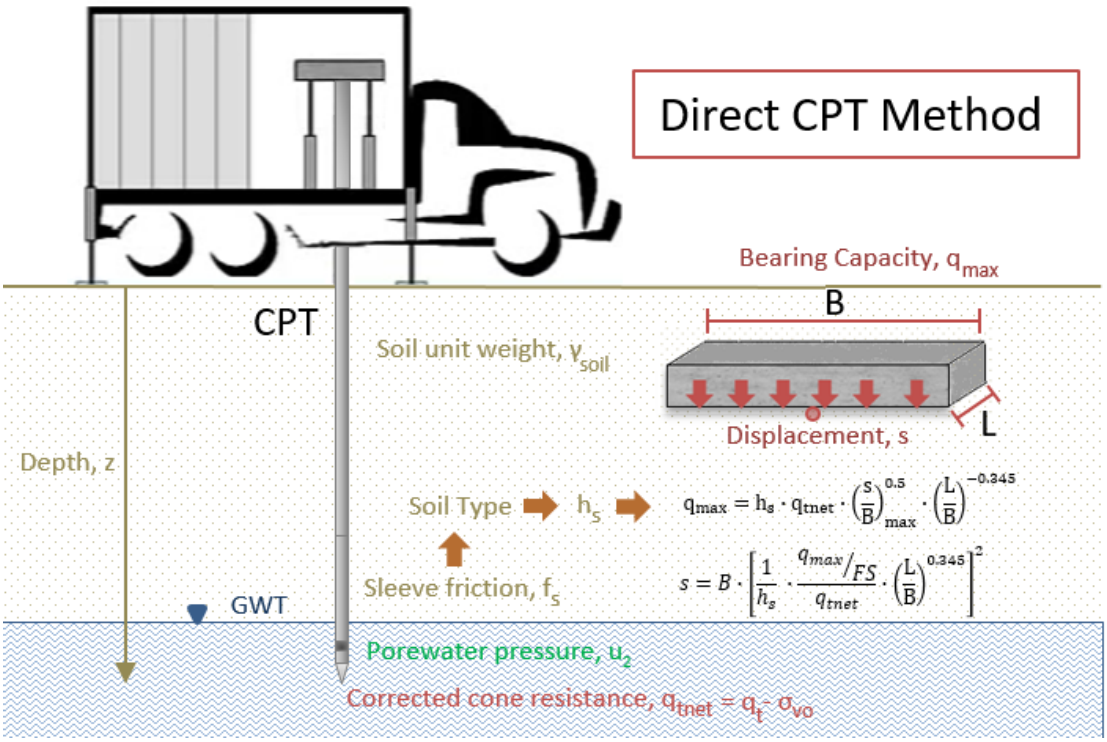

Figure 22. Direct CPT method for shallow foundations.

Equation 27 may be used to calculate all footing stresses from zero to the bearing capacity (q_{max}). To calculate q_{max} for a sized footing of width (B), length (L) and thickness (t), follow steps 1 through 7 provided. The settlement (s) can be determined after the calculation of q_{max} by simply rearranging

Equation 27, where the allowable stress (q_{allow}) is defined as q_{max} divided by the factor of safety (FS). For shallow footings, a FS value of 3 is commonly used in geotechnical engineering.

$$\boldsymbol{q_{max} = h_s \cdot q_{tnet} \cdot \left(\frac{s}{B}\right)^{0.5}_{max} \cdot \left(\frac{L}{B}\right)^{-0.345}} \quad \textbf{27}$$

$$s = B \cdot \left[\frac{1}{h_s} \cdot \frac{q_{max}/_{FS}}{q_{tnet}} \cdot \left(\frac{L}{B}\right)^{0.345}\right]^2 \quad 28$$

Where:

h_s = the foundation soil formation parameter
q_{tnet} = the net corrected cone tip resistance

3.1.1 Step 1. Estimating Footing Dimensions

In Minnesota, frost heave can have devastating effect on a shallow foundations. It is common practice to place a foundation bearing elevation below the expected maximum frost depth (roughly 4.5 to 6 feet below ground level). With this assumption, estimate a footing size (B x L) for design to obtain representative data from CPT roughly 1.5·B below the foundation depth (D_f) as shown in Figure 23. The CPT data collected will consist of:

- cone tip resistance (q_c)
- measured porewater pressure acting behind the cone tip (u_2), as shown in Figure 24
- sleeve friction (f_s)

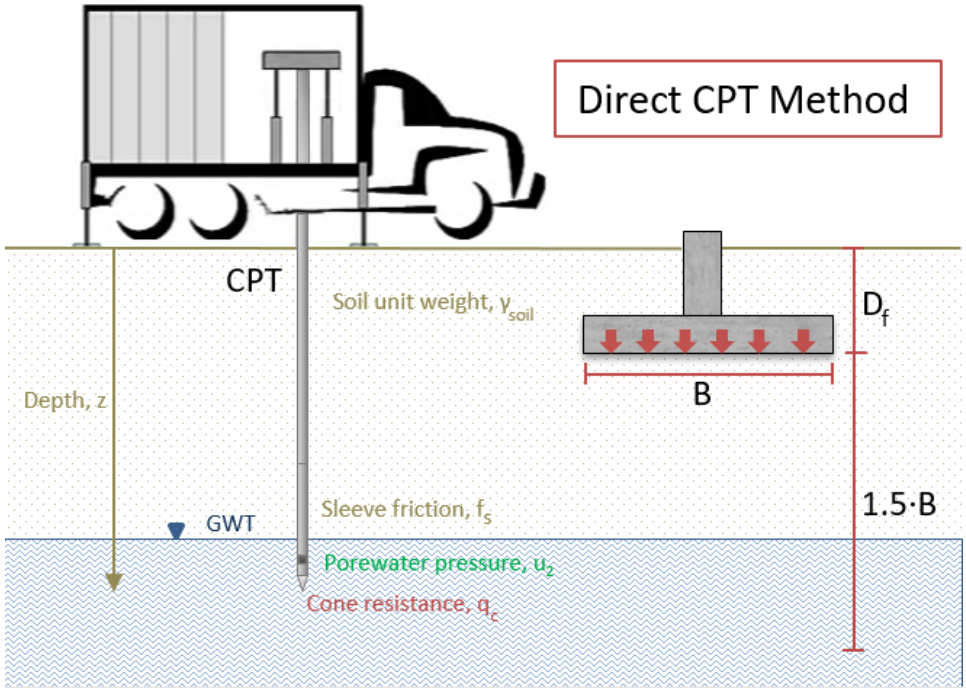

Figure 23. Direct CPT method introduction.

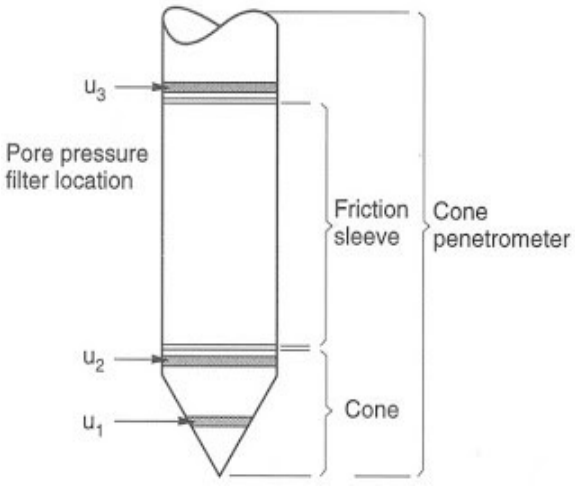

Figure 24. Differentiation of porewater pressure measurement locations (Lunne et al., 1997).

3.1.2 Step 2. Soil Characterization

The soil behavior type (SBT) and CPT material index (I_c) govern the value of the formation factor h_s. The first step is following the steps in Soil Unit Weight to determine soil layering and γ_t values for each layer. To determine a representative unit weight (γ_{soil}) for all the layers in the range of D_f to 1.5·B below

D_f, the user will need to use their engineering judgement on the definition of "representative unit weight". This single value of unit weight is used in further calculations such as the total vertical soil stress (σ_{vo}) from Equation 29 and effective vertical stress (σ'_{vo}) from Equation 30. Values of σ_{vo} and σ'_{vo} will need to be calculated at 1.5·B below D_f.

$$\boldsymbol{\sigma_{vo} = \sum(\gamma_{soil} \cdot z)} \quad \textbf{29}$$

$$\boldsymbol{\sigma'_{vo} = \sigma_{vo} - u_o} \quad \textbf{30}$$

Where:

$z = D_f + 1.5 \cdot B$

$u_o = \gamma_{water} \cdot (z - z_w)$

The q_c will need to be corrected using Equation 31 in the case of fine-grained soils that develop excess porewater pressure during cone penetration. These values will be used in the following calculations.

$$\boldsymbol{q_t = q_c + u_2 \cdot (1 - a)} \quad \textbf{31}$$

Where:

a = cone area ratio = $\frac{A_n}{A_c}$; e.g., MnDOT commonly uses a = 0.8

A_n = cross-sectional area of load cell or shaft

A_c = projected area of the cone

The cone area ratio is determined based on the type of piezocone tip used during in-situ field testing. Manufacturer specifications should provide the measured net area ratio (a) for the particular cone penetrometer as determined by calibration in a pressurized triaxial chamber.

3.1.3 Step 2a. Foundation soil formation parameter

With the representative value γ_{soil}, continue to follow the steps in CPT Material Index through Soil Behavior Type (SBT) to better define the type of soil at depth 1.5·B below D_f,. Use the value of I_c calculated at depth 1.5·B below D_f, to calculate h_s with Equation 36. This parameter is based on the soil type with typical values shown in Figure 25. The data on silts and sands are considered fully drained, whereas the fissured clay subset may be partially drained to undrained.

$$h_s = 2.8 - \frac{2.3}{1+\left(\frac{I_C}{2.4}\right)^{15}} \quad (32)$$

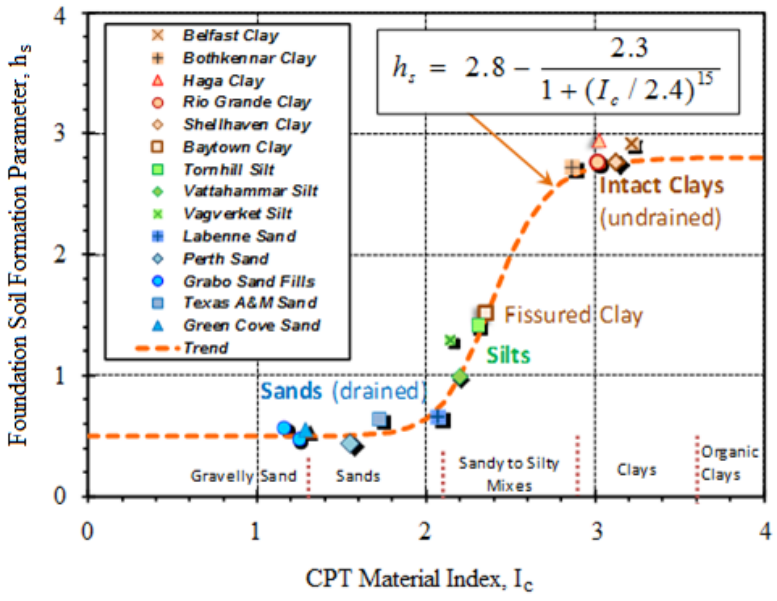

Figure 25. Foundation soil formation parameter hs versus CPT material index, Ic (Mayne 2017).

3.1.4 Step 3. Soil elastic modulus and Poisson's ratio

Details about the soil such as its elastic modulus (E_s) and Poisson's ratio (v) will be needed for further calculations. A representative value for the E_s can be determined from in-situ field tests. Values of v can be assigned as 0.2 for drained sands and as 0.5 for undrained loading cases involving clays (Jardine et al., 1985; Burland, 1989).

3.1.5 Step 4. Net cone tip resistance

Calculate q_{tnet}, the mean value of net cone tip resistance $1.5 \cdot B$ below the foundation bearing elevation using Equation 33.

$$q_{tnet} = q_t - \sigma_{vo} \quad (33)$$

3.1.6 Step 5. Bearing capacity of the soil

Use the assumed B and L, calculated h_s, and q_{tnet}, to determine the soils bearing capacity (q_{max}) from Equation 34. Use Table 6 to calculate q_{max} by using the maximum allowable settlement ratio $(s/B)_{max}$ correlating to the soil type. If h_s is in between the given values, interpolate to acquire $(s/B)_{max}$.

Table 6. Bearing capacity defined by soil type.

Type of Soil	h_s	$(s/B)_{max}$
Clean Sands	0.58	12%
Silts	1.12	10%
Fissured Clays	1.47	7%
Intact Clays	2.70	4%

$$q_{max} = h_s \cdot q_{tnet} \cdot \left(\frac{s}{B}\right)_{max}^{0.5} \cdot \left(\frac{L}{B}\right)^{-0.345} \quad 34$$

3.1.7 Step 6. Settlement

Settlement can be calculated directly using the results from Equation 35. A FS equal to 3 is common in foundation engineering.

$$s = B \cdot \left[\frac{1}{h_s} \cdot \frac{q_{max}/_{FS}}{q_{tnet}} \cdot \left(\frac{L}{B}\right)^{0.345}\right]^2 \quad 35$$

3.1.8 Step 7. Final Check

Check that the applied stress (q) is less than q_{max} using Equation 36. Repeat the process again with a new B and/or new L if $q > q_{max}$.

$$q = h_s \cdot q_{tnet} \cdot \left(\frac{s}{B}\right)^{0.5} \cdot \left(\frac{L}{B}\right)^{-0.345} \quad 36$$

3.2 EXAMPLE PROBLEMS

3.2.1 Example 3: Direct CPT Method on Sands

A footing size needs to be determined based on the given CPT data collected for the South Abutment (Figure 27). The footing stress (q) was determined to be 8,000 psf. Estimate a footing size (B x L) and determine the bearing capacity of the foundation (q_{max}) using the direct CPT method provided. Also determine the expected settlement based on the calculated bearing capacity.

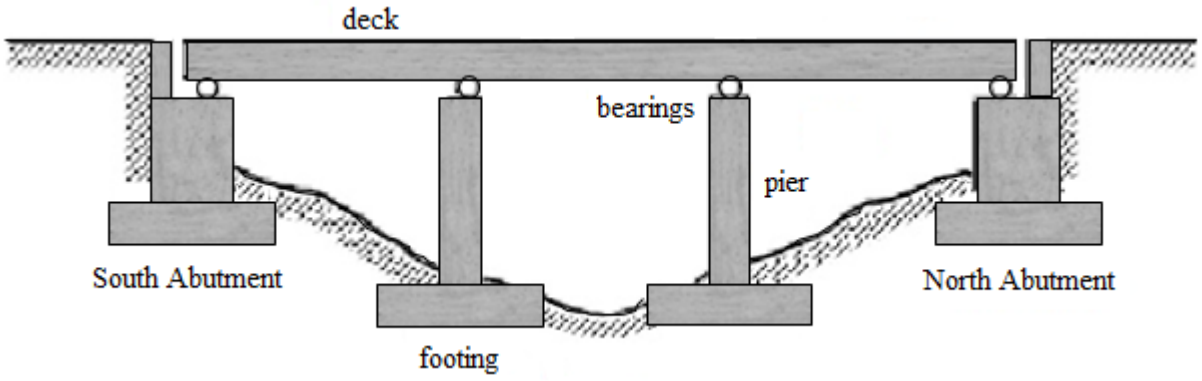

Figure 26. Diagram of footing profiles for Example 3.

The soil elastic modulus determined from seismic CPT (SCPT) are shown in Table 7.

Table 7. SCPT Results

Depth (feet) Bottom of layer	E_s (tsf)
3	557
6	433
9	557
12	695
17	590
22	501
27	571
32	505

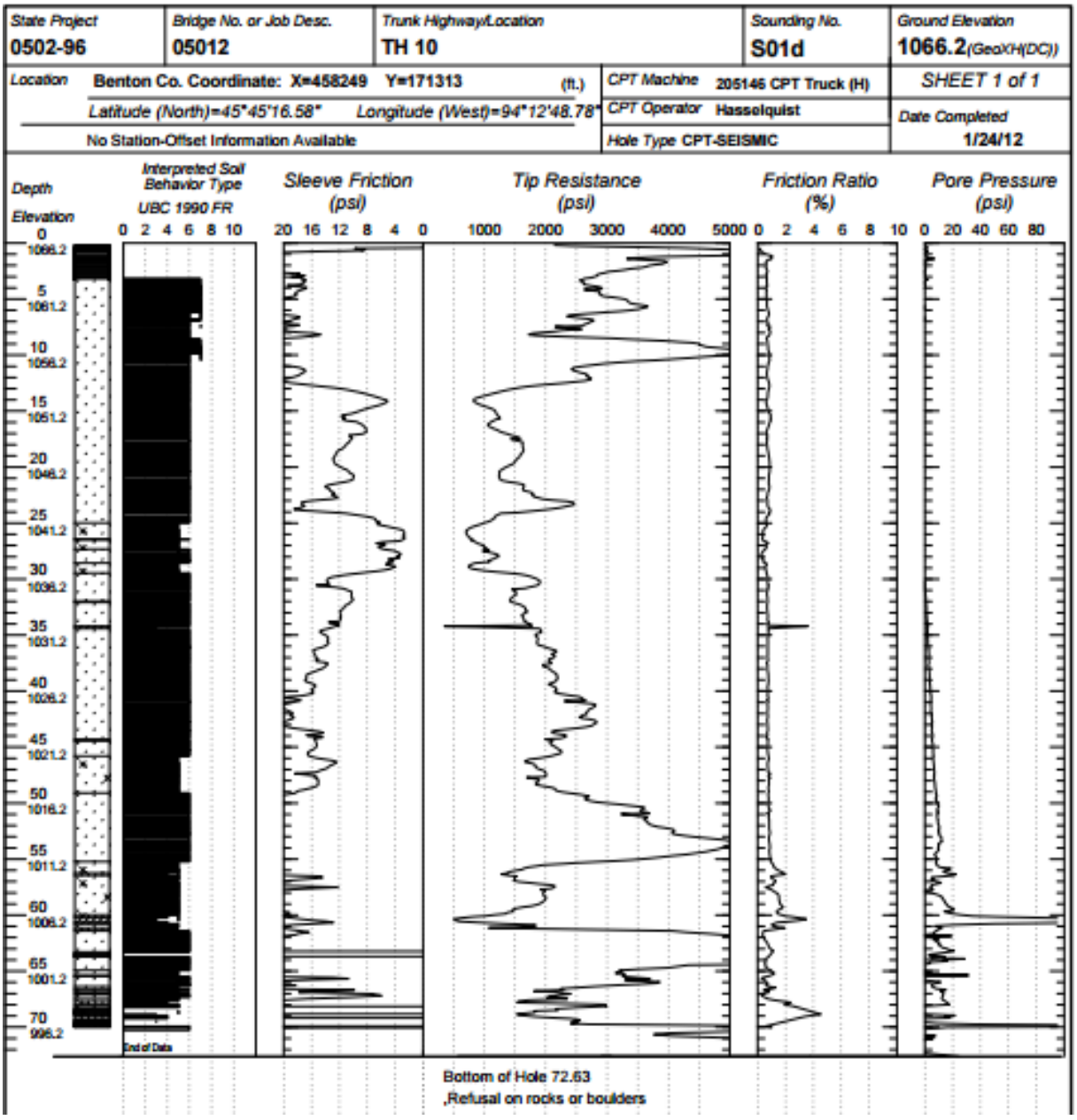

Figure 27. CPT data from Northern Minnesota.

Solution

Step 1. Assume the footing is placed below the frost depth of 6 feet.

Estimate L: L = 50 feet = 600 inches

Estimate B: B = 12 feet = 144 inches

Estimate footing thickness t: t = 2 feet

D_f = 6 feet = 72 inches

$D_f + 1.5 \cdot B$ = 24 feet = 288 inches

Step 2. ***Soil total unit weight***

Estimate soil layering using "rules of thumb."

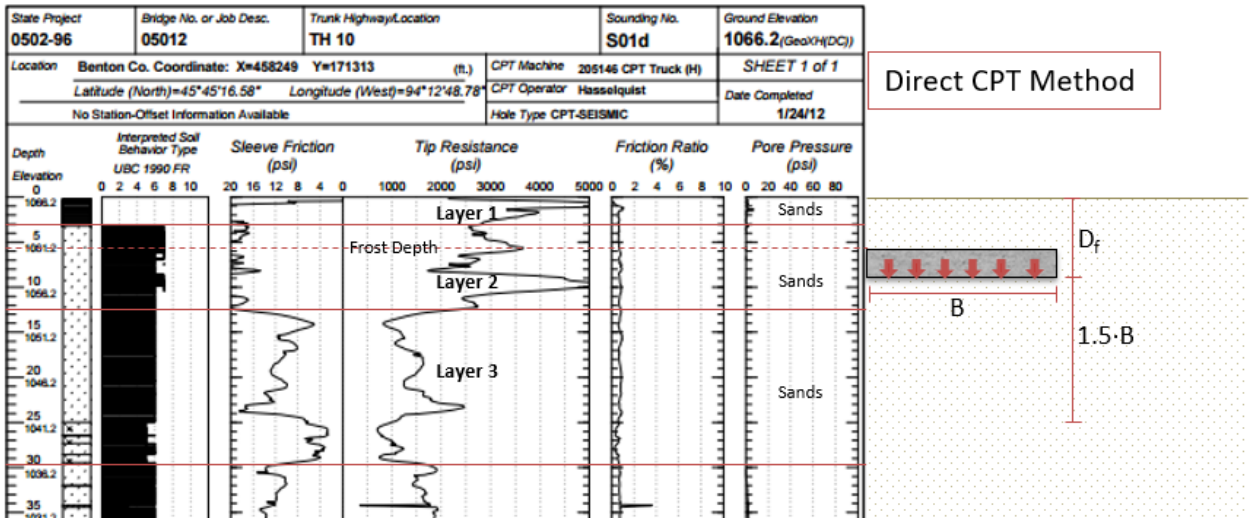

Figure 28. Schematic of foundation design associated with CPT data.

Layer 1

From Figure 28: f_s = 20 psi taken as a representative value of the layer

$$\gamma_t = 62.4 \text{ pcf} \cdot \left[1.22 + 0.15 \cdot \ln\left(100 \cdot \frac{20 \text{ psi}}{14.5 \text{ psi}} + 0.01\right)\right] = 121.9 \text{ pcf}$$

Layer 2

From Figure 28: f_s = 20 psi taken as a representative value of the layer

$$\gamma_t = 62.4 \text{ pcf} \cdot \left[1.22 + 0.15 \cdot \ln\left(100 \cdot \frac{20\text{psi}}{14.5 \text{ psi}} + 0.01\right)\right] = 121.9 \text{ pcf}$$

Layer 3

From Figure 28: f_s = 8 psi taken as a representative value of the layer

$$\gamma_t = 62.4 \text{ pcf} \cdot \left[1.22 + 0.15 \cdot \ln\left(100 \cdot \frac{8 \text{ psi}}{14.5 \text{ psi}} + 0.01\right)\right] = 113.4 \text{ pcf}$$

Using the unit weights calculated between D_f and 1.5B , determine a representative unit weight of the soil to calculate the total and effective soil stresses. Based on layer 3 being the weakest supporting layer, γ_{soil} = 113 pcf.

$$\sigma_{vo} = \gamma_{soil} \cdot (D_f + 1.5 \cdot B) = 113 \text{ lbs/ft}^3 \cdot 24 \text{ feet} = 2721 \text{ psf} = 18.9 \text{ psi}$$

$$\sigma'_{vo} = \sigma_{vo} - u_o = 2721 \text{ psf} - 0 \text{ psf} = 2721 \text{ psf} = 18.9 \text{ psi}$$

Calculate the cone tip resistance between D_f and D_f + 1.5B below the foundation depth.

$$q_t = q_c + u_2 \cdot (1 - a) = 1250 \text{ psi} + 0 \text{ psi} \cdot (1 - 0.8) = 1000 \text{ psi}$$

Step 2a. ***CPT Material Index***

Using Figure 28 the sleeve friction at 1.5B below the foundation depth is about 16 psi.

$$F_r(\%) = 100\% \cdot \frac{f_s}{(q_t - \sigma_{vo})} = 100\% \cdot \frac{16 \text{ psi}}{(1250 \text{ psi} - 18.9 \text{ psi})} = 1.3 \%$$

Iterate to solve for I_c. Steps are not shown for brevity.

$$Q_{tn} = \frac{(q_t - \sigma_{vo})/\sigma_{atm}}{(\sigma'_{vo}/\sigma_{atm})^n} = \frac{(1250 \text{ psi} - 18.9 \text{ psi})/14.5 \text{ psi}}{(18.9 \text{ psi}/14.5 \text{ psi})^n}$$

$$n = 0.381 \cdot I_c + 0.05\left(\frac{\sigma'_{vo}}{\sigma_{atm}}\right) - 0.15 = 0.381 \cdot I_c + 0.05\left(\frac{18.9 \text{ psi}}{14.5 \text{ psi}}\right) - 0.15$$

$$Q_{tn} = 70.3 \qquad n = 0.72 < 1.0 \qquad I_c = 2.10$$

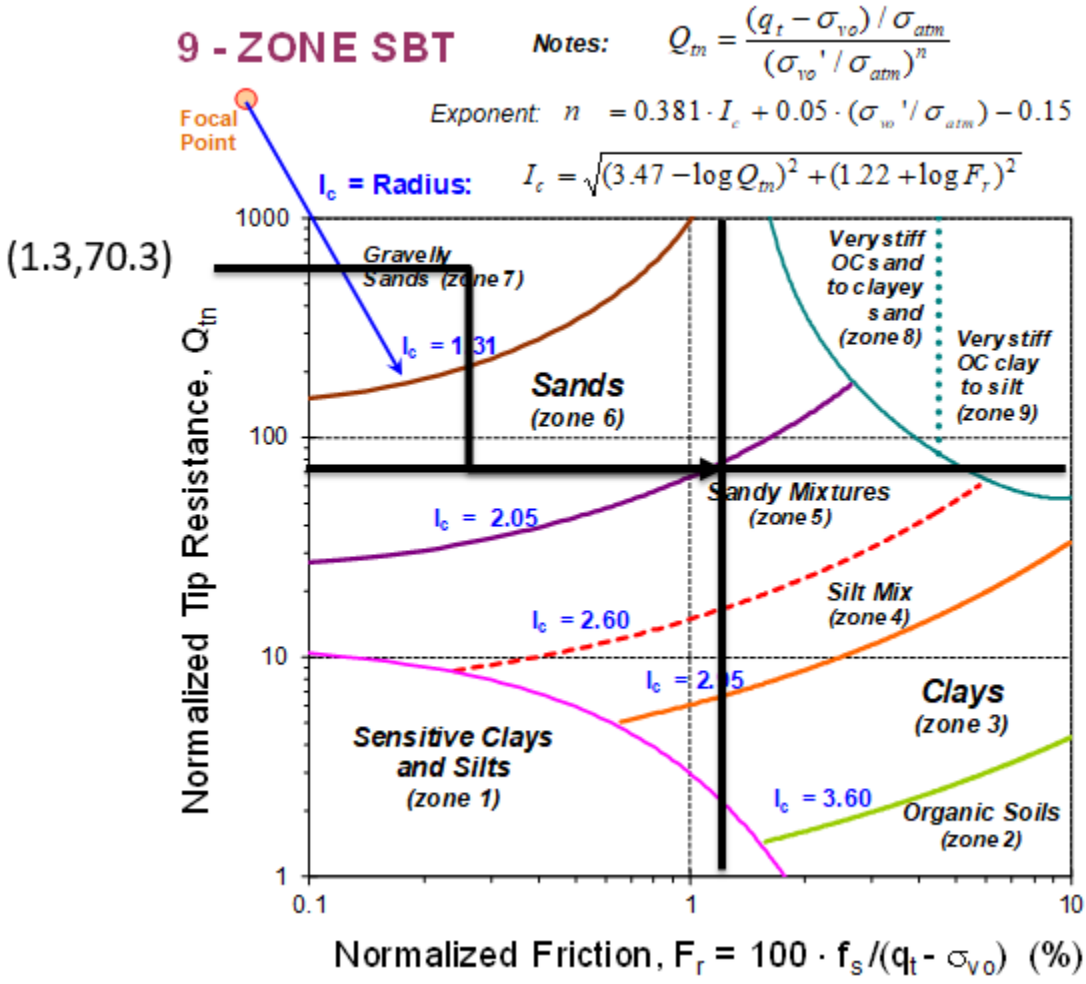

Figure 29. Soil type for example problem 3.

Use the I_c value to determine the foundation soil formation parameter.

Calculate the foundation soil formation parameter. The tip resistance is about 1250 psi at 24 feet and the cone area ratio was determined to be 0.8 from information provided by the manufacturer.

$$h_s = 2.8 - \frac{2.3}{1 + \left(\frac{I_c}{2.4}\right)^{15}} = 2.8 - \frac{2.3}{1 + \left(\frac{2.10}{2.4}\right)^{15}} = 0.78 = \text{"Sand/Silt"}$$

Step 3. Determine representative values of soil elastic modulus from soil testing and Poissons ratio. The soil elastic modulus was taken as the average value between depths of D_f and 1.5·B (6 feet and 24 feet).

$$E_s = \frac{433 + 557 + 695 + 590 + 501}{5} = 555 \text{ tsf} = 708 \text{ psi}$$

"Drained sand/silt" gives a v = 0.20

Step 4. Calculate the net cone tip resistance.

$$q_{tnet} = q_t - \sigma_{vo} = 1250 \text{ psi} - 18.9 \text{ psi} = 1231.1 \text{ psi}$$

Step 5. Calculate the bearing capacity of the sand.

In drained sands/silts the "bearing capacity" is taken as the stress when (s/B) = 0.11 (or 11% foundation width).

$$q_{max} = h_s \cdot q_{tnet} \cdot \left(\frac{s}{B}\right)^{0.5} \cdot \left(\frac{L}{B}\right)^{-0.345} = 0.78 \cdot (979.5) \cdot (0.11)^{0.5} \cdot \left(\frac{600}{144}\right)^{-0.345}$$

$$q_{max} = 193 \text{ psi} = 27{,}860 \text{ psf}$$

Assuming a factor of safety (FS) of 3.

$$\frac{q_{max}}{3} = 64.5 \text{ psi} = 9287 \text{ psf}$$

Step 6. Calculate settlement

$$s = B \cdot \left[\frac{1}{h_s} \cdot \frac{q_{max}/_{FS}}{q_{tnet}} \cdot \left(\frac{\mathrm{L}}{\mathrm{B}}\right)^{0.345} \right]^2$$

$$\mathrm{s} = 144 \text{ inches} \cdot \left[\frac{1}{0.78} \cdot \frac{64.5 \text{ psi}}{1231.1 \text{ psi}} \cdot \left(\frac{600 \text{ inches}}{144 \text{ inches}}\right)^{0.345} \right]^2 = 1.8 \text{ inches}$$

Step 7. Determine if q > q_{max}.

$$\mathrm{q} = 8{,}000 \text{ psf} < 9{,}287 \text{psf} = \mathrm{q_{max}}/3$$

CHAPTER 4: DIRECT CPT METHOD FOR DEEP FOUNDATIONS

4.1 INTRODUCTION

The axial compression capacity (Q_{total}) for a single pile includes a side component (Q_{side}), end bearing component (Q_{base}), and pile weight (W_{pile}) as shown in Figure 30. Since piles commonly push through several layers, a summation of the unit side frictions acting on the pile segments must be considered over the length of the pile. While the examples shown in this Guide resemble hand calculations, computer software is more efficient. Programming the procedure is possible and represents a practical method of designing deep foundations. However, commercial software is frequently available and is MnDOT's most common method of designing deep foundations.

There are upwards of 40 different direct CPT methods that have been developed over the past five decades to determine a piles axial compression capacity. Many of the earliest methods relied on hand-recorded information where q_c data from mechanical CPTs would be collected at 20 cm intervals, whereas the direct CPT method uses scaled penetrometer readings via specified algorithms to obtain the pile unit side friction and unit end bearing. The method that will be used for deep foundation design is the Modified UniCone method which uses all three readings of the electronic piezocone (q_t, f_s, and u_2) while addressing a variety of pile foundation types.

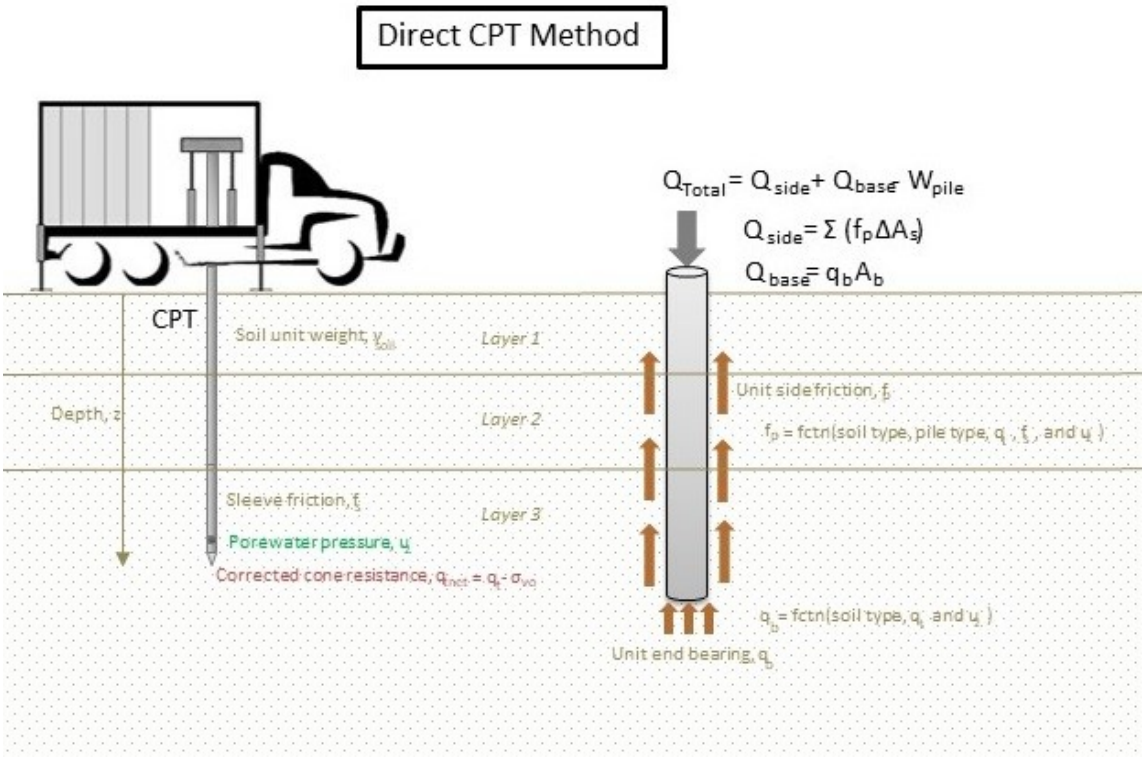

Figure 30. Direct CPT evaluation of axial pile capacity.

The modified UniCone Method is based upon a total of 330 pile load tests (three times the original Unicone database) that were associated with SCPTu data. Originally the UniCone method provided approximate soil classification in five groups via a chart of q_E vs f_s (Figure 31) where $q_E = q_t - u_2$. Later, using the modified approach with a larger data set, provided soil sub classifications as shown in Figure 32. This new 9-zone normalized soil behavior type is determined using CPT data in combination with the CPT Material Index.

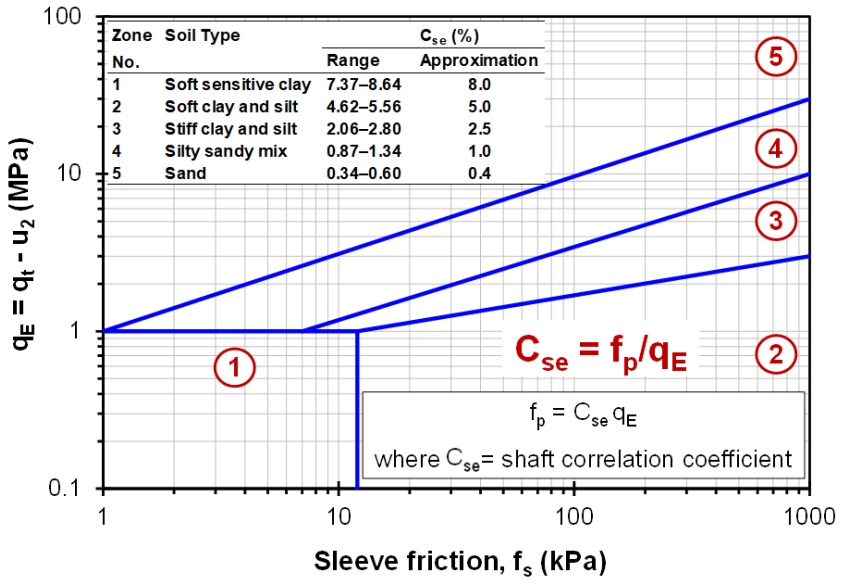

Figure 31. UniCone Method soil behavior type using CPT (Mayne 2017).

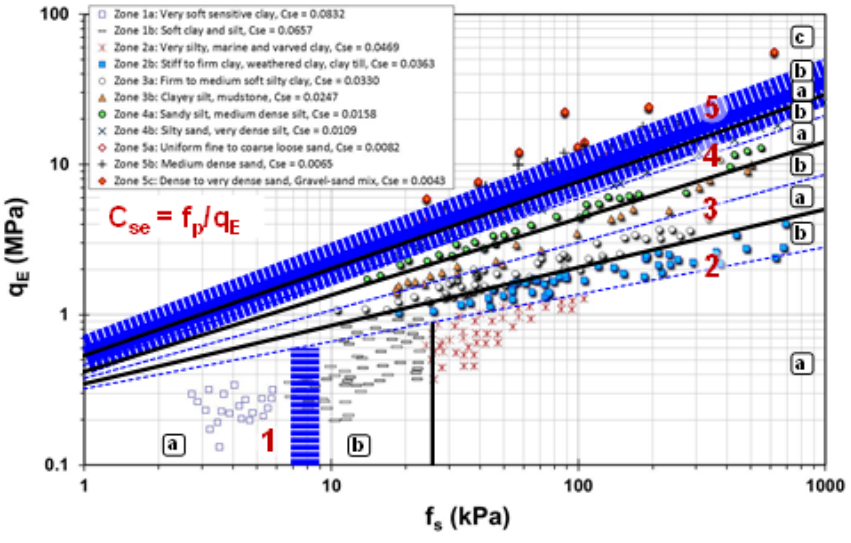

Figure 32. Modified UniCone Method soil behavior type using CPT (Mayne 2017).

4.2 MODIFIED UNICONE METHOD

In order to determine the axial pile capacity using the modified method, the first step requires the determination of geoparameters, as shown in Direct CPT Method for Soil Characterization. Once the soil unit weight and CPT Material index are determined for each soil layer, then the effective cone resistance, pile unit side friction (f_p), and pile end bearing resistance (q_b) can be determined.

4.2.1 Step 1.

Work through the steps provided in CPT Method for Soil Characterization until each soil layer is defined by its CPT material index and soil behavior type using Figure 6. After these steps have been completed, continue to Step 2 to determine q_E, q_b, and f_p.

4.2.2 Step 2.

Once q_t is determined for each layer, the effective cone resistance can be calculated using Equation 37.

$$q_E = q_t - u_2 \tag{37}$$

Where: (a) q_E is the specific value at each elevation along the pile sides for determining f_p; and (b) at the bottom of the pile, q_E is averaged in the vicinity of the pile tip from the tip bearing elevation to about one diameter beneath the tip for determining q_b.

Using CPT material index and q_E, the pile end bearing resistance is calculated using Equation 38.

$$q_b = q_E \cdot 10^{(0.325 \cdot I_c - 1.218)} \tag{38}$$

The pile unit side friction is obtained from q_E and I_c.

$$f_p = q_E \cdot \theta_{PT} \cdot \theta_{TC} \cdot \theta_{RATE} \cdot 10^{(0.732 \cdot I_c - 3.605)} \tag{39}$$

Where:

θ_{PT} = coefficient for pile type (0.84 for bored; 1.02 for jacked; 1.13 for driven piles)
θ_{TC} = coefficient for loading direction (1.11 for compression and 0.85 for tension)
θ_{RATE} = rate coefficient applied to soils in SBT zone 1 through 7 (1.09 for constant rate of penetration test and 0.97 for maintained load tests)

4.2.3 Step 3.

Due to piles extending through multiple layers, the unit side components acting on various pile segments would need to be summed if not using the direct CPT method. Since CPT calculates data at regular intervals of 2 cm to 5 cm along the sides of the pile, the average f_p in each layer can be used directly in Equation 40 to obtain the shaft capacity.

$$Q_{side} = f_p \cdot A_s \quad (40)$$

Where:

f_p = average pile side friction along pile length from eqn 39
$A_s = \pi \cdot d \cdot H$
d = pile diameter and H = length embedded below grade

The base capacity for a pile in compression loading is given by Equation 41. For piles in tension (or uplift) Q_{base} can be taken as 0.

$$Q_{base} = q_b \cdot A_b \quad (41)$$

Where:

q_b = end bearing resistance from eqn 38
$A_b = \pi \cdot d^2/4$ (area of a circular pile)

4.2.4 Step 4.

The final step is to calculate the axial pile capacity using Equation 42.

$$Q_{total} = Q_{side} + Q_{base} - W_{pile} \quad (42)$$

4.3 AXIAL PILE DISPLACEMENTS

Movement of pile foundations can be assessed using elastic continuum theory which has been developed using finite element analyses, boundary elements, and analytical closed-form solutions. In the case of piles passing through several soil layers, the elastic solution can be used by stacking pile segments (each with its own stiffness) as represented by soil Young's modulus. The use of software is recommended for pile groups. Several available programs such as DEFPIG, GROUP, and PIGLET can handle pile groups under axial and lateral/moment loading.

4.4 EXAMPLE PROBLEMS

4.4.1 Example 5: Direct CPT Methods Axial Pile Capacity

Several piles need to be placed beneath the edge of a building. Use the CPT data collected for this site, shown in Figure 34, to determine the axial capacity for one of the piles. Assume round steel driven piles will be used with a diameter of 12.75 inches, wall thickness of 0.25 inches and lengths of 80 feet. Concrete will be used to fill the piles. To solve for all geoparameters use the Direct CPT Method for Soil Characterization section. All sand layers can be assumed “drained” with v = 0.2.

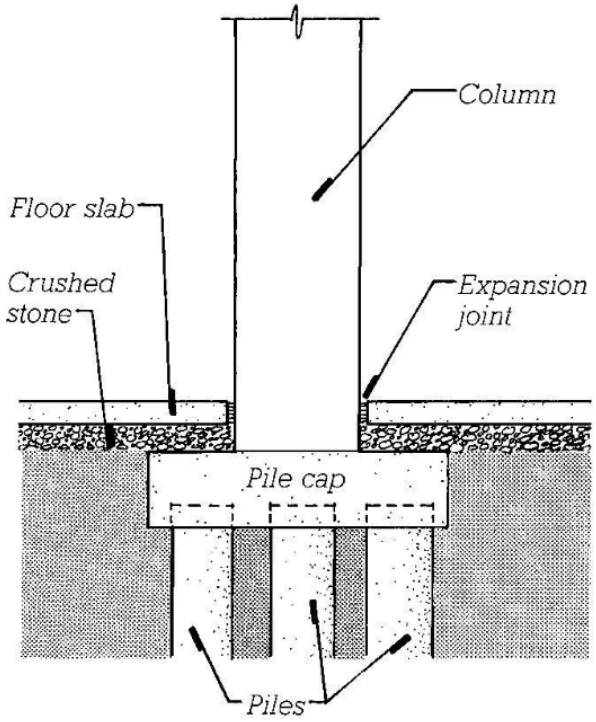

Figure 33. Deep foundation end bearing pile diagram.

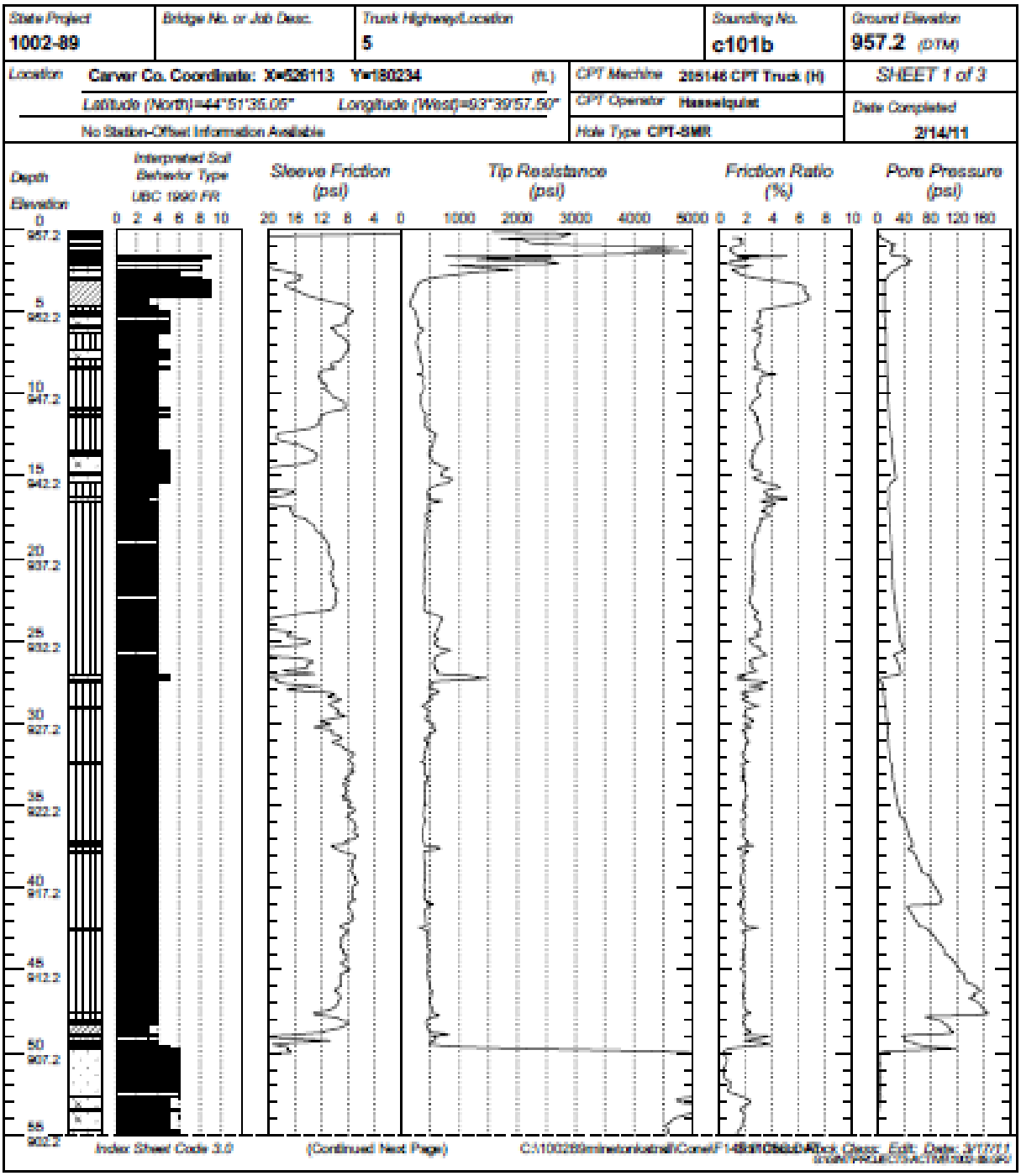

Figure 34. CPT data from Minnesota for example problem 5.

Solution

Soil total unit weight

Estimate soil layering using [“rules of thumb.”]

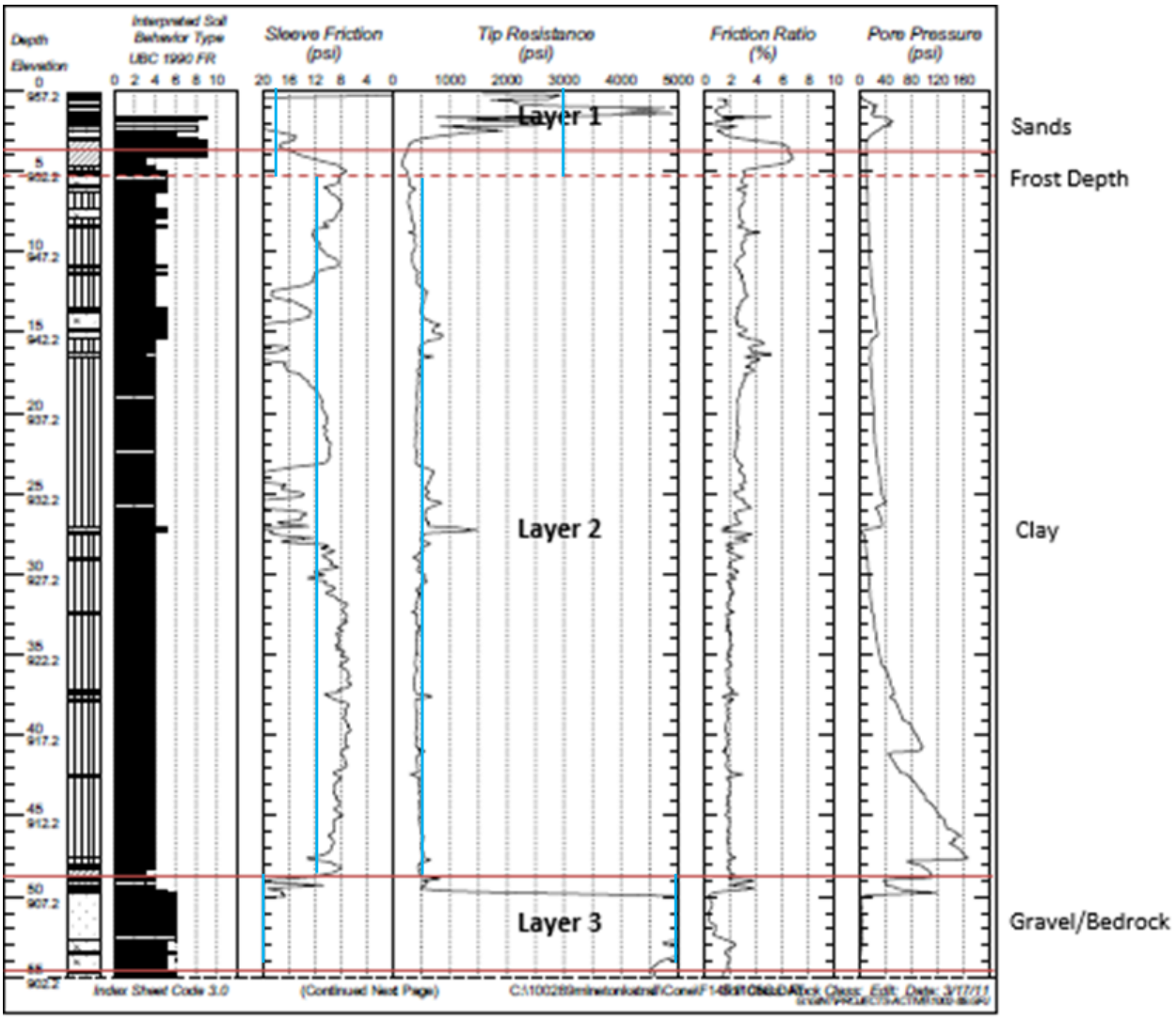

Figure 35. Soil layers using “rules of thumb” for pile capacity example using direct CPT method

Layer 1

From Figure 35: f_s = 18 psi taken as a representative value of the layer

$$\gamma_t = 62.4 \text{ pcf} \cdot \left[1.22 + 0.15 \cdot \ln\left(100 \cdot \frac{18 \text{ psi}}{14.5 \text{ psi}} + 0.01\right)\right] = 121.0 \text{ pcf}$$

Layer 2

From Figure 35: f_s = 12 psi taken as a representative value of the layer

$$\gamma_t = 62.4 \text{ pcf} \cdot \left[1.22 + 0.15 \cdot \ln\left(100 \cdot \frac{12 \text{psi}}{14.5 \text{ psi}} + 0.01\right)\right] = 117.2 \text{ pcf}$$

Layer 3

From Figure 35: f_s = 20 psi taken as a representative value of the layer

$$\gamma_t = 62.4 \text{ pcf} \cdot \left[1.22 + 0.15 \cdot \ln\left(100 \cdot \frac{20 \text{ psi}}{14.5 \text{ psi}} + 0.01\right)\right] = 121.9 \text{ pcf}$$

CPT Material Index

Layer 1

From Figure 35: f_s = 18 psi and q_c = 3000 psi

$$q_t = q_c + u_2 \cdot (1 - a) = 3000 \text{ psi} + 20 \text{ psi} \cdot (1 - 0.8) = 3004 \text{ psi}$$

$$\sigma_{vo} = \gamma_t \cdot 4 \text{ feet} = 121.9 \text{ pcf} \cdot 4 \text{ feet} = 487.7 \text{ psf} = 3.4 \text{ psi}$$

$$F_r(\%) = 100 \cdot \frac{f_s}{(q_t - \sigma_{vo})} = 100 \cdot \frac{18 \text{ psi}}{(3004 \text{ psi} - 3.4 \text{ psi})} = 0.60$$

Step 2. Iterate to solve for I_c. Steps are not shown for brevity.

$$u_o = 0 \text{ psi}$$

$$\sigma'_{vo} = \sigma_{vo} - u_o = 3.4 \text{ psi} - 0 \text{ psi} = 3.4 \text{ psi}$$

$$Q_{tn} = \frac{(q_t - \sigma_{vo})/\sigma_{atm}}{(\sigma'_{vo}/\sigma_{atm})^n} = \frac{(3004 \text{ psi} - 3.4 \text{ psi})/14.5 \text{ psi}}{(3.4 \text{ psi}/14.5 \text{ psi})^n}$$

$$n = 0.381 \cdot I_c + 0.05\left(\frac{\sigma'_{vo}}{\sigma_{atm}}\right) - 0.15 = 0.381 \cdot I_c + 0.05\left(\frac{3.4 \text{ psi}}{14.5 \text{ psi}}\right) - 0.15$$

$$I_c = \sqrt{[3.47 - \log(Q_{tn})]^2 + [1.22 + \log(0.60)]^2}$$

$$Q_{tn} = 359.3 \qquad n = 0.38 < 1.0 \qquad I_c = 1.4 \qquad \text{(i.e., sand)}$$

Layer 2

From Figure 35: f_s = 12 psi and q_c = 500 psi

$$q_t = q_c + u_2 \cdot (1 - a) = 500 \text{ psi} + 40 \text{ psi} \cdot (1 - 0.8) = 508 \text{ psi}$$

$$\sigma_{vo} = 483.8 \text{ psf} + \gamma_t \cdot 45 \text{ feet} = 483.8 \text{ psf} + 117.2 \text{ pcf} \cdot 45 \text{ feet} = 5756 \text{ psf} = 40.0 \text{ psi}$$

$$F_r(\%) = 100 \cdot \frac{f_s}{(q_t - \sigma_{vo})} = 100 \cdot \frac{12 \text{ psi}}{(508 \text{ psi} - 40.0 \text{ psi})} = 2.60$$

Step 2. Iterate to solve for I_c. Steps are not shown for brevity.

$$u_o = 0 \text{ psi}$$

$$\sigma'_{vo} = \sigma_{vo} - u_o = 40.0 \text{ psi} - 0 \text{ psi} = 40.0 \text{ psi}$$

$$Q_{tn} = \frac{(q_t - \sigma_{vo})/\sigma_{atm}}{(\sigma'_{vo}/\sigma_{atm})^n} = \frac{(508 \text{ psi} - 40.0 \text{ psi})/14.5 \text{ psi}}{(40.0 \text{ psi}/14.5 \text{ psi})^n}$$

$$n = 0.381 \cdot I_c + 0.05\left(\frac{\sigma'_{vo}}{\sigma_{atm}}\right) - 0.15 = 0.381 \cdot I_c + 0.05\left(\frac{40.0 \text{ psi}}{14.5 \text{ psi}}\right) - 0.15$$

$$I_c = \sqrt{[3.47 - \log(Q_{tn})]^2 + [1.22 + \log(2.60)]^2}$$

$$Q_{tn} = 11.7 \qquad n = 1.0 \leq 1.0 \qquad I_c = 2.9 \quad \text{(i.e. clayey silt)}$$

Layer 3

From Figure 35: f_s = 20 psi and q_c = 5000 psi

$$q_t = q_c + u_2 \cdot (1 - a) = 5000 \text{ psi} + 0 \text{ psi} \cdot (1 - 0.8) = 5000 \text{ psi}$$

$$\sigma_{vo} = 5756 \text{ psf} + \gamma_t \cdot 6 \text{ feet} = 5756 \text{ psf} + 121.9 \text{ pcf} \cdot 6 \text{ feet} = 6488 \text{ psf} = 45.1 \text{ psi}$$

$$F_r(\%) = 100 \cdot \frac{f_s}{(q_t - \sigma_{vo})} = 100 \cdot \frac{20 \text{ psi}}{(5000 \text{ psi} - 45.1 \text{ psi})} = 0.40$$

Step 2. Iterate to solve for I_c. Steps are not shown for brevity.

$$\sigma'_{vo} = \sigma_{vo} - u_o = 45.1 \text{ psi} - 0 \text{ psi} = 45.1 \text{ psi}$$

$$Q_{tn} = \frac{(q_t - \sigma_{vo})/\sigma_{atm}}{(\sigma'_{vo}/\sigma_{atm})^n} = \frac{(5000 \text{ psi} - 45.1 \text{ psi})/14.5 \text{ psi}}{(45.1 \text{ psi}/14.5 \text{ psi})^n}$$

$$n = 0.381 \cdot I_c + 0.05\left(\frac{\sigma'_{vo}}{\sigma_{atm}}\right) - 0.15 = 0.381 \cdot I_c + 0.05\left(\frac{45.1 \text{ psi}}{14.5 \text{ psi}}\right) - 0.15$$

$$I_c = \sqrt{[3.47 - \log(Q_{tn})]^2 + [1.22 + \log(0.40)]^2}$$

$$Q_{tn} = 180.1 \qquad n = 0.6 < 1.0 \qquad I_c = 1.5 \text{ (i.e. sand)}$$

Soil Behavior Type (SBT)

Layer 1

Based on values of I_c (1.4), Q_{tn} (359), and F_r (0.6), the first layer is defined as a "Gravelly Sand" from Figure 36.

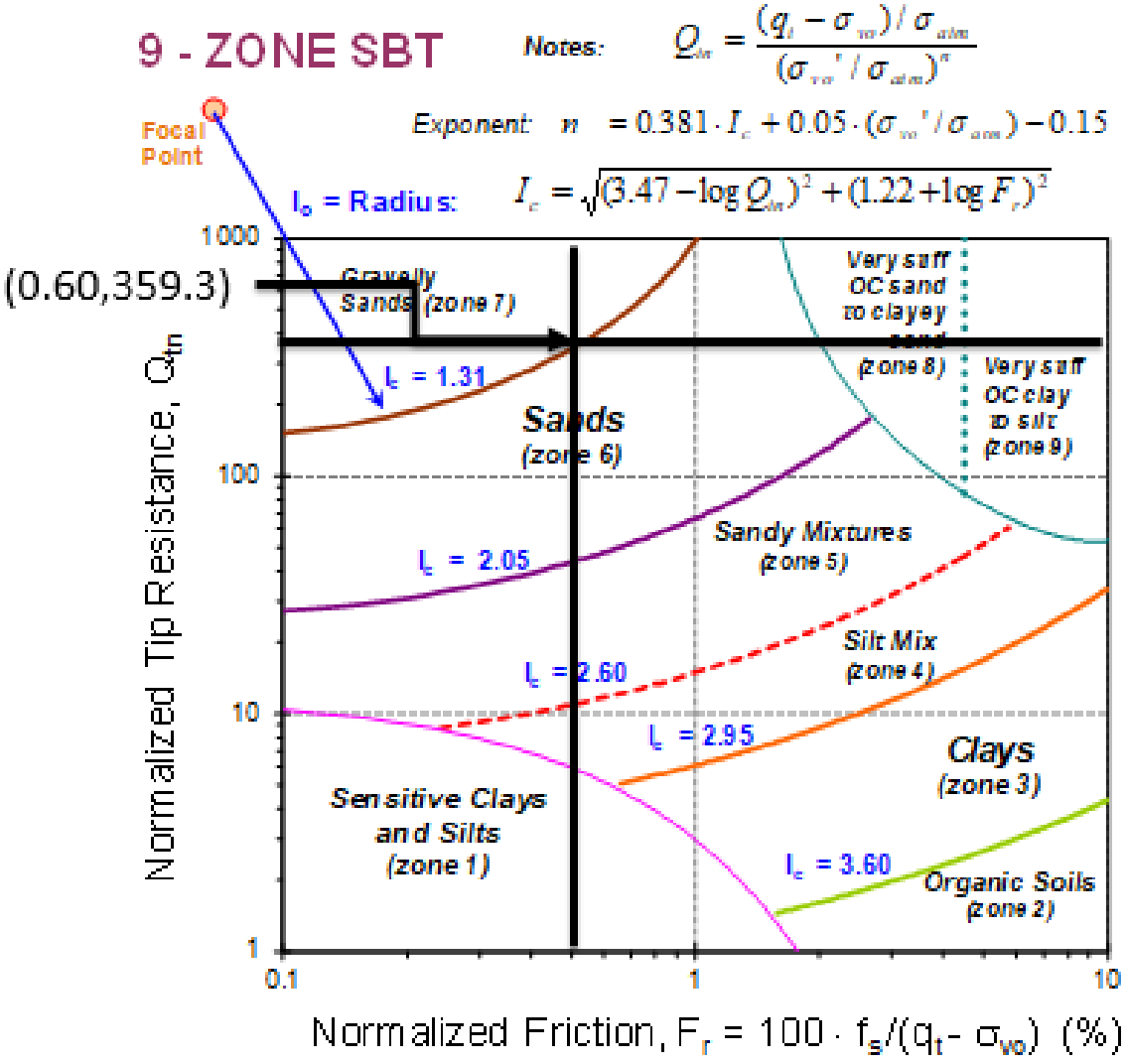

Figure 36. Soil layer 1 using SBT method.

Layer 2

Based on values of I_c (2.9), Q_{tn} (11.7), and F_r (2.6), the second layer is defined as a "Silty Mix" from Figure 37.

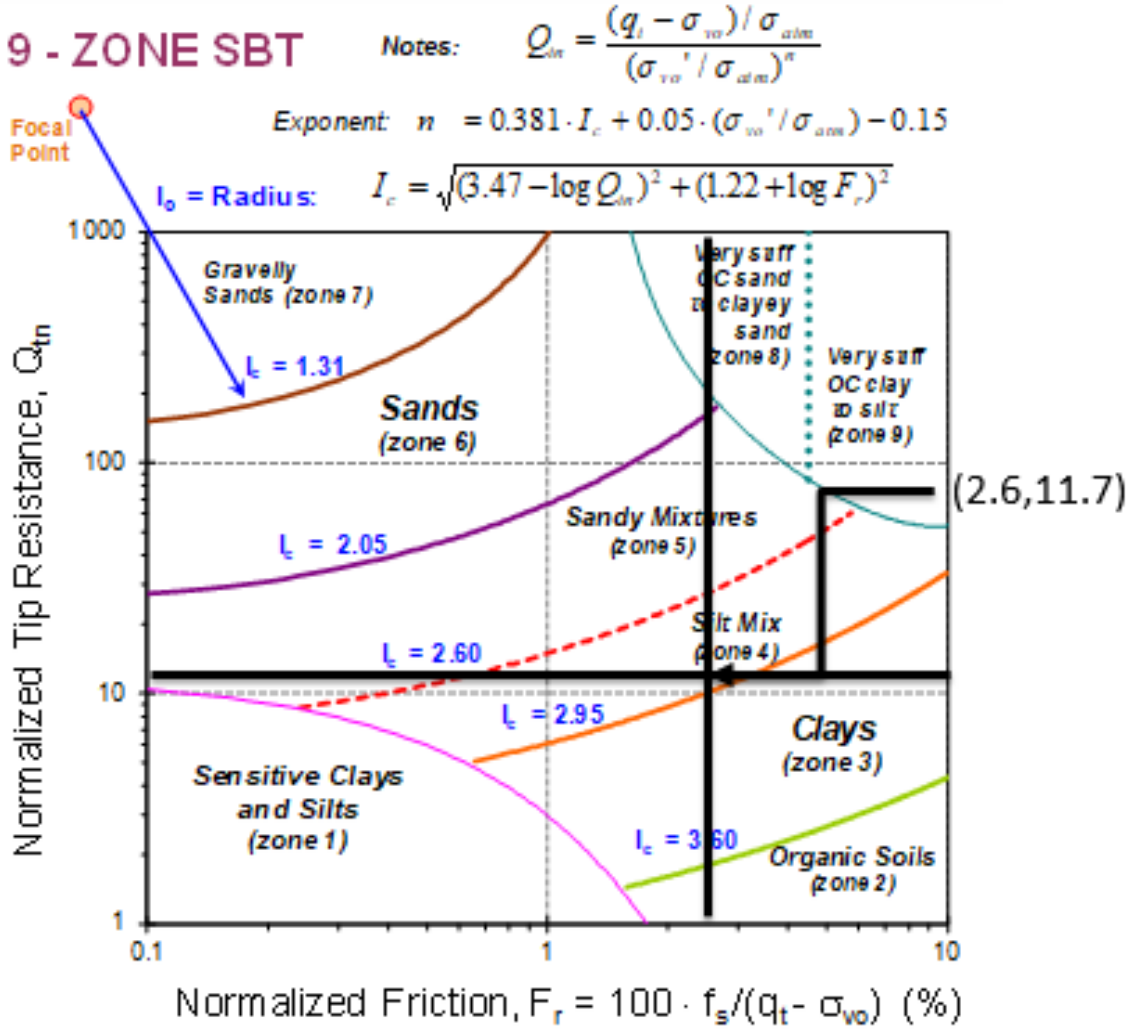

Figure 37. Soil layer 2 using SBT method.

Layer 3

Based on values of I_c (1.5), Q_{tn} (180), and F_r (0.4), the third layer is defined as a "Sand" from Figure 38.

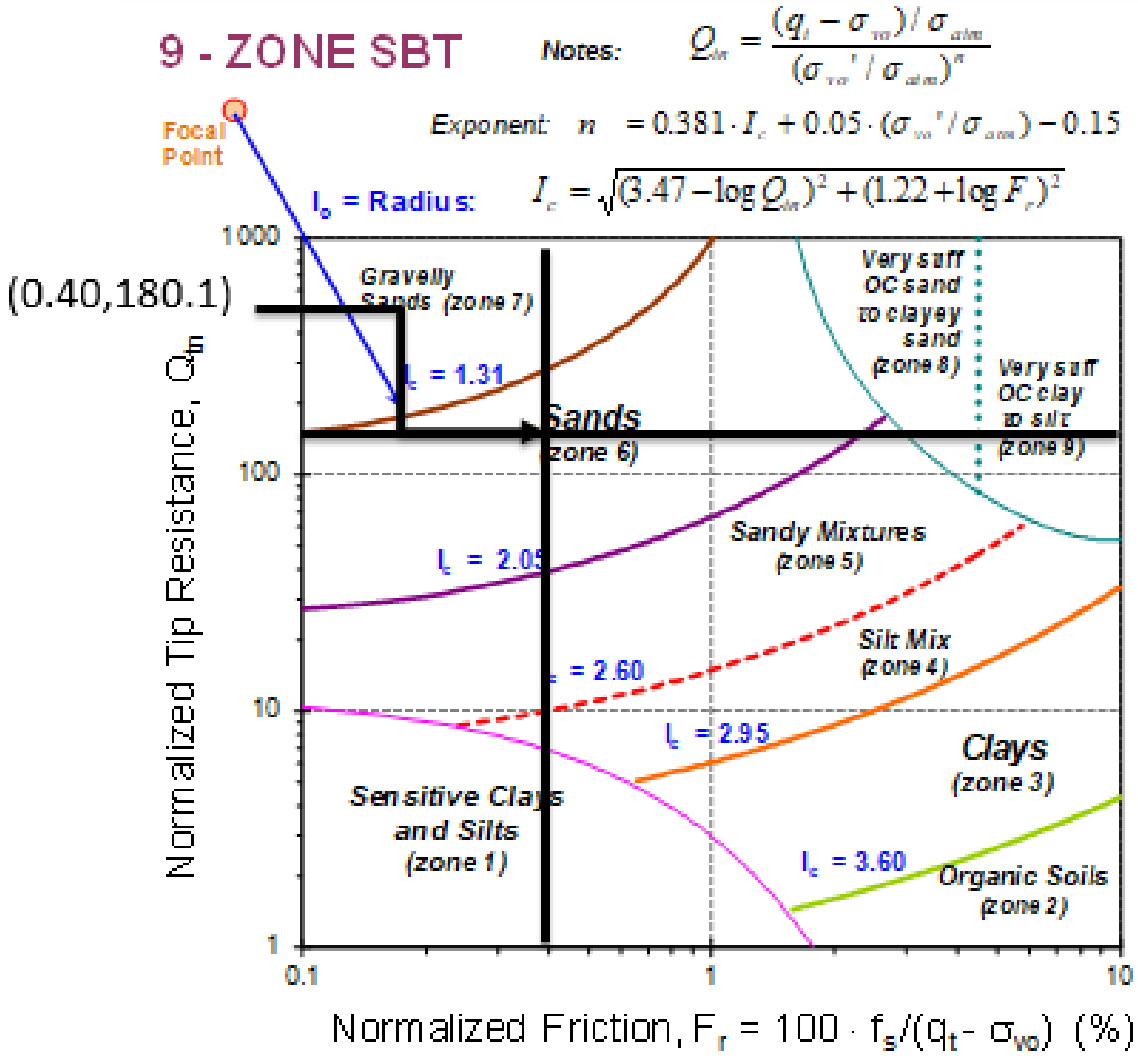

Figure 38. Soil layer 3 using SBT method.

Effective Cone Resistance

Layer 1

$$q_E = q_t - u_2 = 3004 \text{ psi} - 20 \text{ psi} = 2984 \text{ psi}$$

Layer 2

$$q_E = q_t - u_2 = 508 \text{ psi} - 40 \text{ psi} = 468 \text{ psi}$$

Layer 3

$$q_E = q_t - u_2 = 5000 \text{ psi} - 0 \text{ psi} = 5000 \text{ psi}$$

Pile End Bearing Resistance

Layer 3

$$q_b = q_E \cdot 10^{(0.325 \cdot I_c - 1.218)} = 5000 \text{ psi} \cdot 10^{(0.325 \cdot 1.5 - 1.218)} = 908.5 \text{ psi}$$

Pile Unit Side Friction

Layer 1

$$f_p = q_E \cdot \theta_{PT} \cdot \theta_{TC} \cdot \theta_{RATE} \cdot 10^{(0.732 \cdot I_c - 3.605)}$$

$$f_p = 2984 \text{ psi} \cdot 1.13 \cdot 1.11 \cdot 1.09 \cdot 10^{(0.732 \cdot 1.4 - 3.605)} = 9.9 \text{ psi}$$

Layer 2

$$f_p = q_E \cdot \theta_{PT} \cdot \theta_{TC} \cdot \theta_{RATE} \cdot 10^{(0.732 \cdot I_c - 3.605)}$$

$$f_p = 468 \text{ psi} \cdot 1.13 \cdot 1.11 \cdot 1.09 \cdot 10^{(0.732 \cdot 2.9 - 3.605)} = 21.1 \text{ psi}$$

Layer 3

$$f_p = q_E \cdot \theta_{PT} \cdot \theta_{TC} \cdot \theta_{RATE} \cdot 10^{(0.732 \cdot I_c - 3.605)}$$

$$f_p = 5000 \text{ psi} \cdot 1.13 \cdot 1.11 \cdot 1.09 \cdot 10^{(0.732 \cdot 1.5 - 3.605)} = 20.2 \text{ psi}$$

Axial Pile Capacity

The side capacity is based on pile design as shown in Figure 39.

Layer 1

$$Q_{side} = f_p \cdot A_s = 9.9\ psi \cdot (\pi \cdot d \cdot L) = 9.9\ psi \cdot (\pi \cdot 12.75\ in \cdot 48\ in) = 19{,}064\ lb$$

Layer 2

$$Q_{side} = f_p \cdot A_s = 21.1\ psi \cdot (\pi \cdot d \cdot L) = 21.1\ psi \cdot (\pi \cdot 12.75\ in \cdot 588\ in) = 457{,}122\ lb$$

Layer 3

$$Q_{side} = f_p \cdot A_s = 20.2\ psi \cdot (\pi \cdot d \cdot L) = 20.2\ psi \cdot (\pi \cdot 12.75\ in \cdot 240\ in) = 58{,}170\ lb$$

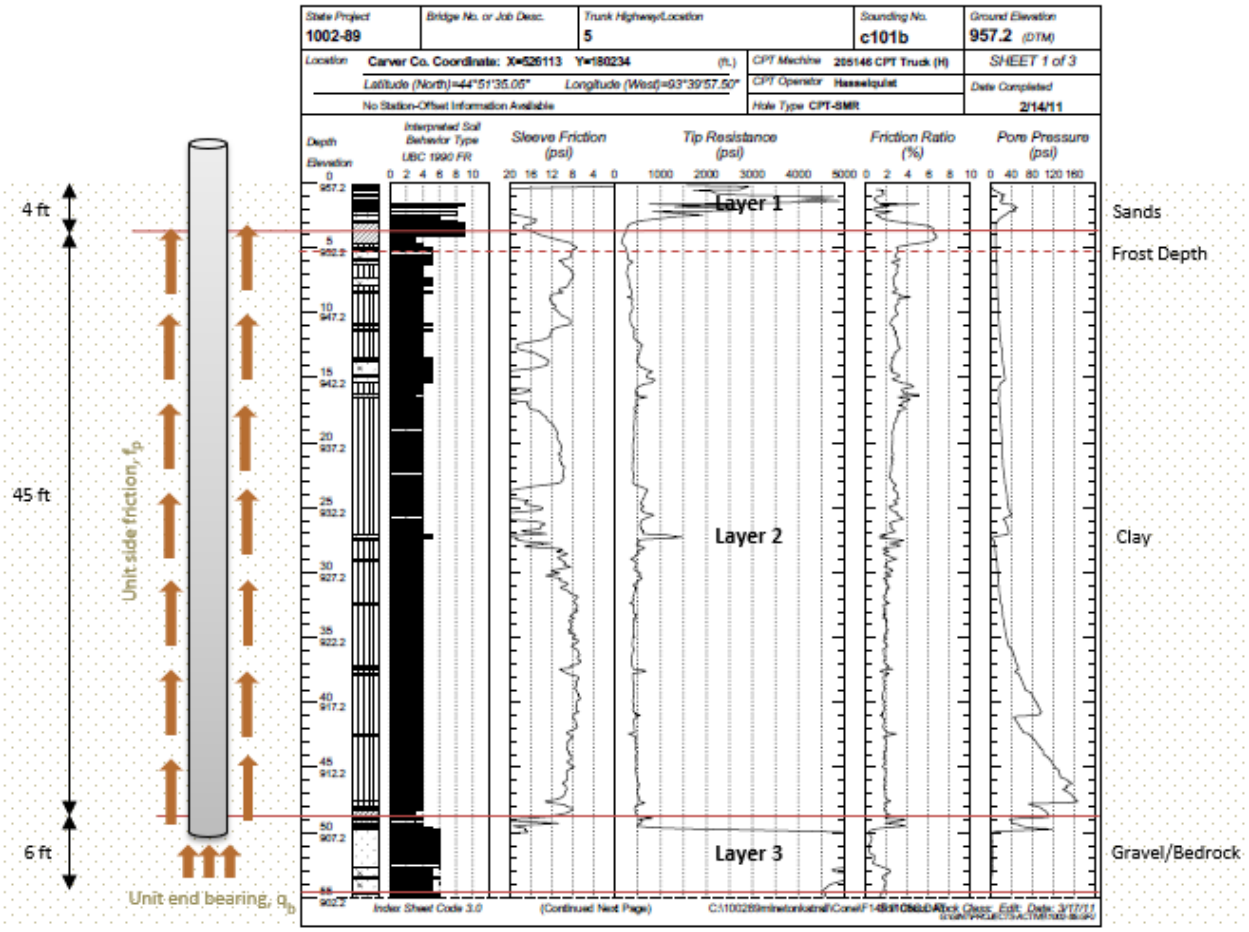

Figure 39. Soil layering compared to pilings.

End Bearing Resistance in Layer 3

$$Q_{base} = q_b \cdot A_b = 908.5 \text{ psi} \cdot \left(\pi \cdot \frac{d^2}{4}\right) = 908.5 \text{ psi} \cdot \left(\pi \cdot \frac{12.75 \text{ in}^2}{4}\right) = 115{,}932 \text{ lb}$$

$$W_p = (\gamma_{steel} \cdot A_{steel} \cdot \text{Depth}) + (\gamma_{steel} \cdot A_{conc} \cdot \text{Depth})$$

$$W_p = (490 \text{ pcf} \cdot 0.03 \text{ ft}^2 \cdot 55 \text{ ft}) + (150 \text{ pcf} \cdot 0.85 \text{ ft}^2 \cdot 55 \text{ ft}) = 7{,}724 \text{ lbs}$$

Layer 3

$$Q_{total} = \Sigma Q_{side} + Q_{b,layer3} - W_p$$

$$Q_{total} = (19{,}064 + 45{,}713 + 58{,}170) \text{ lbs} + 115{,}932 \text{ lbs} - 7{,}724 \text{ lbs} = 642{,}563 \text{ lbs}$$

$Q_{total} = 642$ kips

Table 8. Summary of selected and calculated parameters.

Layer	L (in)	q_c (psi)	f_s (psi)	F_r	I_c	Q_{tn}	q_E (psi)	q_b (psi)	Q_{base} (lb)	f_p (psi)	Q_{side} (lb)	Q_{total} (kip)
1	48	3000	18	0.6	1.4	356	2984	N/A	N/A	9.9	19064	
2	588	500	12	2.6	2.9	11.7	468	N/A	N/A	21.1	457122	
3	240	5000	20	0.4	1.5	180	5000	908.5	115932	20.2	58170	
Total									115932		534355	642

REFERENCES

Abu-Farsakh, M.Y., Zhang, Z., Tumay, M. and Morvant, M. (2008). Computerized cone penetration test for soil classification. *Transportation Research Record* 2053, 47-64.

Agaiby, S.A. (2018). Advancements in the interpretation of seismic piezocone tests in clays and other geomaterials. PhD dissertation, School of Civil & Environmental Engineering, Georgia Institute of Technology, Atlanta, GA.

Agaiby, S.S. and Mayne, P.W. (2018). Interpretation of piezocone penetration and dissipation tests in sensitive Leda Clay at Gloucester Test Site. *Canadian Geotechnical Journal* (accepted for publication 08 March 2018), CGJ-2017-0388.

Amar, S., Baguelin, F., Canepa, Y., and Frank, R. (1998). New design rules for the bearing capacity of shallow foundations based on Menard PMT. *Geotechnical Site Characterization*, Vol. 2 (Proc. ISC-1, Atlanta), 727-733.

American Petroleum Institute (API) (1981). *Planning, designing and constructing fixed offshore platforms. Recommended practice*, API-RP2A, 17th edition. Washington, DC: API.

American Petroleum Institute (API) (1987). *Planning, designing and constructing fixed offshore platforms. Recommended practice*, API-RP2A, 18th edition. Washington, DC: API.

American Petroleum Institute (API) (1989). *Planning, designing and constructing fixed offshore platforms. Recommended practice*, API-RP2A, 19th edition. Washington, DC: API.

Andersen, K.H. and Stenhamar, P. (1982). Static plate loading tests on overconsolidated clay. *Journal of the Geotechnical Engineering Division*, ASCE, 108 (GT7): 919-934.

Basu, D. and Salgado, R. (2012). Load and resistance factor design of drilled shafts in sands. *Journal of Geotechnical & Geoenvironmental Engineering*, 138 (12): 1455-1469.

Berardi, R., Jamiolkowski, M. and Lancellotta, R. (1991). Settlement of shallow foundations in sands: selection of stiffness on the basis of penetration resistance. *Geotechnical Engineering Congress*, Vol. 1, 185-200 (Proc. GSP-27, Boulder), Reston, Virginia: ASCE.

Brand, E.W., Muktabhant, C., and Taechathummarak, A. (1972). Load tests on small foundations in soft clay, *Performance of Earth and Earth-Supported Structures*, Vol. 1, Part 2 903-928 (Proc. PC), ASCE, Reston, Virginia: ASCE.

Briaud, J.L. and Gibbens, R.M. (1999). Behavior of five large spread footings in sand. *Journal of Geotechnical & Geoenvironmental Engineering*, 125 (9): 787-797.

Briaud, J.L. (2007). Spread footings in sand: load-settlement curve approach. *Journal of Geotechnical & Geoenvironmental Engineering*, 133 (8): 905-920.

Brown, D.A., Turner, J.P., and Castelli, R.J. (2010). Drilled Shafts: Construction Procedures and LRFD Design Methods, Geotechnical Engineering Circular GEC 10, Report No. FHWA NHI-10-016, Washington DC: National Highway Institute, US DOT.

Burland, J. B. (1973). Shaft Friction of Piles in Clay -A Simple Fundamental Approach. *Ground Eng.,* 6(3), 30-42.

Cai, G., Liu, S. and Puppala, A. (2012). Reliability assessment of CPTu-based pile capacity predictions in soft clay deposits. *Engineering Geology*: 84-91.

Canadian Geotechnical Society (1992). *Canadian Foundation Engineering Manual*, Third Edition, Vancouver, British Columbia: BiTech Publishers.

Cerato A.B., and Lutenegger, A.J. (2007). Scale effects of shallow foundation bearing capacity on granular material, *Journal of Geotechnical & Geoenvironmental Engineering,* 133 (10): 1192-1201.

Chen, B.S-Y., and Mayne, P.W. (1996). Statistical relationships between piezocone measurements and stress history of clays. *Canadian Geotechnical. Journal*, 33 (3): 488-498.

Cho, W., and Finno, R.J. (2010_. Stress-strain responses of block samples of compressible Chicago glacial clays. *Journal of Geotechnical & Geoenvironmental Engineering*, 136 (1): 178-188.

Chung, S.F., Randolph, M.F., and Schneider, J.A. (2006). Effect of penetration rate on penetrometer resistance in clay. *Journal of Geotechnical & Geoenvironmental Engineering*, 132 (9): 1188-1196.

Clausen, C.J.F., Aas, P.M. and Karlsrud, K. (2005). Bearing capacity of driven piles in sand, the NGI approach. Frontiers in Offshore Geotechnics, (Proc. ISFOG, Perth), London: Taylor & Francis Group.

Consoli, N.C., Schnaid, F., and Milititsky, J. (1998). Interpretation of plate load tests on residual soil site. *Journal of Geotecnical. & Geoenvironmental Engingeering*, 124 (9): 857-867.

Dasenbrock, D.D. (2006). Assessment of pile capacity by static and dynamic methods to reconcile design predictions with observed performance. Proc. 54th Minnesota Geotechnical Engineering Conference, 95-108, edited by Labuz, J., Univ. of Minnesota, St. Paul.

DeBeer, E. and Martens, A. (1957). Method of computation of an upper limit for the influence of heterogeneity of sand layers on the settlement of bridges, 275-282, Proc. ICSMFE-4, Vol. 1, London: ICSMFE.

DeBeer, E.E. (1965). Bearing capacity and settlement of shallow foundations on sand. Proc. Symposium on Bearing Capacity and Settlement of Foundations, 15-33, Duke University: Durham, NC.

Decourt, L. (1999). Behavior of foundations under working load conditions. Proc. PCSMGE-11, Foz do Iguassu, Brazil, Vol. 4, 453-487.

Demers, D., and Leroueil, S. (2002). Evaluation of preconsolidation pressure and the overconsolidation ratio from piezocone tests of clay deposits in Quebec. *Canadian Geotechnical Journal*, 39 (1): 174-192.

Eslaamizaad, S. and Robertson, P.K. (1996). Cone penetration test to evaluate bearing capacity of foundations in sand, 429-438, Proc. CGCFG-49, Vol. 1, St. Johns, Newfoundland.

Eslami, A., Alimirzaei, M., Aflaki, E., and Molaabasi, H. (2017). Deltaic soil behavior classification using CPTu records. *Marine Georesources & Geotechnology* 35 (1): 62-79.

Eslami, A., and Gholami, M. (2005). Bearing capacity analysis of shallow foundations from CPT data, 1463-1466, Proc. ICSMGE- 16, Vol. 3 (Osaka), Millpress, Rotterdam.

Eslami, A., and Gholami, M. (2006). Analytical model for the ultimate bearing capacity of foundations from cone resistance. *Scientia Iranica*, 13 (3), 223-233.

Eslami, A., and Fellenius, B.H. (1997). Pile capacity by direct CPT and CPTu methods applied to 102 case histories. *Canadian Geotechnical Journal* 34 (6): 886-904.

Fellenius, B.H. (2009). *Basics of Foundation Design*, Vancouver: BiTech Publishers.

Fellenius, B.H., and Altaee, A. (1994). Stress and settlement of footings in sand. *Vertical and Horizontal Deformations of Foundations and Embankments*, 2 1760-1773.

Fellenius, B.H., and Eslami, A. (2000). Soil profile interpreted from CPTu data. Proc. Geotechnical Engineering Conference: Year 2000 Geotechnics, Asian Inst. of Technology, Bangkok, Thailand. Available from: www.fellenius.net

Finno, R. J., and Chung, C. K. (1992). Stress-strain-strength responses of compressible Chicago glacial clays. *Journal of Geotechnical Engineering* 118 (10): 1607–1625.

Fleming, K., Weltman, A., Randolph, M. and Elson, K. (2009). Piling Engineering, Third Edition, London: Taylor & Francis Group.

Frank, R., and Magnan, J-P. (1995). Cone penetration testing in France: national report. Proceedings, International Symposium on Cone Penetration Testing, 3 (CPT'95, Linköping), *Swedish Geotechnical Society Report* 3(95): 147-156.

Gavin, K., Adekunte, A., and O'Kelly, B. (2009). A field investigation of vertical footing response on sand. *Geotechnical Engineering*, 162, 257-267.

Hegazy, Y.A. (1998). Delineating geostratigraphy by cluster analysis of piezocone data. PhD dissertation, School of Civil & Environmental Engineering, Georgia Institute of Technology, Atlanta, GA.

Holtz, R.D., Kovacs, W.D. and Sheehan, T.C. (2011). *An Introduction to Geotechnical Engineering*, 2nd Edition, London: Pearson Publishing.

Hunt, C.E., Pestana, J.M., Bray, J.D., and Riemer, M. (2002). Effect of pile driving on static and dynamic properties of soft clay. *Journal of Geotechnical & Geoenvironmental Engineering* 128 (1): 13-24.

Jamiolkowski, M., Ladd, C.C., Germaine, J.T., and Lancellotta, R. (1985). New developments in field and lab testing of soils. *Proc. ICSMFE-11*, 1, 57-154.

Jardine, R., Chow, F., Overy, R., and Standing, J. (2005). ICP design methods for driven piles in sands and clays. London: Thomas Telford Publishing.

Jardine, R.J., Lehane, B.M., Smith, P., and Gildea, P. (1995). Vertical loading experiments on rigid pad foundations at Bothkennar. *Geotechnique*, 45 (4): 573-597.

Karlsrud, K. (2012). Prediction of load-displacement behavior and capacity of axially-loaded piles in clay based on analyses and interpretation of pile load test results. PhD Dissertation, Norwegian Univ. Science & Technology, Trondheim, Norway.

Karlsrud, K., Clausen, C.J.F., and Aas, P.M. (2005). Bearing capacity of driven piles in clay: the NGI approach. Frontiers in Offshore Geotechnics (Proc. ISFOG, Perth), London: Taylor & Francis.

Karlsrud, K., Lunne, T., Kort, D.A. and Strandvik, S. (2001). CPTU correlations for clays. *Proc. 16th ICSMGE*, 2, 683-702.

Kimura, T., Kusakabe, O., and Saitoh, K. (1985). Geotechnical model tests of bearing capacity problems in a centrifuge. *Geotechnique* 35 (1): 33-45.

Knappett, J.A., and Craig, R.F. (2012). Craig's Soil Mechanics, 8th Edition, London: Spon Press, Taylor & Francis.

Kolk, H.J., and Velde, E.V.D. (1996). A reliable method to determine friction capacity of piles driven into clays. Paper No. 7993, Proc. Offshore Technology Conference, Houston.

Kolk, H.J., Baaijens, A.E., and Senders, M. (2005). *Design criteria for pipe piles in silica sands. Frontiers in Offshore Geotechnics*, (Proc. ISFOG, Perth), London: Taylor & Francis Group.

Kulhawy, F.H. (2004). On the axial behavior of drilled shafts. *Geosupport 2004,* 1-18.

Kulhawy, F.H. and Jackson, C.S. (1989). *Foundation Engineering: Current Principles & Practices*, 2 (GSP 22), Reston, VA: ASCE.

Kulhawy, F.H., and Mayne, P.W. (1990). Manual for Estimating Soil Properties for Foundation Design. EPRI Report EL-6800, Electric Power Research Institute, Palo Alto, 306 page. Download from: www.epri.com

Kulhawy, F.H., Trautmann, C.H., Beech, J.F., O'Rourke, T.D., and McGuire, W. (1983). Transmission Line Structure Foundations for Uplift-Compression Loading. *Report EL-2870*, Palo Alto, CA: Electric Power Research Institute. www.epri.com

Ku, T., and Mayne, P.W. (2015). In-situ lateral stress coefficient (K_0) from shear wave velocity measurements in soils. *Journal of Geotechnical & Geoenvironmental Engineering,* 141 (12) 10.1061/(ASCE) GT.1943-5606.0001354.

Ladd, C.C., and DeGroot, D.J. (2003). Recommended practice for soft ground site characterization. *Soil & Rock America 2003*, 3-57.

Larsson, R. (1997). *Investigations and Load Tests in Silty Soils*. SGI Report R-54, Linköping: Swedish Geotechnical Institute.

Larsson, R. (2001). *Investigations and Load Tests in Clay Till*. SGI Report R-59, Linköping: Swedish Geotechnical Institute.

Lee, J., and Salgado, R. (2005). Estimation of bearing capacity of circular footings on sands based on cone penetration tests. *Journal of Geotechnical & Geoenvironmental Engineering*, 131 (4): 442-452.

Lehane, B.M. (2003). Vertically loaded shallow foundation on soft clayey silt. *Geotechnical Engineering*, 156 (1), Thomas Telford, London: 17-26.

Lehane, B.M. (2013). Relating foundation capacity in sands to CPT q_c. Geotechnical & Geophysical Site Characterization, 1, London: Taylor & Francis Group.

Lehane, B.M., Doherty, J.P. and Schneider, J.A. (2008). Settlement prediction for footings on sand. *Deformational Characteristics of Geomaterials* (IS-Atlanta), 1, Rotterdam: Millpress.

Lehane, B.M., Li, Y., and Williams, R. (2013). Shaft capacity of displacement piles in clay using the CPT. *Journal of Geotechnical & Geoenvironmental Engineering,* 139 (2): 253-266.

Lehane, B.M., Schneider, J.A., and Xu, X. (2005). The UWA-05 method for prediction of axial capacity of driven piles in sand. Frontiers in Offshore Geotechnics (Proc. ISFOG, Perth), London: Taylor & Francis.

Low, H.E., Lunne, T., Andersen, K.H., Sjursen, M.A., Li, X. and Randolph, M.F. 2010. Estimation of intact and remoulded undrained shear strengths from penetration tests in soft clays. *Geotechnique,* 60 (11): 843-859.

Lunne, T., Robertson, P.K., and Powell, J.J.M. (1997). *Cone Penetration Testing in Geotechnical Practice*, London: Routledge/Blackie Academic.

Lutenegger, A.J., and DeGroot, D.J. (1995). Settlement of Shallow Foundations on Granular Soils. Report Contract 6332 Task Order 4 submitted to Massachusetts Highway Dept. by University of Mass-Amherst, Amherst, MA.

Lutenegger A.J., and Adams M.T. (2003). Characteristic load-settlement behavior of shallow foundations, Proc. *FONDSUP*, 2, 381-392.

Mase, T., and Hashiguchi, K. (2009). Numerical analysis of footing settlement problem by subloading surface model. *Soils & Foundations*, 49 (2): 207-220.

Mayne, P.W. (1987). Determining preconsolidation stress and penetration pore pressures from DMT contact pressures. *Geotechnical Testing Journal*, 10(3), 146-150.

Mayne, P.W. (1991). Determination of OCR in Clays by Piezocone Tests Using Cavity Expansion and Critical State Concepts. *Soils and Foundations*, 31 (2): 65-76.

Mayne, P.W. (2007). *NCHRP Synthesis 368 on Cone Penetration Test*. Washington, D.C., Transportation Research Board, National Academies Press. www.trb.org

Mayne, P.W. (2009). *Geoengineering Design Using the Cone Penetration Test*. Richmond, BC, Canada: ConeTec Inc.

Mayne, P.W. (2014). Keynote: Interpretation of geotechnical parameters from seismic piezocone tests. *Proceedings, 3rd Intl. Symp. on Cone Penetration Testing*, 47-73.

Mayne, P.W. (2016). Evaluating effective stress parameters and undrained shear strengths of soft-firm clays from CPT and DMT. *Australian Geomechanics Journal*, 51 (4): 27-55.

Mayne, P.W. (2017). Stress history of soils from cone penetration tests. 34th Manual Rocha Lecture, Soils & Rocks, Vol. 40 (3), Saö Paulo: ABMS.

Mayne, P.W., Christopher, B., Berg, R., and DeJong, J. (2002). Subsurface Investigations -Geotechnical Site Characterization. Publication No. FHWA-NHI-01-031, Washington, D.C., National Highway Institute, Federal Highway Administration.

Mayne, P.W., Coop, M.R., Springman, S., Huang, A-B., and Zornberg, J. (2009). Geomaterial Behavior and Testing. Proc. 17th Intl. Conf. Soil Mechanics & Geotechnical Engineering, 4, Rotterdam: Millpress/IOS Press.

Mayne, P.W., and Illingworth, F. (2010). Direct CPT method for footings on sand using a database approach. *Proc. ISCPT-2*, 3, 315-322.

Mayne, P.W., and Niazi, F. (2017). Recent developments and applications in field investigations for deep foundations. *Proceedings, 3rd Bolivian Conference on Deep Foundations*, 1, 141-160.

Mayne, P.W., Peuchen, J., and Baltoukas, D. (2015). Piezocone evaluation of undrained strength in soft to firm offshore clays. *Frontiers in Offshore Geotechnics III*, 2, 1091-1096.

Mayne, P.W., and Poulos, H.G. (1999). Approximate displacement influence factors for elastic shallow foundation systems. ASCE *Journal of Geotechnical & Geoenvironmental Engineering*, 125 (6): 453-460.

Mayne, P.W., Uzielli, M. and Illingworth, F. (2012). Shallow footing response on sands using a direct method based on cone penetration tests. *Full Scale Testing and Foundation Design* (GSP 227), Reston, Virginia: ASCE.

Mayne, P.W., and Woeller, D.J. (2014). Direct CPT method for footings on sands, silts, and clays. *Geocharacterization for Modeling and Sustainability* (GSP 234), 1983-1997.

McClelland, B. (1974). Design of Deep Penetration Piles for Ocean Structures. *Journal Geot. Eng. Div.,* 100(GT7), 705-747.

Mesri, G. (1975). Discussion on new design procedure for stability of soft clays. ASCE *Journal of the Geotechnical Engineering Division*, 101(GT4), pp. 409-412.

Meyerhof, G.G. (1956). Penetration tests and bearing capacity of cohesionless soils. *Journal of Soil Mechanics & Foundations Division*, 82 (SM1): 1-19.

Meyerhof, G.G. (1974). General Report: Penetration testing outside Europe, Proceedings ESOPT-1, Vol. 2.1, Swedish Geotechnical Society, Stockholm.

Meyerhof, G.G. (1976). Bearing capacity and settlement of pile foundations. *Journal of Geotechnical Engineering Division*, 102(3), 197-228.

Missiaen, T., Verhegge, J., Heirman, K., and Crobe, P. (2015). Potential of cone penetrating testing for mapping deeply buried palaeolandscapes in the context of archaeological surveys in polder areas. *Journal of Archaeological Science,* 55, 174-187.

Mlynarek, Z., Wierzbicki, J., Goglik, S., and Bogucki, M. (2014). Shear strength and deformation parameters of peat and gyttja from CPTu, DMT and VST. Proceedings 5th International Workshop on CPTu and DMT in soft clays and organic soils, 193-210, Poznan, Poland, Polish Committee on Geotechnics, Menard Polska, Tensar Internationa.

Nejaim, P.F., Jannuzzi, G.M.F., and Danziger, F.A.B. (2016). Soil behavior type of the Sarapuí II test site. *Geotechnical & Geophysical Site Characterization*, 5, 1009-1014.

Niazi, F.S., and Mayne, P.W. (2013). Cone penetration test based direct methods for evaluating static axial capacity of single piles. *Geotechnical and Geological Engineering,* 31 (4), 979-1009.

Niazi, F.S., and Mayne, P.W. (2015). Enhanced Unicone expressions for axial pile capacity evaluation from piezocone tests, *Proc. International Foundations Conference & Equipment Expo*, Reston/VA: ASCE.

Niazi, F.S., and Mayne, P.W. (2016). CPTu-based enhanced UniCone method for pile capacity. *Engineering Geology,* 212, 21-34.

Nowacki, F., Karlsrud, K., and Sparrevik, P. (1996). Comparison of recent tests on OC clay and implications for design. Large Scale Pile Tests in Clay, London: Thomas Telford.

O'Neill, M.W. (2001). Side resistance in piles and drilled shafts. *Journal of Geotechnical & Geoenvironmental Engineering,* 127 (1): 3-16.

Ouyang, Z., and Mayne, P.W. (2018). Effective friction angle of clays and silts from piezocone. *Canadian Geotechnical Journal*. in press. doi.org/10.1139/cgj-2017-0451.

Paikowsky, S.G., Canniff, M.C., Lesny, K., Kisse, A., Amatya, S., and Muganga, R. (2010). LRFD *Design and Construction of Shallow Foundations for Highway Bridge Structures*. NCHRP Report 651, Washington, DC: National Cooperative Highway Research Program, Transportation Research Board.

Pestana, J.M., Hunt, C.E., and Bray, J.D. (2002). Soil deformation and excess pore pressure filed around a closed-ended pile. *Journal of Geotechnical & Geoenvironmental Engineering,* 128 (1), 1-12.

Poulos, H.G., and Davis, E.H. (1974). *Elastic Solutions for Soil and Rock Mechanics*. New York: Wiley & Sons.

Poulos, H.G., and Davis, E. (1980). *Pile Foundation Analysis & Design*, New York: John Wiley & Sons.

Powell, J.J.M., and Lunne, T. (2005). Use of CPTU data in clays and fine-grained soils. *Studia Geotechnica et Mechanica*, XXVII(3), 29-66.

Randolph, M.F. (2003). Rankine Lecture: Science and empiricism in pile foundation design. *Geotechnique,* 53 (10), 847-875.

Robertson, P.K. (1990, 1991). Soil classification using the cone penetration test. *Canadian Geotechnical Journal*, 27 (1), 151-158. Closure 28 (1), 176-178.

Robertson, P.K. (1991). Estimation of foundation settlements in sand from CPT. *Geotechnical Engineering Congress*, 2, Reston, Virginia: ASCE.

Robertson, P.K. (2009). Cone penetration testing: a unified approach. *Canadian Geotechnical J.,* 46 (11), 1337-1355.

Robertson, P.K. (2009a). Performance based earthquake design using the CPT. Keynote Lecture, *International Conference on Performance-Based Design in Earthquake Geotechnical Engineering*, IS Tokyo, Tsukuba, Japan.

Robertson, P.K. (2009b). Interpretation of cone penetration tests: a unified approach. *Canadian Geotechnical Journal*, 46 (11), 1337-1355.

Robertson, P.K., and Cabal, K.L. (2007). *Guide to cone penetration testing.* Second Edition. Signal Hill, California: Gregg In-Situ.

Robertson, P.K., and Cabal, K.L. (2015). *Guide to Cone Penetration Testing for Geotechnical Engineering*, 6th Edition, Signal Hill, California: Gregg Drilling & Testing, Inc.

Schmertmann, J.H. (1970). Static cone to compute static settlement over sand. *Journal of the Soil Mechanics and Foundations Division*, 95 (SM3), 1011-1043.

Schmertmann, J.H. (1978). *Guidelines for cone penetration test: performance and design.* Report FHWA-TS-78-209, Washington, DC: Federal Highway Administration.

Schnaid, F., Wood, W.R., Smith, A.K.C., and Jubb, P. (1993). Investigation of bearing capacity and settlements of soft clay deposits at Shellhaven. *Predictive Soil Mechanics*, London: Thomas Telford.

Schneider, J.A., Xu, X., and Lehane, B.M. (2008). Database assessment of CPT-based design methods for axial capacity of driven piles in siliceous sands. *J. Geotechnical and Geoenvironmental Engineering,* 134 (9), 1227-1244.

Semple, D. (1980). *Recent Developments in the Design & Construction of Piles*, London: Institution of Civil Engineers.

Senneset, K., Sandven, R., & Janbu, N. (1989). Evaluation of soil parameters from piezocone tests. In-Situ Testing of Soil Properties for Transportation, *Transportation Research Record,* 1235: 24-37.

Shahri, A.A., Melehmir, A., and Juhlin, C. (2015). Soil classification analysis based on piezocone penetration test data. *Engineering Geology,* 189: 32-47.

Stuedlein, A.W., and Holtz, R.D. (2010). Undrained displacement behavior of spread footings in clay, *The Art of Foundation Engineering Practice,* GSP 198, Reston, Virginia: ASCE.

Takesue, K., Sasao, H., and Matsumoto, T. (1998). Correlation between ultimate pile skin friction and CPT data. *Geotechnical Site Characterization*, 2, 1177–1182.

Tand, K.E., Funegard, E.G., and Briaud, J-L. (1986). Bearing capacity of footings on clay: CPT method. *Use of In-Situ Tests in Geotechnical Engineering*, GSP 6, 1017-1033.

Tand, K.E., Warden, P.E., and Funegård, E.G. (1995). Predicted-measured bearing capacity of shallow footings on sand. *PISCPT*, 2, 589-594.

Thomas, D. (1968). Deep soundings test results and the settlement of spread footings on normally consolidated sands. *Geotechnique*, 18 (2), 472-488.

Tomlinson, M.J. (1957). The adhesion of piles driven into clay soils. *Proc. 4th Intl. Conf. on Soil Mechanics and Foundation Engineering*, 2, 66-71.

Tomlinson, M.J. (1986). *Foundation Design & Construction*. London: Longman Scientific.

Tomlinson, M.J. (1987). *Pile Design and Construction Practice*, London: Viewpoint Publication.

Trofimenkov, J.G. (1974). Penetration testing in the USSR. *Proceedings ESOPT-1*, 1, 147-154.

Tumay, M.T., Hatipkarasulu, Y., Marx, E.R., and Cotton, B. (2013). CPT/PCPT-based organic material profiling. *Proc. 18th Intl. Conf. on Soil Mechanics & Geotechnical Engineering*, Paris: 633-636.

Uzielli, M., and Mayne, P.W. (2011). Statistical characterization and stochastic simulation of load-displacement behavior of shallow footings. Proc*. Georisk 2011: Geotechnical Risk Management & Assessment* (GSP 224), 672-679.

Uzielli, M., and Mayne, P.W. (2012). Load-displacement uncertainty of vertically-loaded shallow footings on sands and effects on probabilistic settlement estimation. *Georisk: Assessment and Management of Risk for Engineered Systems and GeoHazards*. 6 (1), 50-69.

Valsson, S.M. (2016). Detecting quick clay with CPTu. Proceedings, *17th Nordic Geotechnical Meeting*, Reykajavik, Iceland: Challenges in Nordic Geotechnics.

Van Dijk, B.F.J., and Kolk, H.J. (2011). CPT-based design method for axial capacity of offshore piles in clay. *Frontiers in Offshore Geotechnics II*, 555-560.

Vesić, A.S. (1975). Bearing capacity of shallow foundations. *Foundation Engineering Handbook*, New York: Van Nostrand Reinhold Publishers.

Vesic, A.S. (1977). *NCHRP Synthesis of Highway Practice 42: Design of Pile Foundations*, Washington, DC: Transportation Research Board.

Yu, F., and Yang, J. (2012). Base capacity of open-ended steel pipe piles in sand. *J. Geotechnical and Geoenvironmental Engineering*, 138 (9), 1116-1128.

Zawrzykraj, P., Rydelek, P., and Bakowska, A. (2017). Geoengineering properties of Eemian peats from Radsymin (central Poland) in the light of static cone penetration and dilatometer tests. *Engineering Geology,* 226, 290-300.

APPENDIX A

List of Figures

List of Tables

A1. INTERPRETATION OF SOIL PARAMETERS FROM CONE PENETRATION TESTS

A1.1 Introduction

Geotechnical site characterization is an important first step towards the evaluation of subsurface conditions and determination of soil layering, geomaterial classification, and the evaluation of soil engineering parameters for the analysis and design of foundations, retaining walls, tunnels, excavations, embankments, and slope stability. Increasing use of the electronic cone penetrometer in highway applications is prominent in the USA because the results are obtained much faster and less expensive than traditional methods that rely on rotary drilling, augering, sampling, and laboratory testing. Moreover, the cone penetration test (CPT) provides at least three independent and continuous readings on soil behavior that are digitally recorded and fully available at the end of the sounding. As such, the reliable and consistent interpretation of CPT data is important, since civil engineering works will best realize the efficiency and economy of this technology in constructed facilities for county, state, and interstate projects.

A1.1.1 Cone Penetration Testing

The cone penetrometer is an electronically-instrumented steel probe that is vertically pushed into the ground at constant rate of 20 mm/s (0.8 in/sec) using a hydraulic system. The penetrometer is outfitted with load cells, pressure transducers, and inclinometers that measure at least three readings continuously with depth: (a) cone tip resistance, q_t, (b) sleeve friction, f_s, and (c) porewater pressure, u_2. With the latter reading, the device is called a piezocone, thus the designation CPTu is used to indicate porewater pressure. Additional sensors are available that can be used to measure: inclination, resistivity, pH, temperature, shear wave velocity, and other readings, if desired.

Figure A1 shows a schematic rendering of the cone penetration test that is performed in the field per ASTM D 5778 procedures. The hydraulic system is nominally rated at 180 kN (20 tons) capacity and often mounted on a truck but can also be positioned on tracked vehicles or

anchored frames. Figure A2 shows a MnDOT cone truck that uses the full dead weight of the rig for the hydraulic reaction forces which are applied at the center of the vehicle. The cab is enclosed so that soundings may proceed during inclement weather and the data acquisition system and operator are protected.

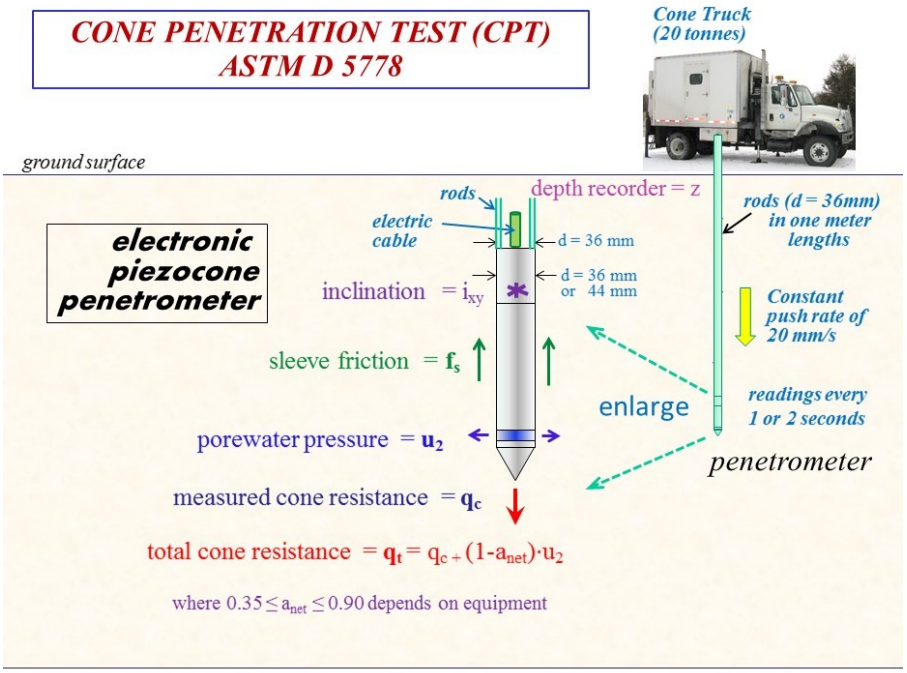

Figure A1. Setup and procedures for cone penetration testing (CPT).

Figure A2. CPT truck-mounted rig used by MnDOT.

A representative sounding taken at the I-35 test site just northeast of Saint Paul is presented in Figure A3. Here the separate profiles of q_t, f_s, and u_2 with depth are shown in side-by-side plots. In the last graph, the hydrostatic porewater pressure (u_o) due to the groundwater table is indicated by the blue dashed line.

These readings are used to interpret the soil layers, types, and properties of the ground, as discussed in the following sections.

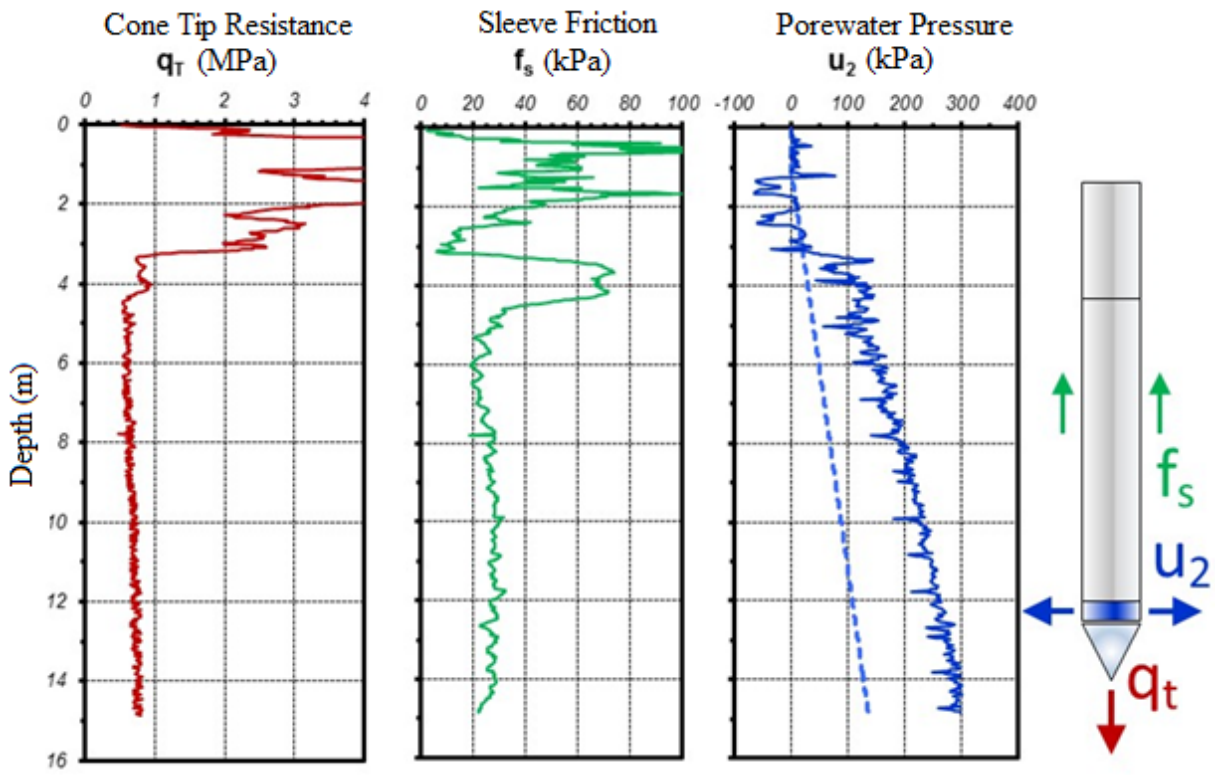

Figure A3. Representative CPT sounding at I-35 test site northeast of St. Paul, MN showing profiles of: (a) cone resistance, (b) sleeve friction, and (c) penetration porewater pressures.

A1.1.2 Soil Parameter Interpretation

A variety of soil engineering parameters can be interpreted from CPT results on the basis of theoretical frameworks, analytical models, or numerical simulations, otherwise by empirical methods based on correlations and statistics of databases. Figure A4 shows a conceptual utilization of the readings from the CPT for interpretation of geostratigraphy, compressibility, flow characteristics, and stress-strain-strength behavior of soils.

Table A1 lists a selection of geoparameters that have been addressed for these purposes. The most common or useful relationships will be discussed in subsequent sections and reference is made to other sources (Lunne et al. 1997; Mayne 2007; Robertson & Cabal 2015) for additional details.

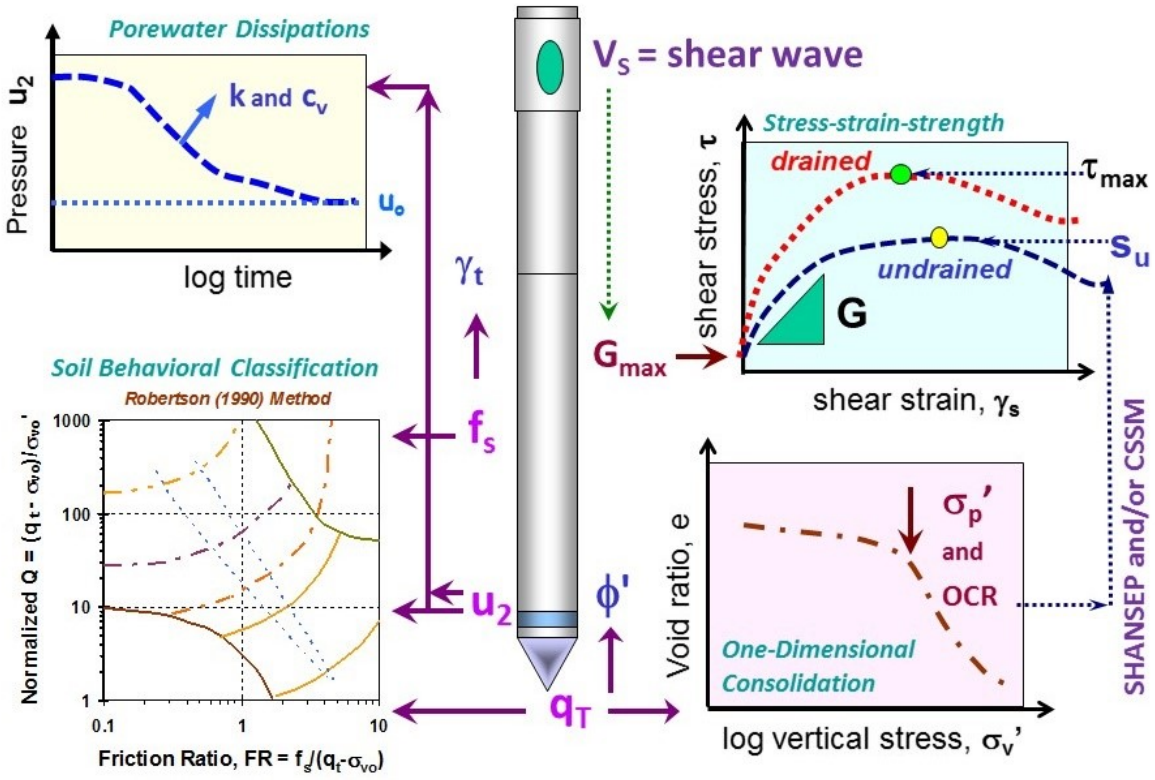

Figure A4. Conceptual post-processing of CPT results for geoparameter evaluation.

Table A1. List of common geoparameters interpreted from CPT data.

Symbol	Parameter	Remarks / Notes
SBT	Soil behavior type (SBT)	
I_c	CPT material index	
γ_t	Unit weight	
ρ_t	Mass Density	
σ_{vo}	Overburden stress	
u_0	Hydrostatic pressure	

σ_{vo}'	Effective stress

Table A1. Continued

Symbol	Parameter	Remarks / Notes
σ_p'	Preconsolidation stress (or Effective Yield Stress)	$\sigma_p' = 0.33 (q_{net})^{m'}$ where m' = fctn (I_c) where stresses are in kPa
YSR	Yield stress ratio	YSR = σ_p'/σ_{vo}' (formerly OCR)
c'	Effective cohesion intercept	
φ'	Effective friction angle	
s_u	Undrained shear strength	
D'	Constrained modulus	
G_0	Small-strain modulus	
G	Shear modulus	
E	Young's modulus	
c_{vh}	Coefficient of consolidation	
K'	Bulk modulus	

K_0 Lateral stress coefficient

k Hydraulic conductivity

LI Liquefaction index

A1.2. Geostratigraphy and Soil Behavioral Type (SBT)

In routine CPT, soil samples are not normally taken and thus the measured stress, friction, and/or porewater pressure readings are used to infer the types of soils. This can be accomplished using three basic approaches:

a. "Rules of Thumb" or approximate guidelines for a quick visual assessment.

b. Soil Behavioral Type (SBT) Charts that are based on either the three readings (q_t, f_s, u_2), net readings, including net cone resistance ($q_{net} = (q_t - \sigma_{vo})$, effective cone resistance ($q_E = q_t - u_2$), friction ratio (R_f % = $100 \cdot f_s/q_t$), and excess porewater pressures; or using normalized CPT readings, such as Q, F, B_q, or U*;

c. Probabilistic methods where the CPT readings have been calibrated from lab tests on recovered soil samples (e.g., Tumay et al. 2013).

A1.2.1 Approximate Rules of Thumb

The approximate rules of thumb provide simple guidelines for soil type and suggest that sands are identified when $q_t > 5$ MPa and $u_2 \approx u_0$, whereas intact clays are prevalent when $q_t < 5$ MPa and $u_2 > u_0$ (Mayne et al. 2002). The magnitude of porewater pressures reflects the consistency of the intact clay, such that: soft ($u_2 \approx 2 \cdot u_0$), firm ($u_2 \approx 4 \cdot u_0$), stiff ($u_2 \approx 8 \cdot u_0$), and hard ($u_2 \approx 20 \cdot u_0$). However, for fissured overconsolidated clays, the measured porewater pressures are less than hydrostatic, in fact, often negative: $u_2 < 0$. On land, negative porewater pressure readings at the shoulder filter element of the piezocone should be greater than -1 bar; i.e., $u_2 > -100$ kPa (-14.7 psi). Also, for clean sands, the friction ratio (FR = $100 \cdot f_s/q_t < 1\%$) while for insensitive clays (FR > 4%).

Figure A5 presents a 36-m deep piezocone sounding from the MnDOT Wakota Bridge site which crosses the Mississippi River at I-494 (Dasenbrock 2006). The q_t and u_2 readings have been annotated using the aforementioned "rules of thumb", indicating the predominance of sands at this site. As noted, there are five interbedded clay layers evident at depths of 1 m, 3-4 m, 7 - 12 m, 17 m, and 22-27 m.

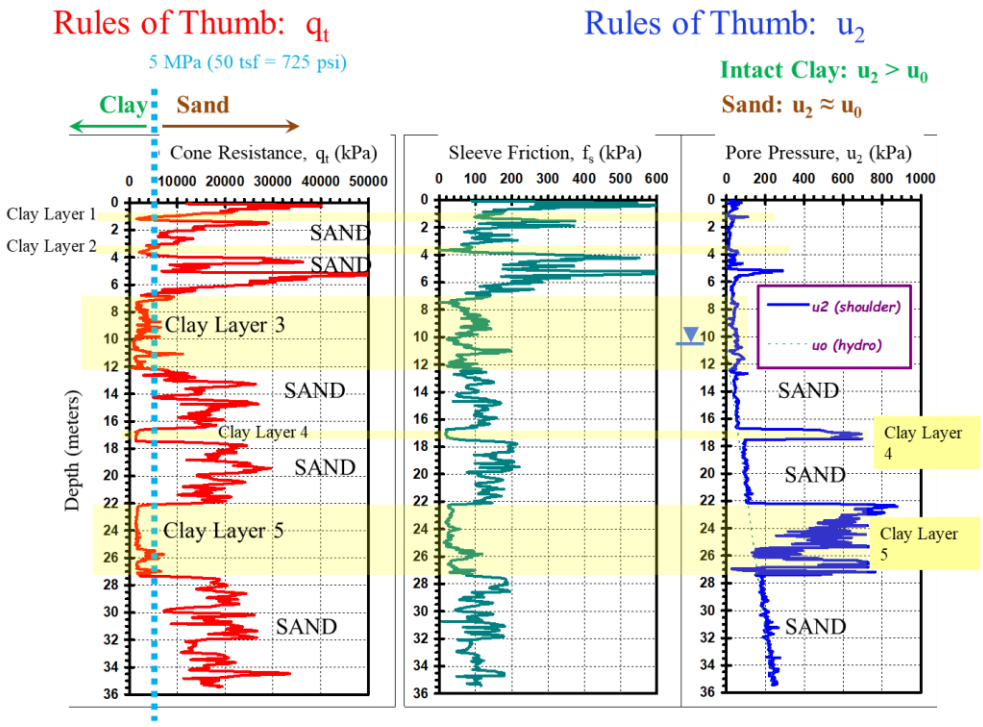

Figure A5. Interpretation of soil types from CPT data taken from the Wakota Bridge on I-494 using approximate "rules of thumb."

A1.2.2 Soil Behavioral Type Charts

The most common approach for identification of soil types is based on soil behavioral charts. Reviews of several chart methods are provided elsewhere (Kulhawy & Mayne 1990; Fellenius & Eslami 2000; Shahri et al. 2015). Current popularity favors the 9-zone classification system to evaluate soil behavioral type (SBT) that uses normalized piezocone readings (Robertson 1990, 1991; Lunne et al. 1997):

(a) normalized tip resistance: $$Q = \frac{(q_t - \sigma_{vo})}{\sigma'_{vo}}$$ A1.1

(b) normalized sleeve friction: $$F(\%) = \frac{100 \cdot f_s}{(q_t - \sigma_{vo})}$$ A1.2

(c) normalized porewater pressure: $$B_q = \frac{(u_2 - u_0)}{(q_t - \sigma_{vo})}$$ A1.3

While the Q-F-B_q classification is a three-dimensional plot, it is often presented as a set of two-dimensional plots, specifically: Q vs. F and Q vs. B_q, as shown in Figure A6. Data are grouped according to layers and can be superimposed to identify their association with the nine soil behavioral types. All indirect CPT soil classification approaches should be cross-checked and verified for a particular geologic setting and local geotechnical conditions before routine use in practice.

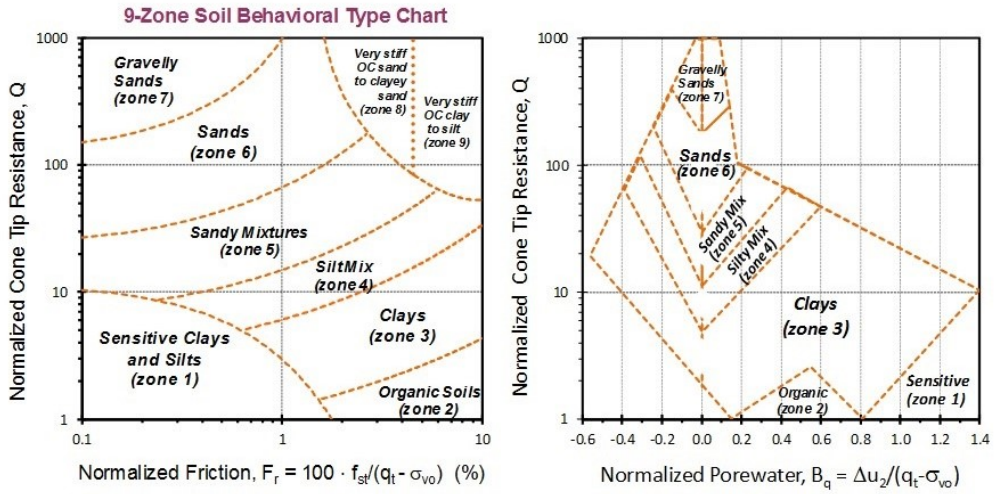

Figure A6. Nine-zone soil behavioral type charts: (a) normalized cone resistance vs. normalized sleeve friction; (b) normalized cone resistance vs. normalized porewater pressure parameters (adapted after Robertson 1991; Lunne et al. 1997).

The development of a CPT material index (I_c) has been found advantageous in the initial screening of soil types and helps to organize the sounding into their respective SBT zones of similar soil response. In this case, the CPT index is found from (Robertson 2009):

$$I_c = \sqrt{(3.47 - \log Q_{tn})^2 + (1.22 + \log F_r)^2} \quad \text{A2}$$

where Q_{tn} = modfied stress-normalized net cone resistance, given by:

$$Q = \frac{(q_t - \sigma_{vo})/\sigma_{atm}}{(\sigma'_{vo}/\sigma_{atm})^n} \quad \text{A3.1}$$

where σ_{atm} = reference stress equal to atmospheric pressure (1 atm ≈ 1 bar = 100 kPa ≈ 1 tsf ≈ 14.7 psi). The exponent n is soil-type dependent: n = 1 (clays); n ≈ 0.75 (silts); and n ≈ 0.5 (sands). If units of bars are used, then Q_{tn} (units of bars) is simply:

$$Q = \frac{(q_t - \sigma_{vo})}{(\sigma'_{vo})^n} \quad \text{A3.2}$$

The operational value of exponent n is found by iteration. Initially, an exponent n = 1 is used to calculate the starting value of I_c (i.e., $Q_{tn} = Q$) and then the exponent is upgraded to:

$$n = 0.381 \cdot I_c + 0.05\left(\frac{\sigma'_{vo}}{\sigma_{atm}}\right) - 0.15 \leq 1.0 \quad \text{A4}$$

Then the index I_c is recalculated. Iteration converges quickly and generally only 3 cycles are needed to secure the operational I_c at each depth. The soil zones and associated I_c values are detailed in Figure A7.

The sensitive soils of zone 1 can be screened using the following expression:

Zone 1: $$Q_{tn} < 12exp(-1.4 \cdot F_r)$$ A5

If any soil layers are found within zone 1 (sensitive soils), then caution should be exercised as these structured clays are prone to instability, collapses, and difficulties in construction and performance. Another indicator of zone 1 sensitive soils is when the normalized porewater parameter $B_q > 0.8$. When these criteria are evident, the geoengineer should consult with senior geotechnical personnel or the chief engineer for guidance.

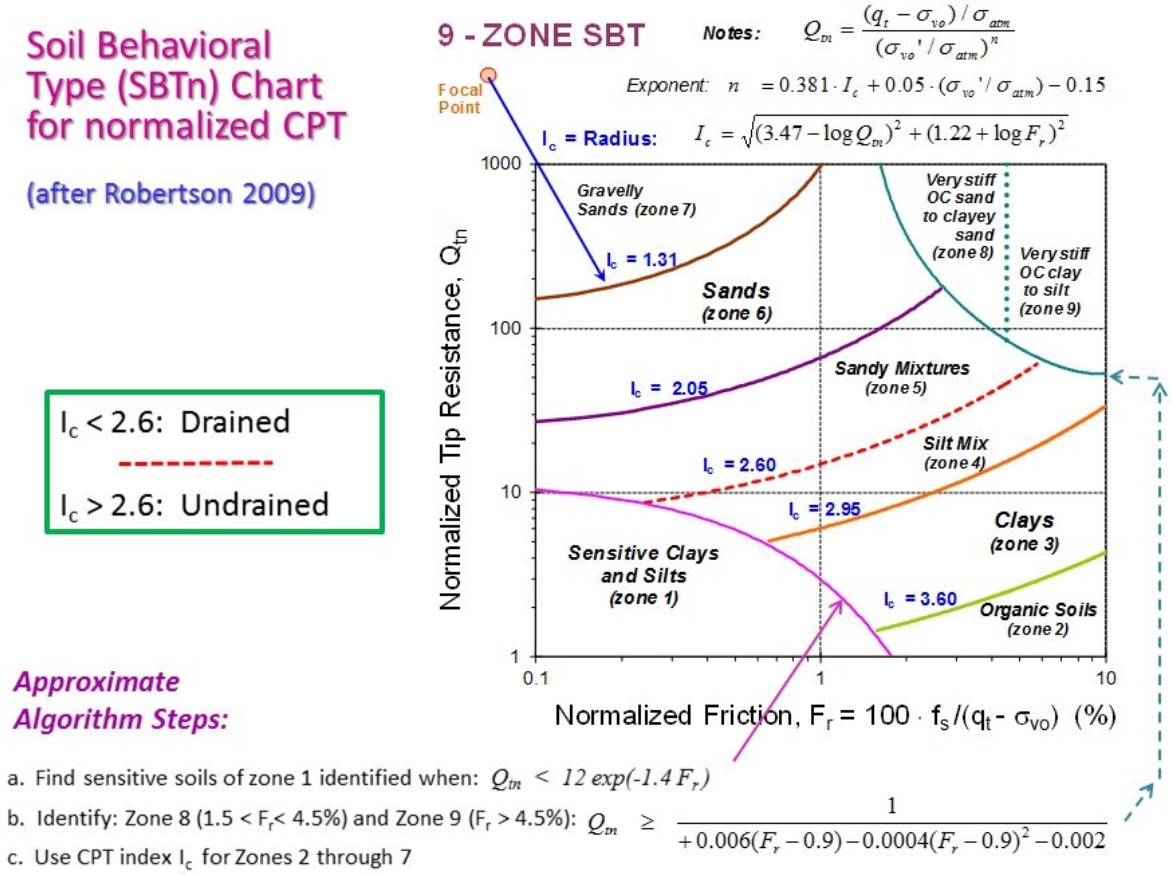

Figure A7. Delineation of soil behavioral type zones using CPT material index, I_c.

Stiff overconsolidated clayey sands and sandy clays soils of zone 8 (1.5% < F_r < 4.5%) and zone 9 (F_r > 4.5%) can be identified from the following criterion:

Zones 8 and 9:
$$Q_{tn} > \frac{1}{0.005(F_r - 1) - 0.0003(F_r - 1)^2 - 0.002} \quad \text{A6}$$

The remaining soil types are identified by the CPT material index: Zone 2 (organic clayey soils: $I_c \geq 3.60$); Zone 3 (clays to silty clays: $2.95 \leq I_c < 3.60$); Zone 4 (silt mixtures: $2.60 \leq I_c < 2.95$); Zone 5 (sand mixtures: $2.05 \leq I_c < 2.60$); Zone 6 (clean sands: $1.31 \leq I_c < 2.05$); and Zone 7 (gravelly to dense sands: $I_c \leq 1.31$).

The red dashed line at $I_c = 2.60$ represents an approximate boundary separating *drained* ($I_c < 2.60$) from undrained behavior ($I_c > 2.60$).

Once the specific zone has been assigned to a layer, a visual representation can be made to show either the zone number or colorization so that the predominant layers and soil types can be realized.

A1.2.3 Probabilistic Soil Types from CPT

The inference of soil type has been addressed using probabilistic methods, as discussed by Abu-Farshakh et al. (2008) and Tumay et al. (2013). Here, the CPT readings can be post-processed to provide the percentage of sand, silt, and clay components with depth. The output is consistent and compatible with the current MnDOT soil classification chart (Figure A8) which is similar in content to that used by the USDA.

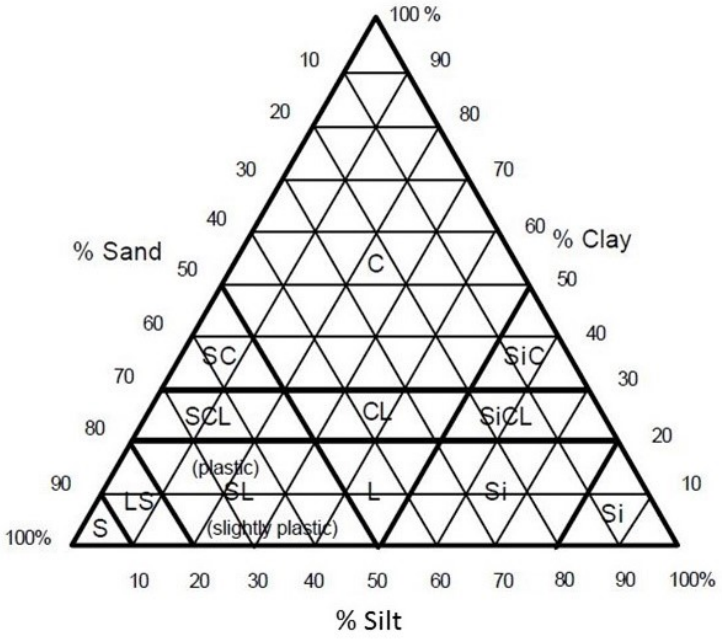

Figure A8. Chart for soil classification system by MnDOT.

A1.3. Identifying Soft Organic Soils

The identification of soil type using cone penetration tests (CPT) is usually done on the basis of empirical soil behavioral type (SBT) charts that use the measured readings (q_t, f_s, and/or u_2). While there at least 25 different sets of charts available (i.e. Hegazy, 1998; Eslami et al., 2017; Valsson, 2016), one of the most widely used and popular is the 9-zone SBT system that uses three normalized cone readings: Q_{tn}, F_r, and B_q (Robertson & Cabal, 2007; Lunne et al., 1997). The system is denoted as SBTn and plotted on charts in terms of Q vs. F and Q vs B_q, as shown in Figure A9.

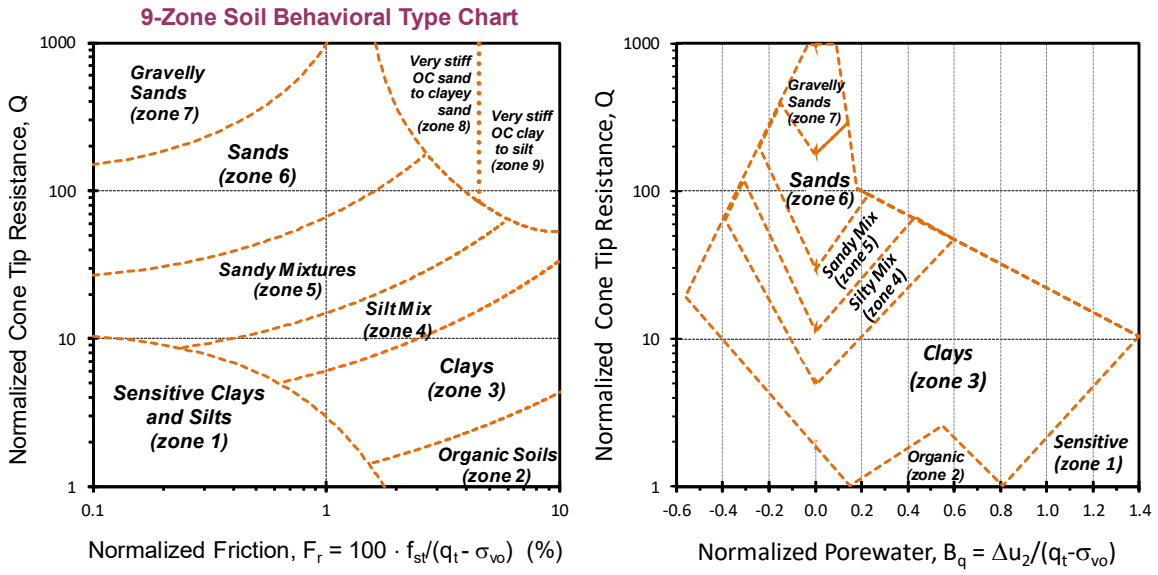

Figure A9. CPT charts for SBTn system: (a) Q versus F; (b) Q versus B_q.

Of particular concern in geotechnical site characterization is the proper identification of soft organic soils, such as organic clays and silts (OL and OH) and peats (Pt). These soils often cause difficulties and problems during construction and performance of civil engineering works because of bio-degradation, long-term creep, excessive settlements, and/or other issues.

The SBTn system has a category labelled Zone 2 recognizes organic soils. However, several recent studies have noted that data from CPTu soundings do not always fall within the bounds delineated using Zone 2, even though laboratory tests and field inspections clearly note the presence of organic soils. Lab tests to classify organic soils includes loss on ignition (LOI > 5%) and two pairs of Atterberg limits testings per ASTM standards, as well as the visual-manual identification of strong organic odor and smell, and dark color, notably black and dark gray.

Results by Mlynarek et al. (2014) show that organic soils in Poland are not adequately identified by the Q-F chart, as seen in Figure A10. Moreover, studies by Zawrzykraj et al. (2017) found that neither the Q-

F and Q-B_q plots worked well to recognize organic soils and peats in Poland. Nejaim et al. (2016) found that Brazilian soft organic clays were misclassified as Zone 3 (clays), rather than Zone 2 (organic clays).

Similarly, a recent study on CPTu data from organic clays located at 24 sites in the USA, Sweden, Mexico, Brazil, and Australia have been compiled (Agaiby, 2018). These data are shown to generally avoid falling with the Zone 2 boundaries in either Q-F or Q-B_q charts, thus are not recognized during these soundings, as indicated by Figure A11. The exception in this case is the Mexico City clay which is correctly identified, however the other 23 sites are generally not properly recognized and categorized. Additional findings by Missiaen et al. (2015) found that the CPTu results in Belgian soils also did not identify organic clays and peats in the non-normalized version of these charts that uses Q_t versus friction ratio ($R_f = 100 \cdot f_s/q_t$), as detailed by Robertson & Cabal (2007).

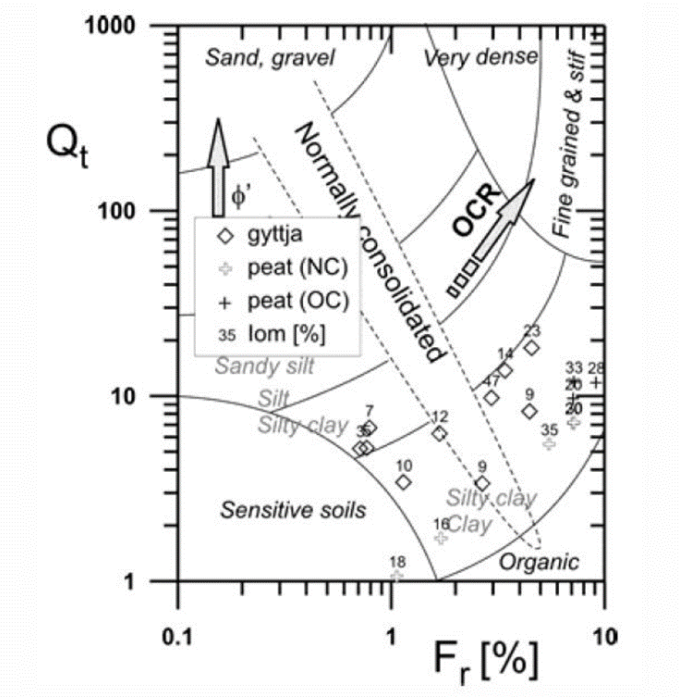

Figure A10. Soil behavioral chart with superimposed CPTu data from Polish organic soils

(from Mlynarek et al., 2014).

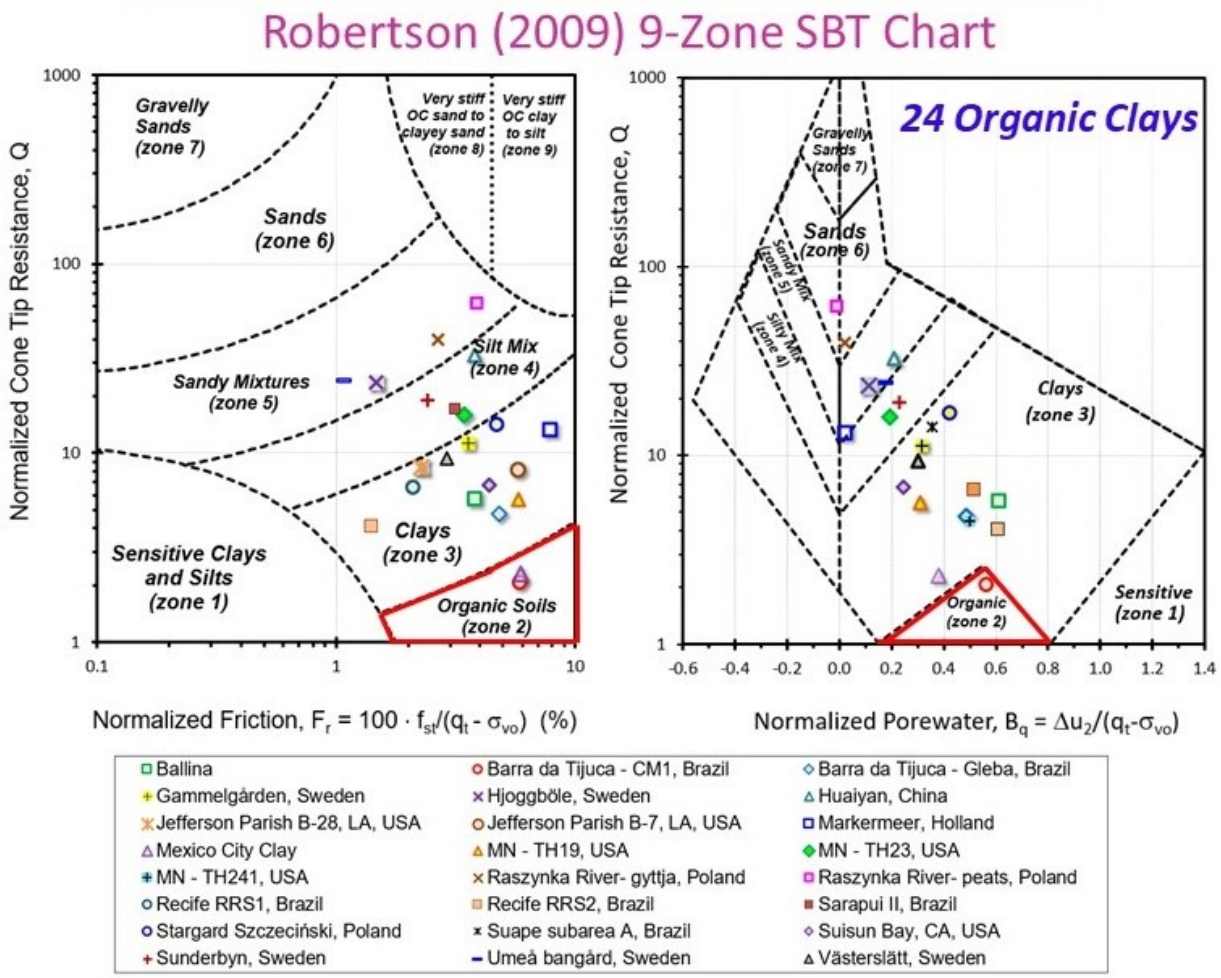

Figure A11. Paired SBTn charts with CPTu data from 24 organic clay sites, indicating non-compliance with Zone 2 (organic soils)

(compiled by Agaiby, 2018)

A1.4. Simplified Yield Stress Evaluation in Clays by CPTu

From the development of a hybrid formulation of spherical cavity expansion (SCE) theory with critical-state soil mechanics (CSSM), the effective preconsolidation stress, or yield stress (σ_p'), of clays can be expressed in terms of three piezocone parameters: (a) net cone tip resistance: $q_{net} = q_t - \sigma_{vo}$; (b) measured excess porewater pressure: $\Delta u_2 = u_2 - u_0$; and (c) effective cone resistance: $q_E = q_t - u_2$. Details on the SCE-CSSM solutions are given elsewhere (Mayne, 1991; Mayne, 2017; Agaiby & Mayne, 2018).

For "normal" and "well-behaved" clays, which include inorganic fine-grained soils such as clays and silts of low sensitivity, a set of simple relationships can be derived. By adopting characteristic default values for effective friction angle φ' = 30° and rigidity index (I_R = 100), linear expressions for the effective preconsolidation stress are obtained:

$$\sigma'_p = 0.33 \cdot q_{net} \quad \text{A7}$$

$$\sigma'_p = 0.53 \cdot \Delta u_2 \quad \text{A8}$$

$$\sigma'_p = 0.60 \cdot q_E \quad \text{A9}$$

A1.4.1 Application to soft Chicago clay

An example of a common geomaterial in this category includes the infamous soft Chicago clays that were deposited in a glacio-lacustrine environment (Cho & Finno, 2010). The soft clay has a mean water content of 20%, liquid limit of 38% and plasticity index PI= 12%. Results of CPTu tests conducted at the national geotechnical experimentation site (NGES) at Northwestern University are shown in Figure A12 (Ouyang & Mayne, 2017). As seen in the profile, a thin soft clay resides between depths of 9 to 10.5 m with a thicker soft clay layer in the range of 12 to 18 m.

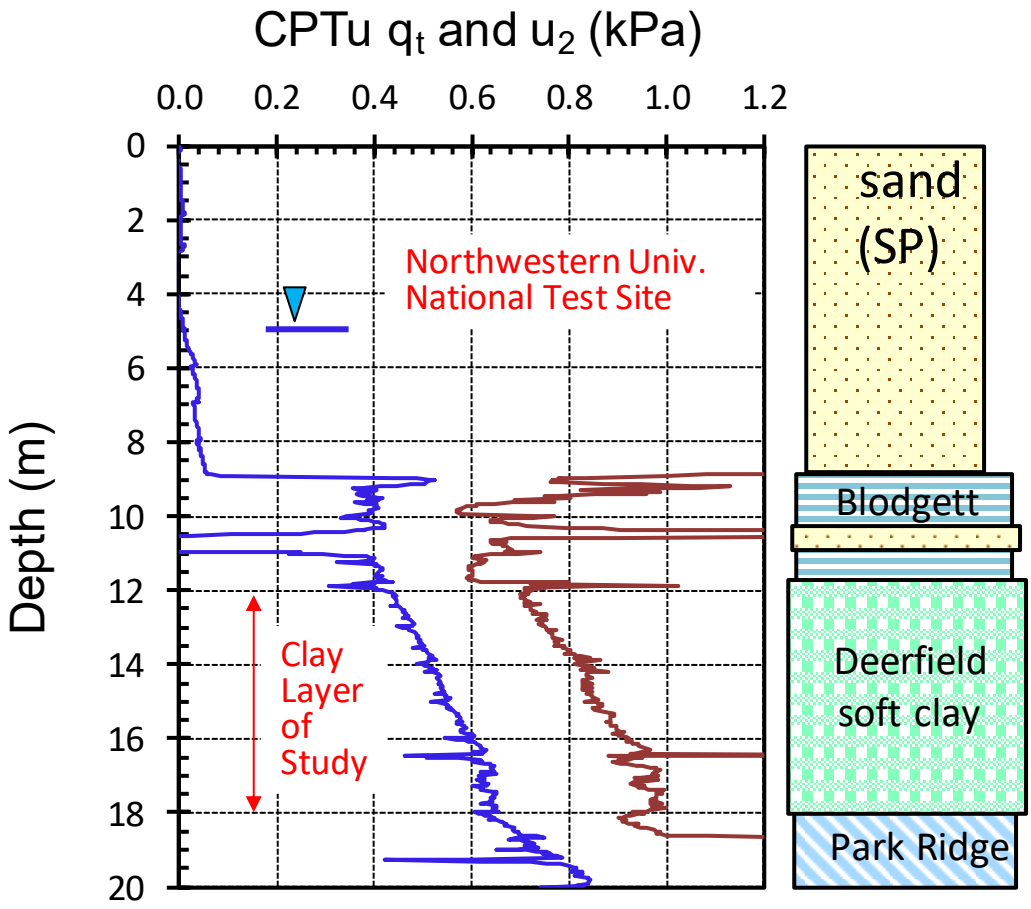

Figure A12. Results of CPTu sounding at the NGES at Northwestern University, Illinois

Post-processing of the CPTu data using Equations A7, A8, and A9 show good agreement in evaluating the profile of effective yield stress in this clay layer compared with results from one-dimensional consolidation tests made on undisturbed samples taken at the site.

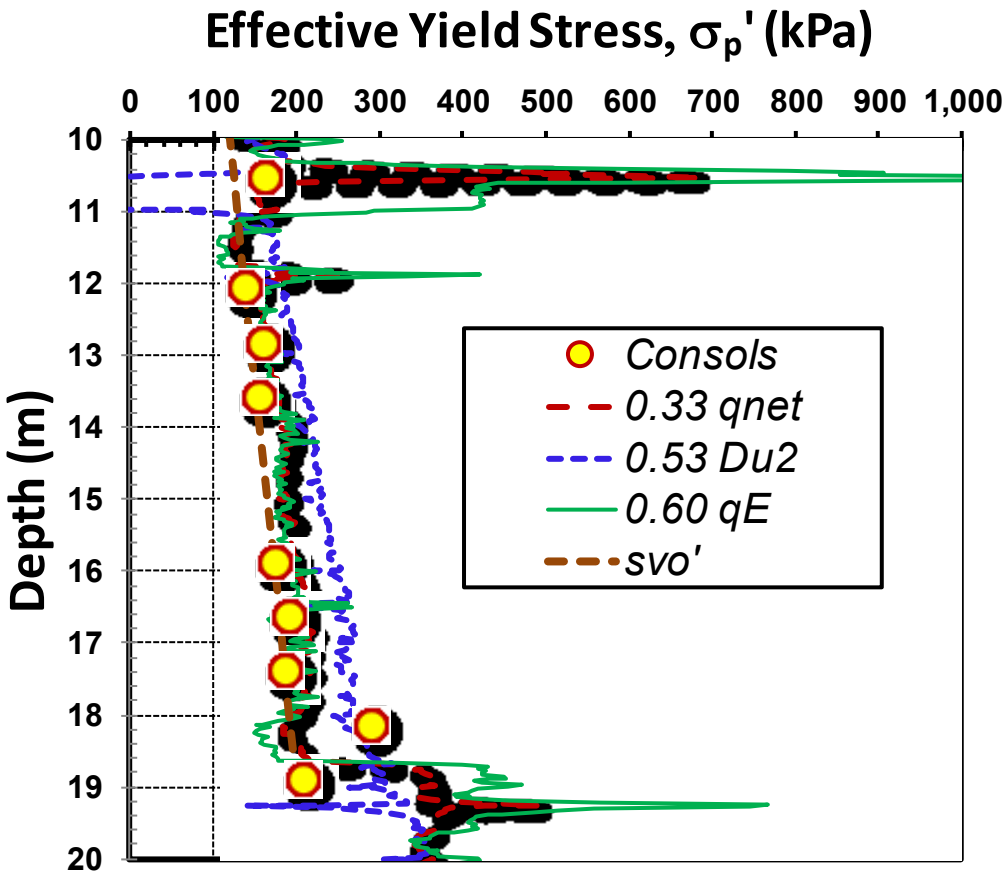

Figure A13. Evaluation of effective yield stresses at NWU using consolidation tests and CPTu

A1.4.2 Application to soft Bay Mud, California

Another example of a "well-behaved" fine-grained soil is the San Francisco Bay Mud which is a soft clay deposit in northern California. Results of a representative CPTu are shown in Figure A14 and indicate the soil profile at a site in eastern San Francisco (Hunt et al., 2002). For this site, index values include: $70 < w_n < 90\%$, $60 < LL < 80\%$, and $35 < PI < 45$ %. Post-processing the CPTu data using Equations A7, A8, and A9 show good agreement with each other, as well as with the results of consolidation tests, as seen in

Figure A15. The consolidation tests were performed using a CRS device as reported by Pestana et al. (2002).

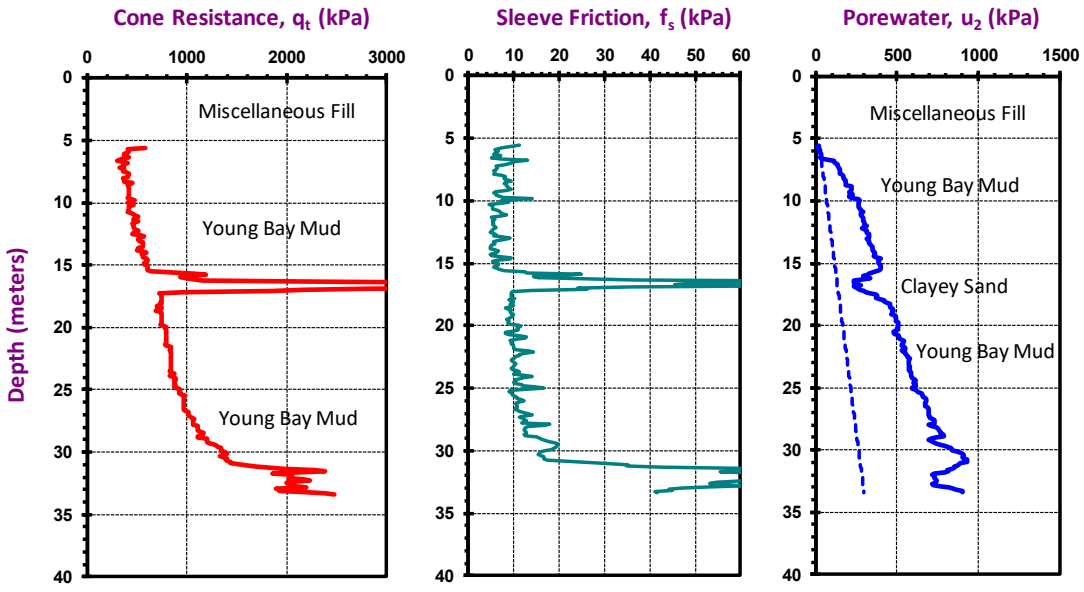

Figure A14. Representative CPTu in San Francisco Bay Mud (data from Hunt et al., 2002).

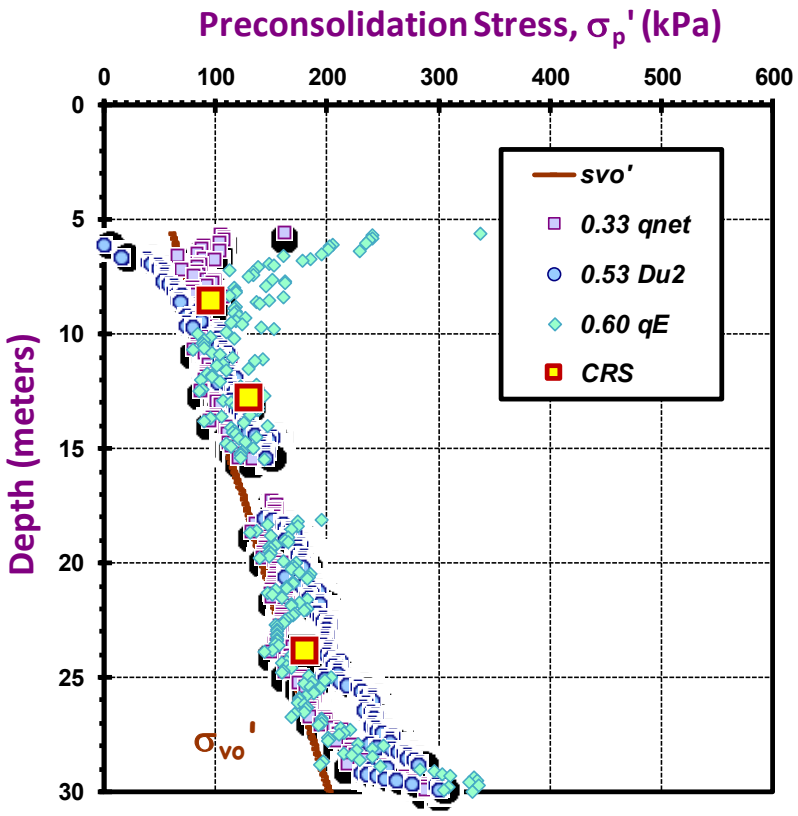

Figure A15. Evaluation of effective yield stresses in Bay Mud from consolidation tests and CPTu.

A1.5. CPTu Screening of Soft Organic Clays

For soft organic clays, the Equations A7, A8, and A8 will not apply, thus can serve as a means to screen such geomaterials from the soil profile. Two examples of CPTu soundings in soft organic clays are presented to illustrate the approach. Additional case records and documentation of CPTu data in organic clays are given in Agaiby (2018).

A1.5.1 Soft organic alluvial soils in Washington, DC

Results of in-situ tests including CPTu soundings in soft organic clayey silts along the Potomac River at the Anacostia Naval Air Station are presented by Mayne (1987). Here the soft soils are categorized as organic clayey silts (OH) per the Unified Soils Classification Systems (USCS) with mean values (and plus and minus

one standard deviations) of w_n = 68 ± 16 %, LL = 83 ± 25 %, and PI = 37 ± 17 %. A representative piezocone sounding is depicted in Figure A16. For the post-processing of CPTu data, the use of the Q-F and Q-B_q graphs do not find any points within the Zone 2 category for organic soils. When the data are evaluated to determine the profile of effective yield stress, the Equations A7, A8, and A9 do not agree, as shown by Figure A17.

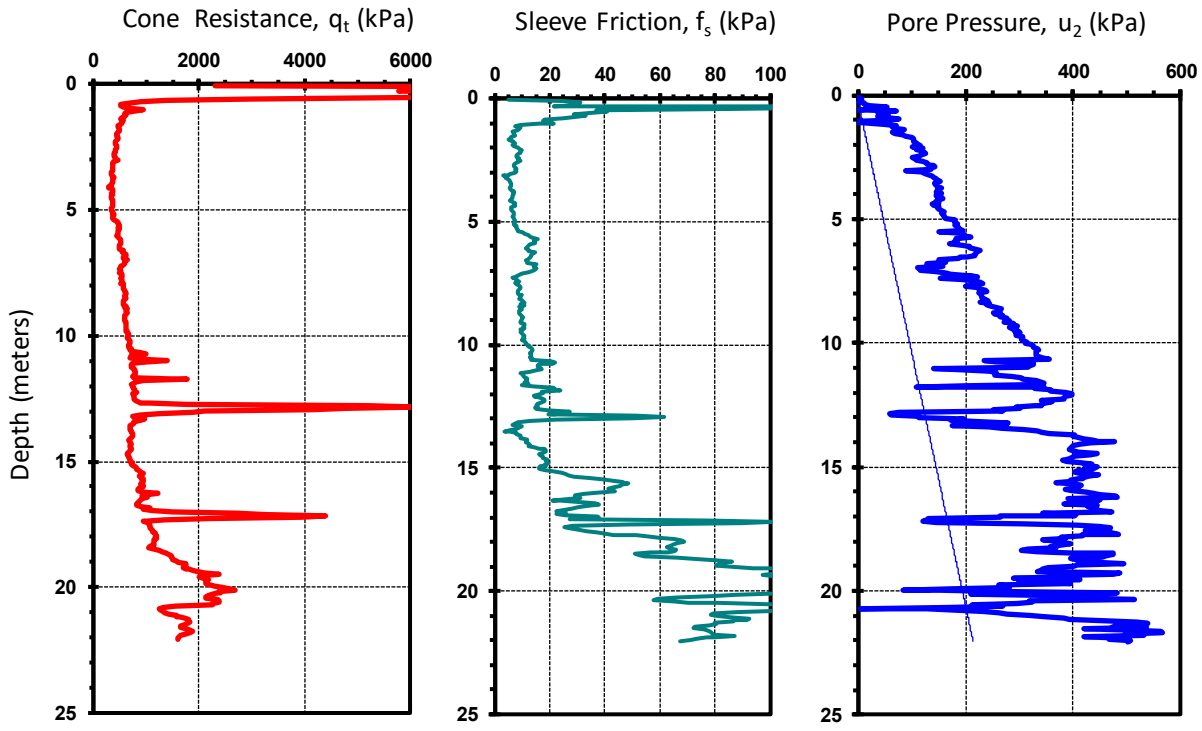

Figure A16. Representative CPTu in soft organic clay along the Potomac River, DC.

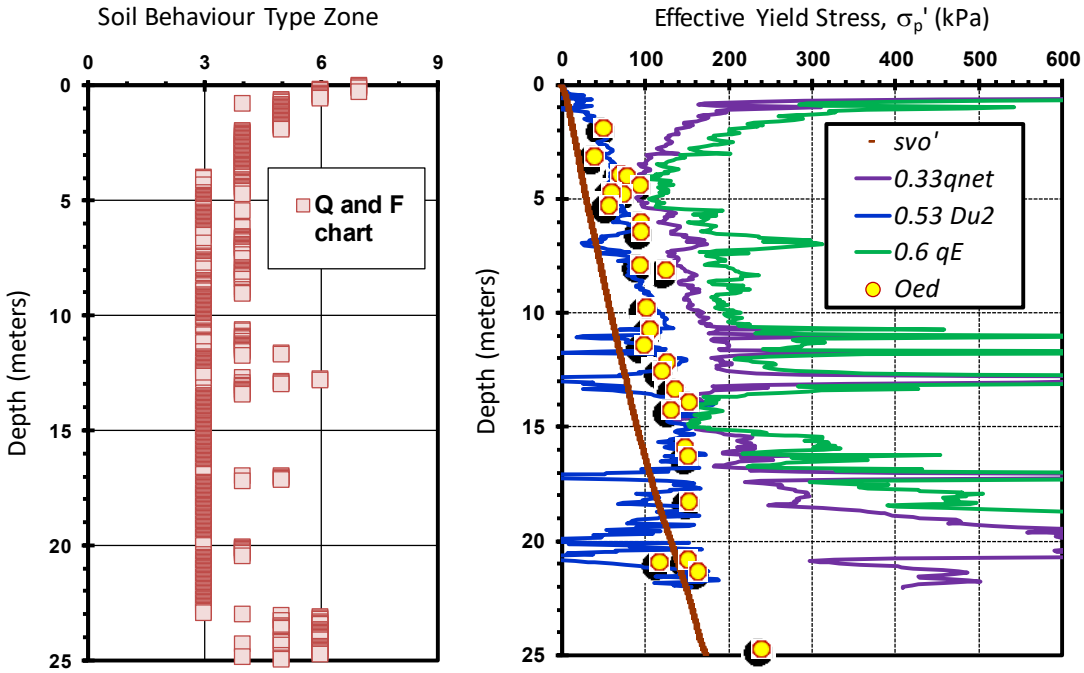

Figure A17. Post-processing of CPTu data from Anacostia-Bolling: (a) SBTn zones using CPT material index, Ic; (b) CPTu screening equations for yield stress.

Note that the hierarchy of the results from Equations A7, A8 and A9 show that the CPTu evaluations for preconsolidation stress in soft organic clays indicates:

[A10] $\sigma_p' = 0.53\ \Delta u_2 < 0.33\ q_{net} < 0.60\ q_E$

A1.5.2 Soft organic peaty clay in Saint Paul, MN

Results of CPTu tests were collected during a training exercise underneath I-35E just northeast of Saint Paul, MN in 2007. All three MnDOT CPT rigs available at the time were used to obtain in-situ test data at the site. The site is well known as having soft organic soils and samples were obtained from three borings made at the site (Boring ID # T523, T542, and T518). Boring logs

indicate the presence of highly organic silt loams, with marl and spongy organic clayey silts. From 12 samples, the natural water contents ranged from 30% to 191%, with a mean of 112 ± 58%.

A representative piezocone sounding from the site (MnDOT CPTu ID #F22Y0703C) is used for this illustration and is presented as Figure A18. Post-processing these data using the SBTn algorithms and CPT material index show that the soils classify primarily as Zone 3 (clays) and Zone 4 (silty mix), thus do not identify the geomaterials properly as Zone 2 (organic soils).

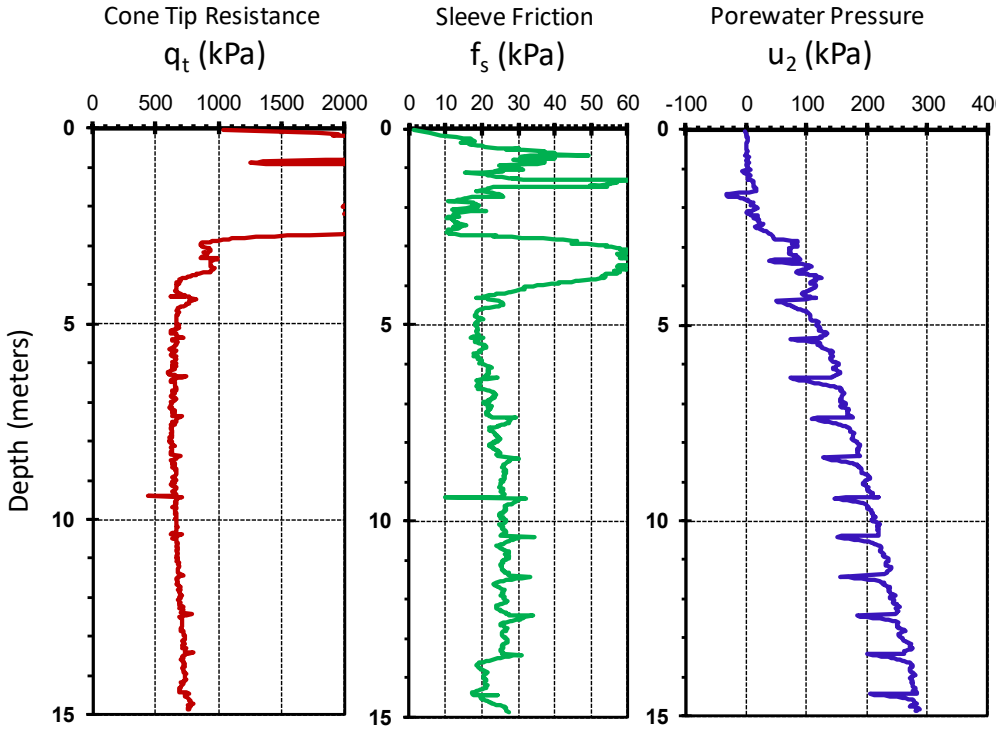

Figure A18. MnDOT CPTu sounding at the I-35E test site near St. Paul, Minnesota

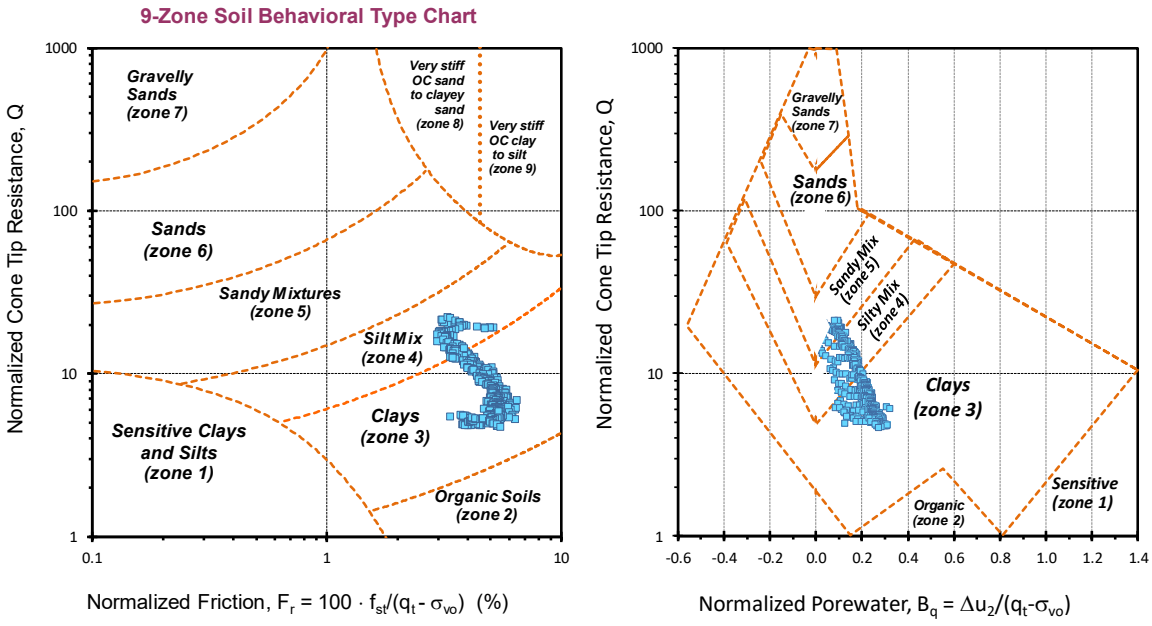

Figure A19. Post-processing St. Paul sounding using the 9-zone SBTn classification system.

Using the recommended approach Figure A20 shows the CPT-evaluated yield stress profiles from equations A7, A8, and A9. Here again, the three estimates of σ_p' do not agree but show the same hierarchy as detailed in Equation A10.

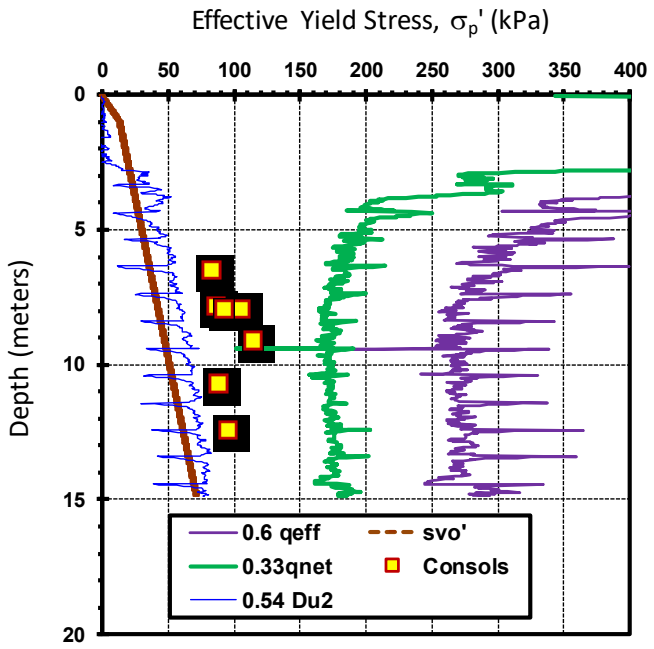

Figure A20. CPTu screening of soft organic soils at St. Paul test site

A1.6. CPTu Evaluations of Yield Stress in Soft Organic Soils

Once the presence of soft organic clays and silts is identified using the aforementioned CPT screening algorithms, the evaluation of effective yield stress is conducted using the procedure outlined in Chapter 2 of this MnDOT manual. For soft organic soils, an exponent of m' = 0.90 is recommended (Mayne et al., 2009). Therefore, the preconsolidation stress is obtained from (units of kPa):

$$\sigma'_p = 0.33 \cdot (q_{net})^{0.90} \quad \text{A11}$$

The algorithm can be expressed in dimensionless form by:

$$\sigma'_p = 0.33 \cdot (q_t - \sigma_{vo})^{m'} \cdot (\sigma_{atm}/100)^{1-m'} \quad \text{A12}$$

where σ_{atm} = reference stress (= 100 kPa = 14.7 psi) and m' = 0.90 for soft organic silts and clays.

The approach is applied to the two former example case studies in Figure A21 (Washington DC) and Figure A22 (St. Paul, MN), respectively, showing good agreement with benchmark results taken from laboratory consolidation tests on undisturbed samples of these sites in both cases.

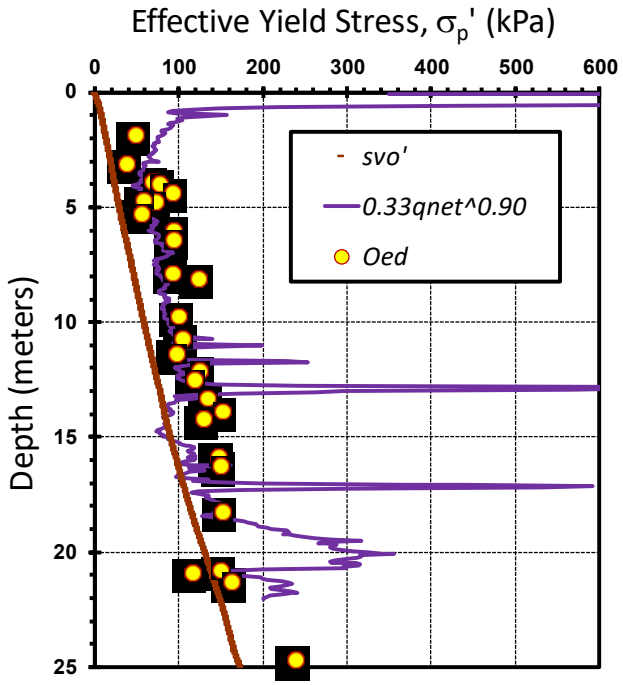

Figure A21. Profiles of yield stress from consolidation tests and CPTu method for organic clayey silts at Anacostia-Bolling site in Washington, DC.

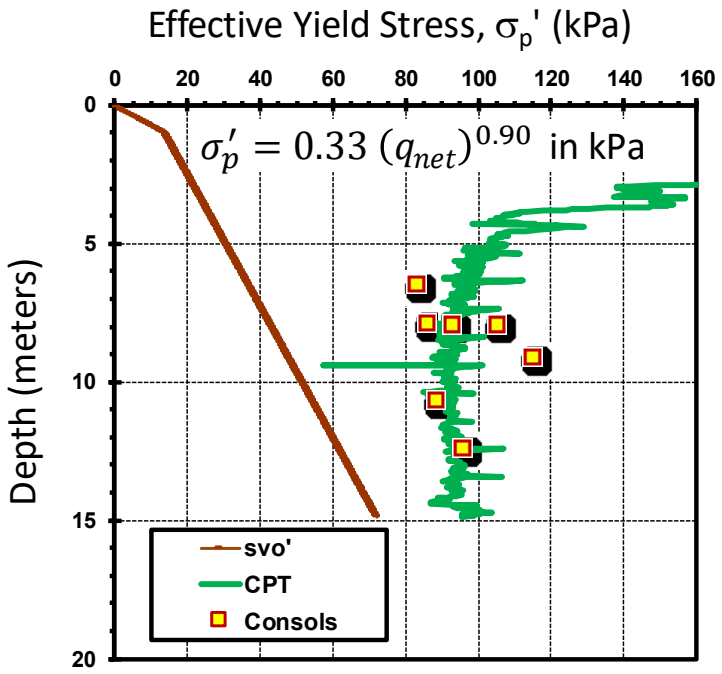

Figure A22. Profiles of yield stress from consolidation tests and CPTu method for organic clayey silts at MnDOT test site near Saint Paul, Minnesota

A1.7. Soil Unit Weight

As shown by Figure A23, total soil unit weight (γ_t) can be estimated from the CPT sleeve friction resistance (Mayne 2014). The equation can be expressed by:

$$\gamma_t = \gamma_w \cdot [1.22 + 0.15 \cdot ln\,(100 * f_s/\sigma_{atm} + 0.01)] \quad \text{A13}$$

where γ_w = unit weight of water and σ_{atm} = atmospheric pressure.

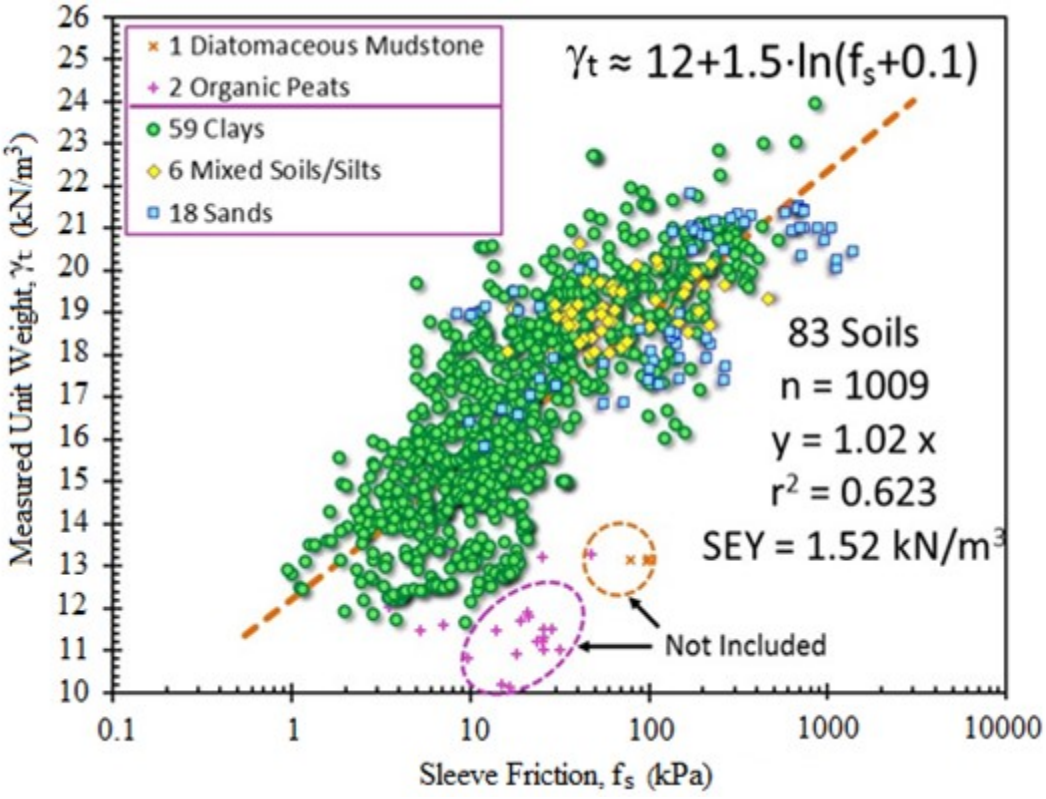

Figure A23. Evaluation of soil unit weight from CPT sleeve friction.

A1.8. Effective Stress Friction Angle

Sands

The effective stress friction angle (ϕ') is one of the most important soil properties as it governs the strength of geomaterials, as well as affects soil-pile interface and pile side friction. While an effective cohesion intercept (c') can also be considered, this is usually reserved for cemented or bonded geomaterials or unsaturated soils and may lose its magnitude with time, ageing, or with prolonged environmental changes.

For clean quartz to silica sands where porewater pressures are essentially hydrostatic (B_q = 0), the following expression has been calibrated with triaxial compression test results from undisturbed sand samples and normalized cone resistances, as presented in Figure A24 (Mayne 2007; 2014)

$$\phi'(deg) = 17.6° + 11.0° \, log\,(q_{t1}) \qquad \text{A14}$$

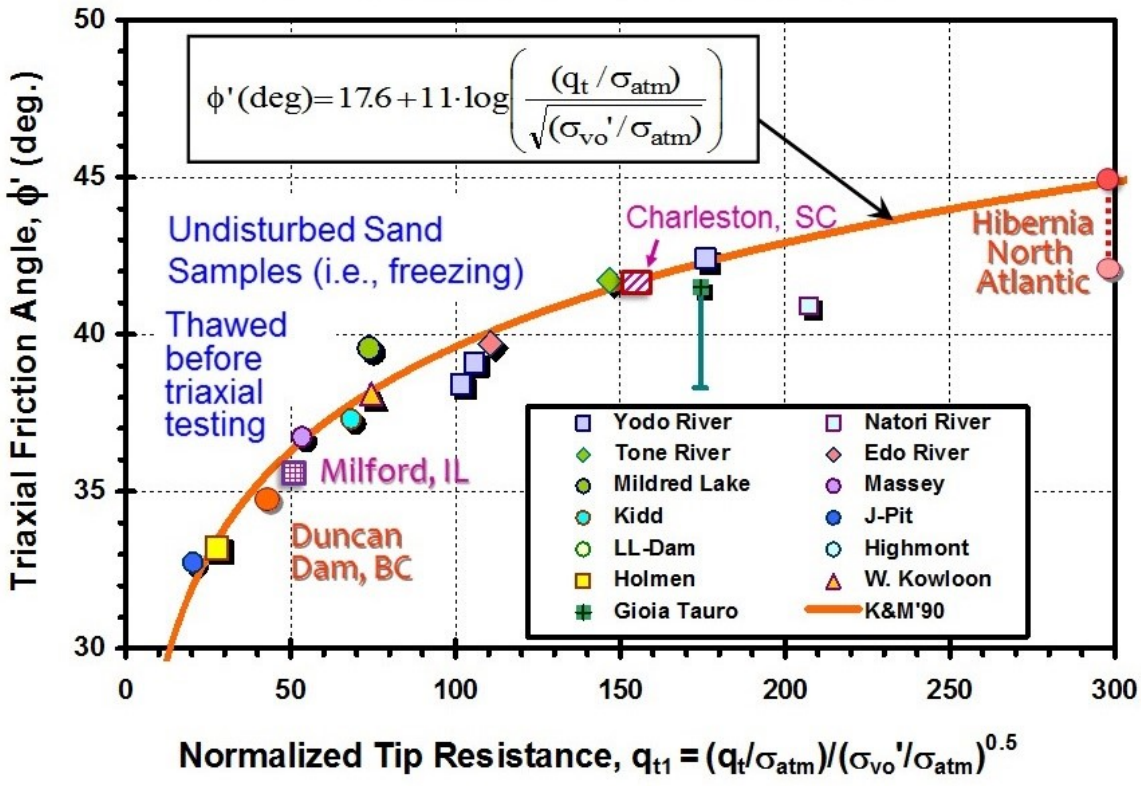

Figure A24. Evaluation of effective stress friction angle in quartz-silica sands from CPT.

Note: Relationship applies to drained soil behavior when $I_c < 2.6$ and/or $B_q < 0.1$

where q_{t1} is an earlier form of stress normalized cone tip resistance for sands given by:

$$q_{t1} = \frac{(q_t / \sigma_{atm})}{(\sigma'_{vo}/\sigma_{atm})^{0.5}} \qquad \text{A15.1}$$

In terms of units of bars, this is expressed simply as (in units of bars):

$$q_{t1} = \frac{q_t}{(\sigma'_{vo})^{0.5}} \quad \text{A15.2}$$

Recently, Robertson & Cabal (2015) recommended the use of the modified form of normalized cone resistance (Q_{tn}) in Equation A10.

$$\phi' (deg) = 17.6° + 11.0° \, log \, (Q_{tn}) \quad \text{A16}$$

In sands, $q_{net} \approx q_t$ since the overburden term is small relative to the cone tip resistance. Figure A25 shows that the two normalizations give very comparable results.

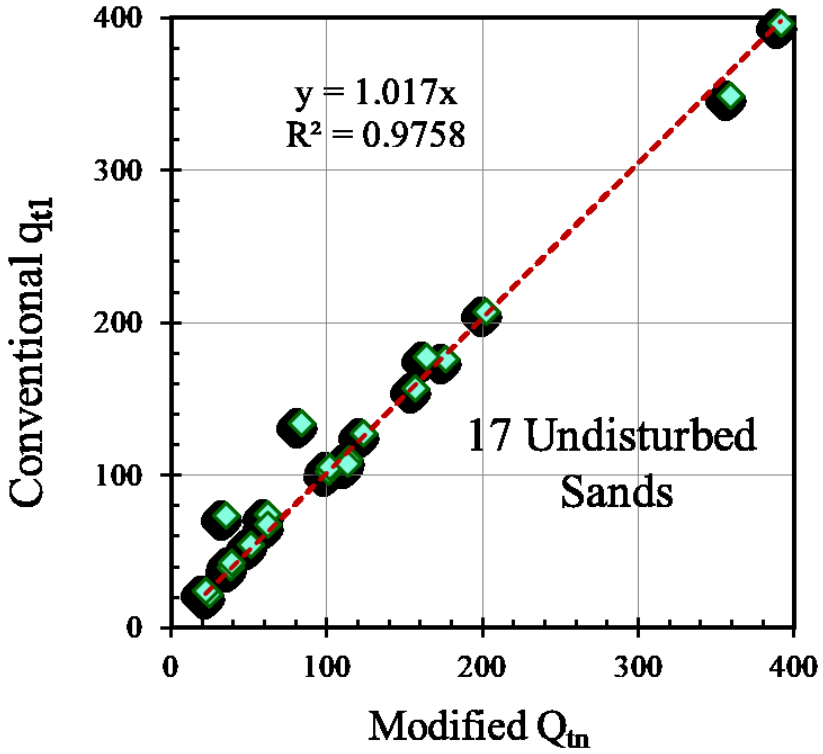

Figure A25. Comparable values from q_{t1} and Q_{tn} normalization schemes for CPTs in sands

Clays and Silts

In the case of soft to firm intact clays and silty clays, the effective friction angles are determined from the normalized cone resistance and porewater pressure parameters (Senneset et al. 1989; Mayne 2016), as shown in Figure A26. The exact solution when the angle of plastification $\beta = 0$ is given as:

$$Q = \frac{\tan^2(45° + \phi'/2) \cdot \exp(\pi \cdot \tan\phi') - 1}{1 + 6 \cdot \tan\phi' \cdot (1 + \tan\phi') \cdot B_q} \qquad \text{A17}$$

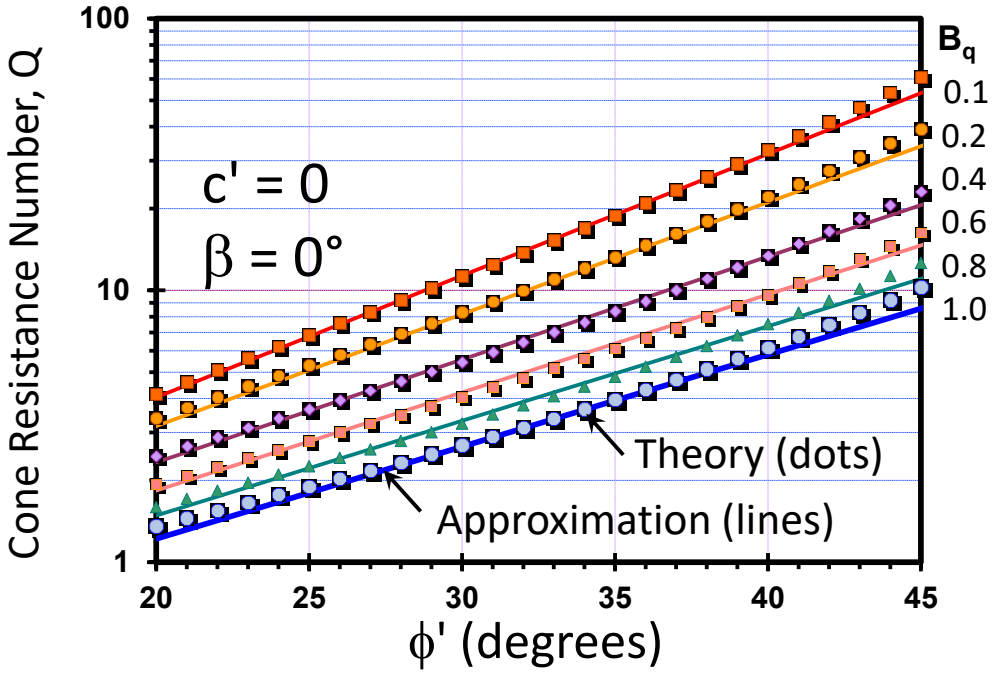

Figure A26. Evaluation of effective stress friction angle in clays and silts from CPTu results

Note: Relationship applies to undrained soil behavior when $I_c \geq 2.6$ and/or $B_q \geq 0.1$.

which can be approximately inverted into the form (Mayne 2007):

$$\phi' = 29.5° \cdot B_q^{0.121} \cdot [0.256 + 0.336 \cdot B_q + \log(Q)] \quad \text{A18}$$

This algorithm is specifically applicable for the following ranges of porewater pressure parameter ($0.1 \leq B_q < 1$) and effective stress friction angles ($20° \leq \phi' < 45°$).

A1.9. Stress History

The stress history can be characterized by an apparent yield stress or preconsolidation stress (σ_p'), as well as by its normalized and dimensionless form, YSR = σ_p'/σ_{vo}' = yield stress ratio. The YSR is in effect the same as overconsolidation ratio (OCR), however, now generalized to accommodate mechanisms of preconsolidation that occur beyond just erosion, glaciation, and removal of overburden stresses, but also due to ageing, desiccation, repeated cycles of wetting-drying, bonding, repeated freeze-thaw cycles, groundwater changes, and other factors.

A generalized approach for evaluating the yield stress or preconsolidation in soils using net cone resistance has been formulated, as presented in Figure A27 (Mayne 2015).

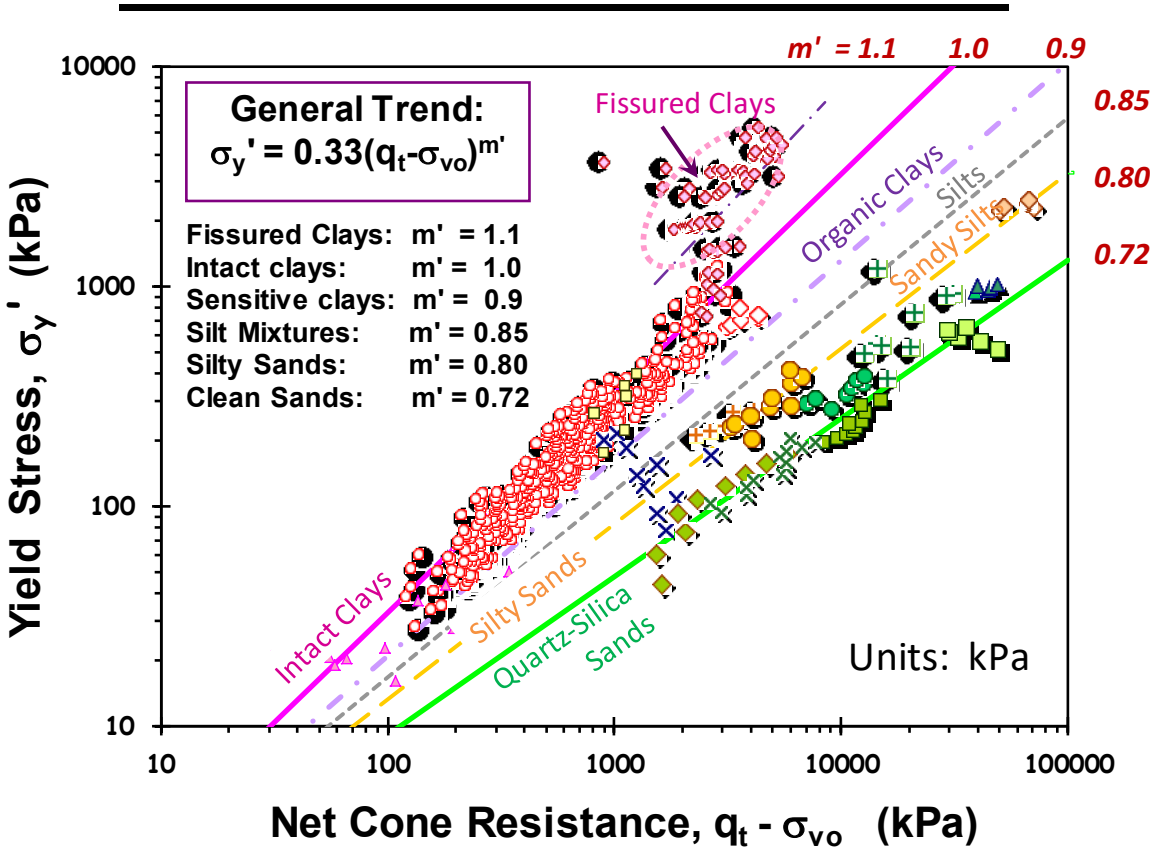

Figure A27. Evaluation of yield stress or preconsolidation stress in soils from CPT.

The algorithm can be expressed in dimensionless form by:

$$\sigma_p' = 0.33 \cdot (q_t - \sigma_{vo})^{m'} \left(\frac{\sigma_{atm}}{100}\right)^{1-m'} \quad \text{A19}$$

where m' = exponent depends on soil type: m' = 1 (intact clays); 0.85 (silts); 0.80 (sandy silts to silty sands), and 0.72 (sands), For fissured clays, the exponent m' may be 1.1 or higher, depending upon the age of the

formation and degree of jointing and discontinuities. Note that fissured clays can be identified when I_c < 2.6 and B_q < 0.1.

The exponent m' has also been calibrated with CPT material index, as presented in Figure A28. An algorithm to express this relationship for non-fissured soils is given by:

$$m' = 1 - \frac{0.28}{1+(I_c/2.65)^{25}} \quad \text{A20}$$

This allows the post-processing of CPT to automatically choose the appropriate exponent m' for a layer by layer analysis.

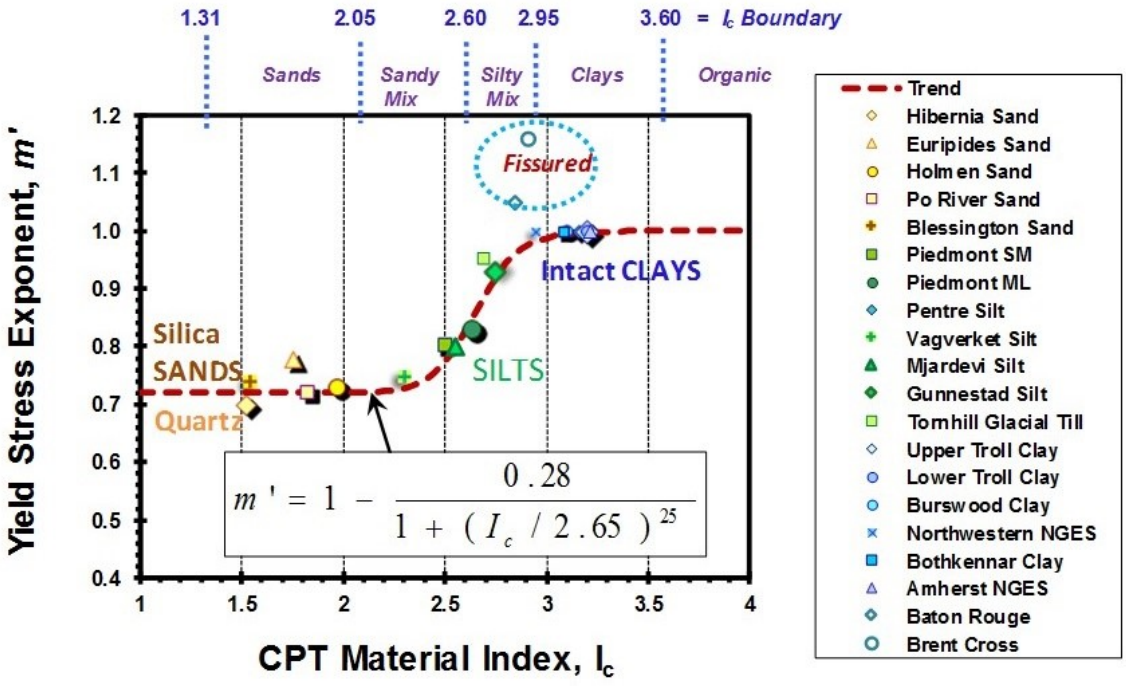

Figure A28. Yield stress exponent m' in terms of CPT material index, I_c.

A1.10. Lateral Stress Coefficient

The horizontal geostatic state of stress is represented by the lateral stress coefficient, $K_0 = \sigma_{ho}'/\sigma_{vo}'$, commonly referred to as the at-rest condition. The magnitude of K_0 for soils that have been loaded and unloaded can be approximately estimated from:

$$K_o = (1 - sin\phi') \cdot OCR^{sin\phi'} \quad \text{A21}$$

Data compiled from in-situ K_0 measurements using self-boring pressuremeter tests (SBPMT), total stress cells (TSC) or push-in spade cells, and/or laboratory methods (instrumented consolidometers, triaxials, and/or suction measurements) on a variety of clays, silts, and sands have been compiled and reported by Ku & Mayne (2015), as shown in Figure A29, verifying Equation A15 as a means for evaluating K_0 in soils.

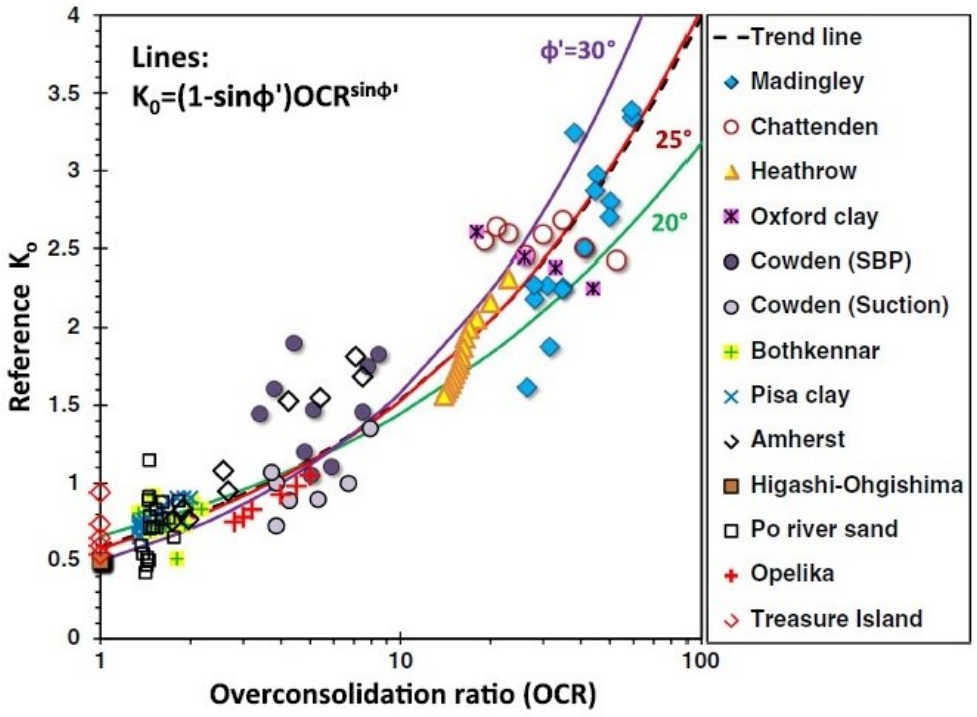

Figure A29. Relationship between lateral stress coefficient K_0 and YSR or OCR in soils (Ku & Mayne 2015).

A1.11. Undrained Shear Strength

The loading of soils can occur under conditions of being fully drained ($\Delta u = 0$), partially drained, or full undrained ($\Delta V/V_0$), where Δu = excess porewater pressures (above hydrostatic) and $\Delta V/V_0$ = volumetric strain. Further details on specific stress paths are best explained in terms of critical state soil mechanics, or CSSM (Mayne et al. 2009; Holtz, Kovacs, & Sheahan 2011). The prevailing drainage conditions depend upon the rate of loading and permeability characteristics of the soil. Normally, in sands that are pervious and exhibit high permeability, a drained response occurs. Exception to this may occur in loose sands during fast earthquake loading, resulting in soil liquefaction. In clays that exhibit low permeability, a fast rate of loading will result in undrained loading at constant volume. This, in fact is a temporary and transient condition, often termed short term loading. In the long term, eventually porewater pressures will dissipate (albeit slowly), and a drained response will prevail, thus termed long term loading.

The overall soil strength is controlled by the effective stress strength envelope. Most commonly, this is represented by a simple linear relationship termed the Mohr-Coulomb criterion where the maximum shear stress (τ_{max}, called the "shear strength) is given as:

$$\tau_{max} = c' + \sigma' \cdot tan\,\phi' \qquad \text{A22}$$

where c' = effective cohesion intercept, σ' = effective normal stress, and ϕ' = effective stress friction angle. As a starting point, values of c' = 0 and ϕ' = 30° can be adopted for all soil types, at least until the specific soil type, geologic formation, and results from high-quality laboratory or field test data are available.

Peak Undrained Shear Strength from Stress History

Using simplified critical state soil mechanics, the peak undrained shear strength ($\tau_{max} = s_u$) can be evaluated from the effective stress strength envelope (c' = 0; effective friction angle ϕ') and stress history (i.e., OCR) in the form:

DSS: $$s_u = (sin\phi'/2) \cdot (OCR)^{\Lambda} \cdot \sigma'_{vo} \qquad \text{A23}$$

which corresponds to a simple shear mode. Figure A30 presents the aforementioned relationship together with data from 17 different clays tested in simple shear.

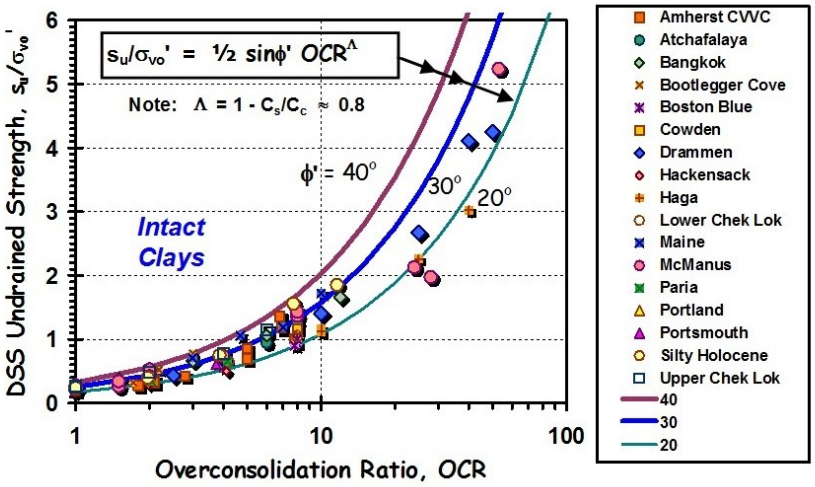

Figure A30. Normalized undrained shear strength from simple shear tests on various clays versus YSR or OCR.

For the triaxial compression (TC) mode, the equation would give slightly higher strengths that are calculated from:

$$\text{TC:} \quad s_u = (M_c/2) \cdot (OCR/2)^{\Lambda} \cdot \sigma'_{vo} \qquad \text{A24}$$

where $M_c = (6 \cdot \sin\phi')/(3-\sin\phi')$.

Peak Undrained Shear Strength from CPTu

A more direct approach to assessing undrained shear strength is via bearing capacity theory whereby:

$$s_u = \frac{q_t - \sigma_{vo}}{N_{kt}} \quad \text{A25}$$

where N_{kt} = bearing factor that depends on mode of shearing, sensitivity of the clay, degree of overconsolidation, and other factors. For soft offshore clays, the back figured N_{kt} from data collected at 14 well-documented sites (Low et al. 2010) determined mean values based on mode of shearing: N_{kt} = 11.9 (triaxial compression), N_{kt} = 13.6 (simple shear), and N_{kt} = 13.3 (vane).

A recent study of 51 clays that were tested by both field piezocone and laboratory CAUC triaxial tests showed that essentially N_{kt} = 12 for intact clays and clayey silts of low to medium sensitivity (Mayne, Peuchen & Baltoukas 2015). Figure A31 shows the slightly different trends for offshore versus onshore clays. For sensitive clays, a lower value of N_{kt} = 10 would be appropriate and for fissured clays, a higher value of N_{kt} would be in the range of 20 to 30.

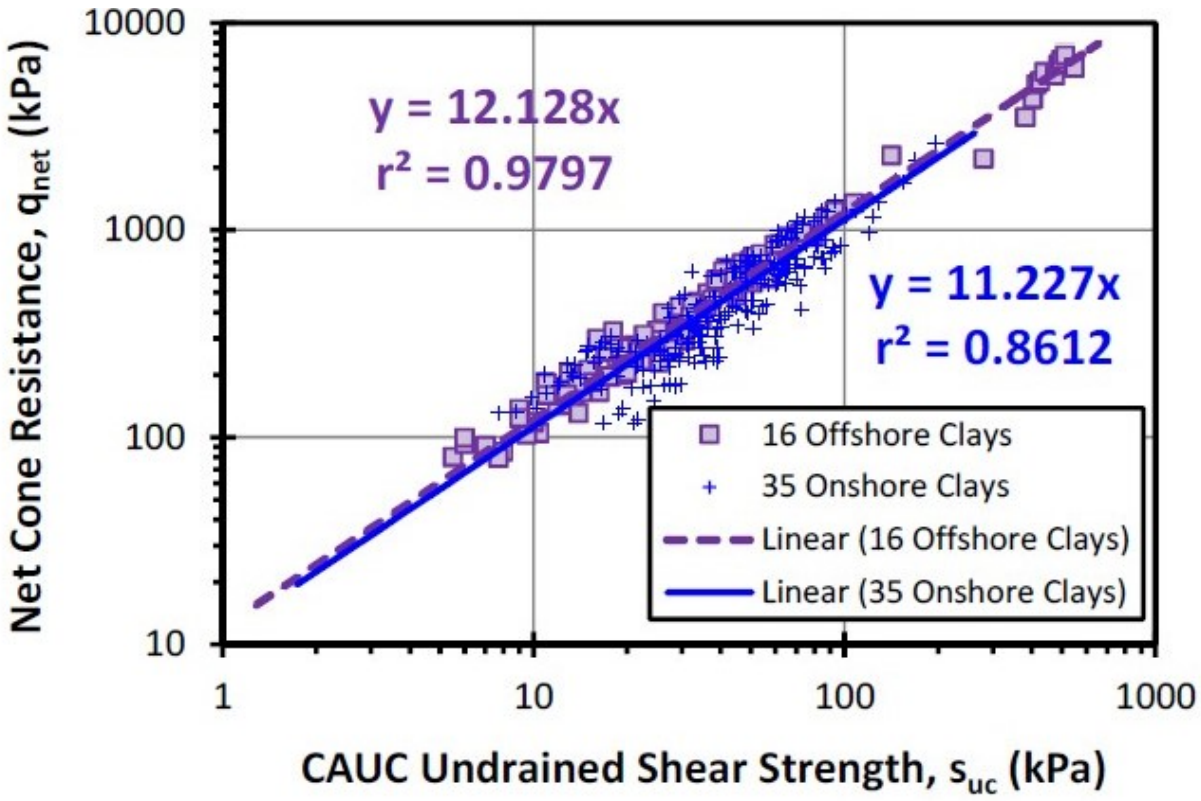

Figure A31. Database from 51 clays with CPT q_{net} versus lab measured triaxial shear strength (Mayne, Peuchen, & Baltoukas 2015).

For soft to firm clays, an alternate means to evaluate undrained shear strength is via the excess porewater pressures ($\Delta u = u_2 - u_0$) from the following:

$$s_u = \frac{\Delta u_2}{N_{\Delta u}} \qquad \text{A26}$$

where $N_{\Delta u}$ = porewater bearing factor, also dependent on the aforementioned factors. The study by Low et al. (2010) found $N_{\Delta u}$ = 5.9 (triaxial compression), $N_{\Delta u}$ = 6.9 (simple shear), and $N_{\Delta u}$ = 7.1 (vane shear).

A third alternate is found from the effective cone resistance ($q_E = q_t - u_2$) whereby:

$$s_u = \frac{q_t - u_2}{N_{kE}} \quad \text{A27}$$

where N_{kE} is a bearing term for this approach. Mayne et al. (2015) indicated a mean value of $N_{kE} = 8$ for soft-firm intact clays.

Remolded Undrained Shear Strength from CPT

The remolded undrained shear strength (s_{ur}) is obtained from either field vane tests, lab mini-vane shear tests, or lab fall cone devices. This affords the evaluation of the clay sensitivity (S_t) which is defined as the ratio of peak to remolded strengths at a given water content:

$$S_t = {}^{s_{u(peak)}}/_{s_{ur}} \quad \text{A28}$$

For the CPT, the sleeve friction has been noted to give values that are comparable to the remolded undrained shear strength (Powell & Lunne 2015). Therefore,

$$s_{ur} \approx f_s \quad \text{A29}$$

A1.12. Ground Stiffness and Soil Moduli

The stiffness of the ground can be represented by several geoparameters, including the compressibility indices (C_r, C_c, C_s), spring constants (k_v), and moduli. Regarding the latter, there are several moduli that are used in geotechnical engineering, including: shear modulus (G and G_u), Young's modulus (E and E_u), constrained modulus (D'), bulk modulus (K'), resilient modulus (M_R), and subgrade reaction modulus (k_s).

Soil Modulus

The definition of modulus is taken as E = $\Delta\sigma/\Delta\varepsilon$, with Figure A32 showing a typical deviator stress (q = σ_1 - σ_3) versus axial strain (ε_a) curve. Theoretical interrelationships between the elastic moduli: G, E, D, and K have a dependence on the Poisson's ratio, v. The value of Poisson's ratio can be taken as v_u = 0.5 for undrained loading (i.e., constant volume), while for drained loading which is accompanied by volumetric strains, a value of v' = 0.2 may be used. If we adopt the reference modulus as E', then the interrelationships with the other elastic moduli are given by:

a. Reference Stiffness: E' = drained Young's modulus A30

b. Shear Modulus: $$G' = \frac{E'}{[2(1+\nu')]}$$ A31

c. Constrained Modulus: $$D' = \frac{E'\,(1-\nu')}{[(1+\nu')(1-2\nu')]}$$ A32

d. Bulk Modulus: $$K' = \frac{E'}{[3\cdot(1-2\nu')]}$$ A33

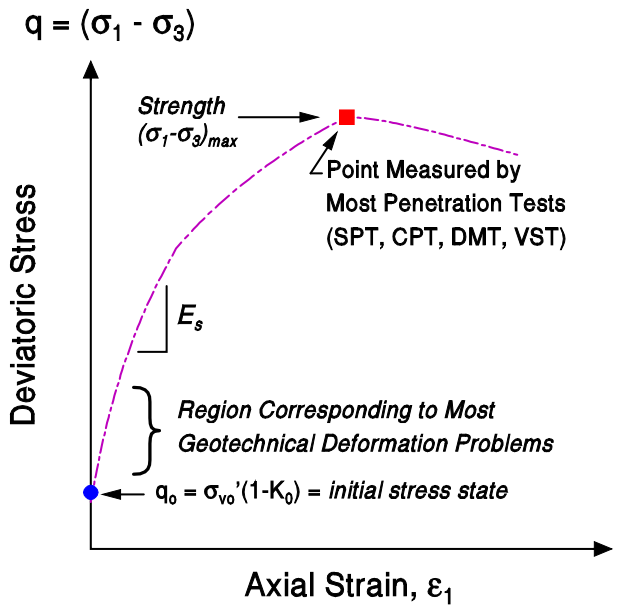

Figure A32. Representative stress-strain-strength curve for soils in triaxial compression.

For the extreme case when $\nu' = 0$, in fact D' = E'. When $\nu' = 0.2$, the two moduli are only 10% different: D' = 1.1·E', thus the constrained modulus and drained Young's modulus are often considered somewhat interchangeable.

The resilient modulus (M_R) applies to pavement analysis and design, most commonly measured by cyclic triaxial testing under repeated load applications. In fact, M_R is a special case of Young's modulus that relates to the small strain stiffness measured in the nondestructive range but has developed permanent plastic strains after many cycles of loading (Brown 1996; Dehler & Labuz 2007).

The subgrade reaction modulus is actually a combined soil-structural parameter, as its value depends on the ground stiffness and the size of the loaded element. The subgrade modulus is defined as: $k_s = q/\delta$, where q = applied stress and δ = measured deflection. In terms of elasticity solutions, the deflection of a flexible circle of diameter d is given by: $\delta = q \cdot d \cdot (1-\nu^2)/E'$. Therefore,

$$k_s = \frac{E'}{[d \cdot (1-\nu^2)]} \qquad \text{A34}$$

which has units of kN/m^3 or pcf.

Table A2 summarizes several selected studies towards the approximate evaluation of these moduli obtained directly from measured CPT data. Note however that the results from in-situ penetrometer tests generally represent a peak strength, as indicated in Figure A32. Thus, the measured cone tip resistance (q_t) reflects the top of the stress-strain curve, either the undrained strength in clays (s_u) or the effective friction angle (ϕ') of sands, or even a strength intermediate between these two values. Thus,

q_t is probably not the best means to obtain the slope of the stress-strain curve. Instead, the SCPTu that provides the initial tangent shear modulus (G_{max}) from the shear wave velocity (V_s) is a better choice.

Table A2. Selected Modulus Relationships with Cone Penetration Test Measurements.

Source	Soils Studied	Reference Modulus	Findings
Kulhawy & Mayne 1990	8 stiff OC clays	Lab constrained modulus	$D' \approx 8.25 \cdot (q_t - \sigma_{vo})$
Mohammed et al. (2000)		Resilient modulus	
Abu-Farsakh 2004	7 Louisiana sites	Lab constrained modulus	$D' \approx 3.58 \cdot (q_t - \sigma_{vo})$
Mayne (2007b)	All soil types	Constrained moduli from lab consolidation	First-order estimate: $D' \approx 5 \cdot (q_t - \sigma_{vo})$
Robertson (2009)	All soil types	Constrained modulus from consolidation	$D' = \alpha_m \cdot (q_t - \sigma_{vo})$ when $I_c > 2.2$: 1. $\alpha_m = Q_{tn}$ when $Q_{tn} \leq 14$ 2. $\alpha_m = 14$ when $Q_{tn} > 14$. when $I_c < 2.2$, then: $\alpha_m = 0.03 \cdot 10^{0.55\, Ic + 1.68}$
Liu et al. (2016)	16 clay sites in China	Resilient modulus	$M_R = (1.46 q_t^{0.53} + 13.55\, f_s^{1.4} + 2.36)^{2.44}$ (all in MPa)
Casey et al. (2016)	8 clays	Triaxial tests for undrained Young's modulus	$E_u/(\sigma_{vc}')^{0.7} = 316 - 2.3 \cdot LL$ where E_u and σ_{vc}' (MPa) and LL = liquid limit (%)

Nonlinear Modulus

The small-strain shear modulus (G_{max} or G_0) represents the initial stiffness of all soils and rocks. It is the beginning of all stress-strain-strength curves for geomaterials and obtained from elasticity theory:

$$G_{max} = G_0 = \rho_t \cdot V_s^2 \quad \text{A35}$$

where V_s = shear wave velocity, $\rho_t = \gamma_t/g_a$ = total soil mass density, γ_t = total soil unit weight, and g_a = gravitational acceleration constant (9.8 m/s^2).

From a general viewpoint on stiffness, the shear modulus G of soil is defined as the slope of shear stress versus shear strain: $G = \Delta\tau/\Delta\gamma_s$ for a tangent definition, and by: $G = \tau/\gamma_s$ as a secant definition. The shear modulus is related to its associated Young's modulus: E = 2G(1+v). Both moduli are in fact highly nonlinear, ranging from a maximum value at the small-strain stiffness ($G_{max} = G_0 = \rho_t \cdot V_s^2$, where ρ_t = total soil mass density and V_s = shear wave velocity) to intermediate G values at medium strains (≈ 1%) to low values at peak strength. As such, a variety of algorithms and formulae have been developed to represent either a partial range or the full stress-strain-strength behavior of soils over a range of interests (e.g., Mayne 2005). In these formulations, a variable number of input parameters may be required in order to produce a stress-strain-strength curve.

A modified hyperbolic form suggested by Fahey & Carter (1993) has favorable attributes in that the modulus reduction factor can be established with only a single variable. This allows the initial stiffness to the be small-strain stiffness (G_0) that is reduced in terms of level of mobilized strength, e.g. $\tau/\tau_{max} = q/q_{max} = 1/FS$, which is simply the reciprocal of the calculated factor of safety (FS). The magnitude of secant shear modulus (G) corresponding to the particular level of loading is given by:

$$G = MRF \cdot G_0 = (G/G_0) \cdot G_0 \quad \text{A36}$$

where the MRF = modulus reduction factor determined as:

$$MRF = (G/G_0) = 1 - (\tau/\tau_{max})^g \quad \text{A37}$$

and g = empirical exponent term. Figure A33 shows the relationships for normalized shear stress (τ) versus shear strain (γ_s) and corresponding normalized secant shear modulus ($G = \tau/\gamma_s$) with shear strain over a range of exponent values: $0.1 \leq g \leq 1.0$. For a discussion of tangent G, please see Fahey & Carter (1993).

Using laboratory data from resonant column-torsional shear tests and triaxial specimens with local strain measurements for G_{max} reference values, modulus reduction curves for a selection of sands and clays are presented in Figure A34. The data indicate that the exponent g falls within the range: $0.2 < g < 0.5$ for many soils, tested drained and undrained. A mean value of g = 0.3 is recommended for preliminary site investigations and designs, until additional information can be obtained.

The value of τ_{max} is the shear strength of the soil, generally taken as either: (1) drained (c' = 0): $\tau_{max} = \sigma_{vo}' \cdot \tan\phi'$, or (2) undrained, where $\tau_{max} = s_u$ = undrained shear strength, as discussed earlier. Thus, each shear stress (τ) can be associated with its shear modulus (G) and the relevant shear strain is found from: $\gamma_s = \tau/G$. This allows for generation of nonlinear stress-strain-strength curves at all depths from SCPTu data, in clays, sands, and mixed soil types.

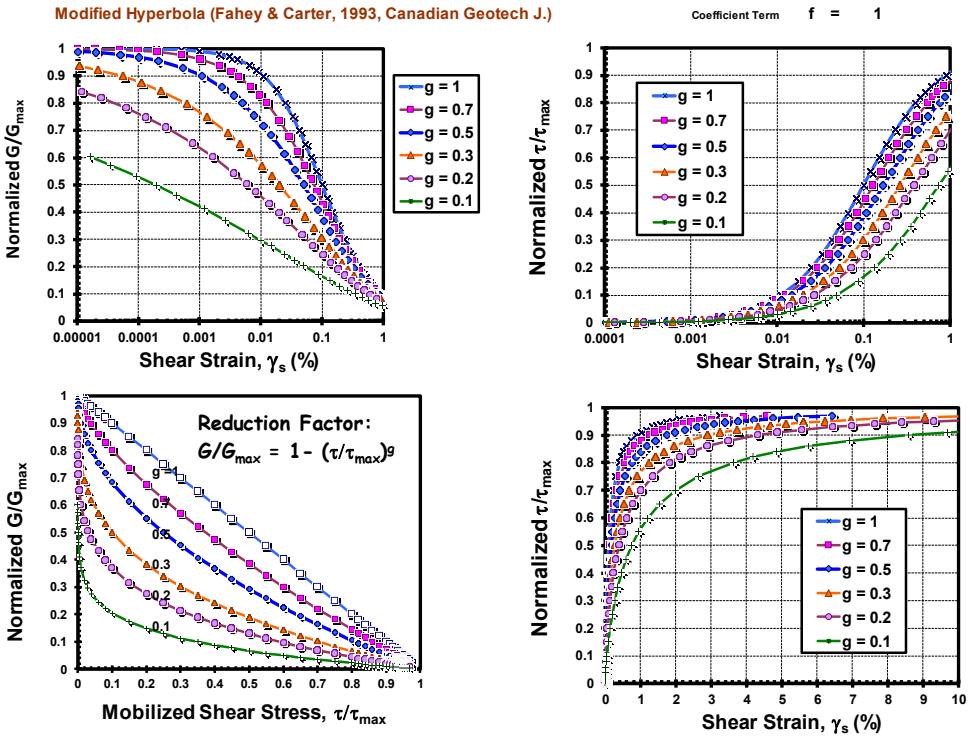

Figure A33. Normalized modulus (G/G_{max}) and normalized shear stress (τ/τ_{max}) versus shear strain (γ_s) for modified hyperbolic relationship of Fahey & Carter (1993).

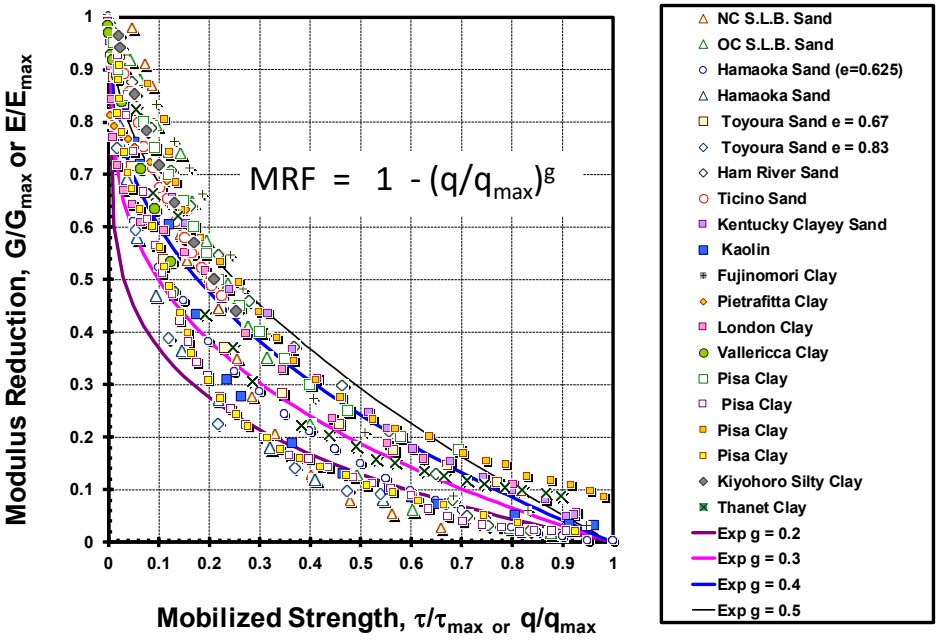

Figure A34. Modulus Reduction Factors (MRF) with mobilized strength of clays and sands.

A1.13. Coefficient of Consolidation

The rate at which foundation and embankment settlements occur, as well as the dissipation of excess porewater pressures, is controlled by the coefficient of consolidation (c_v). The magnitude of c_v is also required in the design of vertical wick drains that can be installed in soft ground to expedite the time for consolidation. Using the results of CPTu dissipation tests, which measure the rate at which the u_2 readings vary with time, the in-situ profile of c_v can be evaluated. Often, the piezocone-interpreted values of c_v are validated by comparison with results from laboratory one-dimensional consolidation tests (e.g. Abu-Farsakh, M.Y. 2004). Alternatively, a better method is to cross-check the values with the measured full-scale performance of instrumented embankments that are constructed over the ground and the recorded time-rate of consolidation and settlements can provide the best c_v for that site (Abu-Farsakh, M.Y., et al. 2011).

Monotonic Dissipation Tests

An illustrative dissipation curve from piezocone testing at IDT State Highway 95 at an embankment and bridge crossing is presented in Figure A35. After the CPTu sounding was halted at a depth of 51.2 feet, the recorded decay of porewater pressures was observed to be monotonic with time until the dissipations were ended at 1000 seconds. During that time, the u_2 readings decreased from 115 psi to 47 psi. At this location, the depth to the groundwater table is about 16 feet, thus the calculated equilibrium water pressure is 15 psi. Commonly, a characteristic time for piezo-dissipations is taken at 50% degree of consolidation, although other degrees may be adopted. By evaluating the value of u_2 at 50%, as shown in Figure A35, the characteristic t_{50} = 404 s can be obtained.

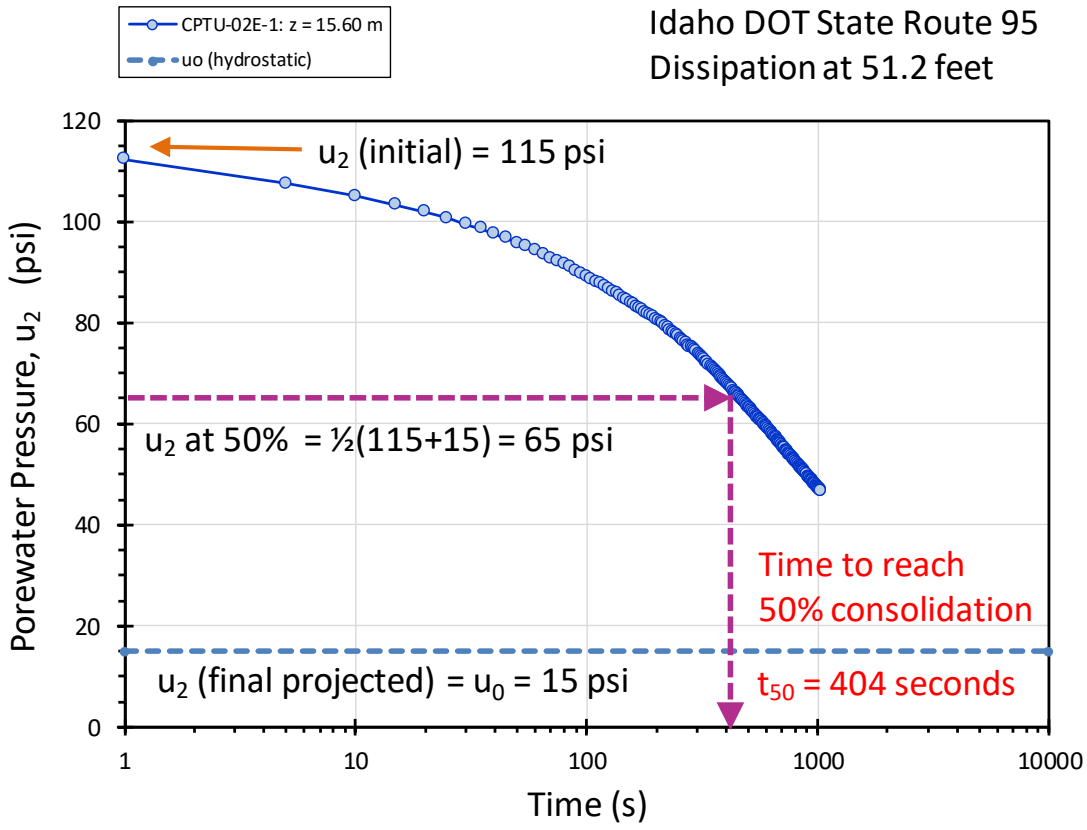

Figure A35. Piezo-dissipation at Sandpoint Bridge Crossing, Idaho for depth z = 51.2 feet illustrating the evaluation of characteristic time t_{50}.

It is also common to plot normalized excess porewater pressures relative to the measured initial Δu_2 that is obtained during penetration at the constant rate of 20 mm/s, i.e. $\Delta u/\Delta u_i$ versus time. Figure A36 shows a set of piezo-dissipation records for a bridge and embankment site in southern Louisiana reported by the LTRC. While the porewater pressure axis is arithmetic, the time scale is often plotted on either logarithmic or square root scales. In either case, the t_{50} is then found from the measured dissipation curve when $\Delta u/\Delta u_i = 0.50$.

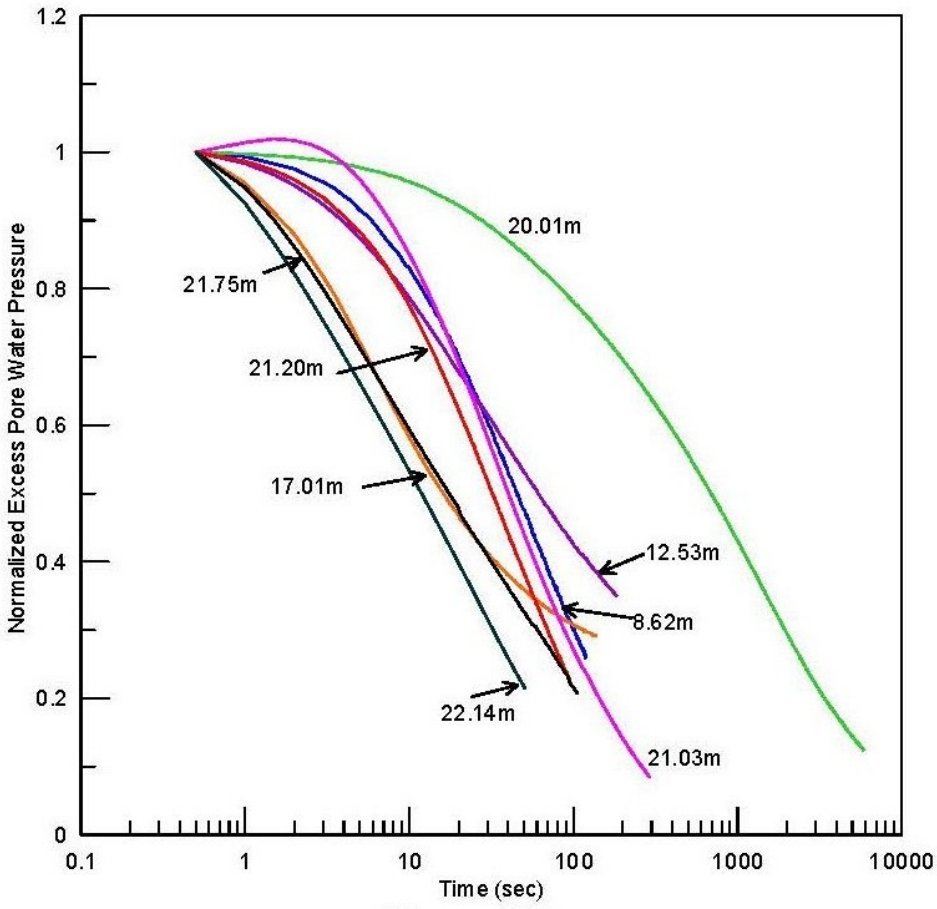

Figure A36. Set of monotonic piezo-dissipations taken at various depths for Courtableau Bridge Site on Louisana State Highway 103 (Abu-Farsakh et al. 2011).

Dilatory Dissipation Curves

In a number of situations, a monotonic type dissipation does not occur on the onset but instead a dilatory type curve is observed. Here, after stopping the push of the penetrometer, the recorded porewater pressures initially begin to rise and eventually reach a peak value, then afterwards follow a phase where the Δu values decrease to hydrostatic (Figure A37). A full solution is available for both cases (Burns & Mayne 2002). Dilatory responses are most often associated with overconsolidated clays and silts, although occasionally are observed in fine-grained soils with low OCRs.

The selection of the characteristic t_{50} value may found by using a square root of time plot to find the initial u_2 value by projection of the post-peak dissipatory data back to the ordinate axis, as shown by the example in Figure A38. In this example, the initial u_2 = 480 kPa, and then the same procedures in Figure A35may apply.

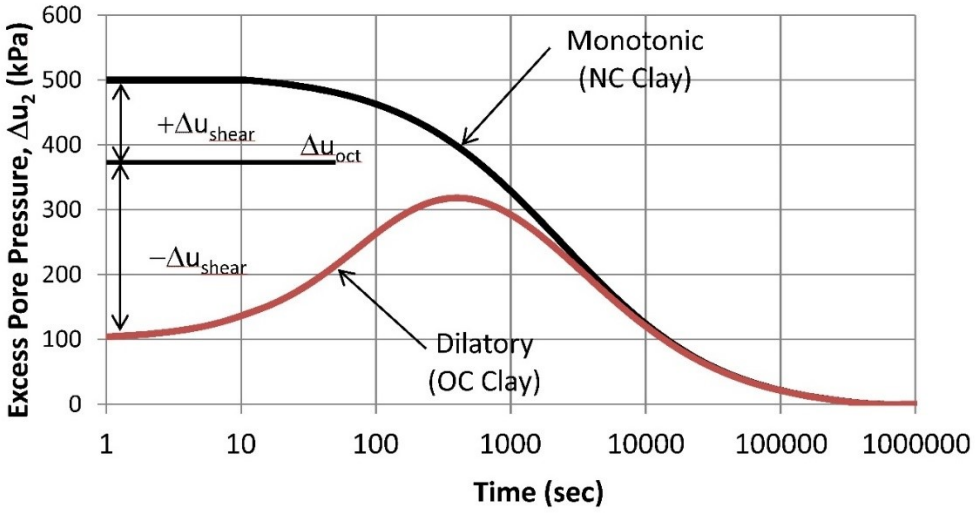

Figure A37. Monotonic and dilatory porewater dissipation responses in soils

(after Burns & Mayne 1998).

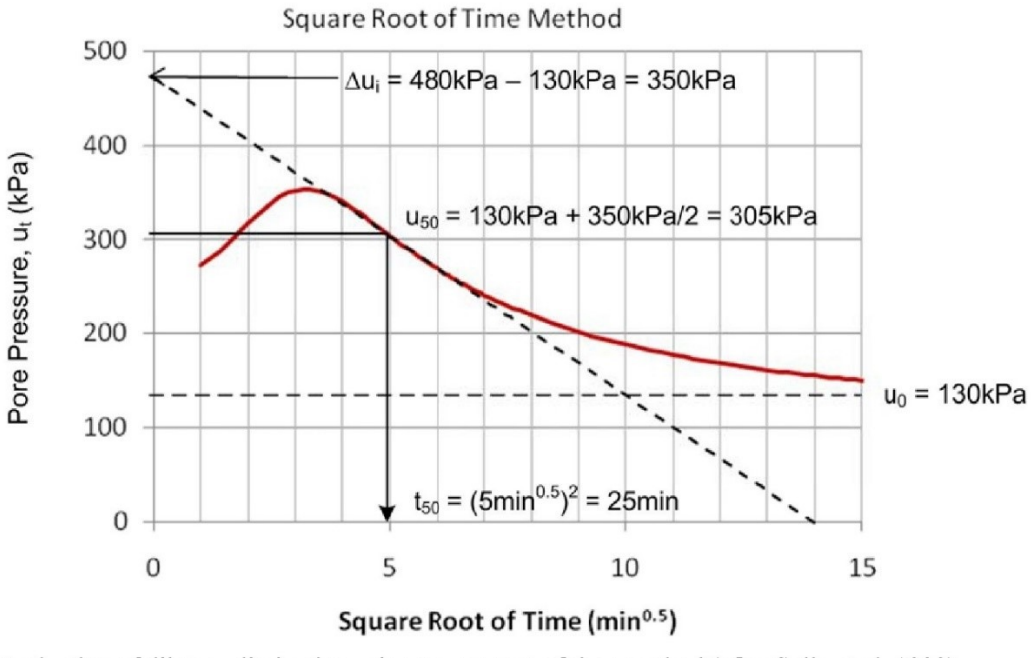

Figure A38. Method for obtaining t_{50} from dilatory dissipation curves

(Schneider & Hotstream 2010).

Interpretation of Dissipation Test Data

There are a number of different solutions available for the interpretation of the coefficient of consolidation (c_v) from the piezocone dissipation curves. For monotonic type response, the strain path method (SPM) developed at Oxford University (Teh & Houlsby 1991) is well-recognized, while the Georgia Tech solution by Burns & Mayne (2002) is based on spherical cavity expansion and critical state soil mechanics (SCE-CSSM) and handles both monotonic and dilatory curves. For both solutions, a simplified procedure can be recommended that relies on the aforementioned t_{50} value obtained from the measured field data, as given in Table A3. The units for c_v are in cm^2/s, as shown, or equivalent.

Table A3. Recommended procedures for calculating c_v from t_{50} obtained in dissipation tests

Method	Equation for coefficient of consolidation, c_v	Remarks/Notes	Eqn No.
SPM (Teh & Houlsby 1991)	$c_v = \frac{0.245 \cdot (a_c)^2 \cdot \sqrt{I_R}}{t_{50}}$	t_{50} = measured time to reach 50% dissipation $I_R = G/s_u$ = undrained rigidity index G = shear modulus s_u = undrained shear strength a_c = penetrometer radius (a_c = 1.78 cm for 10-cm^2 cone; a_c = 2.20 for a 15-cm^2 size)	A32
SCE-CSSM (Burns & Mayne 2002)	$c_v = \frac{0.030 \cdot (a_c)^2 \cdot (I_R)^{0.75}}{t_{50}}$		A33

Evaluating rigidity index

Both the SPM and SCE-CSSM solutions require an estimate of the in-situ rigidity index ($I_R = G/s_u$) of the soil. If the results of SCPTU are available, Krage et al. (2014) have derived an expression for I_R that depends upon the small-strain shear modulus, net cone tip resistance, and effective overburden stress:

$$I_{R50} = 1.811 \cdot \frac{G_{\max}}{q_{net}^{0.75} \cdot \sigma_{vo}'^{0.25}} \quad \text{A38}$$

where consistent units are input for G_{max}, q_{net}, and σ_{vo}'. The value of G_{max} is obtained from B29 using the measured shear wave velocity (V_s) and unit weight evaluated from B7.

If the shear wave velocity is not measured, it can be estimated from the CPT data. A number of methods have been reviewed for CALTRANS by Wair et al. (2012), including one that is applicable to sands, silts, and clays of low sensitivity that are inorganic and uncemented:

$$V_s\ (m/s) = [10.1 \cdot log(q_t) - 11.4]^{1.67} \cdot (100 \cdot f_s/q_t)^{0.3} \quad \text{A39}$$

where q_t is in units of kPa (Hegazy & Mayne 1995). An alternative relationship is given by Robertson & Cabal (2015).

A1.14. Hydraulic Conductivity

The hydraulic conductivity is a parameter that expresses the flow characteristics of the soil. In geotechnics, it is also called the coefficient of permeability (k) and has units of cm/s, or feet/day. Through consolidation theory, the hydraulic conductivity relates directly to the coefficient of consolidation:

$$k = \frac{c_v \cdot \gamma_w}{D'} \quad \text{A40}$$

where γ_w = unit weight of water and D' = constrained modulus.

Therefore, one approach to evaluating k can be from the site-specific c_v obtained from the dissipation tests using an estimate of D' from one of the relationships given in Table A2.

An approach developed for soft normally-consolidated soils that uses t_{50} directly to assess the magnitude of k is presented in

Figure A39 (Parez and Fauriel 1988). The mean trendline through the wedges of soil type can be approximated by:

$$k_h(cm/s) \approx \left(\frac{1}{251 \cdot t_{50}(\text{sec})} \right)^{1.25} \quad \text{A41}$$

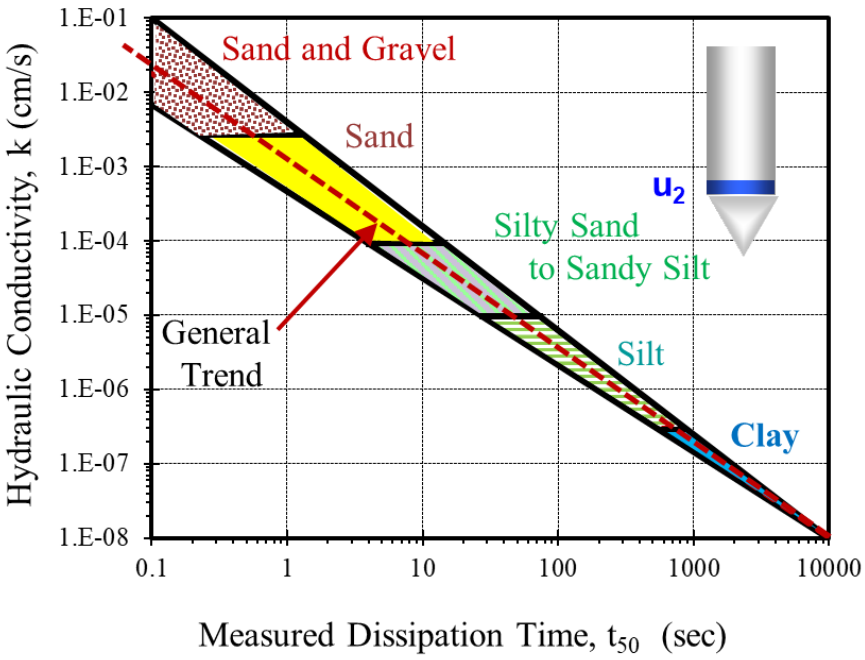

Figure A39. Hydraulic conductivity versus dissipation time for 50% consolidation (Parez & Fauriel 1988).

APPENDIX B

List of Figures

List of Tables

B1. DIRECT CPT METHOD FOR SHALLOW FOUNDATIONS

B1.1. Introduction

The analysis of shallow foundations on soils is classically handled as a two-step and two-part set of calculations involving: (a) bearing capacity, commonly reliant on limit plasticity solutions, and (b) settlement, or more appropriately termed displacements that are assessed via elastic continuum theory. The utilization of cone penetration tests (CPT) provides the necessary geotechnical data for the site-specific information on the subsurface conditions at the project site, including the geostratigraphy and evaluation of input parameters. This is still a viable approach where the CPT readings are interpreted to give the soil unit weight (γ_t), effective friction angle (φ'), undrained shear strength (s_u), preconsolidation stress (σ_p'), and elastic moduli (D' and E') for analysis.

An alternative approach is the use of CPT results to provide direct assessments of bearing capacity and/or settlements. A comparison of these two distinctly different and alternate paths is depicted in Figure B1.

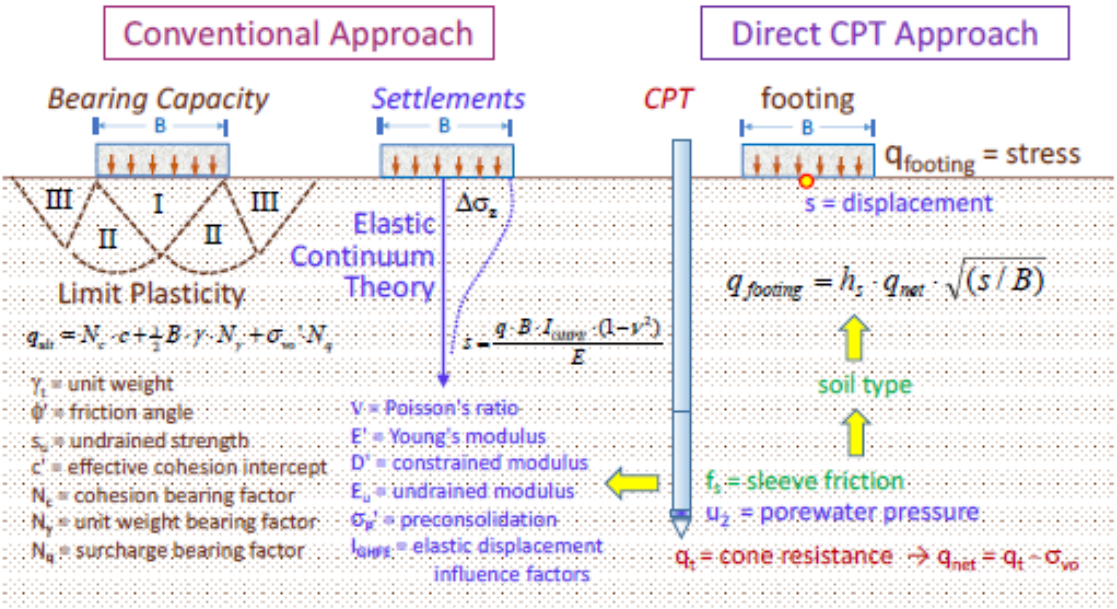

Figure B1. Conventional methods versus direct CPT approach to shallow foundation response.

A number of available direct CPT approaches for shallow footings are reviewed within this report. Moreover, as the entire load-displacement-capacity response of shallow foundations to loading occurs as a continuous nonlinear phenomenon, a single direct CPT solution is presented for the behavior of

footings on sands (drained) and clays (undrained). The methods discussed herein are specifically to address the general case of vertical loading of shallow foundations. Additional more complex situations that consider load eccentricity, moments, inclined forces, sloping ground, and other facets may be handled using well-established procedures that are discussed elsewhere (e.g., Vesić, 1975; Kulhawy et al., 1983).

This report focuses on foundations on granular soils and/or soils exhibiting drained behavior, since Federal Highway Administration (FHWA) studies have concluded that less than 1% of shallow foundations for highway bridges are placed on clay soils (Paikowsky et al., 2010). One reason for this is because soft-firm intact clays require a more complicated process that assesses both a short-term analysis (undrained) as well as long-term analysis (drained), thus requiring undrained bearing capacity, undrained distortion displacements, drained bearing capacity, and drained primary consolidation settlements.

B1.2. Direct CPT Methods for Bearing Capacity of Footings on Sands

Classical bearing capacity solutions are based most often in limit plasticity theory, albeit can be formulated from limit equilibrium, cavity expansion, and numerical methods. Because the limit plasticity solutions are prevalent and adopt total stress analysis, they are usually developed as either fully drained ($\Delta u = 0$) or fully undrained ($\Delta V/V = 0$), where Δu equals excess porewater pressure and $\Delta V/V$ equals volumetric strain. Paikowski et al. (2010) provides an extensive review of various solutions.

There are a number of direct CPT methods for the evaluation of the bearing capacity of footings and shallow foundations. Table B1 lists a variety of these direct CPT approaches for footings on sands. In the direct approach, a one-step process is used to scale the measured cone penetrometer readings (i.e., measured cone tip resistance (q_c), total cone tip resistance (q_t), sleeve friction (f_s), and/or measured porewater pressure u_2)) to obtain the ultimate bearing stress (q_{ult}) of the foundation.

Table B1. Direct CPT methods for bearing capacity of footings on clean sands.

Method	Surface Footing	Remarks and Embedment	Notes
Meyerhof (1956)	$q_{ult} = q_c\,(B/12)\cdot c_w$	$q_{ult} = q_c\,(B/12)(1+D_e/B)c_w$ Note: for silty sand, reduce by 0.5	$c_w = 1.0$ dry or moist sand $c_w = 0.5$ submerged sand
Meyerhof (1974)	$q_{ult} = q_c\,(B + D)/40$ with stresses in tsf	Presumably dry sands	B = fdn width (feet) and D = depth (feet)
Schmertmann (1978)	N/A (applies to embedded footings)	Square: $q_{ult} = 0.55\sigma_{atm}(q_c/\sigma_{atm})^{0.78}$ Strip: $q_{ult} = 0.36\sigma_{atm}(q_c/\sigma_{atm})^{0.78}$ See Figure A2	Embedment applies: $D_e > 0.5(1+B)$ for B<1m $D_e > 1.2$ m for B >1m

Canadian Geotech Society (CFEM, 1992)	$q_{ult} = R_{k0} \cdot q_c$ where $R_{k0} = 0.3$		Applied to FS = 3 where FS = factor of safety
Tand et al (1995)	N/A	$q_{ult} = R_k \cdot q_c + \sigma_{vo}$ where R_k = fctn(D_e, B)	See Figure A3

Table B1. Continued

Frank and Magnan (1995)	$q_{ult} = R_{k0} \cdot q_c$ where R_{k0} = fctn(sand consistency): Loose: $R_{k0} = 0.14$ Medium: $R_{k0} = 0.11$ Dense: $R_{k0} = 0.08$	$q_{ult} = R_{k1} \cdot q_c + \sigma_{vo}$ where R_{k1} = function (D_e, B, L, & sand consistency). Factor $R_{k1} = R_{k0}[1+R_{k2}\{0.6+0.4(B/L)\}(D_e/B)]$ and $R_{k2} = 0.35$ (loose), 0.50 (medium), and 0.85 (dense)	Loose sand: $q_c < 5$ MPa Medium sand: 8 MPa < q_c < 15MPa Dense sand: $q_c > 20$ MPa
Eslaamizaad & Robertson (1996)	$q_{ult} = K_\Phi \cdot q_c$ See Figure A4	See surface footing equation	K_Φ = function (B/D_e, shape, and density)
Lee & Salgado (2005)	$q_{bL} = \beta_{bc} \cdot q_{c(AVG)}$ where q_c averaged over distance B beneath the base	Not addressed	See Figure A5 for factor β_{bc} = fctn(B, D_R, K_0, and s/B)
Eslami & Gholami (2005, 2006)	See embedded footing solution	$q_{ult} = R_{k1} \cdot q_c$ where R_{k1} = function (ratio D_e/B and normalized q_c/σ_{vo}') See Figure A6	Measured q_c and q_c/σ_{vo}' are geometric means over 2B deep beneath footing
Robertson & Cabal (2007)	$q_{ult} = K_\Phi \cdot q_c$ with $K_\Phi = 0.16$	See surface footing equation	
Briaud (2007)	$q_{ult} = K_\Phi \cdot q_c$ with $K_\Phi = 0.23$		Based on full-scale tests at Texas A&M
Mayne & Illingworth (2010)	$q_{ult} = 0.18\ q_{c\text{-Mean}}$	Note: q_c-Mean is averaged CPT cone resistance over depth of influence z = 1.5 B deep	Based on 30 footing load tests on 12 sands
Lehane (2013)	$q_{ult} = 0.16\ q_{c\text{-AVE}}$	Note: $q_{c\text{-AVE}}$ is averaged CPT cone resistance within z (m) = [B (m)]$^{0.7}$	Based on 47 load tests

Notes: B = minimum footing width (or diameter), L = footing length, D_e = embedment depth, c_w = water table correction, σ_{vo} = total overburden stress at bearing elevation and σ_{vo}' = the effective vertical stress

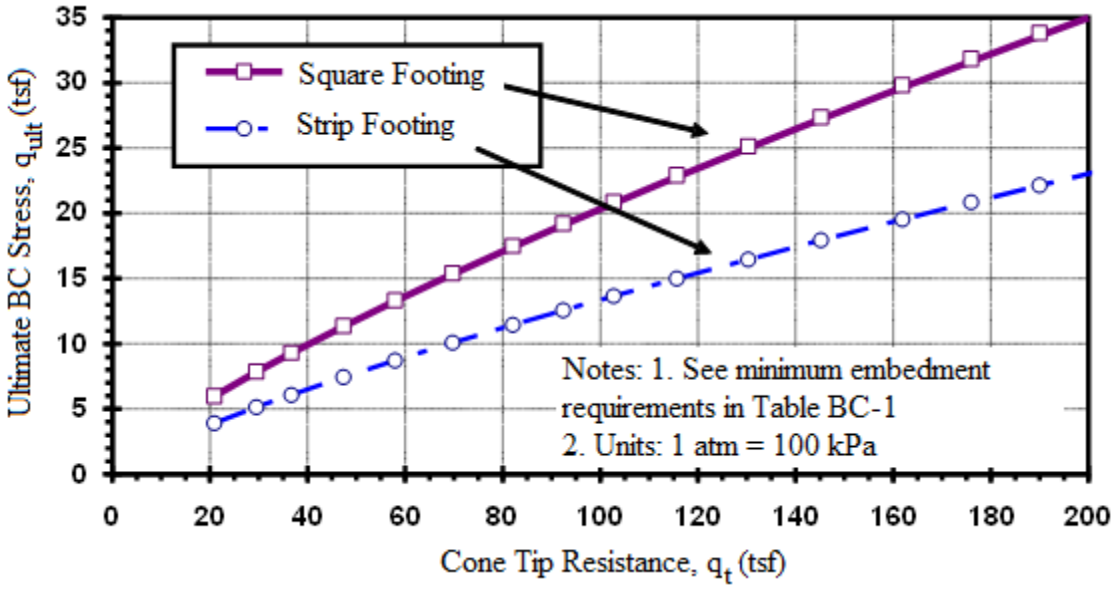

Figure B2. Direct bearing capacity relationship for embedded square and strip footings situated on clean sands (after Schmertmann, 1978).

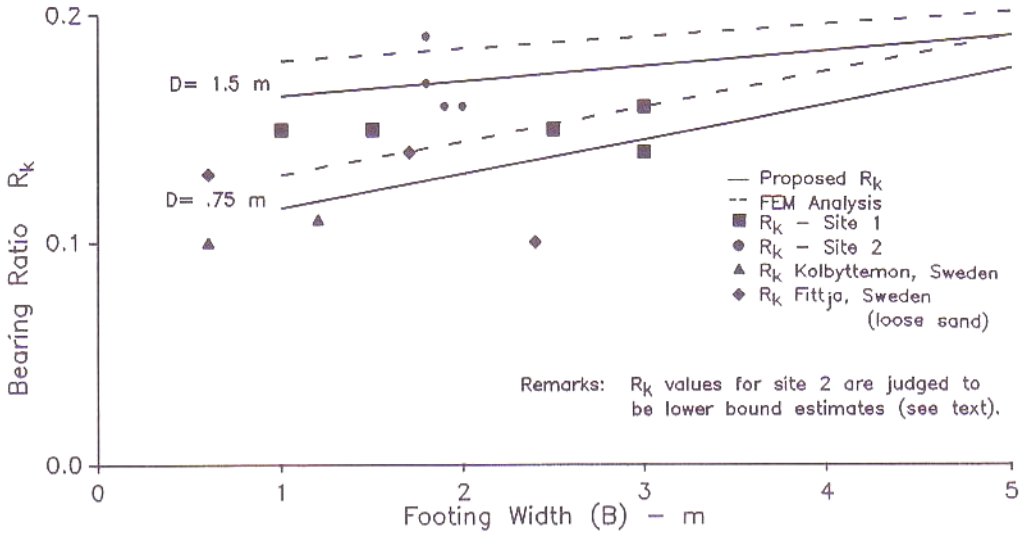

Figure B3. Direct CPT bearing factor Rk as function of footing width B and embedment depth from finite element analyses (Tand, et al., 1995).

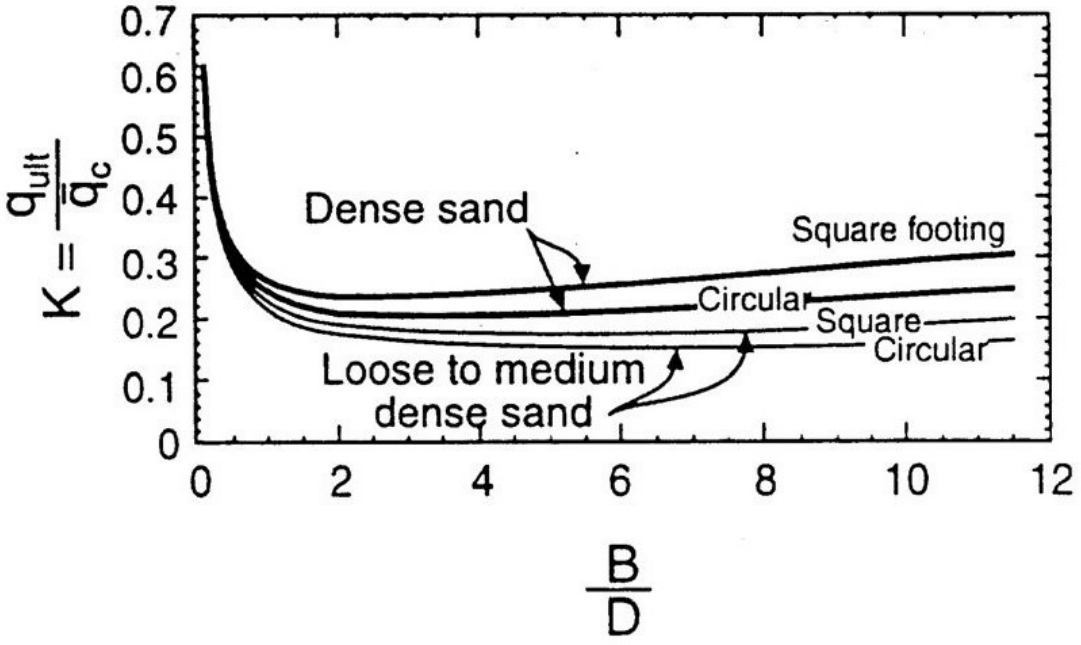

Figure B4. Direct CPT bearing factor Rk as function of footing shape, size-to-embedment ratio, and sand consistency (Eslaamizaad & Robertson, 1996).

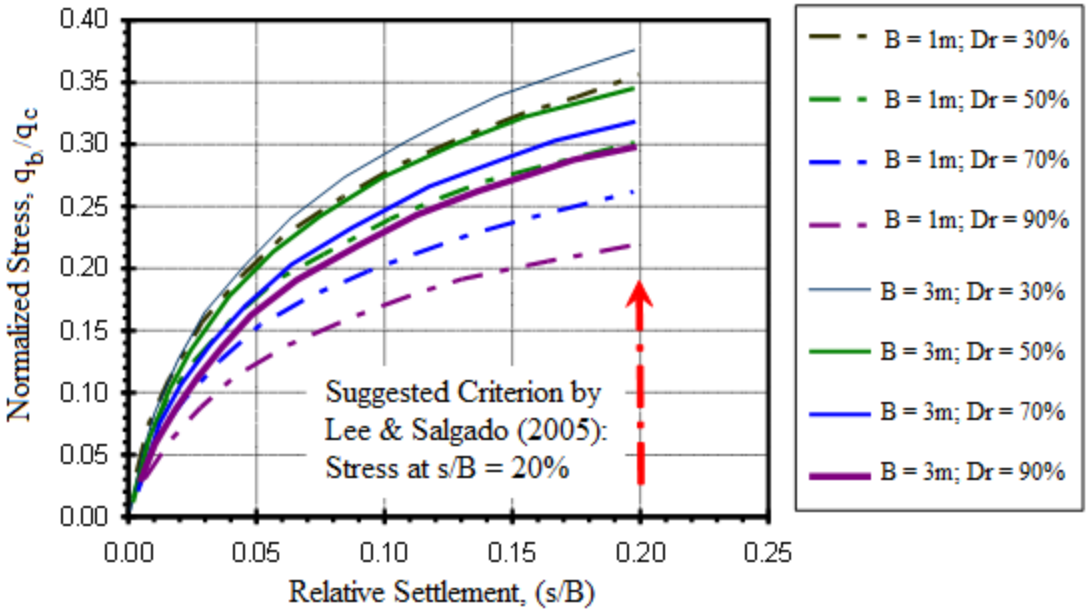

Figure B5. Direct CPT factors for bearing capacity of sands from FEM analysis by Lee & Salgado (2005) in terms of footing size, relative density, and base settlement.

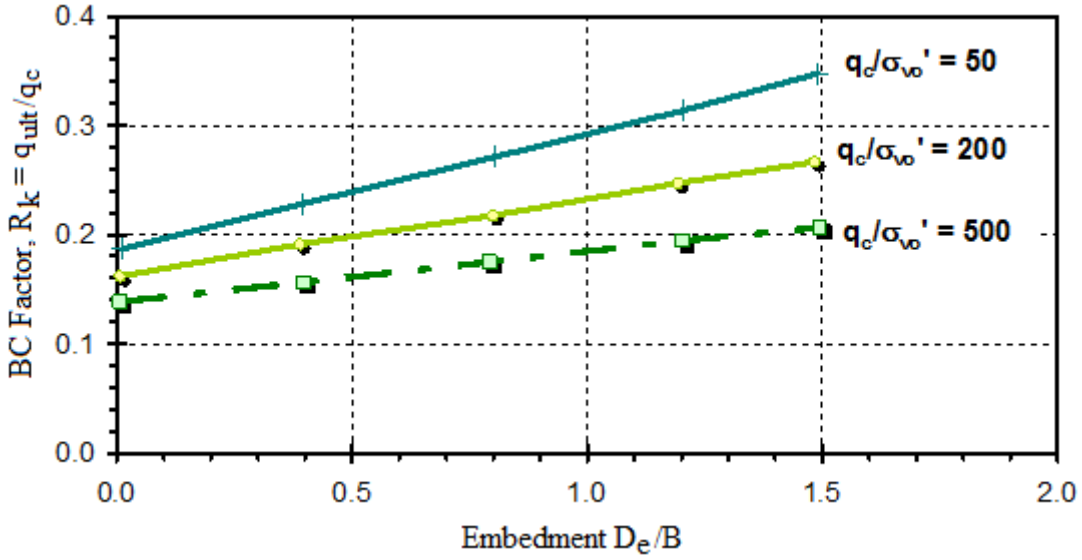

Figure B6. Direct CPT bearing factor Rk as function of footing embedment to size ratio and normalized cone tip resistance (after Eslami & Gholami 2005).

B1.3. Direct CPT Methods for Bearing Capacity of Footings on Clays

For direct CPT evaluations of foundation bearing capacity in clays, Table B2 summarizes some of the well-documented methods that are available. Generally, these assume that the loading is fast enough and the permeability of the clay is also sufficiently low, such that an undrained (i.e., constant volume) condition is maintained. This is fine for short term loading of foundations, particularly for soft to firm intact clays. However, the undrained case is not permanent. Given sufficient time, excess porewater pressures in the clay will eventually dissipate and hydrostatic conditions will return to equilibrium. During this dissipation phase, primary consolidation will occur that results in drained settlements. Also, a drained bearing capacity condition will prevail. As the CPT is advanced at a constant rate of 20 mm/s, the recorded readings normally constitute undrained behavior from a direct measurement viewpoint. Thus, direct CPT methods are normally focused at an undrained foundation response. Nevertheless, the drained footing case can be addressed using CPT results via use of conventional analysis approach and effective stress limit plasticity solutions that require piezocone penetrometers with porewater pressure measurements.

Many of the earlier solutions were based on data from mechanical penetrometers and/or older electric cones that measure the uncorrected tip resistance (q_c). It is now well-recognized that this measurement must be updated to the corrected cone resistance (q_t) because of porewater pressure effects that act on the mechanics of the load cell and geometry of the particular penetrometer design. The results are particularly significant in clays, silts, and mixed soils that are soft to firm to stiff where excess porewater pressures are recorded.

Table B2. Direct CPT methods for bearing capacity of footings on clays.

Method	Footing	Comments	Notes/Remarks
Meyerhof (1974)	$q_{ult} = \alpha_{bc} \cdot q_c$ where $0.25 \le \alpha_{bc} \le 0.50$	Applicable to saturated insensitive clays under short-term loading	Cone tip resistance measured by mechanical CPT
Trofimenkov (1974)	Approximation: $q_{ult} \approx (q_c/33)^{0.9}$ (Assuming FS = 3)	Strip footings on clays and sandy clays: 0.6m ≤ B ≤ 1.5m; 1m ≤ z_{emb} ≤ 2.5m	Mechanical CPT with q_c and q_{ult} in kg/cm^2
Schmertmann (1978)	q_{ult} = function (q_c and foundation shape)	Relationship shown in Figure A7 for square and strip footings	Cone tip resistance measured by mechanical CPT
Tand et al. (1986)	$q_{ult} = R_k \cdot (*q_c - \sigma_{vo}) + \sigma_{vo}$ Factor R_k obtained from Figure A8 accounts for surface and deep footings. Separate R_k factor for intact and jointed clays	$*q_c = (q_{c1} \cdot q_{c2})^{0.5}$ where q_{c1} is geometric mean from bearing elevation to 0.5B deeper and q_{c2} is geometric mean from 0.5B to 1.5B beneath foundation base	Mix of data from mechanical CPT q_c and electric CPT q_c
LCPC Method (Frank & Magnan, 1995)	Footing a surface: $q_{ult} = k_c \cdot q_c + \sigma_{vo}$ where $k_c = 0.32$	Embedment case: $k_c = 0.32\left[1 + 0.35(0.6 + 0.4\frac{B}{L}) \cdot \frac{D}{B}\right]$	

Note: Methods above generally consider undrained bearing capacity

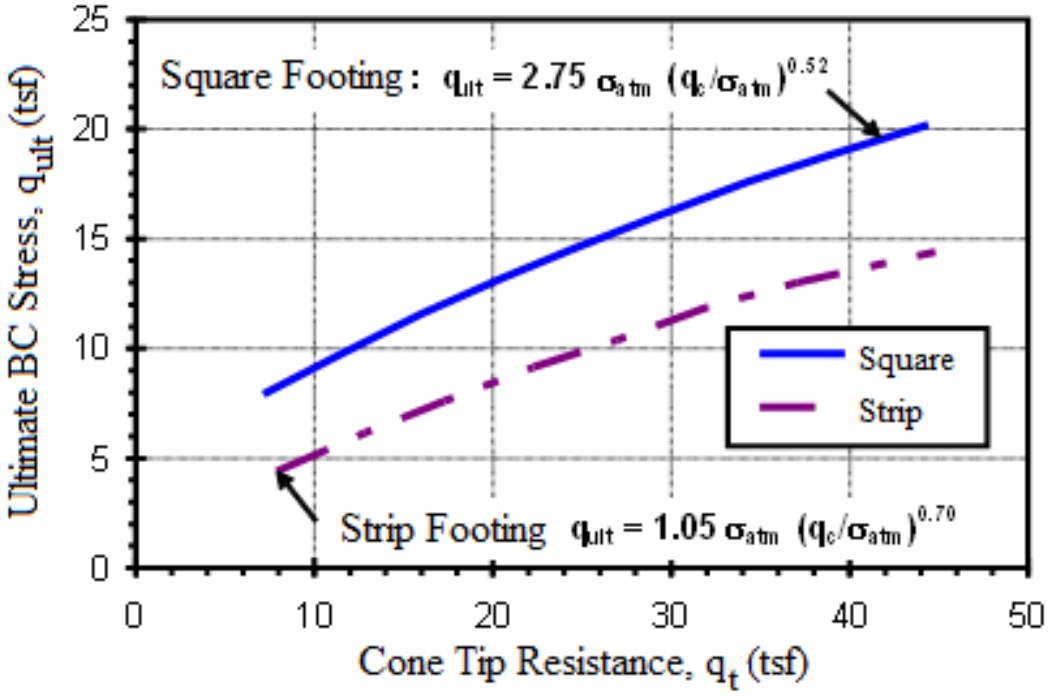

Figure B7. Direct relationship between ultimate bearing stress in clays and measured cone tip resistance (Schmertmann, 1978).

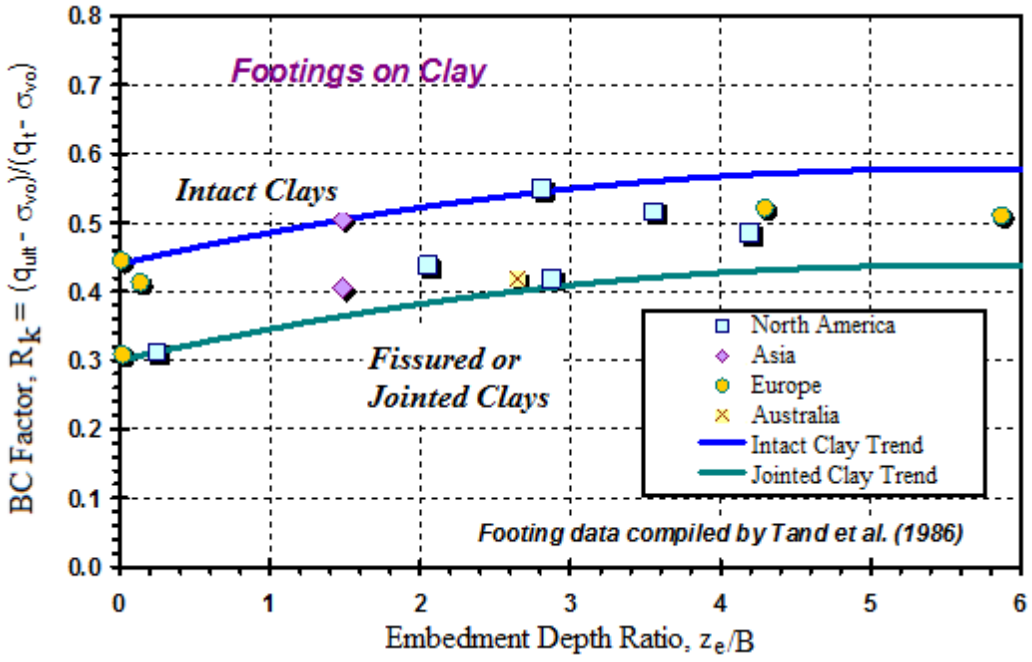

Figure B8. Direct relationship between ultimate foundation bearing stress in clays and net cone tip resistance (after Tand, et al. 1986).

B1.4. Direct CPT Assessments of Settlement and Displacements of Shallow Foundations

Methods for evaluating the magnitude of foundation displacements (s) can be found using elastic theory, subgrade reaction methods, spring models, and numerical simulations. The classical approach to footing settlement calculations on sands is to utilize elastic theory solutions (e.g., Poulos & Davis 1974) which take on the form:

$$s = \frac{q \cdot B \cdot I \cdot (1-\nu^2)}{E_s} \quad \text{B1}$$

where q = applied footing stress and I = displacement influence factor from elasticity theory.

The value of I depends upon foundation geometry, footing rigidity, embedment depth, variation of soil modulus with depth, compressible layer thickness, and other factors, as discussed by Mayne & Poulos (1999). For instance, for a flexible circular footing of diameter B resting on an infinitely deep soil formation having a constant modulus E_s with depth, the influence factor I is equal to 1 for the center point. The results of in-situ field tests such as pressuremeter tests (PMT), standard penetration tests (SPT), cone penetration tests (CPT), flat dilatometer tests (DMT), and other methods can be used to ascertain the input value of soil modulus, E_s.

Alternatively, direct CPT methods have been investigated to provide a one-step assessment of foundation displacements. Selected methods for direct CPT evaluation of shallow foundation settlements on granular soils is include DeBeers & Martens (1957), Meyerhof (1965), DeBeer (1965), Thomas (1968), Schmertmann (1970), Meyerhof (1974), Berardi & Jamiolkowski & Lancellotta (1991), Robertson (1991), Lutenegger & DeGroot (1995), Lehane & Dougherty & Schneider (2008), Gavin & Adekunte & O'Kelly (2009), Mayne & Illingworth (2010) and Uzielli & Mayne (2012).

B1.4.1 Large Scale Footing Load Tests

The measured load-displacement response of shallow foundations is conducted in the field using either stepped loading procedures or continuous rate of displacement methods. Results from the well-documented test program at the Texas A&M University (TAMU) site (Briaud & Gibbens, 1999; Briaud, 2007) for five spread footings on sand are shown in Figure B9. Each footing clearly shows a nonlinear

behavior to loading over the range of testing. This site is one of the national geotechnical experimentation sites (NGES) funded by the National Science Foundation (NSF), FHWA, and American Society of Civil Engineering (ASCE).

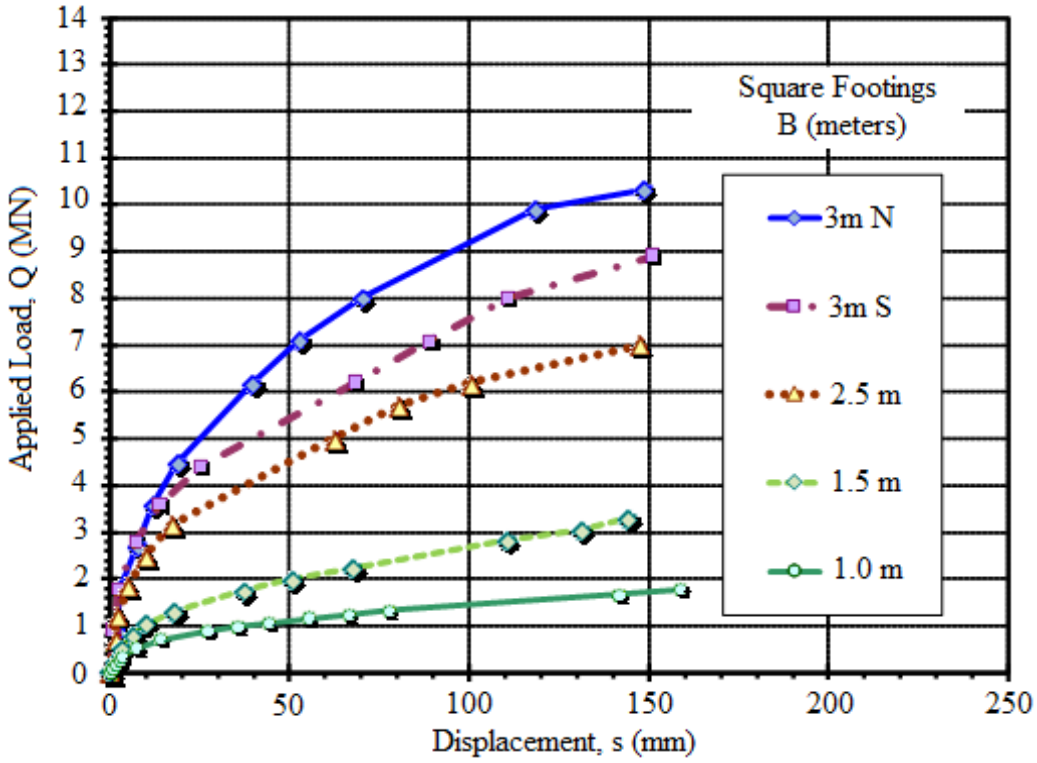

Figure B9. Measured load-displacements for each of the five large footings at TAMU (Briaud & Gibbens, 1994) sand site.

B1.4.2 Generalized Direct CPT Method for Footing Response on Soils

The use of applied foundation stress versus normalized displacement curves (q vs. s/B) is generalized to footings on sands, silts, intact clays, and fissured clays. A square root plotting of the normalized displacements (s/B) permits a single parameter characterization for each specific soil type that in turn, correlates with the net cone tip resistance. The generalization is based on a statistical review of data from large foundations (B > 0.5m) involving 70 full-scale load tests with available CPT data. For fine-grained soils, the data are from electronic piezocone tests where the proper correction from q_c to q_t has been obtained to allow the best possible results. The methodology permits an evaluation of the load-displacement-capacity response of shallow square footings based on CPTs performed in the four types

of ground conditions. For the TAMU footings, the characteristic stress-normalized displacement response is shown in Figure B10 where all five foundations can be represented by a single curve.

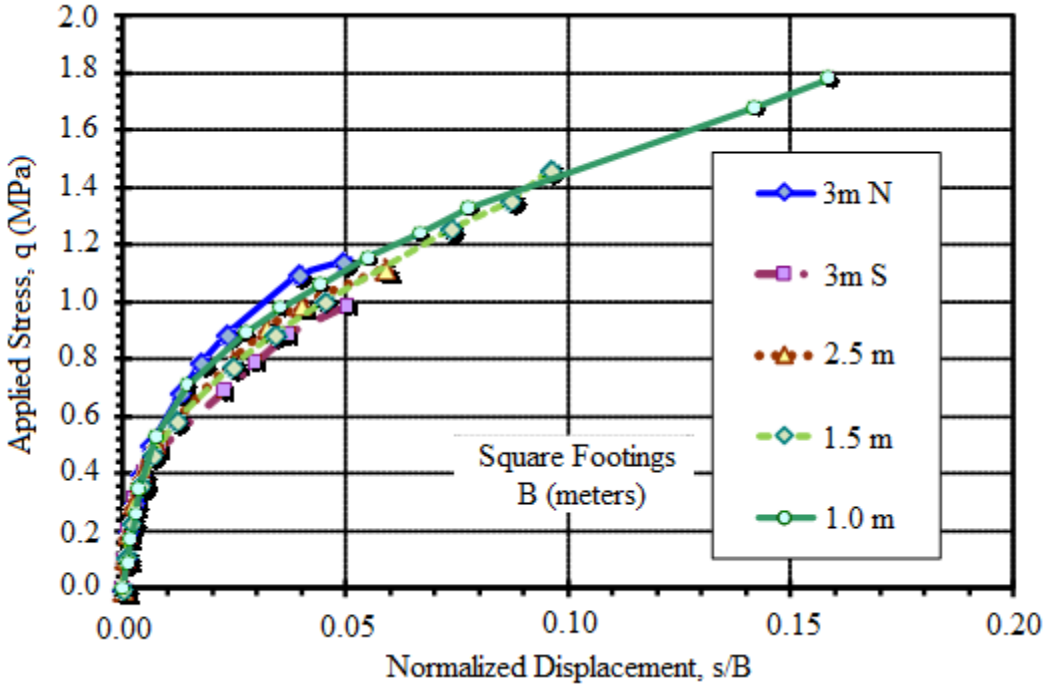

Figure B10. Characteristic nonlinear stress-normalized displacement curve for the five TAMU (Briaud & Gibbens, 1994) footings.

B1.4.3 Characteristic Stress-Displacement Curves

Fellenius & Altaee (1994) recommended the concept of a characteristic stress (q) vs. normalized displacement (s/B) curve for foundation response on a given soil formation, later supported by Decourt (1999), Briaud & Gibbens (1999), Lutenegger & Adams (2003), and Briaud (2007). In this approach, the measured load (Q) vs. displacement from individual footings of various sizes that rest on the same soil conditions collapse to a unified relationship given in Equation B2:

$$q_{applied} = a_f \left(\frac{s}{B}\right)^{bf} \quad \textbf{B2}$$

where a_f and b_f are empirical fitting coefficients (Decourt 1999; Uzielli & Mayne 2011, 2012).

In a review of measured load tests data from large spread footings situated on different sands, it has been suggested that Equation B2 can be reduced to a single parameter expression by use of square root plotting where the exponent bf is equal to 0.5 (Mayne & Illingworth 2010; Mayne et al. 2012):

$$q_{applied} = r_s \sqrt{\frac{s}{B}} \qquad \textbf{B3}$$

where r_s = fitted soil parameter from best fit line regression. In the case of sands, the coefficient r_s represents the supporting soil conditions including particle size, relative density, and fines content, as well as geologic origin, aging, and overconsolidation effects.

The results from the five TAMU footings are presented in this format in Figure B11 that shows the formation factor r_s = 4.86 MPa for this sand deposit. This single coefficient can be used to express the nonlinear load versus settlement of any size footing on this sand site. Moreover, one criterion, from Eurocode, for "bearing capacity" that is used by the European community identifies that stress (or load) which corresponds to (s/B) = 10%. That is, when the displacement equals ten percent of the footing width, then the "capacity" has been reached. Therefore, adopting this criterion for footings on sands, the ultimate bearing stress (q_{ult}) for footings on sand can be taken when (s/B) equals 0.10, or when square root of (s/B) equals 0.316. In that case, this gives: q_{ult} equal to 0.316 · r_s. For the TAMU site, this gives q_{ult} equal to 0.316 times (4.86) which equals 1.53 MPa, as illustrated by Figure B12.

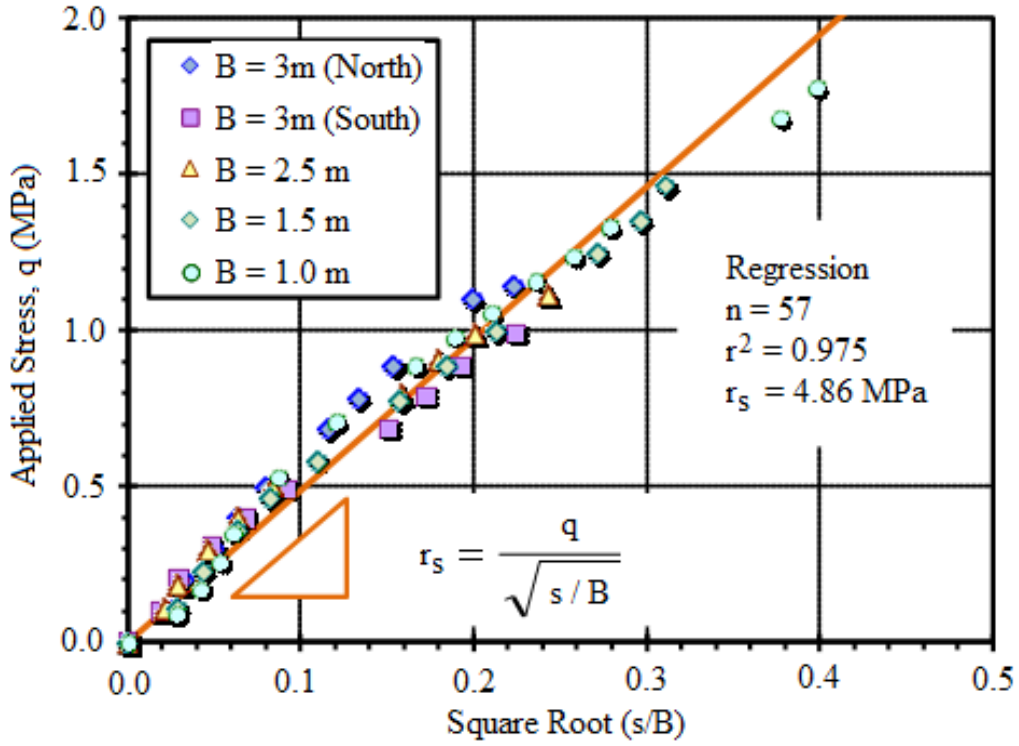

Figure B11. Characteristic stress versus square root normalized displacements for TAMU footings.

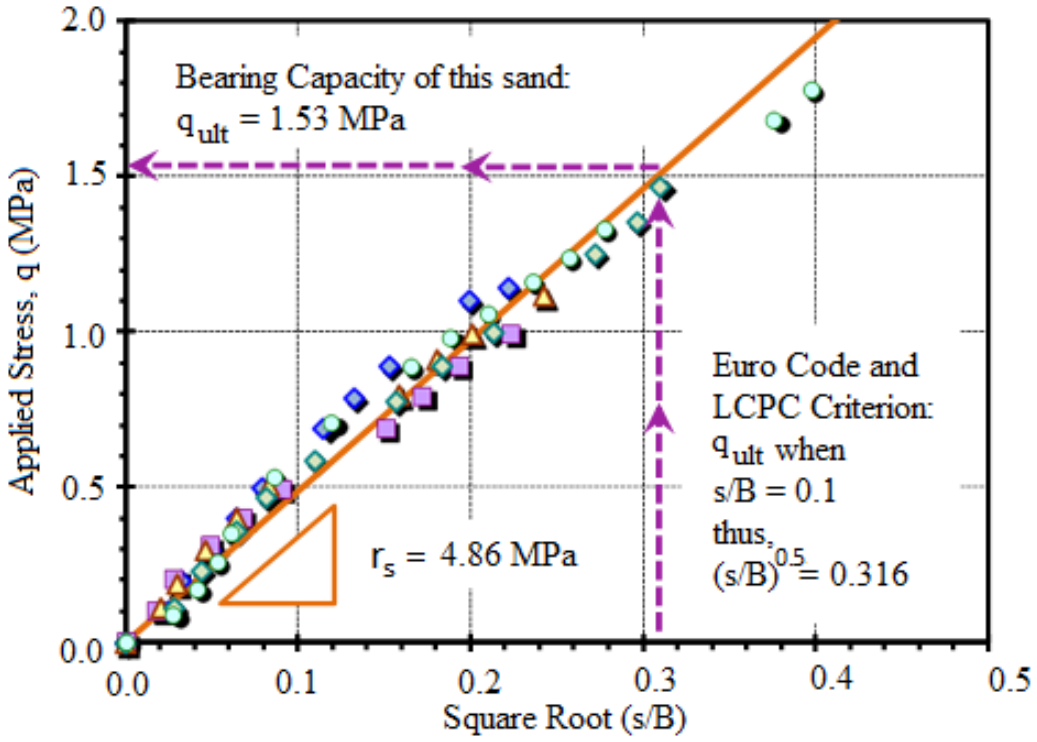

Figure B12. Eurocode or LCPC criterion applied to determine bearing capacity of TAMU sand.

B1.5. Footing Database

A database of spread footings and large plates was assembled which considers only full-size shallow foundations (0.5 ≤ B ≤ 6 m) that rest on sands, silts, and clays. Sites for the foundations were also subjected to CPT. The inclusion solely of large footings are significant because results from small-scale model footings exhibit scale effects. In fact, experimental centrifuge work and numerical simulation studies have shown that bearing capacity factors are size-dependent, especially for factor N_γ decreasing with footing width B (Kimura et al., 1985; Cerato & Lutenegger, 2007; Mase & Hashiguchi, 2009). A direct approach based on full-size footings provides a more reliable means for foundation evaluation.

The compiled database is given in Table B3 with a total of 70 large footings and plates. These include a listing of 34 foundations on 13 sands, 11 footings on 4 silt deposits, 13 footings or large plate load tests on 6 intact clays, and 12 foundations on 5 fissured clays. Most of the footings were square or nearly square (80%), while the remaining were circular. The largest foundation was a mat 5 m by 14 m in plan, loaded by stacking Kentledge concrete blocks to cause a bearing failure in the underlying soft clay. For sands, the largest footing consisted of the 6-m square concrete pad. In terms of equivalent square footings, mean footing sizes were 1.55 m (sands), 1.14 m (silts), and 1.26 m (clays).

Additional details on the individual load tests and site conditions are given elsewhere (Mayne 2009; Mayne & Illingworth, 2010; Uzielli & Mayne, 2011, 2012; Mayne et al., 2012; Mayne & Woeller, 2014).

Table B3. Summary of large footings, soil conditions, and reference sources of database

Sand Site	**Location**	**Soil Conditions**	**Footings: Numbers, Shapes and Sizes**	**References/Source**
College Station	Texas	Pleistocene sand	5 Square: 1, 1.5, 2.5, 3,3 m	Briaud & Gibbens (1999)
Kolbyttemon	Sweden	Glaciofluvial sand	4 Rect: B = 0.6, 1.2, 1.7, 2.4 m	Bergdahl et al. (1985, 1986)
Fittija	Sweden	Glaciofluvial sand	3 Rect: B = 0.6, 1.7, 2.4 m	Bergdahl et al. (1984, 1985)
Alvin West	Texas	Alluvial sand	2 Circular: D = 2.35 m	Tand et al. (1994)
Alvin East	Texas	Alluvial sand	2 Circular: D = 2.2 m	Tand et al. (1994)
Perth	Australia	Silceous dune sand	4 Square: B = 0.5 and 1.0 m	Lehane (2008)
Grabo T1C	Sweden	Compacted sand fill	1 Square: B = 0.46 m	Long (1993)
Grabo T2C	Sweden	Compacted sand fill	1 Square: B = 0.63 m	Long (1993)
Grabo T3C	Sweden	Compacted sand fill	1 Square: B = 0.80 m	Long (1993)
Labenne	France	Dune sand	6 Square: B = 0.7 and 1.0 m	Amar et al. (1998)
Green Cove	Florida	Brown silty sand	1 Circular: D = 1.82 m	Anderson et al. (2006)
Durbin	South Africa	White fine sand	1 Square: B = 6.09 m	Kantley (1965)
Porto	Portugal	Residual clayey sands	1 Circular D = 1.2 m and 1 plate	Viana da Fonseca (2003)
Jossigny	France	Soft clayey silt	2 Square: B = 1 m	Amar et al. (1998)
Tornhill	Sweden	Glacial Baltic till	3 Square: B = 0.5, 1, 2 m	Larsson (2001)
Vagverkel	Sweden	Stiff medium silt	3 Square: B = 0.5, 1, 2 m	Larsson (1997)
Vattahammar	Sweden	Brn-Gry layered silt	3 Square: B = 0.5, 1, 2 m	Larsson (1997)

Table B3. Continued

Clay Site	Location	Soil Conditions	Footings: Numbers, Shapes and Sizes	References/Source
Baytown	Texas	Fissured Beaumont	2 plates with d = 0.76 m	Stuedlein & Holtz (2008)
Belfast	Ireland	Soft clay silt "sleech"	1 Square Pad: B = 2.0 m	Lehane (Geot Engr 2003)
Bothkennar	Scotland	Soft silty clay	2 Square Pads: B = 2.2, 2.4 m	Jardine et al. (1995)
Bangkok	Thailand	Soft to stiff clay	4 Square: 0.67, 0.75, 0.90, 1.0 m	Brand et al. (1972)
Haga	Norway	Stiff OC clay	2 Square Footings: B = 1.0 m	Andersen & Stenhammar (1982)
Rio Grande	Brazil	Sandy residual clay	3 Square: 0.4, 0.7, and 1.0 m	Consoli et al. (1998)
Shellhaven	England	Soft estuarine clay	Rectangular: 5 m by 14 m	Schnaid et al. (1993)
Texas City A	Texas Coast	Fissured Beaumont	3 circular plates: d = 0.58 m	Tand et al. (1986)
Texas City B1	Texas Coast	Fissured Beaumont	2 circular plates: d = 0.58 m	Tand et al. (1986)
Texas City B2	Texas Coast	Fissured Beaumont	1 circular plate: d = 0.58 m	Tand et al. (1986)
Alvin, Texas	Texas Coast	Fissured Beaumont	3 circular plates: d = 0.58 m	Tand et al. (1986)

For the series of footings on sands, Figure B13 shows the summary of measure formation factors (r_s) for the 34 foundation load tests. Also, indicated on the graph are the corresponding mean q_c values of the sands, averaged over 1.5·B beneath the bearing elevations.

Note also in sands that the q_t and net resistance (q_{net}) are all very close to the measured q_c, since: (a) porewater pressure corrections for the a-net value are negligible in clean sands; and (b) overburden stresses are typically only 1% to 3% of the magnitude of q_c. This is especially true of shallow depths. Therefore, for clean sands, q_{net} is approximately q_t which is approximately q_c.

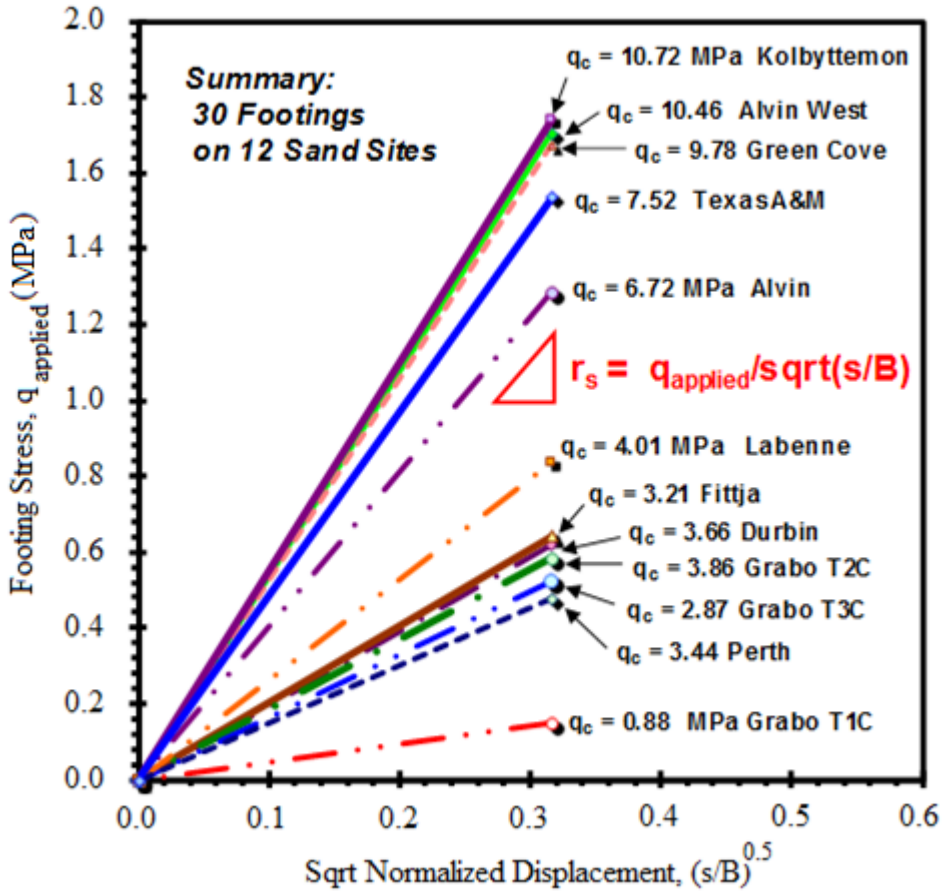

Figure B13. Summary of sand formation factors with corresponding CPT resistances.

As suggested by Briaud (2007), various in-situ measurements can be used to normalize the results, from cone penetration tests in this case. Herein, the q_c from the CPT soundings in the sands are used to normalize the footing stress axis, as presented in Figure B14. It is evident that the results of the load-displacement response of all 34 footings on 13 different sands can be captured by the characteristic stress versus normalized displacement with the inclusion of the site-specific cone tip resistance. In this case, the mean trend for all footings and sand sites indicates a simple expression shown in Equation B4.

Clean quartz-silica sands:

$$\frac{q_{footing}}{q_c} = 0.585\sqrt{\frac{s}{B}} \qquad \textbf{B4}$$

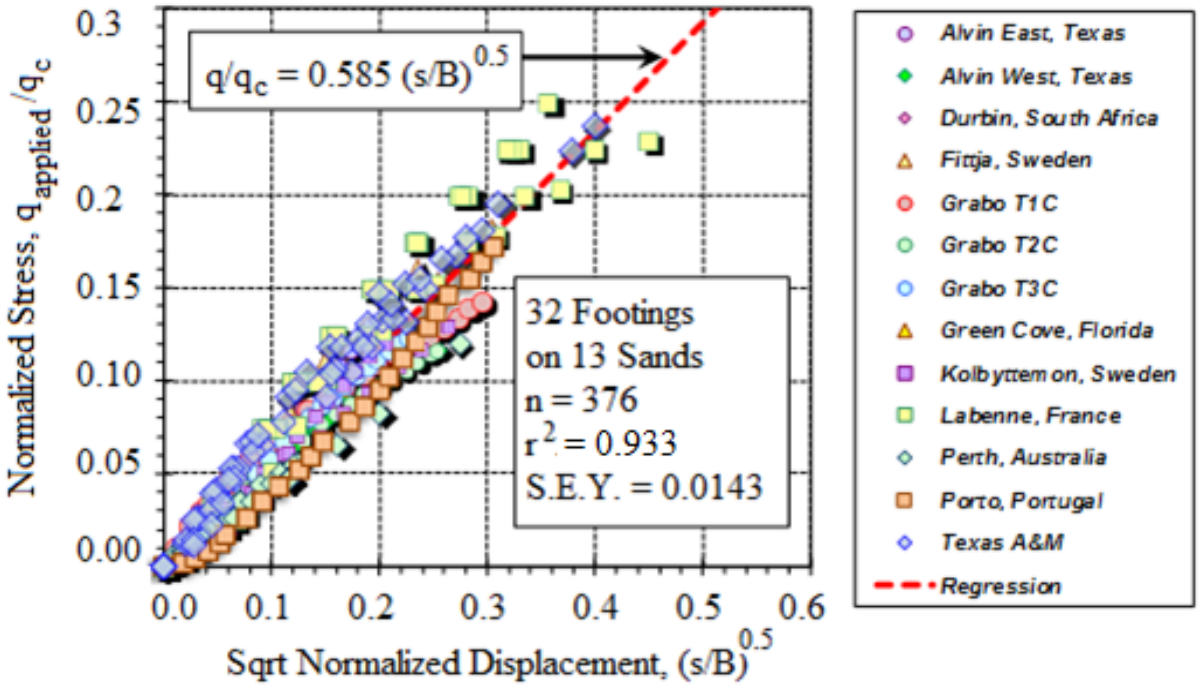

Figure B14. Normalized foundation stresses vs. square root of normalized displacement for spread footings on sand (modified after Mayne et al., 2012)

The results of measured force-displacement curves (Q vs s) from footing load tests are nonlinear and, thus, the definition of "capacity" must be addressed. Kulhawy (2004) identified three main curve types that occur during load testing, depicted in Figure B15. The most common response (Type A) shows no clear peak and is observed in sands and silts, as well as slow loading of insensitive clays and fissured clays. In this case, “capacity” can be defined by the Eurocode corresponding to the load (or stress) when s/B=10% (Amar et al., 1998). For foundations situated on many clays, a plateau capacity is reached, as depicted as Type B response. In rare cases where sensitive clays or structured soils are encountered, a Type C relationship occurs whereby the load-displacement curve reaches a peak followed by strain softening. In the one case observed in this study for Type C loading (Haga clay), the corresponding “peak capacity” was reached at a pseudo-strain of s/B = 4%, as shown in Figure B16 followed by some strain softening. In the cases of soft clays at Belfast and Bothkennar, a plunging type (plateau failure) was achieved at around s/B=7%.

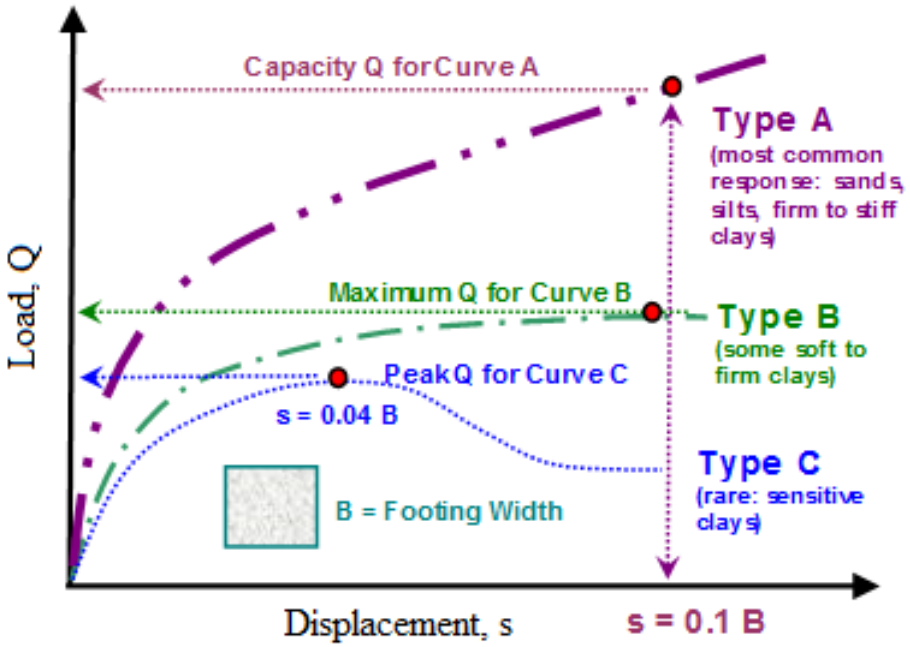

Figure B15. Definitions of "capacity" from three types of observed foundation load test responses (modified after Kulhawy, 2004).

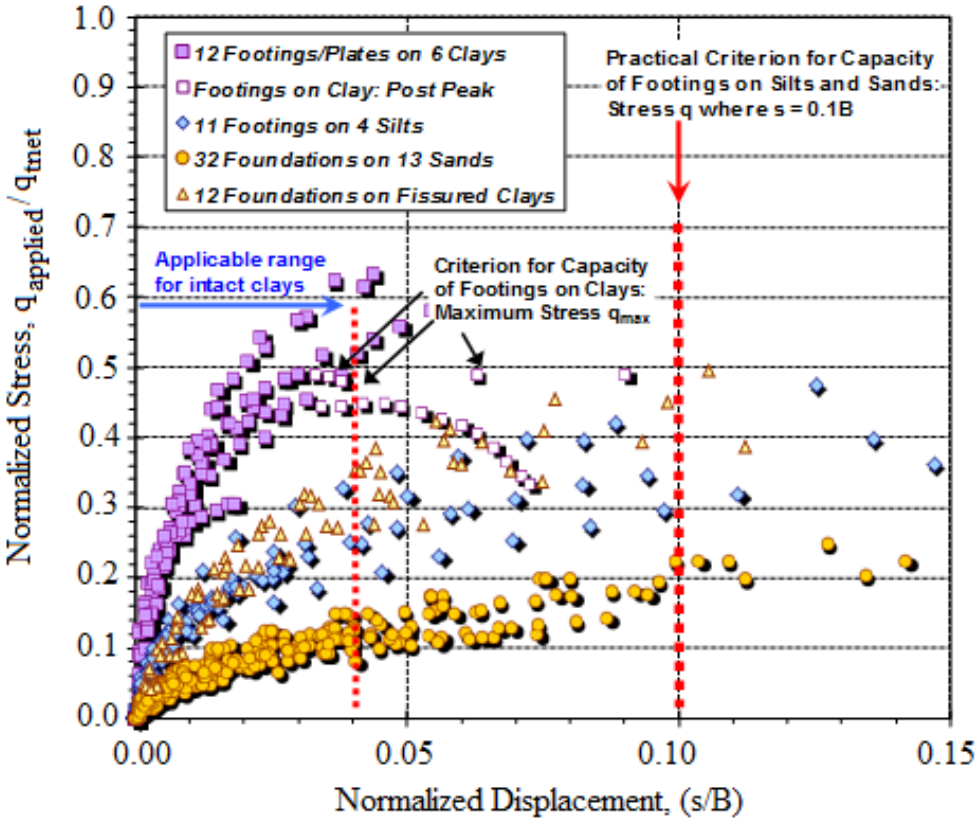

Figure B16. Summary of applied footing stresses normalized to CPT net cone resistance vs pseudo-strains (s/B) for all footings.

In the case of fine-grained soils that develop excess porewater pressure during cone penetration, the use of the net total cone resistance (q_{tnet}), which equals the cone tip resistance minus the total stress, must be considered (Lunne et al., 1997). As noted earlier, the correction of CPT data in sands is minimal because of the low value of penetration porewater pressures and the fact that total overburden stress is small relative to the cone resistance, especially for shallow soundings. Thus, the use of q_{tnet} may be substituted for q_c into the trend of Figure B1.

B1.6. Undrained and Drained Capacity

The footings on sands typically show drained response with no excess porewater pressures developed during loading. For the foundations situated on silts, analyses by Larsson (1997, 2001) concluded that these too show drained conditions. For shallow foundations on clays, the entire range of drainage cases are possible, ranging from undrained to partially-drained to fully-drained, depending upon the applied rate of loading relative to the permeability of the geomaterial. If sufficient data were available for each of the clay sites, then the recent evaluation of drainage condition could be assessed using normalized velocity criteria (Chung et al., 2006). However, this was not possible with the current data set. Instead,

the test loadings of footings on clays have essentially been assumed to primarily occur under undrained conditions, following recommendations by Tand et al., (1986). For this case, a limiting bearing stress can be calculated from bearing capacity analyses and related directly to the CPT readings.

From classical bearing capacity calculations using limit plasticity solutions, the ultimate foundation stress is shown in Equation B5.

$$q_{ult} = N_c \cdot s_u \quad \textbf{B5}$$

where N_c equals the bearing factor for constant volume (5.14 for strip and 6.14 for square or circular plan) and s_u equals the undrained shear strength of the clay. For the case of soft to firm clays of low to medium sensitivity, the operational strength can be related to the preconsolidation stress (Mesri 1975; Jamiolkowski et al., 1985) as shown in Equation B6.

$$s_u = 0.22\sigma'_p \quad \textbf{B6}$$

Finally, the effective preconsolidation stress has been linked directly to the net cone resistance (Chen & Mayne 1996; Demers & Leroueil 2002) as shown in Equation B7.

$$\sigma'_p = 0.33(q_t - \sigma_{vo}) \quad \textbf{B7}$$

Combining Equations (B5), (B6), and (B7) results in direct expressions for undrained bearing capacity on intact clays from CPT results as shown in Equations B8 and B8-2.

Strip footing: $$q_{ult} = 0.373(q_t - \sigma_{vo}) \quad \textbf{B8}$$

Square/circle: $$q_{ult} = 0.445(q_t - \sigma_{vo})$$ B8-2

Equation (B8-2) is in excellent agreement with Tand et al., (1986) database study for the case of intact clays and footings with no embedment. Their study also provided a lower relationship for foundations situated on jointed clays, specifically recommending that the bearing stress not exceed 0.30 q_{tnet}. Review of the available data in Figure 3 shows this to be rather conservative and a more realistic value may be taken at 0.40 q_{tnet} for fissured clays.

B1.6.1 Normalized Undrained Footing Response

The characteristic stress vs. normalized displacement curves for footings on clays exhibiting undrained conditions can be verified using a relatively recent case study on Beaumont clay by Stuedlein & Holtz (2010). The Baytown, Texas site was investigated using an exploration program of soil borings, piezocone soundings, and laboratory testing. The field testing included a large square footing (B = 2.76 m) and two small circular plates (D = 0.76 m). The measured load-displacement responses for all three foundations are presented in Figure B17. Of course, the large footing carried considerably higher loads than the two small plates on the same soil deposit. Yet, using the aforementioned characteristic stress (q) vs. square root of normalized displacement (s/B) essentially gave a unique relationship for all 3 foundations, as presented in Figure B18. In this case, utilizing the form of Equation B2, the characteristic coefficient r_s is 1.77 MPa for this deltaic clay formation.

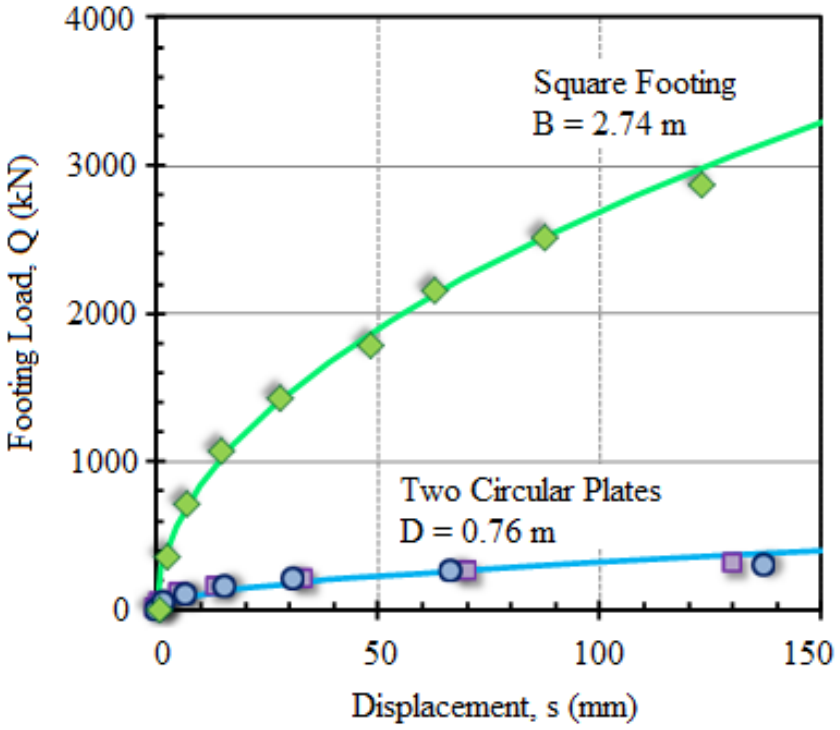

Figure B17. Measured load vs. displacement curves for 3 shallow foundations on clay at Baytown, Texas (Stuedlein & Holtz 2010).

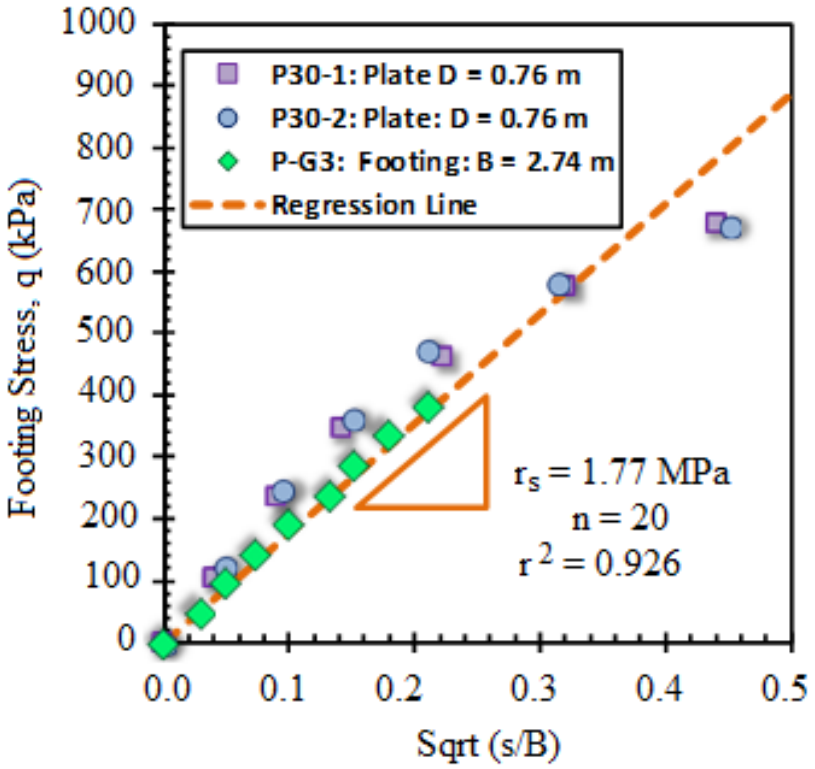

Figure B18. Characteristic stress vs. square root of normalized displacement for all three foundations at Baytown site (Stuedlein & Holtz 2010).

B1.7. General Direct CPT Method

In a manner, analogous to the normalization of applied foundation stresses shown in Figure B14 for footings on sands, a generalized direct CPT method for shallow foundations on different soils can be made in Equation B9.

$$q = h_s \cdot q_{tnet} \cdot \left(\frac{s}{B}\right)^{0.5} < q_{capacity} \qquad \text{B9}$$

where $q_{capacity}$ is equal to the foundation bearing capacity of the ground and h_s is equal to the empirical fitting term that depends on soil type. Specifically: h_s equals 0.58 for sands, 1.12 for silts, 1.47 for fissured fine-grained soils, and 2.70 for clays. A summary of the normalized stress versus the normalized displacement curves for these four soil types is presented in Figure B19 where the data fitting to obtain the h_s parameter on clays are limited to (s/B) < 0.04, corresponding to undrained loading. The data on

silts and sands are considered fully drained, whereas the fissured clay subset may be partially drained to undrained. The statistical measures for obtaining the fitted parameter h_s are quite good as shown in Figure B20 with the coefficient of determinations (r^2) values of 0.947 for sands, 0.88 for silts, 0.935 for fissured, and 0.925 for intact clays. Additional statistical evaluations on the database are provided by Uzielli & Mayne (2011).

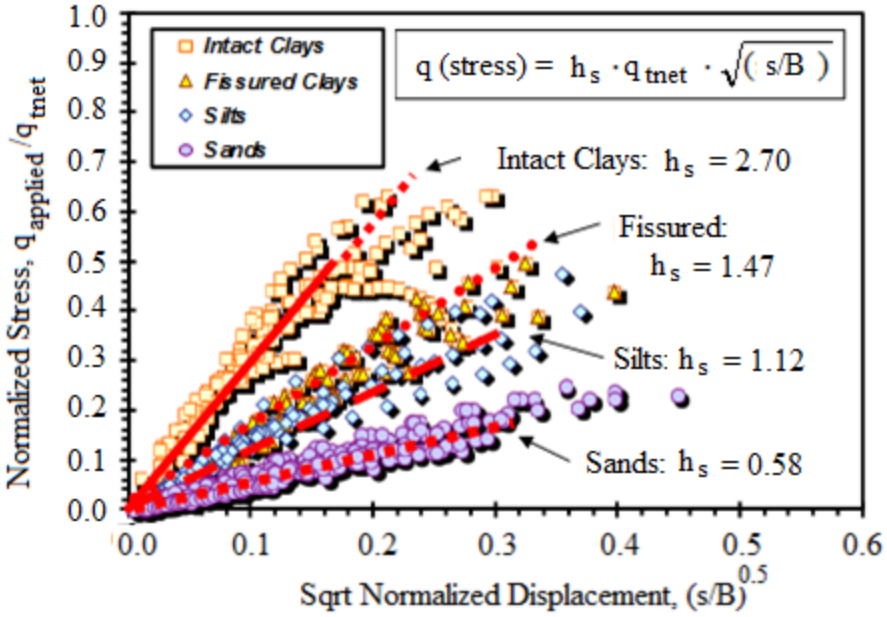

Figure B19. Normalized foundation stress vs square root of normalized displacements.

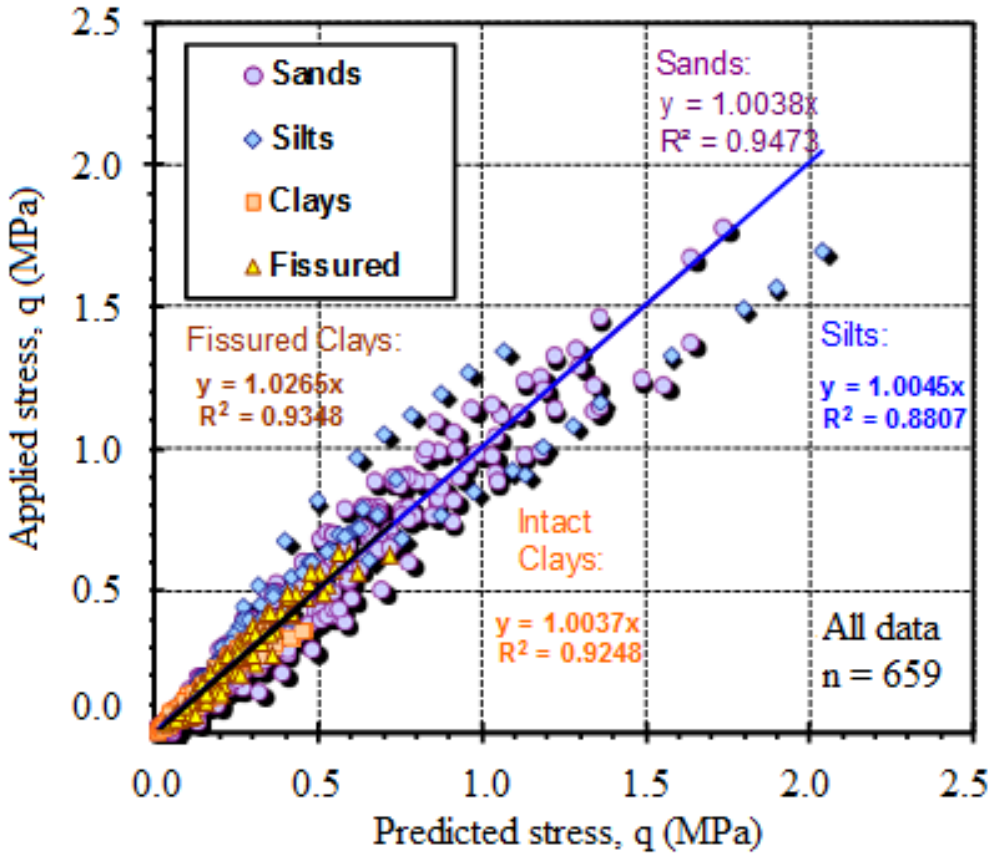

Figure B20. Applied foundation stress vs. CPT-calculated stress for 67 footings.

The same data are shown on Figure B21 in a log-log plot to emphasize the early parts of the load-displacement responses of these footings. The best fit line from regression analyses shows excellent statistical correlations. As detailed earlier, the undrained bearing capacity of square or circular footings on clays can be taken as approximately 0.40 times q_{tnet}. For silts and sands that experience drained loading with no excess porewater pressures being developed and no clear peak value for capacity, the (s/B) =10% criterion can be used. In this case, Equation 7 can be used directly to obtain stress q equal to $q_{capacity}$ when $(s/B)^{0.5}$ is 0.316.

An alternate approach is presented in Figure B22, summarizing the direct CPT method for estimating the load-displacement-capacity of shallow square footings on four soil types. The maximum values of soil bearing capacity (q_{max}) can be capped at stresses corresponding to a percentage of the average measured q_{tnet}, determined over the depth interval from the foundation bearing elevation to 1.5·B below the foundation. In such an approach, the foundation bearing capacity can be taken as ($q_{capacity}/q_{tnet}$) of 0.2 for sands, 0.35 for silts, 0.40 for fissured, and 0.45 for intact clays. Using the assigned values of the h_s parameter, the corresponding cut-off for the general stress-normalized displacement relationship given by Equation 7 can be established, specifically giving corresponding values of the

normalized displacements, which can also be considered as pseudo-strains, equal to $(s/B)_{max}$ of 4% for clays, 7% for fissured clays, 10% for silts, and 12% for sands.

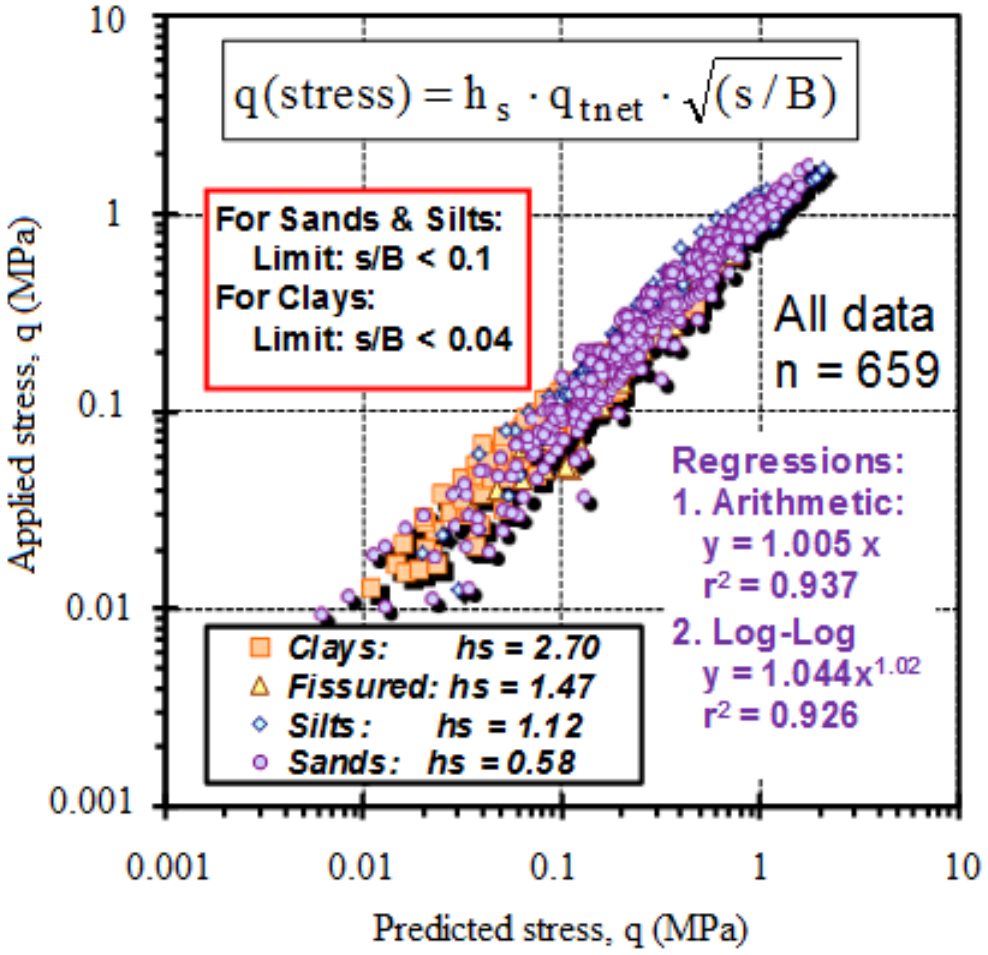

Figure B21. Applied footing stress vs. CPT calculated stress on logarithmic scales

B1.7.1 CPT Soil Material Index, I_c

The soil behavioral type can be assessed indirectly by CPT using a material index (I_c) as defined by Robertson (2009a, b) shown in Equation B10.

$$I_c = \sqrt{[3.47 - logQ_{tn}]^2 + [1.22 + logF_r]^2} \quad \text{B10}$$

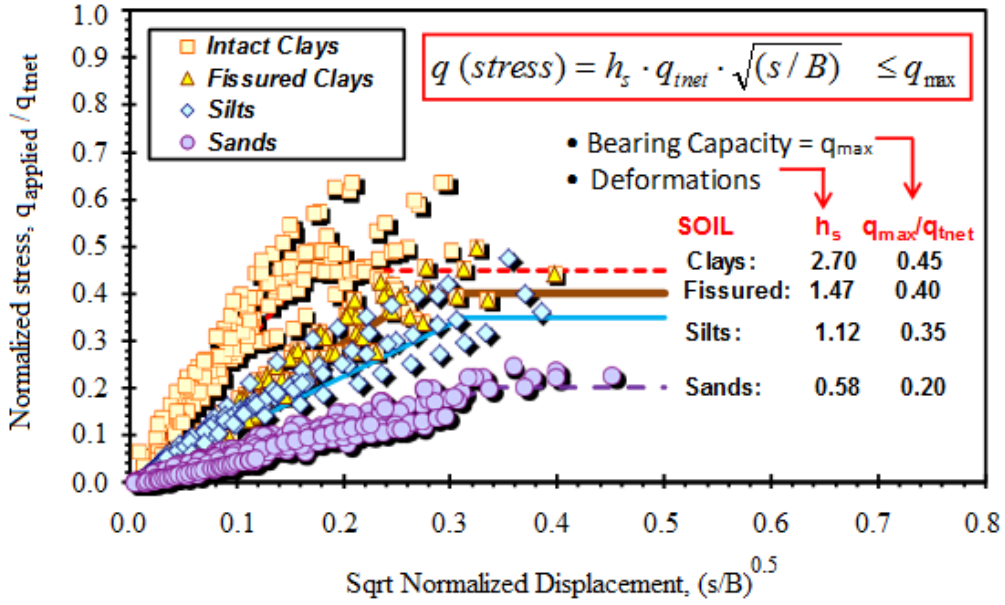

Figure B22. Summary graph and equations of direct CPT method for evaluating the vertical

where Q_{tn} equals the stress-normalized cone tip resistance and F_r equals the normalized sleeve friction calculated from the cone penetrometer readings as shown in Equations B11 and B12 respectably.

$$Q_{tn} = \frac{(q_t - \sigma_{vo})/\sigma_{atm}}{(\sigma'_{vo}/\sigma_{atm})^n} \qquad \textbf{B11}$$

$$F_r(\%) = 100 \cdot \frac{f_s}{(q_t - \sigma_{vo})} \qquad \textbf{B12}$$

where σ_{atm} equals a reference stress equal to atmospheric pressure (σ_{atm} = 1 atm ≈ 1 bar ≈ 100 kPa). In the initial evaluation, the exponent *n* is set to n = 1 to find the soil behavioral type (SBT), based on a 9-zonal chart as shown in Figure 23. The value of exponent *n* varies with soil type; ranging from n = 1 in intact clays and decreasing with increasing grain size to around approximately 0.75 in silts and

approximately 0.5 ± 0.2 in clean sands. The appropriate value of exponent *n* is found by iteration until conversion using the relationship (Robertson 2009b) shown in Equation B13.

$$n = 0.381 \cdot I_c + 0.05\left(\frac{\sigma'_{vo}}{\sigma_{atm}}\right) - 0.15 \leq 1.0 \qquad \textbf{B13}$$

As the distinction that footings on intact clays subjected to fast loading are behaving primarily under undrained conditions (i.e., constant volume), Robertson (2009a) suggested that this occurs when $I_c > 2.7$, while in contrast, $I_c < 2.5$ corresponds more or less to drained loading (i.e., no excess porewater pressures).

The CPT material index can be used to identify soil type and the corresponding characteristic h_s value for estimating footing load-displacement response. In a number of the case studies investigated, the results of the sleeve friction readings were also available to allow the calculation of I_c with depth at these sites. Figure B23 shows the tentative relationship between the values of the h_s parameter plotted versus the corresponding CPT material index, with an approximate trend given by Equation B14.

$$h_s = 2.8 - \frac{2.3}{1+\left(\frac{I_c}{2.4}\right)^{15}} \qquad \textbf{B14}$$

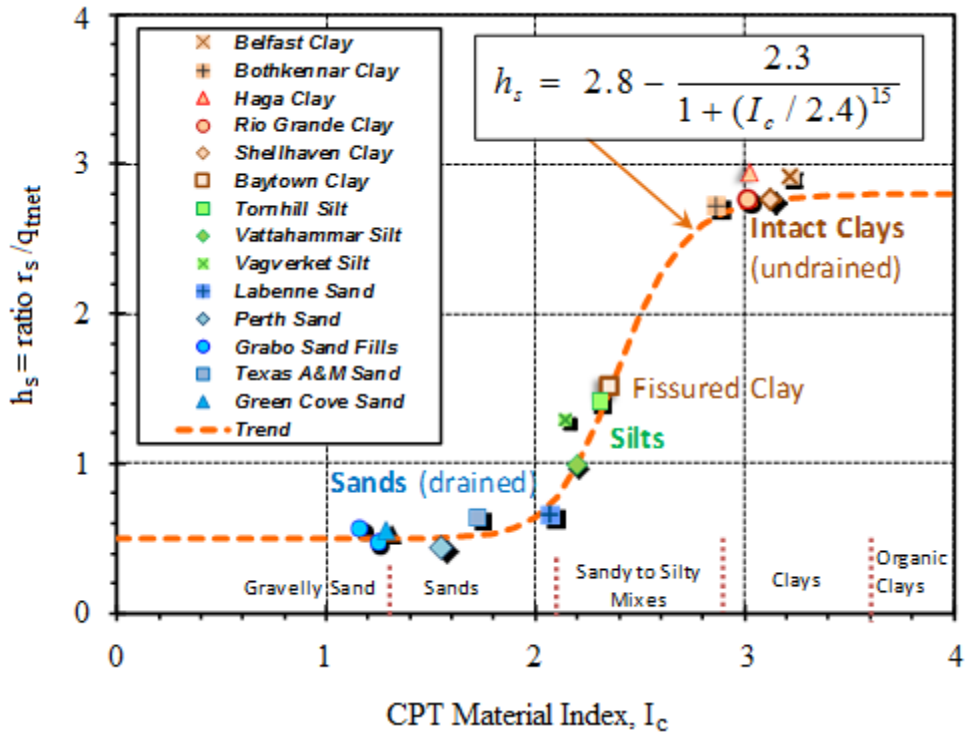

Figure B23. Foundation soil formation parameter h_s versus CPT material index, I_c.

Soil behavioral type from the I_c ranges given by Robertson (2009b) and are shown in Figure B23 with an overall general agreement with the known soil classifications. In summary, the CPT can provide an evaluation of the load-displacement-capacity response directly via Equation B15 which may be of interest in mixed soil types, such as silty sands, sandy silts, and the like.

Footing stress:
$$q = q_{net} \cdot \sqrt{(s/B)} \cdot \left[2.8 - \frac{2.3}{1+(I_c/2.4)^{15}}\right] \qquad \textbf{B15}$$

As discussed earlier, foundation bearing capacity may be taken by a limiting value of pseudo-strain, $(s/B)_{max}$, or by q_{max} as specified as a percentage of q_{tnet}. This definition of bearing capacity can be seen in comparison to soil type as seen in Figure B24.

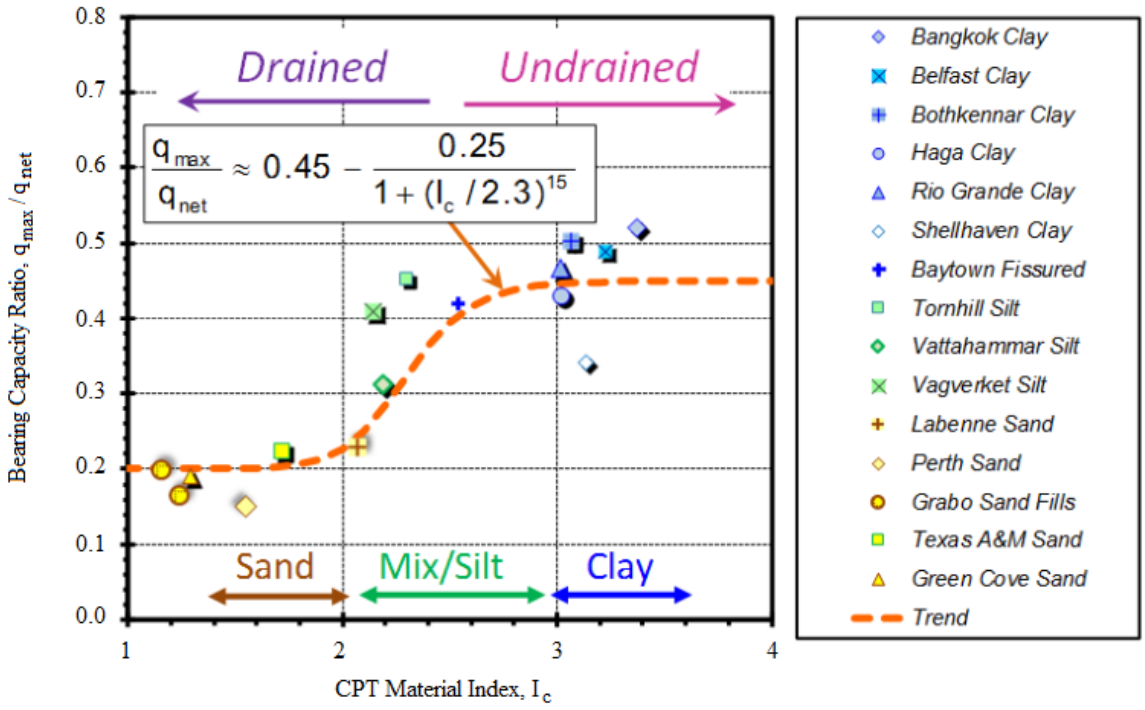

Figure B24. Bearing capacity ratio, q_{max}/q_{net} versus CPT material index, I_c.

B1.7.2. Rectangular Foundations

This same elastic solution from Giroud (1968) for a CPT method for square and circular foundations were utilized for rectangular foundations. The study covered rectangular distortions (A/B) ranging from 1 (square) to very long foundations with A/B equal to 20, where A represents the foundation length and B represents the foundation width (Mayne & Dasenbrock 2017). The influence factor for rectangular shaped foundations is given in Figure B25 and the expression in Equation B16.

$$I_{A/B} = (A/B)^{0.345} \quad \textbf{B16}$$

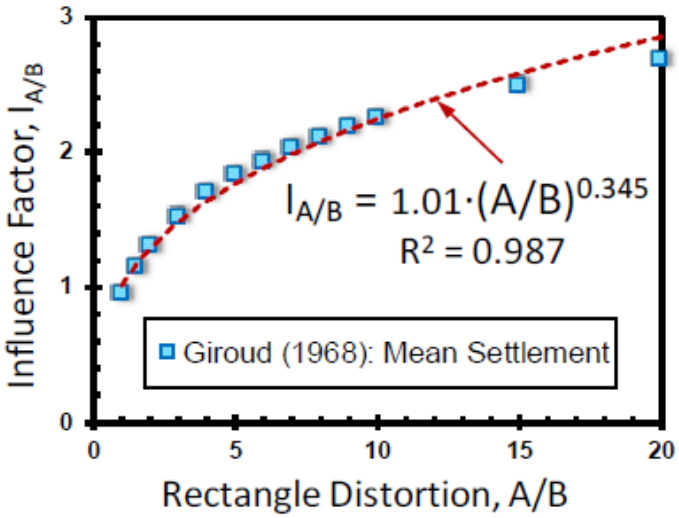

Figure B25. Influence factor for rectangular foundations from elastic theory solution (Mayne & Dasenbrock 2017).

Including 32 full scale load tests on sands, results from an additional 98 shallow foundations have been reported in previous studies. The foundations were primarily square or circular and among these include large spread footings with measured settlements and bearing capacity. Table B4 shows a summary of the number of footings and footing sizes used in the study. The range of length to width ratios varied from $1 < (A/B) < 23$, with an average value of (A/B) equal to 2.38. The embedment depth to footing width ranged from $0 < De/B < 2.22$ and averaged 0.46.

Table B4. Sources for shallow foundation performace

Source of Data	No. of Footings	Mean B (m)	Max. B (m)	Min. B (m)	Mean A (m)	Max. A (m)	Min. A (m)
Mayne et al., (2012)	32	1.49	6.09	0.46	1.49	6.09	0.46
Lehane (2011)	8	0.41	0.27	0.60	0.41	0.60	0.27
Gifford et al., (1987)	17	8.46	15.88	5.27	15.91	35.96	7.01
Jeyapalan & Boehm (1986)	13	10.22	28.92	4.00	16.71	30.49	6.40

Schmertmann (1970)	31	9.45	56.08	0.61	12.88	86.68	0.61
Papadopoulos (1992)	29	8.70	36.00	1.00	13.00	72.90	1.00
Total	*130*	*6.71*	*56.08*	*0.27*	*10.12*	*86.68*	*0.27*

The solution for shallow foundation settlements, given back in Equation B1, combined with the expression in Equation B16 takes on the form:

$$s = \frac{q \cdot B \cdot I_{A/B} \cdot (1-\nu^2)}{E_s} \qquad \textbf{B17}$$

Combining the direct CPT equation developed from the 32 full scale load tests (Equation B15) together with the influence factor for rectangular shaped foundations becomes:

Footing stress:
$$q = q_{net} \cdot \sqrt{(s/B)} \cdot \left[2.8 - \frac{2.3}{1+(I_c/2.4)^{15}}\right] \cdot \left[\frac{A}{B}\right]^{-0.345} \qquad \textbf{B18}$$

B1.8. Conclusions

A direct CPT method for square, rectangular and circular shallow footings is developed using a database of 166 full-scale field load tests where the minimum footing size of an equivalent square width of 0.5 m is established to avoid scaling issues. The use of load vs. displacement is generalized by characteristic stress vs. normalized displacement (s/B) and further simplified by a square root plotting technique that captures the ground response in a single parameter that is related to the q_{tnet}. Data are grouped according to four main soil categories: sands, silts, fissured clays, and intact clays. It is generally believed that the footings on sands and silts exhibit fully drained behavior, while in intact clays, an undrained response occurs under conditions of constant volume.

The summary equation for evaluating the vertical stress-displacement-capacity of square, rectangular and circular footings is given by:

$$q_{footing} = h_s \cdot q_{tnet} \cdot \sqrt{\frac{s}{B}} \cdot \left(\frac{A}{B}\right)^{-0.345} < q_{max} \qquad \textbf{B19}$$

where the parameter h_s also relates directly to I_c. The foundation capacity depends upon the mode of failure, as well as drainage conditions, and can be taken as a fraction of q_{tnet}, where q_{max}/q_{tnet} is 0.20 in sands, 0.35 in silts, 0.40 in fissured clays, and 0.45 in intact clays as shown in Figure 24. Alternatively, the capacity can be defined using a limiting pseudo-strain, given by $(s/B)_{max}$ of 4% in clays, 7% in fissured, 10% in silts, and 12% in sands.

APPENDIX C

List of Figures

List of Tables

C1. EVALUATING DEEP FOUNDATION RESPONSE FROM CONE PENETRATION TESTS

C1.1. Introduction

The axial response of deep foundations includes the load-displacement-capacity and axial load transfer when driven pilings and drilled shafts are loaded in compression and uplift. The use of cone penetration testing (CPT), especially seismic piezocone tests (SCPTu), are advantageous since they provide information on the subsurface soils and their geomaterial properties. The SCPTu provides at least four measurements on soil behavior with depth, including: (a) cone tip resistance, q_t, (b) sleeve friction, f_s, (c) penetration porewater pressure, u_2, and (d) shear wave velocity, V_s. This offers the opportunity to determine the geostratigraphy, unit weight, effective overburden stress, shear strength, stress state, and stiffness of the ground from a single exploratory sounding, thus values in economic, expediency, and reliability. The axial pile capacity can be calculated based on static equilibrium of forces acting along the sides and base of the pile foundation. The displacement of the pile can be ascertained using elasticity theory from closed-form solutions, boundary elements, and/or finite element analyses. Load transfer occurs along the length of the pile and only a portion of axial forces are transmitted to the base or toe or tip of the pile. These too can be assessed using elasticity solutions.

An alternate approach to pile capacity involves the utilization of direct CPT methods, available since the 1970's, but in the past 10+ years a number of new and statistically reliable algorithms have been developed which can be implemented for highway design and construction.

C1.1.1 Axial Pile Capacity

The axial compression capacity of a single pile foundation is composed of a shaft or side component and end-bearing component at the base, as depicted in Figure 1. For a circular pile, the side capacity (Q_s) is determined from the unit side friction (f_p) acting along the surface area of the shaft which is: $A_s = \pi \cdot d \cdot L$, where d = pile diameter and L = length embedded below grade.

If the magnitude of side friction is uniform and constant with depth, the side capacity is simply:

$$Q_s = f_p \cdot A_s \qquad \text{C1}$$

Moreover, however, many piles extend through multiple layers and a summation of unit side frictions acting on various pile segments must be tabulated over the length of the pile, as suggested by Figure C1.

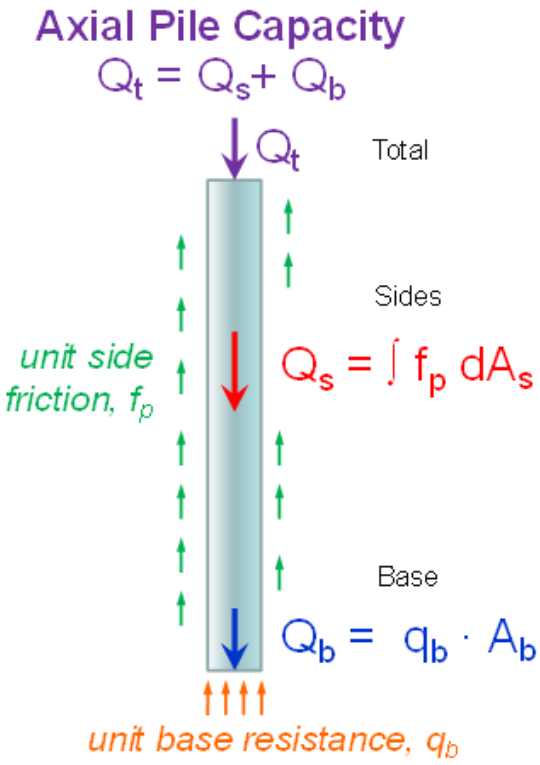

Figure C1. Components of Axial Pile Capacity

The unit-end bearing resistance (q_b) acts over the base of the pile tip, where the area of a circular pile is given by $A_b = \pi \cdot d^2/4$. For piles in compression loading, the base capacity is determined from Equation C2.

$$Q_b = q_b \cdot A_b \qquad \text{C2}$$

and for piles in tension (or uplift), it is normally taken that $Q_b = 0$.

C1.1.2 Pile Unit Side Friction

Several different approaches can be adopted for evaluating the unit pile side friction (f_p) prior to full-scale load testing and construction (Poulos & Davis 1980; O'Neill 2001). The most common types including the alpha and beta methods, as summarized in Tables 1 and 2, respectively. In the alpha method, an empirical coefficient (α) is applied to the undrained shear strength (s_u) of clay soils to obtain:

$$f_p = \alpha \cdot s_u \qquad \text{C3}$$

An illustrative example of alpha curves is shown in Figure C2. A difficulty with the alpha method is the evolution of many variants and changes to the expressions for its estimation. It is also restricted in its use for specific types of piles in clays and fine-grained soils.

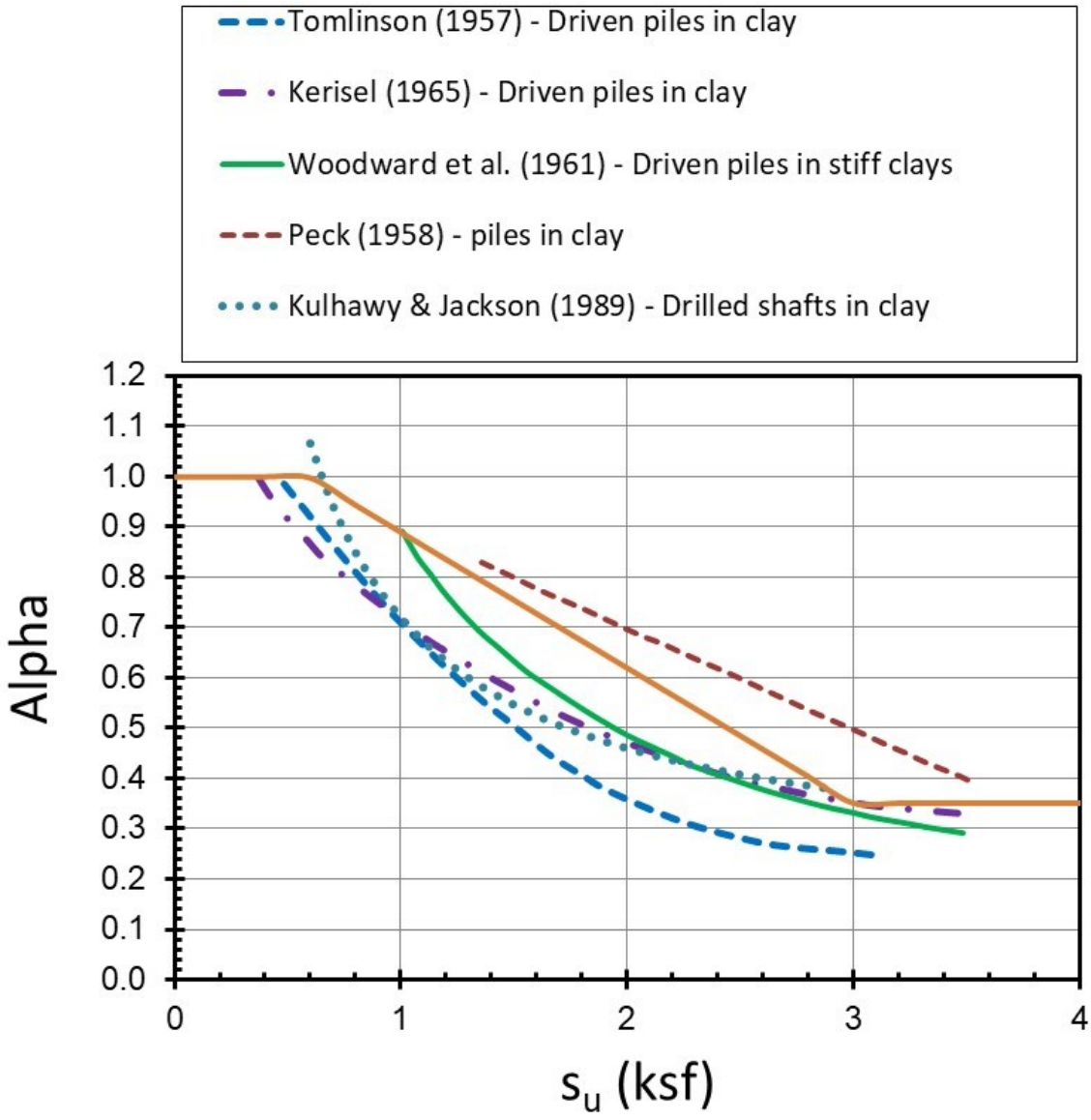

Figure C2. Selected alpha relationships as function of the undrained shear strength.

Table C1. Alpha Methods for Axial Pile Side Friction where $f_p = \alpha \cdot s_u$

Reference Source	Alpha Equation	Remarks
Tomlinson (1957)	$\alpha = 0.11 \cdot s_u^{\,2} - 0.68 \cdot s_u + 1.27$	All pile types (steel, concrete, timber) Note: s_u in ksf
Tomlinson (1957)	$\alpha = 0.11 \cdot s_u^{\,2} - 0.62 \cdot s_u + 1.26$	Concrete piles Note: s_u in ksf
McClelland (1974)	Kerisel: $\alpha = 0.7 - 0.31 \cdot \ln(s_u)$ Peck: $\alpha = 1.0 - 0.2 \cdot s_u$ Woodward: $\alpha = 0.91 \cdot (s_u)^{0.91}$	Driven piles in clay Note: s_u in ksf
Semple (1980)	$\alpha = 1 - \frac{(OCR-1)}{1+1.5 \cdot (OCR-1)}$	Summary from 9 series of pile load tests
American Petroleum Institute (API 1981)	For $s_u/\sigma_{vo}' \leq 0.35$: $\alpha = 1.0$ For $s_u/\sigma_{vo}' > 0.80$: $\alpha = 0.5$ Otherwise: $\alpha = 1 + 1.111 \cdot (0.35 - s_u/\sigma_{vo}')$	Driven steel pipe piles
Tomlinson (1986)	1. $\alpha = 55\ (s_u)^{-0.91}$ 2. $\alpha = 78.5\ (s_u)^{-1.02}$ 3. $\alpha = 60.5\ (s_u)^{-1.00}$ where $75 < s_u$ (kPa) < 210	1. Driven piles 2. Bored piles 3. Driven piles in till with L < 10·d
API (1987) *	1. $\alpha = 1.0$ for $s_u < 25$ kPa	Driven piles in clay other than Gulf of Mexico

	2. $\alpha = 1.25 - 0.01 \cdot s_u$ for $25 < s_u < 75$ kPa 3. $\alpha = 0.50$ for $s_u > 75$ kPa	
Kulhawy & Jackson (1989)	$\alpha = 0.21 + 0.26 \cdot (\sigma_{atm} / s_u) \leq 1$	Analyses of 106 drilled shaft foundations

Table C1. Continued

API (1989)	For $s_u/\sigma'_{vo} \leq 1$: $\alpha = \frac{0.5}{\sqrt{s_u/\sigma'_{vo}}}$ For $s_u/\sigma'_{vo} > 1$: $\alpha = 0.5 \cdot \left(s_u/\sigma'_{vo}\right)^{-0.25}$	Driven steel pipe piles
Kulhawy & Jackson (1989)	$\alpha = \frac{(1-\sin\phi') \cdot \tan\phi' \cdot OCR^{\sin\phi'}}{0.5 \cdot \sin\phi' \cdot OCR^{\Lambda}}$	$\Lambda = (1-C_s/C_c) \approx 0.80$ for insensitive clays
Nowacki et al. (1996)	For $s_u/\sigma'_{vo} \leq 0.7$: $\alpha = 0.5 \cdot \left(s_u/\sigma'_{vo}\right)^{-0.5}$ For $s_u/\sigma'_{vo} > 0.7$: $\alpha = 0.55 \cdot \left(s_u/\sigma'_{vo}\right)^{-0.2}$	Driven pile foundations
Kolk and van der Velde (1996)	$\alpha = 0.9 \cdot F_L \cdot (s_u/\sigma'_{vo})^{-0.3} < 1.0$ $F_L = [(L - z)/d]^{-0.2}$ = length term L = pile length	Note: s_u obtained from UU lab tests Applicable to driven piles in clays

	z = depth at point considered d = outside diameter of pile	
Karlsrud et al. (2005, NGI Method)	α = function (s_u/σ'_{vo} and plasticity index)	Driven pilings
Fleming et al. (2009)	For $s_u/\sigma'_{vo} \le 1$: $\alpha = \left(s_u/\sigma'_{vo}\right)_{NC}^{0.5} \cdot \left(s_u/\sigma'_{vo}\right)^{-0.5}$ For $s_u/\sigma'_{vo} > 1$: $\alpha = \left(s_u/\sigma'_{vo}\right)_{NC}^{0.5} \cdot \left(s_u/\sigma'_{vo}\right)^{-0.25}$	For driven piles in clay where $(s_u/\sigma'_{vo})NC$ is the normalized shear strength for normally-consolidated clay
Brown, et al. (2010)	α = 0 for 0 < z ≤ 5 feet α = 0.55 for z > 5 feet and $(s_u/\sigma_{atm}) \le 1.5$ $\alpha = 0.55-0.1\cdot(s_u/\sigma_{atm}-1.5)$ for $1.5 \le (s_u/\sigma_{atm}) \le 2.5$	Drilled Shafts and Bored Piles

Table C1. Continued

Knappett & Craig (2012)	α = 1 for $s_u \le 30$ kPa α = 1.16 - $(s_u/185)$ for 30 kPa ≤ s_u ≤ 150 kPa α = 0.35 for s_u > 150 kPa	Non-displacement piles in fine-grained soils
Knappett & Craig (2012)	$\alpha = 0.55 \cdot \left(\frac{40}{(L/D)}\right)^{0.2} \cdot \left(s_u/\sigma'_{vo}\right)^{-0.3}$	Displacement piles in fine-grained soils

Karlsrud (2012)	α = function (s_u /σ'$_{vo}$ and plasticity index)	Driven pilings

*Note: as reported by Karlsrud (2012)

In the beta method, the coefficient β is applied to the effective overburden stress (σ'$_{vo}$) at the point of concern along the pile length:

$$f_p = \beta \cdot \sigma'_{vo} \qquad \text{C4}$$

Table C2. Beta Methods for Axial Pile Side Friction where $f_p = \beta \cdot \sigma'_{vo}$

Reference Source	**Beta Equation**	**Remarks**
Burland (1973)	β = (1-sinφ') · tan φ'	Piles in NC clays
Meyerhof (1976)	β = K·tanδ	where K = K_0 = for NC clays K = 1.5·K_0 for OC clays $K_0 = (1-\sin\phi')\cdot\sqrt{OCR}$
Poulos & Davis (1980)	β = (1-sinφ') · tan φ' · $OCR^{0.5}$	Piles in OC stiff clays

Table C2. Continued

Kulhawy & Jackson (1989)	$\beta = (1\text{-}\sin\varphi') \cdot \tan\varphi' \cdot OCR^{\sin\varphi'}$	Piles in quartz sands and insensitive clays
O'Neill (2001)	$\beta = (1\text{-}\sin\varphi') \cdot \tan\theta' \cdot OCR^{\sin\varphi'}$	Drilled shafts where $\theta = (\delta/\varphi')\cdot\varphi'$ and δ = interface friction between pile and soil
Fleming et al. (2009)	$\beta = K\cdot\tan\delta$	K = lateral stress coefficient and δ = friction angle between soil and pile material
Karlsrud (2012)	β = fctn (OCR and PI)	PI = plasticity index of the clay (%)
Mayne and Niazi (2017)	$\beta = C_M \cdot C_K \cdot K_0 \cdot \tan\varphi'$ where $K_0 = (1\text{-}\sin\varphi') \cdot OCR^{\sin\varphi'}$ for soils that are virgin loaded then unloaded	C_M = pile material factor = 1 (drilled; augered); 0.9 (prestressed or precast concrete); 0.8 (timber); and 0.7 (steel); and C_K = pile installation factor = 0.9 (bored or augered); 1.0 (low displacement, e.g. H-pile or open-end pipe); and 1.1 (driven high displacement, e.g. prestressed concrete, closed-end pipe)

As the beta approach applies to all types of soils (gravels, sands, silts, and clays) and more or less has remained unchanged since its advent circa 1970, it has been selected for further discussion herein. In the direct form for calculation of unit pile side friction, the expression is given by:

$$f_p = C_M \cdot C_K \cdot (1 - sin\phi') \cdot OCR^{sin\phi'} \cdot tan\phi' \cdot \sigma'_{vo} \qquad \text{C5}$$

where C_M is a soil-pile interface friction coefficient and C_K = pile installation factor. Values of C_M are in the range: $0.7 < C_M < 1.0$ depending upon pile material (steel, wood, concrete) and ranges for C_K vary: $0.9 < C_K < 1.1$ depending upon method of installation (auger, drill, driven), as detailed in Table 2.

The value of K_0 is limited to the passive stress coefficient which for the simple Rankine case is given by: $K_P = (1+\sin \varphi') / (1 - \sin \varphi')$. Thus, there is a maximum value of overconsolidation ratio for which Equation C5 applies, given by: $OCR_{limit} = [(1+\sin \varphi') / (1 - \sin \varphi')^2]^{(1/\sin\varphi')}$.

The corresponding graph in Figure C3 shows the relationship for β in terms of φ ' and OCR.

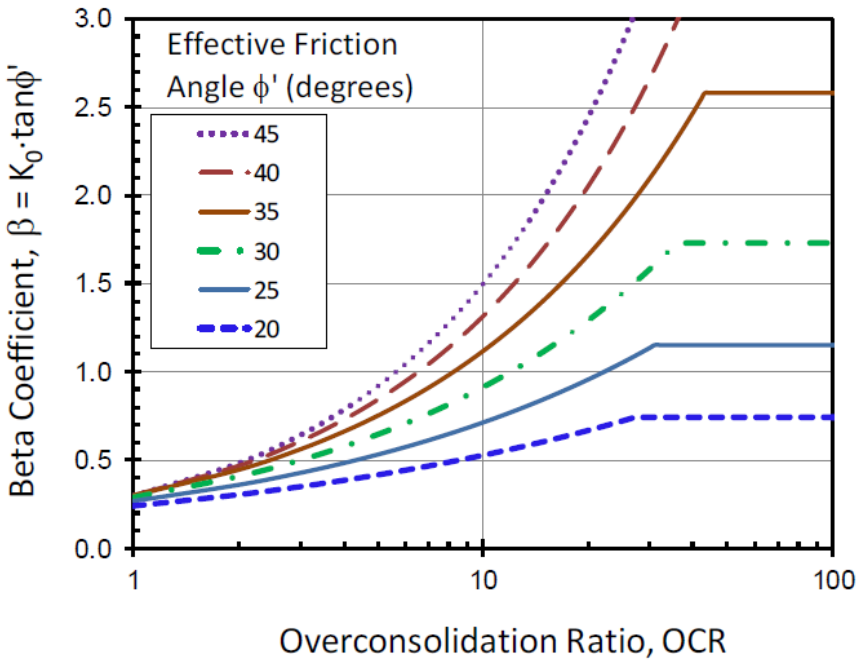

Figure C3. Pile side friction coefficient β in terms of effective friction angle and overconsolidation ratio.

C1.1.3 Pile Unit End Bearing

C1.1.3.1 Theoretical Considerations

The evaluation of the end bearing resistance of pile foundations is commonly determined using limit plasticity theory where:

Drained loading: $$q_b = N_q \cdot \sigma'_{vo}$$ C6

Undrained loading: $$q_b = N_c \cdot s_u$$ C7

where the value of σ'_{vo} is calculated at the depth z = L and the value of s_u is the average undrained shear strength from z = L to a depth z = L + d beneath the pile tip. For a circular pile, the limit plasticity solution for undrained loading gives (Vesic 1977) a value N_c = 9.33 while a deep strip foundation would employ a value of N_c = 8.24. For drained loading, the expression for N_q for a deep foundation is given by (Vesic 1977):

$$N_q = \exp(\pi \cdot \tan\phi') \frac{1+\sin\phi'}{1-\sin\phi'} \cdot [1+\tan\phi'(B/A)] \cdot [1+2\tan\phi'(1-\sin\phi')^2 \arctan(L/B)] \quad \text{C8}$$

where A and B are the pile plan dimensions (for a circular pile, A = B) and L = pile length. For a circular pile, this can be approximated by:

$$N_q \approx 0.77^{(\phi'/7.5°)} \quad \text{C9}$$

over a range of effective friction angles: 20° ≤ φ' ≤ 45°.

C1.1.3.2 Practical Considerations

For drained loading of sands, the full calculated end bearing capacity will never be realized because it would require the pile to move a distance equal to its diameter. This is beyond practical use and therefore the limit plasticity solutions must be clipped to a fraction of the calculated value. Another reason for using a reduced end-bearing capacity is due to strain incompatibility since the side capacity is mobilized early while the end-bearing is engaged much later. So, to have compatible values of Q_s and Q_b, the q_b must be reduced using the following guidelines (Randolph 2003; Mayne 2007):

$$q_b = N_q \cdot \sigma'_{vo} \cdot f'_x \quad \text{C10}$$

where f_x' = strain incompatibility factor

f_x' = 0.10 for drilled shafts, augered cast-in-place, and bored piles

f_x' = 0.20 for driven low displacement piles (opened-ended steel pipe and H-piles)

f_x' = 0.30 for driven high-displacement piles (i.e., solid piles, PSC, and closed-ended pipe)

For undrained loading of circular piles in compression, no reduction of end-bearing is necessary, therefore:

$$q_b = 9.33 \cdot s_u \qquad \text{C11}$$

C1.2. Direct CPT Methods for Pile Capacity

In the direct CPT method, the penetrometer readings are scaled directly via specified algorithms to obtain the pile unit side friction and end-bearing, as depicted in Figure C4. As many as 40 different direct CPT methods have been developed over the past five decades, as summarized by Niazi & Mayne (2013). Starting circa 1970, many of these early methods relied on hand-recorded data from field mechanical CPTs where only q_c data were obtained at 20 cm intervals, or later with mechanical readings of both q_c and f_s using special sets of inner and outer rods that recorded vertical load for tip and loads for tip plus sleeve in alternating increments. Also, early pile load test data were often obtained from top-down measurements of load-displacement.

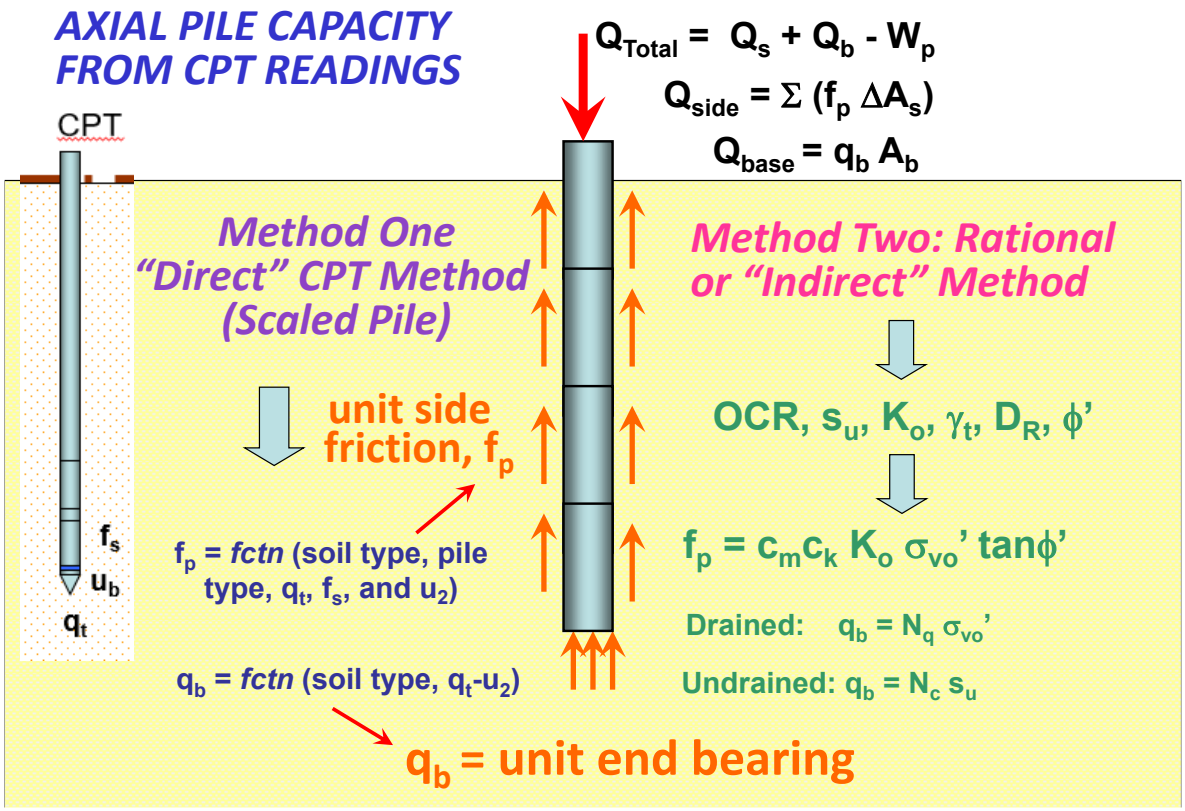

Figure C4. Concept of Direct versus Rational Method for CPT evaluation of axial pile capacity

Beginning in the mid-1990's, as the modern electric piezocone (CPTu) was implemented, the newer equipment offered improved data and better resolution because of the additional reading of porewater pressures and correction of raw measured q_c to total resistance q_t. In addition, the use of electronic digital data collection and field computers proved superior in field measurements and recordings. As a consequence, several reliable CPT methods for axial pile capacity have been developed. Moreover, parallel improvements in full-scale pile load testing occurred and now include modern strain gage instrumentation, digital data recording, and automated testing procedures. Also, the testing can be single direction (compression or tension) or bi-directional, as in the Osterberg cell.

Table C3 provides a selection of recent direct CPT methods that have become available over the past two decades. A number of these (namely ICP, NGI, UWA, and Fugro) were funded by the offshore industry because of the growth of oil & gas reserves and windfarm installations, thus necessitating increased concerns on risk, probability, and reliability in the site investigations for offshore platforms and design of large driven monopile foundations. These direct CPT methods are often statistically based on large datasets compiled from full-scale load tests made worldwide (e.g., Schneider et al. 2008).

Table C3. Selection of Direct CPT Methods for Axial Pile Capacity

Method	**Pile Types**	**Soil Types**	**References**	**CPT data**	**Additional parameters needed**
Unicone Method	all types	Sands, silts, clays	Eslami and Fellenius (1997); Fellenius (2009)	q_t, f_s, u_2	
KTRI = Kajima Technical Research Institute	all types	Sands, mixed, clays	Takesue et al. (1998)	f_s and u_2	No guidance given on end bearing resistance
Imperial College Procedure (ICP)*	OE and CE	Sands	Chow et al. (1997; PhD) Jardine et al. (2005)	q_t	Interface friction angle (δ) from ring shear tests; Correlated to mean grain size (D_{50})

	OE and CE	Clays	Jardine et al. (2005)	q_t	Interface friction angle (δ); correlated to PI

Table C3. Continued

NGI Method (Norwegian Geotechnical Institute)	OE and CE	Sands	Clausen et al. (2005)	q_t	D_R from q_t
		Clays	a. Alpha method (Karlsrud et al. 2005; 2012) b. Beta method (Karlsrud 2012)	q_t for s_u q_t for OCR	PI = plasticity index (%) PI = plasticity index (%)
Fugro Method	OE and CE	Sands	Kolk et al. (2005)	q_t	
		Clays	Van Dijk and Kolk (2011)	q_t	
	OE and CE	Sands	Lehane et al. (2005)	q_t	IFR = infilling ratio related to amount of plugging

UWA (Univ. of Western Australia)					R_a = pile roughness
		Clays	Lehane et al. (2012)	q_t	Interface friction angle (δ) from ring shear tests; and also method without δ
HKU Method (Hong Kong Univ.)	OE and CE (end resistance only)	Sands	Yu and Yang (2012)	q_t	End bearing only. PLR = plug length ratio Note: PLR can be estimated from OE inner diam.

Table C3. Continued

Purdue LFRD	Drilled shafts	Sands	Basu & Salgado (2012)	q_t	LRFD = load resistance factored design
Enhanced Unicone Method	Various	Sands, silts, clays, and mixed soils	Niazi and Mayne (2015, 2016)	q_t, u_2, and f_s	Based on 330 load tests, including bored, augered, jacked, and driven piles

*Note: previously called "Marine Technical Directorate" (MTD)

Many of the offshore CPT methods relate to driven piles, either in sand or clay, as that is common deep foundation for those purposes. Of particular interest are the Unicone and Modified Unicone Methods, since they use all three readings of the piezocone (qt, fs, and u2) and address a variety of pile foundation types.

C1.3. Modified UniCone Method

The modified UniCone Method was developed based on a total 330 pile load tests which were associated with SCPTu data during their site investigations (Niazi and Mayne, 2015, 2016). This represents a threefold increase over the original UniCone database that was built upon data from 106 pile load tests (Eslami & Fellenius 1997).

For the original UniCone algorithms, use is made of the effective cone resistance (q_E):

$$q_E = q_t - u_2 \qquad \text{C12}$$

and a chart of q_E vs f_s provided an approximate soil classification in five distinct groups, as shown by Figure C5. Later, in the modified approach, a better delineation of the larger dataset gave soil subclassifications, as indicated by Figure C6.

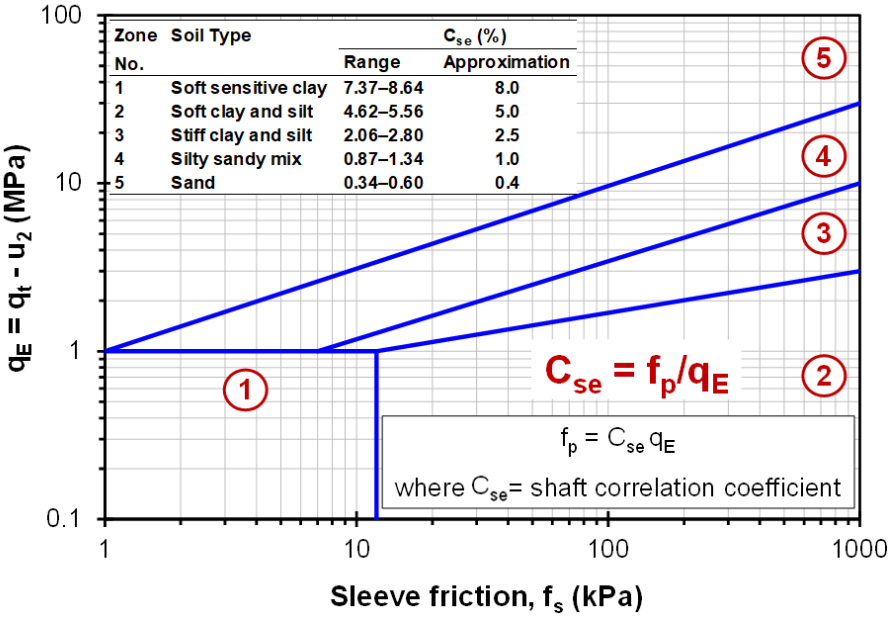

Figure C5. Soil behavior type using CPT via original UniCone.

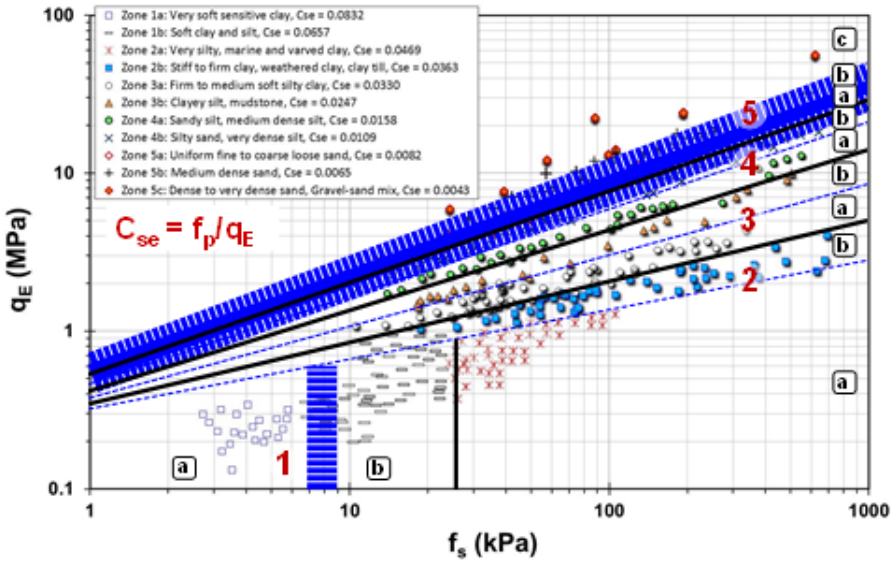

Figure C6. Soil behavior type using CPT via Modified UniCone.

In the modified approach, the 9-zone normalized soil behavioral type (SBTn) is ascertained using CPT data in conjunction with the Robertson (2009) charts, as shown in Figure C7. As discussed in Appendix A and B, the SBTn method uses the normalized cone resistance (Q_{tn}), normalized sleeve friction (F_r(%)), and CPT material index, I_c. This permits a much wider range in the calculated pile side friction because f_p is related as a continuous curve with I_c, rather than only 5 values that are assigned in the original scheme.

The pile unit side friction (f_p) is obtained from q_E and the CPT material index, I_c, using the following expression at each elevation along the sides of the pile:

$$f_p = q_E \cdot \theta_{PT} \cdot \theta_{TC} \cdot \theta_{RATE} \cdot 10^{(0.732 \cdot I_c - 3.605)} \quad \text{C13}$$

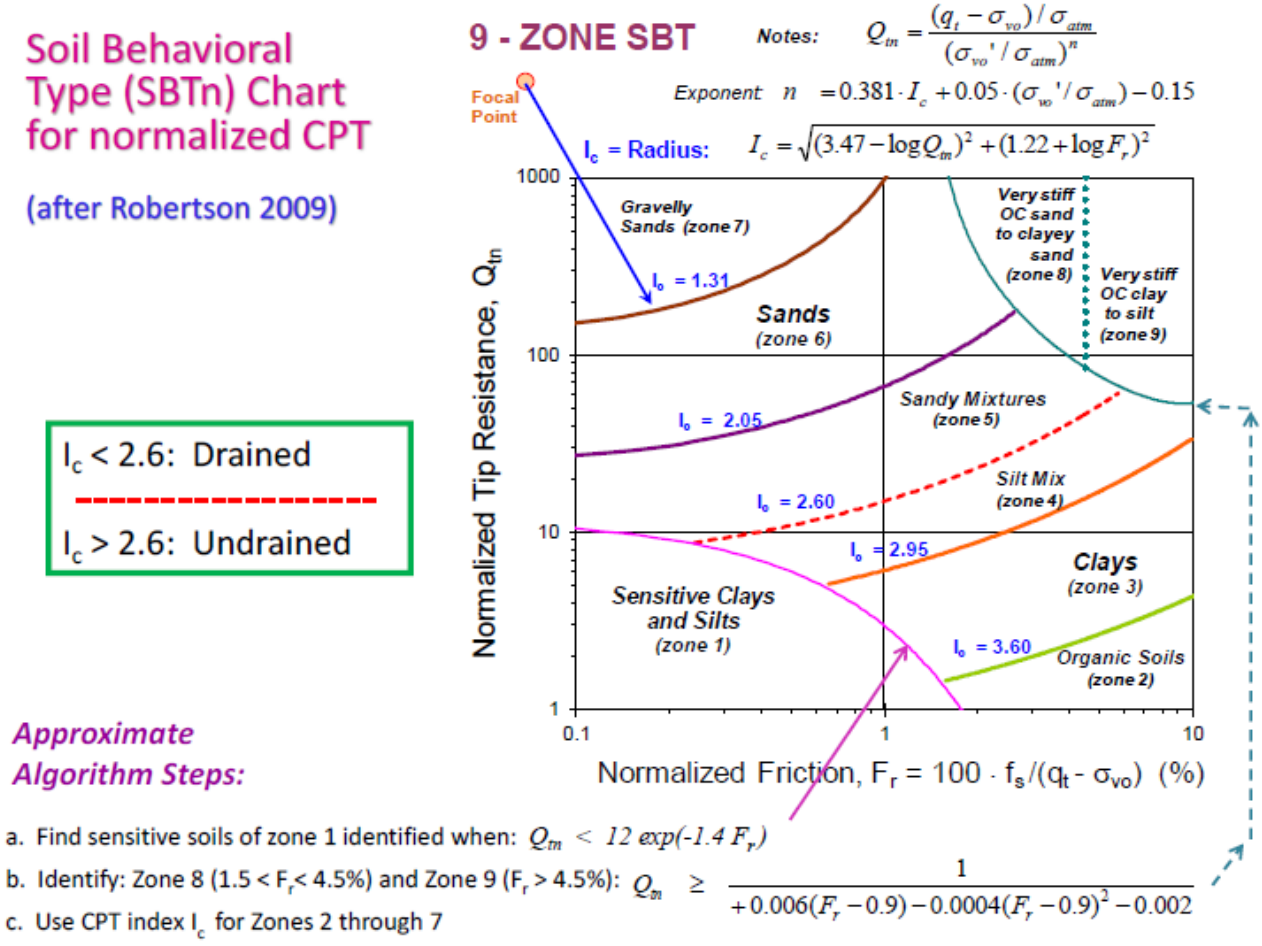

Figure C7. Nine-zone soil behavioral soil type using normalized piezocone parameters (after Robertson 2009; Mayne 2014).

where θ_{PT} = coefficient for pile type (θ_{PT} = 0.84 for bored piles; 1.02 for jacked piles; 1.13 for driven piles), θ_{TC} = coefficient for loading direction (θ_{TC} = 1.11 for compression and 0.85 for tension); and θ_{RATE} = rate coefficient applied to soils in SBT zones 1 through 7 (θ_{RATE} = 1.09 for constant rate of penetration tests and 0.97 for maintained load tests). Since CPT provides data at regular intervals of 2 cm to 5 cm along the sides of the pile, the average f_p from z = 0 to z = L can be used directly in Equation 1 to obtain the shaft capacity Q_s.

The pile end bearing resistance is obtained from:

$$q_b = q_E \cdot 10^{(0.325 \cdot I_c - 1.218)} \qquad \text{C14}$$

where q_E is averaged in the vicinity of the pile tip. Figure C8 shows the Modified Unicone Method in graphical format. For sensitive clays of zone 1, please see additional discussions by Niazi & Mayne (2016).

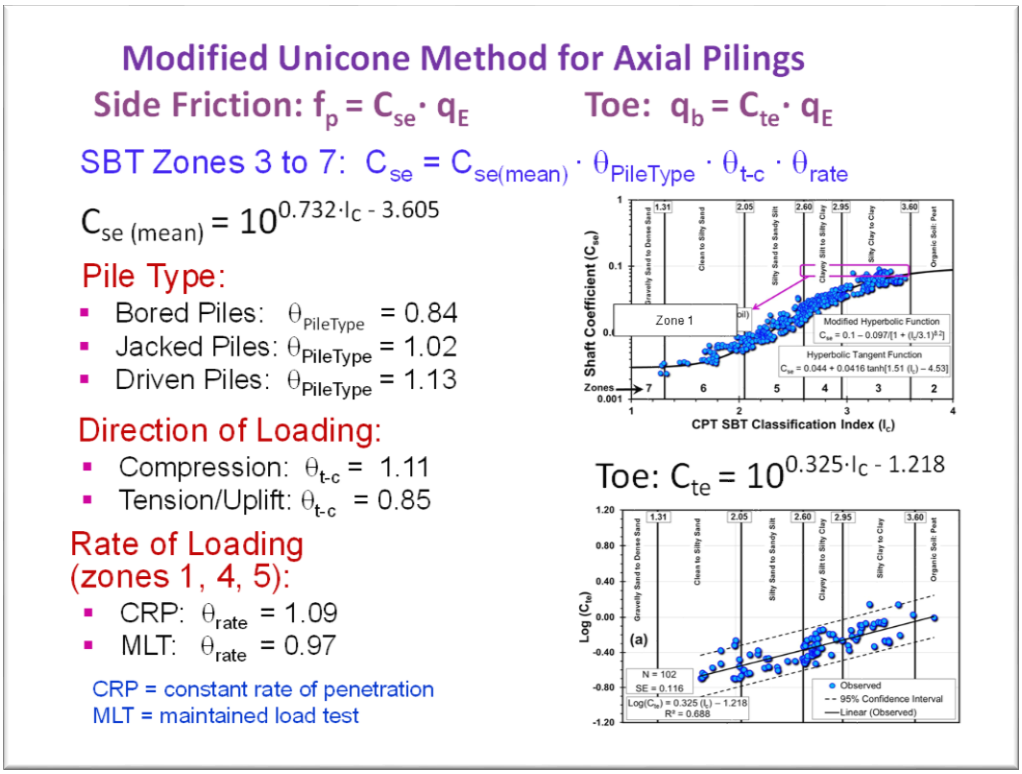

Figure C8. Summary of Modified UniCone Method for direct CPT assessment of axial pile capacity.

C1.4. Axial Pile Displacement

The movement of pile foundations can be assessed using elastic continuum theory (Poulos & Davis 1980; Randolph 2003; Mayne & Niazi 2017). These relationships have been developed using finite element analyses, boundary elements, and analytical closed-form solutions. For the latter approach, the top displacement of a rigid pile subjected to a vertical force is shown in Figure C9. This gives the movement at the top of a pile subjected to either compression or tension (uplift) loading. Also, the percentage of axial load transferred to the pile toe is determined. For piles extending through various soil layers, the elastic solution can be implemented by using a set of stacked pile segments, each with its own stiffness, as represented by a soil Young's modulus.

For pile groups, the use of computer software is recommended. Several available programs can handle pile groups under axial and lateral / moment loading, such as DEFPIG (Univ. Sydney) and PIGLET (Univ. Western Australia). A full listing of pile foundation software is given at the Geotechnical & GeoEnvironmental Service Directory: www.ggsd.com

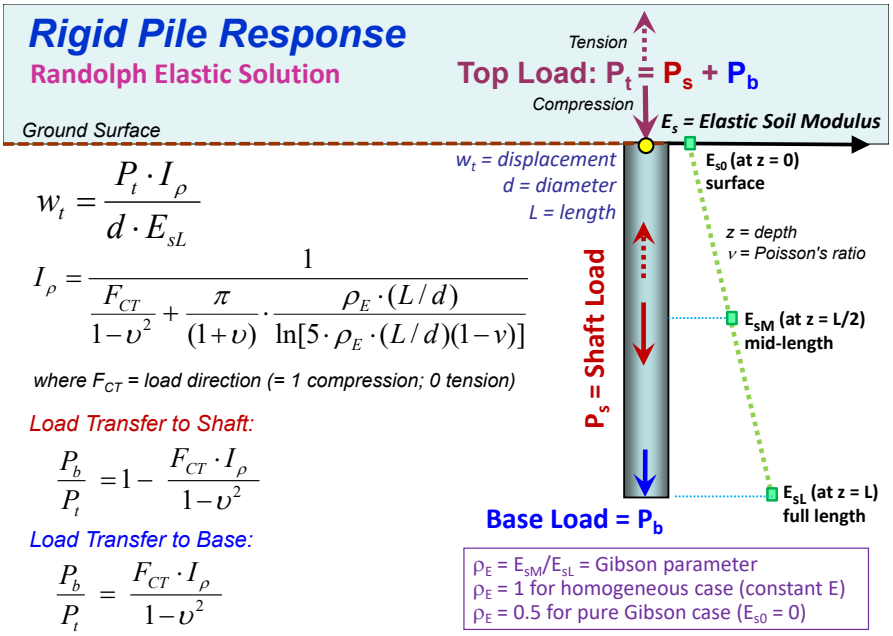

Figure C9. Elastic continuum solution for axial pile response under compression and tension loading.

C1.5. Acknowledgements

The author appreciates the help of Fernando Illingworth of Pons/Ecuador, Meena Viswanth of GeoSyntec/Atlanta, and Dr. Marco Uzielli of GeoRisk/Italy in helping to collect and process the data. Funding support was provided by David Woeller of ConeTec, Richmond, BC.